

**RESPONSE TO QUESTIONS 1, 2, 3, 4, 5, 7,
10, 11, 12, 13, 14, and 16**

August 1989

This volume responds to 12 of 19 questions asked of PG&E by the Nuclear Regulatory Commission (NRC) on June 1, 1989. Responses to the remaining 7 questions will be submitted later. These responses provide data requested to augment or clarify information regarding seismic ground motions presented in the Final Report of the Long Term Seismic Program, submitted by PG&E to the NRC on July 31, 1988, and in the responses to Questions 4 through 18 and 20, submitted by PG&E to the NRC in January and February 1989.

8909140143 890831
PDR ADOCK 05000275
P PDC



Pacific Gas and Electric Company

Diablo Canyon Power Plant
Long Term Seismic Program



QUESTION 1

What are the potential effects on the ground motion regression analysis results of including the very hard rock sites in the empirical data set.

Examination of data used in the Long Term Seismic Program empirical ground motion studies (presented in response to Question 6, January 1989) indicates there are no clear systematic differences in ground motions recorded at soft-rock and hard-rock sites.

Our rock-site data consist of recordings from both soft-rock (primarily sedimentary rock) and hard-rock (primarily crystalline rock) stations. In our data base, more than 55 percent of the rock-site recordings for earthquakes of magnitude 6.3 M_w or greater (including several close-in recordings) are from hard-rock sites. Therefore, including hard-rock recordings significantly enhanced the data set of rock recordings, and provided sufficient close-in recordings to allow robust estimates of regression coefficients for the ground-motion parameters analyzed.





QUESTION 2

Provide a justification of the methods used for the selection and adjustment of the data used in the near-source ground motion and empirical ground motion estimates. The justification should demonstrate that the methods used do not bias the ground motion to the low side.

The empirical near-source ground-motion statistical and regression analyses were performed to provide a realistic characterization of site-specific ground motions for a magnitude 7.2 M_w earthquake 4.5 km from the plant site. Ideally, the strong-motion data used for these analyses should be selected from recording sites having tectonic setting and local site conditions similar to those at the plant site. However, in reality, there are only so many strong-motion records available for selection, and not all the recording sites of the selected records have the same tectonic setting and local site conditions as the plant site. We have dealt with this situation in two ways.

First, to achieve robust statistical and regression analyses results, we chose selection criteria that were general enough to include as many records as possible in our data base, but specific enough to require only limited adjustment of the selected records for the effects of tectonic setting and site conditions. These selection criteria specified shallow crustal earthquakes as the seismic sources, and rock or rock-like recording sites. The selection criteria were applied to all available worldwide records. As a result, we established a large empirical ground-motion data base, as described in the Final Report, July 1988, as well as in our response to Question 6, January 1989.

Second, the selected records were evaluated in terms of their compatibility with the site-specific seismic conditions. Our site is located in a plate boundary zone, and does not have significant topographic relief or unusual subsurface geologic conditions, so a few records had to be adjusted. In the case of the Pacoima Dam record of the 1971 San Fernando earthquake, the peak ground acceleration and the response spectral acceleration above 10 Hz were reduced to account for the topographic amplification of the high-frequency components of ground motion. The reductions were based on several published empirical and numerical modeling studies, and documented in the Final Report, as well as in our response to Question 9, January 1989. Fractional weightings were applied to five records (Gazli, Koyna, and Nahanni Sites 1, 2, and 3) obtained from recording sites within plate interiors at large distances from the plate boundaries, as there is evidence that high-frequency ground motions may be enhanced at such locations. Two of these five records, Nahanni Site 1 and Site 2, as well as the Mexicali Valley record, were known to have possible topographic or unusual subsurface geologic effects. Thus, weighting factors were applied to these three records, as described in our response to Question 9, January 1989.

It should be noted that the weightings were based on available information about tectonic setting or local site conditions considered to have caused some effects on the recorded ground motions. Once the weightings were selected, they were applied to the individual records regardless of their ground-motion amplitudes. The adjustments and weightings were applied to the records used in both the statistical and the regression analyses.

In the case of the statistical analysis of near-source ground-motion records, additional criteria for magnitude and distance were used. The magnitude and distance criteria adopted for selecting our original record set were a moment magnitude of 6.3 or greater, and a source-to-site distance of 20 km or less. This resulted in a set of 18 strong-ground-motion records, consisting of 11 records from thrust events and 7 records from strike-slip events. The selected records were scaled to a moment magnitude of 7.2 and a distance of 4.5 km, as described in our response to Question 9, January 1989.

Effects of Magnitude and Distance Selection Criteria

To assess the effects of the selection criteria for magnitude and distance, we have performed sensitivity studies of the near-source statistical analyses using four sets of records that have been expanded by relaxing the selection criteria. In the current sensitivity studies, we expanded the





magnitude range to include earthquakes having magnitudes as low as 6.0 and 6.1, and we extended the source-to-site distance range to include recordings within 25 km and 30 km, respectively. As a result, five sets of recordings (including the original set presented in the Final Report) were used in the analyses. The number of records in each set and their composition are listed in Table Q2-1. A plot showing the magnitude versus distance distribution of the recordings is presented on Figure Q2-1.

The response spectrum for each record (based on the average of the two horizontal components) was scaled from the magnitude and source-to-site distance of that particular record to a magnitude of 7.2 M_w and a source-to-site distance of 4.5 km, and weighted for style of faulting. The relative scaling relationships were described in our response to Question 9, January 1989.

The results of the statistical analyses for each data set, using the adjustments and weighting factors described above, are presented for the entire frequency range on Figure Q2-2 for the 84th-percentile level of ground-motion estimates. The results are summarized in Table Q2-1 for the peak ground acceleration values and for the spectral acceleration values averaged in the frequency bands of 3 to 8.5 Hz and 5 to 14 Hz, at the median and 84th-percentile levels. An examination of the results shows that the differences between the five cases considered are not significant. Specifically, changing the selection criteria resulted in a maximum difference in peak ground acceleration values between any of the five cases at the median level of about 6 percent; at the 84th-percentile level, it is about 9 percent. In the case of spectral acceleration values at 3 to 8.5 Hz, the maximum difference between any of the five cases at the median level is about 4 percent; at the 84th-percentile level, it is about 7 percent. For spectral acceleration values at 5 to 14 Hz, the maximum difference between any of the five cases at the median level is about 18 percent; at the 84th-percentile level, it is about 16 percent.

The results shown on Figure Q2-2 show that the methods used for selecting the data for the near-source empirical ground motions do not bias the ground-motion estimates to the low side in the high frequency range (above about 3 Hz), which is the frequency range of interest. The estimates for the low frequency range tend to be lower; this, however, has no bearing on the selected site-specific response spectrum obtained from the regression analysis. As can be seen from this figure, Case 5 gives the most conservative ground-motion estimate, thus, we selected this case for comparison with the original record set (Case 1), as well as with the site-specific spectrum from the regression analysis.

A plot showing a comparison of the site-specific spectrum developed from the regression analysis, the original record set (Case 1), and the most conservative estimate of the near-source statistics sensitivity set in the 3 to 8.5 Hz range (Case 5) is presented in Figure Q2-3. Comparison of the response spectra, which are shown for the 84th-percentile level, for the original record set and the most conservative case shows that relaxing the magnitude and distance selection criteria results in a small reduction of computed spectral values in the high frequency range, and a slight increase in the low frequency range. It should be emphasized that the site-specific response spectrum adopted for the Long Term Seismic Program is rich throughout the frequency range of interest. It essentially equals or envelops the computed spectral values in different frequency regions from various individual sensitivity analyses.

Effects of Adjustments and Weighting Factors

To evaluate the effects of adjustments and weighting factors on the near-source statistical analyses, we examined each of the 18 records used. Six records had required adjustment or the application of weighting factors, because they did not satisfy one or both of the two selection criteria adopted for this study: compatibility of tectonic setting, and similarity of site conditions. Of these six records, two (Nahanni Sites 1 and 2) were from sites having both differing tectonic setting and site conditions. The remaining four records satisfied one or the other of the two criteria. In the current sensitivity study, a statistical analysis was made by including the above four recordings using no adjustment or weighting, and excluding the two Nahanni recordings that failed both criteria. The results are compared with the original record set spectrum and with the site specific spectrum



Table Q2-1

STATISTICS OF NEAR-SOURCE RECORDS USED IN SENSITIVITY STUDIES
 Scaled to 7.2 M_w and 4.5 km source-to-site distance, and weighted for style of
 faulting: 0.65, strike-slip; 0.30, oblique; and 0.5, thrust

Case No.	Selection Criteria		Number of Records	Earthquake Mechanism		Peak Ground Acceleration		Spectral Acceleration (3 to 8.5 Hz)		Spectral Acceleration (5 to 14 Hz)	
	Minimum Magnitude (M _w)	Maximum Distance (km)		Thrust	Strike-Slip	Median	84th	Median	84th	Median	84th
1	6.3	20	18*	11	7	0.545	0.765	1.189	1.807	1.088	1.685
2	6.1	25	22	14	8	0.532	0.783	1.156	1.828	0.964	1.448
3	6.1	30	29	19	10	0.530	0.777	1.167	1.876	0.924	1.496
4	6.0	25	28	15	13	0.561	0.834	1.202	1.917	0.98	1.519
5	6.0	30	35	30	15	0.553	0.818	1.199	1.935	0.953	1.545
6	Site-Specific Spectrum (from regression analysis)					0.578	0.829	1.299	1.938	1.196	1.756

* Includes five soil-site records from the Imperial Valley modified to rock-site conditions.



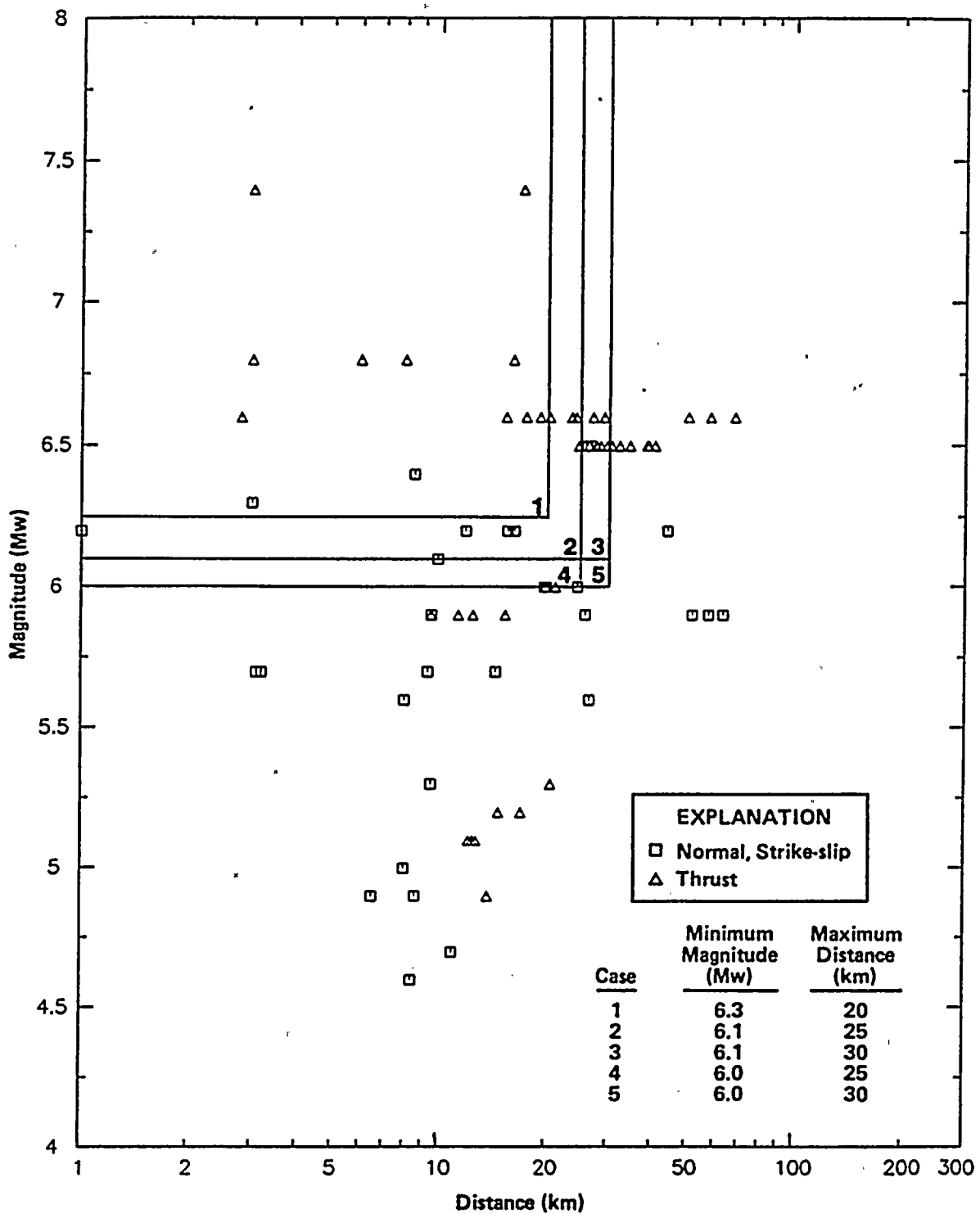


Figure Q2-1

Magnitude versus distance relationships for recordings used in the sensitivity studies.



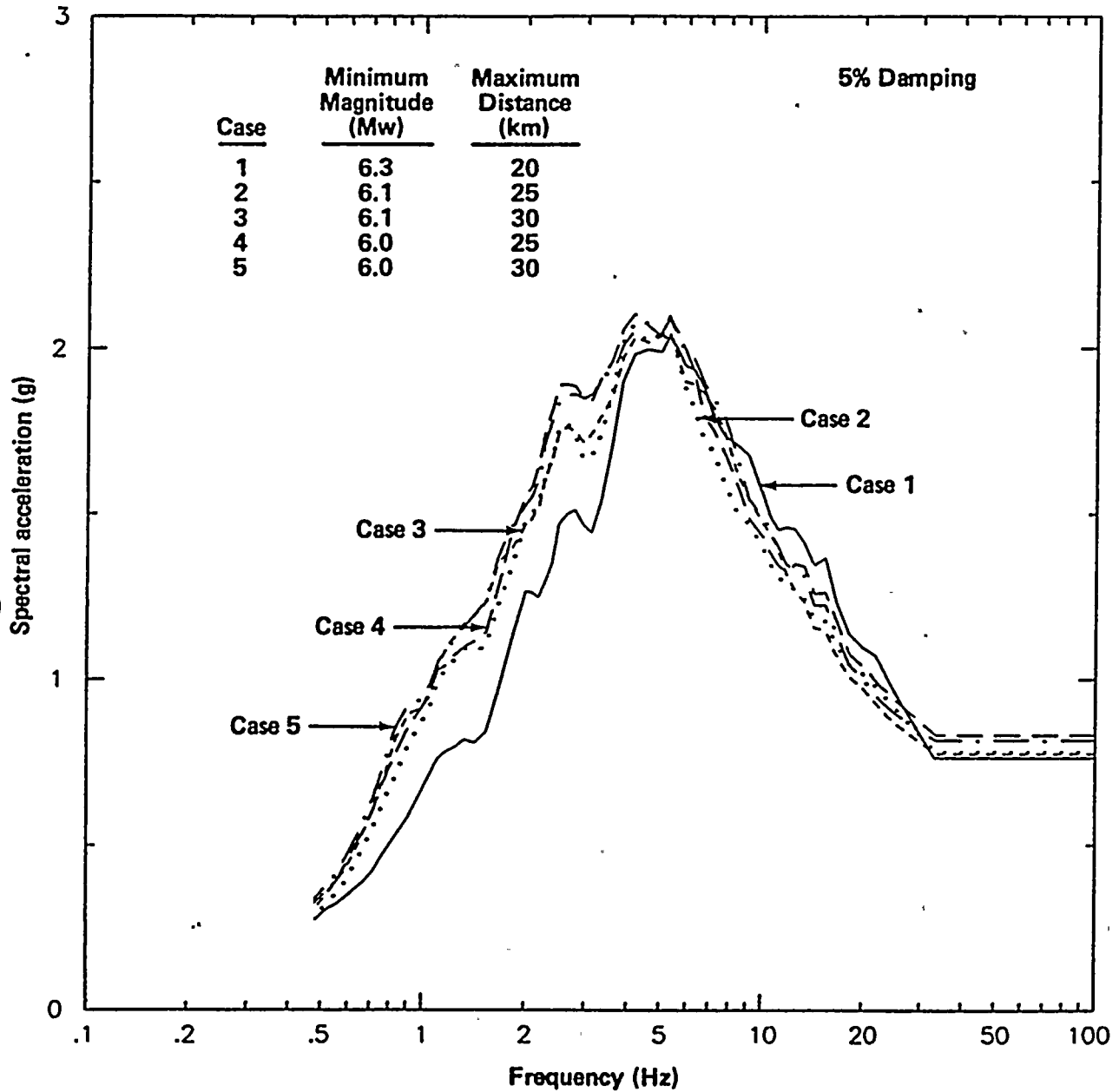


Figure Q2-2

34th-percentile horizontal acceleration response spectra based on statistics of near-source records used in the sensitivity studies for the effects of magnitude and distance selection criteria.



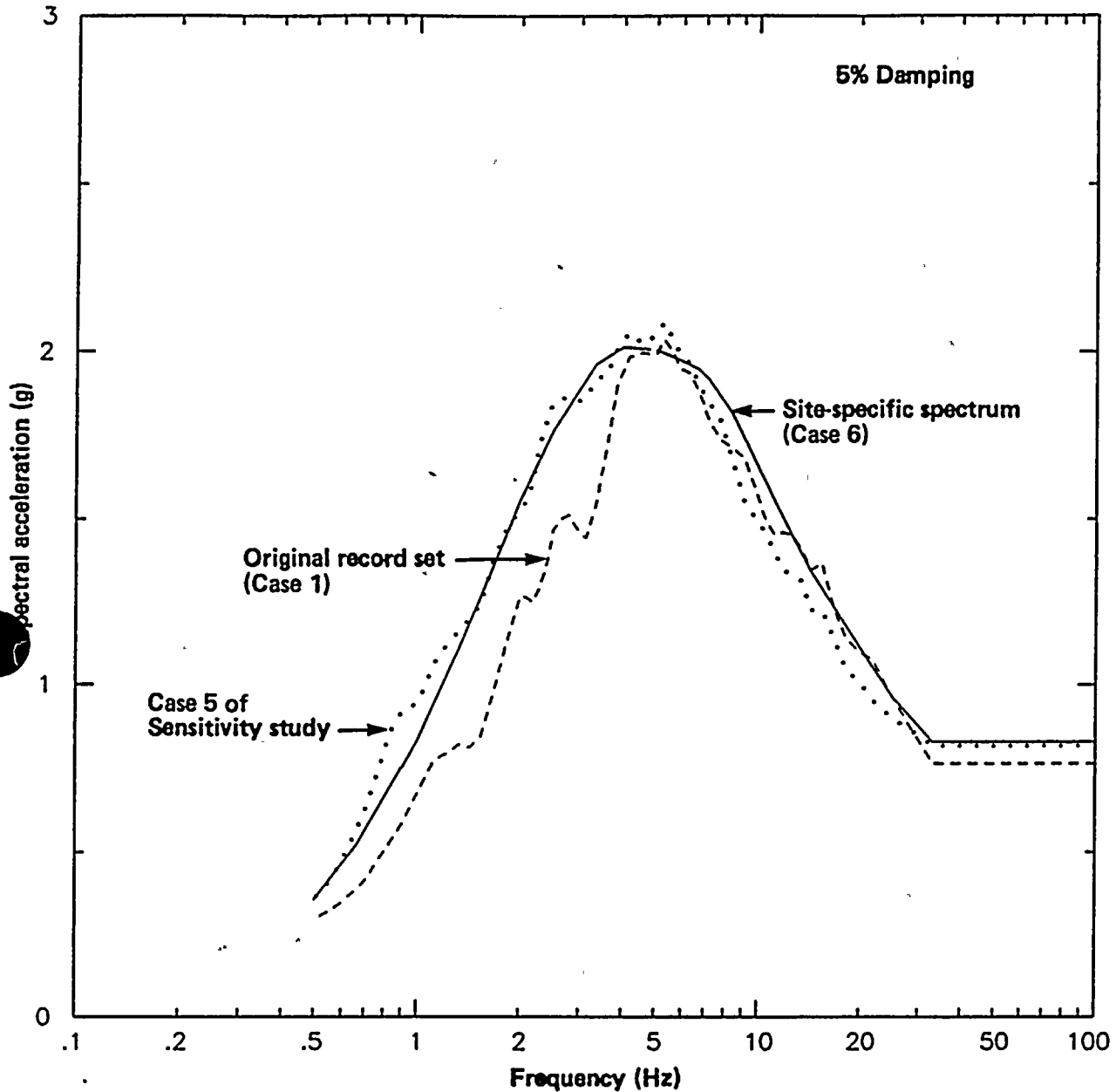
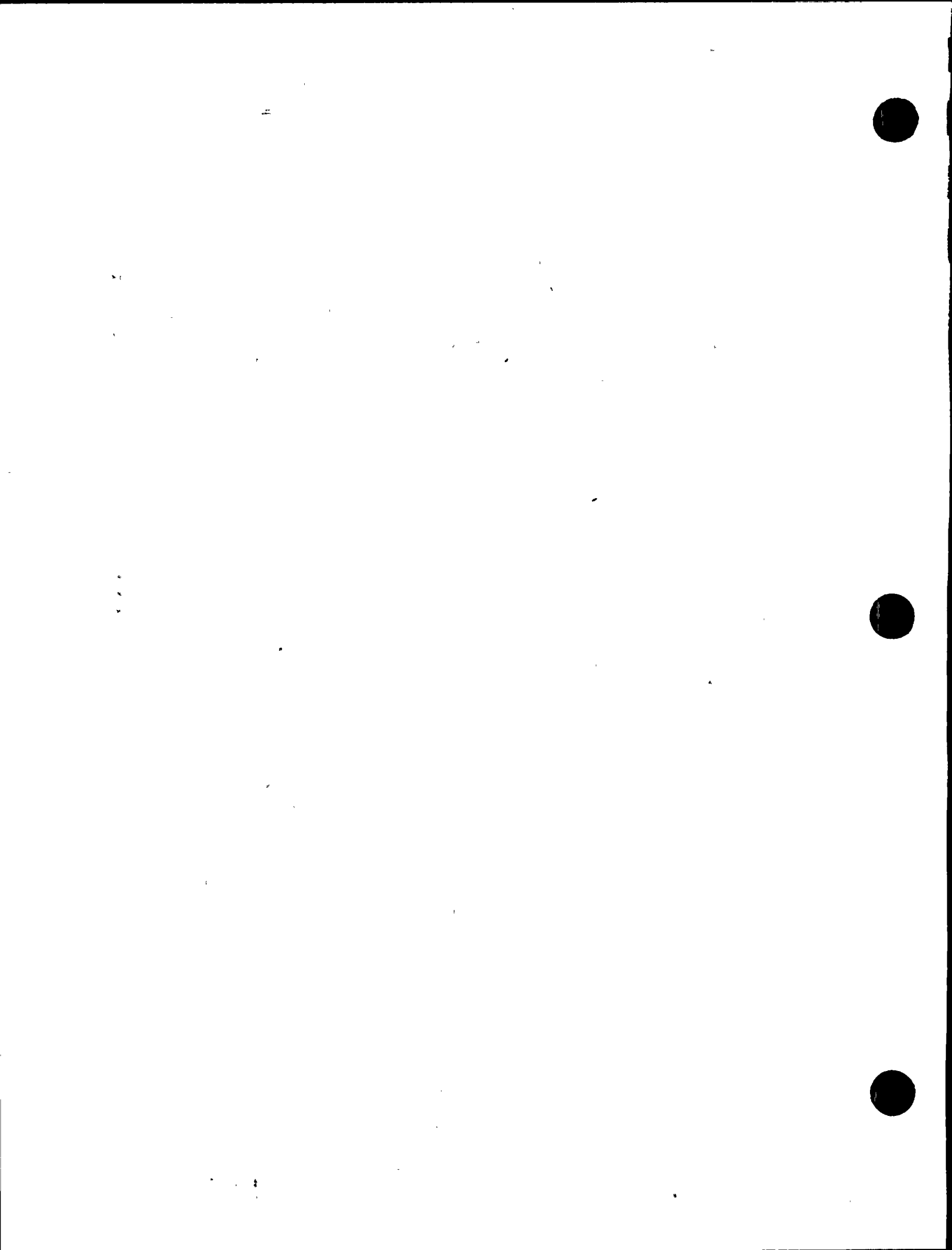


Figure Q2-3

Comparison of the 84th-percentile Long Term Seismic Program site-specific and near-source statistics horizontal response spectra with the spectrum based on statistics of near-source records used in the sensitivity studies for the effects of magnitude and distance selection criteria.



(obtained from the regression analysis) on Figure Q2-4. The results show that eliminating the adjustments or weighting factors did not significantly change the ground-motion estimates. When compared with the site-specific spectrum at the 84th-percentile level, the average spectrum of the 16 unadjusted and unweighted records is within about one percent at the peak ground acceleration level, is lower by about 8 percent in the frequency range of 3 to 8.5 Hz, is lower by about 10 percent in the frequency range of 5 to 14 Hz, and is up to 7 percent higher for frequencies above 15 Hz.

Given the incompatibility of the two Nahanni records with our site conditions, we firmly believe that conducting a statistical analysis on the entire set of unaltered 18 near-source records is inappropriate; however, for this sensitivity evaluation, we have done so. The results are presented in Figure Q2-5, together with the spectrum for the original record set and the spectrum obtained from the unweighted statistics of the 16-record set (excluding the two Nahanni records). When compared with the unweighted statistics of the 16-record set, the 84th-percentile spectrum of the unweighted 18-record set is about 5 percent higher at the peak ground acceleration level, about 2 percent higher in the frequency range of 3 to 8.5 Hz, about 6 percent higher in the frequency range of 5 to 14 Hz, and is higher by about 11 percent in the frequency range of 15 to 25 Hz.

Summary

In summary, our selection criteria, adjustments, and weighting factors were based on a thorough evaluation of the tectonic setting and site conditions at the plant site, and a detailed analysis of the compatibility of the records in our data base. Using appropriate selection criteria, adjustments, and weighting factors to ensure compatibility of data with a specific set of defined conditions is an important part of the scientific method and is commonly practiced. Even though changing our selection criteria, adjustments, and weighting factors do not result in significant changes to our estimates of the site-specific ground motions, we believe that using a carefully selected data base that is compatible with our specific site conditions provides the most appropriate estimate of ground motions.





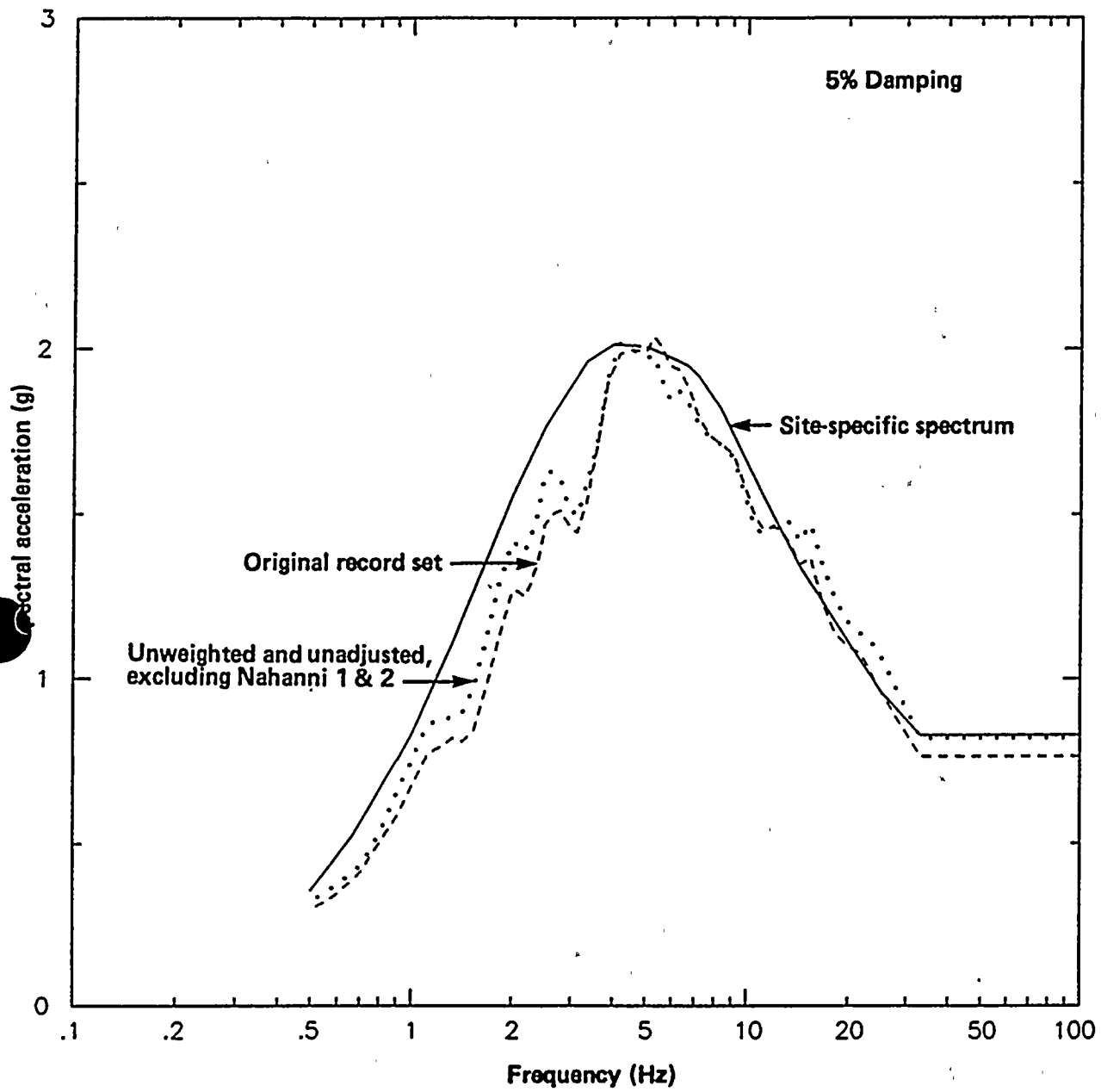


Figure Q2-4

Comparison of the 84th-percentile Long Term Seismic Program site-specific and near-source statistics horizontal response spectra with the spectrum based on statistics of near-source records used in the sensitivity studies for the effects of adjustments and weighting factors.



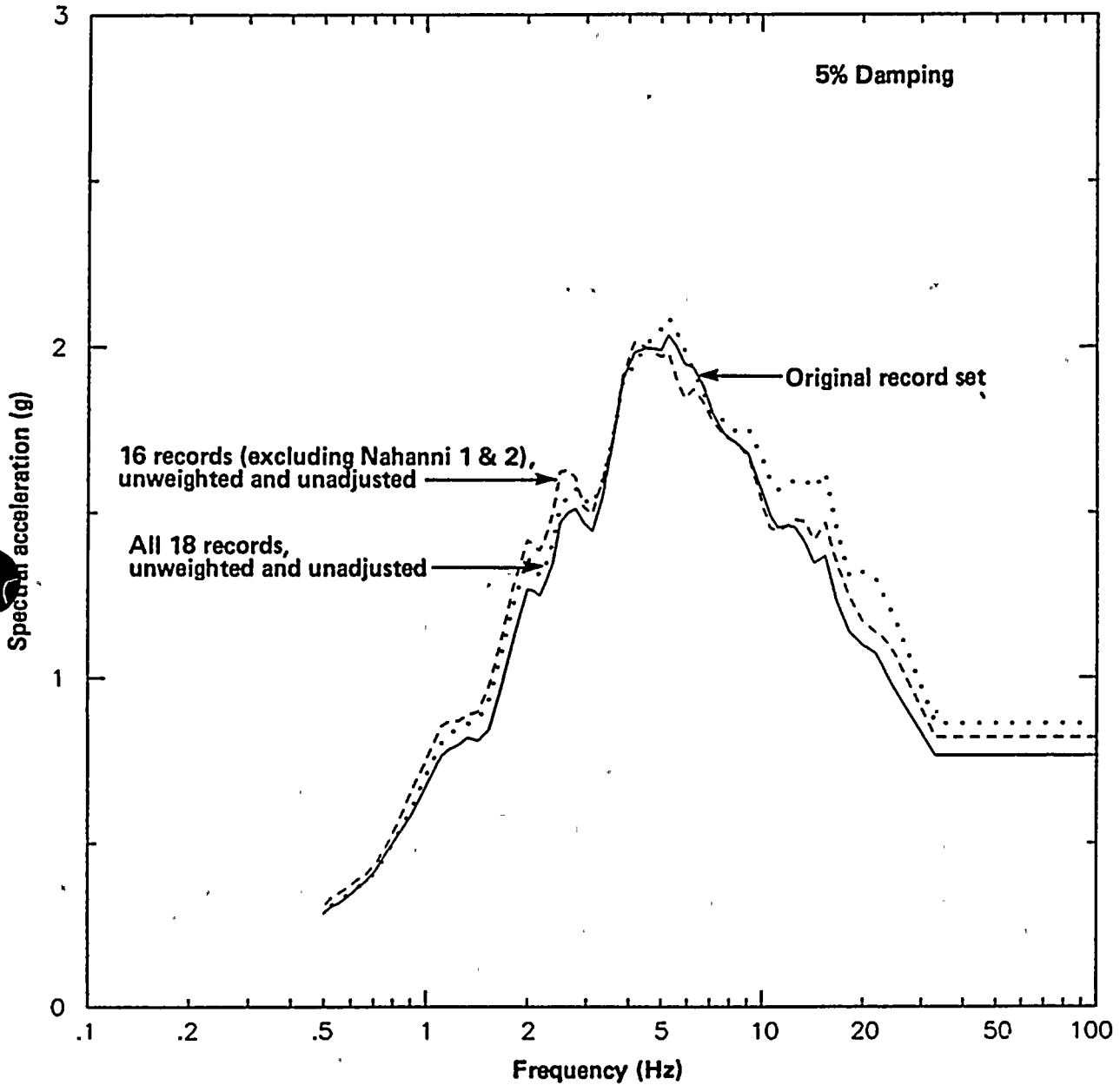


Figure Q2-5

Comparison of the 84th-percentile Long Term Seismic Program near-source statistics horizontal response spectrum with spectra obtained from unadjusted and unweighted records.



**QUESTION 3**

Identify the records which were used in each of the subsets of the empirical data set used for each of the various analyses.

The approach used to develop attenuation relationships for peak ground acceleration and response spectral acceleration at 14 selected periods (in the range of 0.07 to 1.0 second), as well as the analysis results and selected relationships, were presented in our Final Report dated July 31, 1988 and in our response to Question 8, January 1989. A listing of the entire dataset was provided in our response to Question 6, January 1989. The subsets of the empirical data set used for key analyses, including development of attenuation relationships for peak ground acceleration and response spectra, are given below.

As described previously, peak ground acceleration attenuation relationships for rock sites were first developed primarily for thrust faulting. Specifically, two sets of attenuation relationships were developed; one for earthquake magnitudes of $6.5 M_w$ or greater, and another for magnitudes less than $6.5 M_w$. The data base used to develop these two sets of relationships are shown in Table Q3-1 for magnitudes $6.5 M_w$ or greater, and Table Q3-2 for magnitudes less than $6.5 M_w$.

Attenuation relationships for strike-slip faulting were developed by adjusting the relationships for thrust faulting. The adjusted peak ground acceleration attenuation relationships for strike-slip faulting were then compared with the corresponding data for strike-slip earthquakes. The data base used in these comparisons is shown in Table Q3-3.

Attenuation relationships for response spectral acceleration were developed by combining the attenuation relationships for peak acceleration with magnitude-dependent response spectral shape relationships. To develop the spectral shape relationships, the average spectral acceleration data from all the recordings (all magnitudes and all styles of faulting) shown in Table Q3-4 were analyzed.





Table Q3-1

ROCK-SITE STRONG-MOTION RECORDS, REVERSE/THRUST FAULTING
 Data used to develop peak ground acceleration attenuation relationships for
 earthquakes of magnitude 6.5 M_w or greater

Earthquake Name	Date	Rupt Mech	M	Stn #	Dist (km)	Comp	PGA (g)	PGV (cm/s)
Kern County, CA (C)	07/21/52	RV	7.4	136	128.	N51W	0.031	
				136	128.	N39E	0.019	
				136	128.	VERT	0.008	
San Fernando, CA (C)	02/09/71	TH	6.6	279	2.8	S16E	1.170	113.2
				279	2.8	S74W	1.080	57.7
				279	2.8	DOWN	0.710	58.3
				220	15.3	N00E	0.181	12.4
				220	15.3	S90W	0.154	15.0
				220	15.3	DOWN	0.085	5.00
				141	17.4	S00W	0.188	20.5
				141	17.4	S90W	0.180	14.6
				141	17.4	DOWN	0.138	7.40
				266	19.1	S00W	0.096	6.00
				266	19.1	S90W	0.204	11.6
				266	19.1	DOWN	0.093	5.90
				128	20.3	N21E	0.374	14.7
				128	20.3	N69W	0.288	12.8
				128	20.3	DOWN	0.164	4.10
				127	23.5	N21E	0.147	4.80
				127	23.5	N69W	0.131	4.50
				127	23.5	DOWN	0.089	3.00
				126	24.2	S69E	0.200	5.70
				126	24.2	S21W	0.159	8.60
				126	24.2	DOWN	0.170	7.10
				104	27.0	N03E	0.172	5.30
				104	27.0	N87W	0.223	6.70
				104	27.0	DOWN	0.070	4.50
				121	29.1	N56E	0.068	3.80
				121	29.1	N34W	0.103	8.40
				121	29.1	UP	0.034	3.40
				278	50.4	N55E	0.078	4.60
				278	50.4	N35W	0.059	4.40
				278	50.4	DOWN	0.039	2.20
				287	58.1	N15E	0.058	3.10
				287	58.1	N75W	0.081	3.70
287	58.1	DOWN	0.032	1.60				
1027	68.0	S00W	0.026	1.08				
1027	68.0	N90E	0.057	2.13				
1027	68.0	DOWN	0.047	2.07				
111	86.6	S85E	0.021	1.88				
111	86.6	S05W	0.016	1.58				
111	86.6	DOWN	0.010	0.79				
1039	113.	N14E	0.008	1.47				
1039	113.	N76W	0.010	1.21				
1039	113.	DOWN	0.007	1.08				
Gazli, USSR (C)	05/17/76	RV	6.8	9201	3.0	NORT	0.655	44.4
				9201	3.0	EAST	0.699	47.2
				9201	3.0	VERT-	1.413	53.5
Tabas, Iran (C)	09/16/78	TH	7.4	9101	3.0	N16W	0.700	105.0
				9101	3.0	N74E	0.810	91.5
				9101	3.0	VERT	0.739	41.5





Table Q3-1 (continued)

ROCK-SITE STRONG-MOTION RECORDS, REVERSE/THRUST FAULTING
 Data used to develop peak ground acceleration attenuation relationships for
 earthquakes of magnitude 6.5 M_w or greater

Earthquake Name	Date	Rupt Mech	M	Stn #	Dist (km)	Comp	PGA (g)	PGV (cm/s)
-----	-----	-----	---	-----	-----	-----	-----	-----
Tabas, Iran (C)				9102	17.0	N80W	0.379	36.7
(continued)				9102	17.0	N10E	0.391	27.5
				9102	17.0	VERT	0.189	12.2
				9105	148.0	N61W	0.026	4.4
				9105	148.0	N29E	0.024	4.6
				9105	148.0	VERT	0.024	5.5
				9108	172.0	N24E	***	***
				9108	172.0	N66W	0.019	5.1
				9108	172.0	VERT	0.016	3.6
Coalinga, CA; Mainshock (H)	05/02/83	RV	6.5	36177	33.7	N65E	0.179	12.6
				36177	33.7	N25W	0.122	14.6
				36177	33.7	UP	0.069	6.55
				46175	35.0	N45E	0.173	15.7
				46175	35.0	S45E	0.137	15.6
				46175	35.0	UP	0.053	7.22
				36453	39.6	N90E	0.087	6.63
				36453	39.6	N00E	0.079	10.8
				36453	39.6	UP	0.043	5.02
				36176	41.2	S70E	0.139	13.6
				36176	41.2	N20E	0.101	11.7
				36176	41.2	UP	0.056	6.23
				36444	41.3	N90E	0.133	15.9
				36444	41.3	N00E	0.075	16.2
				36444	41.3	UP	0.046	5.92
				36438	43.2	N90E	0.065	8.05
				36438	43.2	N00E	0.074	7.80
				36438	43.2	UP	0.029	3.60
				36422	49.1	N90E	0.089	7.48
				36422	49.1	N00E	0.062	8.12
				36422	49.1	UP	0.033	3.81
				36420	50.2	N90E	0.123	8.17
				36420	50.2	N00E	0.138	11.6
				36420	50.2	UP	0.067	7.63
				36450	52.7	N90E	0.046	6.83
				36450	52.7	N00E	0.044	5.57
				36450	52.7	UP	0.027	3.21
				36230	54.5	N90E	0.039	5.78
				36230	54.5	N00E	0.027	3.65
				36230	54.5	UP	0.017	2.60
Maharni, Canada (C)	12/23/85	TH	6.8	E6097	6.0	N10E	1.101	46.2
				E6097	6.0	N80W	1.345	45.1
				E6097	6.0	VERT	2.367	42.9
				E6098	8.0	N30W	0.390	32.6
				E6098	8.0	S60W	0.545	30.3
				E6098	8.0	VERT	***	***
				E6099	16.0	N00E	0.194	3.43
				E6099	16.0	N90W	0.186	6.29
				E6099	16.0	VERT	0.181	6.09

NOTE:

 (C) Denotes that distance used was closest distance to fault rupture surface
 (H) Denotes that distance used was Hypocentral distance





Table Q3-2

ROCK-SITE STRONG-MOTION RECORDS, REVERSE/THRUST FAULTING
 Data used to develop peak ground acceleration attenuation relationships for
 earthquakes less than magnitude 6.5 M_w

Earthquake Name	Date	Rupt Mech	M	Stn #	Dist (km)	Comp	PGA (g)	PGV (cm/s)
Lytle Creek, CA (H)	09/12/70	RV	5.3	287	19.7	N75W	0.118	
				287	19.7	N15E	0.092	
				287	19.7	VERT	0.030	
				111	20.6	S85E	0.086	5.60
				111	20.6	S05W	0.057	2.00
				111	20.6	DOWN	0.093	2.60
				116	21.9	SOUT	0.164	6.24
				116	21.9	EAST	0.179	3.40
				116	21.9	DOWN	0.094	2.32
				278	32.8	N55E	0.022	0.95
				278	32.8	N34W	0.019	0.88
				278	32.8	DOWN	0.018	0.66
				104	45.9	N03E	0.054	1.70
				104	45.9	N87W	0.020	0.46
				104	45.9	DOWN	0.016	0.43
				266	60.3	SOUT	0.012	
				266	60.3	EAST	0.015	
266	60.3	VERT	0.010					
Santa Barbara, CA (C)	08/13/78	TH	6.0	941	21.0	N53W	0.04	
				941	21.0	N37E	0.04	
				941	21.0	UP	0.03	
				941	21.0	N40W	0.04	
				941	21.0	S50W	0.03	
				941	21.0	UP	0.03	
Coalinga, CA; Aftshck 03 (H)	05/09/83	RV	5.1	65	12.1	N00E	0.177	5.10
				65	12.1	N90W	0.240	7.74
				65	12.1	UP	0.168	3.52
				61	12.4	N00E	0.114	4.99
				61	12.4	N90W	0.152	7.61
				61	12.4	UP	0.128	3.41
				46T06	12.7	N90E	0.353	9.85
				46T06	12.7	N00E	0.302	9.52
46T06	12.7	UP	0.220	3.64				
Coalinga, CA; Aftshck 08 (C)	06/10/83	RV	5.3	46T03	9.7	N90E	0.037	4.33
				46T03	9.7	N00E	0.049	4.99
				46T03	9.7	UP	0.034	3.67
				67	9.8	N00E	0.06	
				67	9.8	S90W	0.06	
				67	9.8	UP	0.04	
Coalinga, CA; Aftshck 10 (H)	07/09/83	TH	5.2	67	10.4	N00E	0.178	9.46
				67	10.4	S90W	0.193	10.3
				67	10.4	UP	0.111	3.10
				65	11.9	N00E	0.098	4.36
				65	11.9	S90W	0.092	3.36
				65	11.9	UP	0.059	1.85
				65	11.9	N00E	0.103	4.26
				65	11.9	S90W	0.094	3.70
				65	11.9	UP	0.076	2.11
				61	12.6	N00E	0.146	5.17
				61	12.6	S90W	0.177	6.93
				61	12.6	UP	0.174	4.01



Table Q3-2 (continued)

ROCK-SITE STRONG-MOTION RECORDS, REVERSE/THRUST FAULTING
 Data used to develop peak ground acceleration attenuation relationships for
 earthquakes less than magnitude 6.5 M_w

Earthquake Name	Date	Rupt Mech	M	Stn #	Dist (km)	Comp	PGA (g)	PGV (cm/s)
-----	-----	-----	---	-----	-----	-----	-----	-----
Coalinga, CA; Aftshck 10 (H)				46T03	17.0	N90E	0.074	2.12
(continued)				46T03	17.0	N00E	0.056	1.94
				46T03	17.0	UP	0.040	1.20
Coalinga, CA; Aftshck 12 (H)	07/21/83	TH	5.9	67	9.5	N00E	0.961	46.8
				67	9.5	N90W	0.838	46.6
				67	9.5	UP	0.426	10.7
				65	11.3	N00E	0.219	16.8
				65	11.3	N90W	0.218	16.9
				65	11.3	UP	0.157	7.33
				65	11.3	N00E	0.194	15.9
				65	11.3	N90W	0.219	16.8
				65	11.3	UP	0.130	6.57
				61	12.4	N00E	0.231	14.9
				61	12.4	N90W	0.375	16.2
				61	12.4	UP	0.247	9.36
				46T03	15.3	N90E	0.116	5.63
				46T03	15.3	N00E	0.136	5.57
				46T03	15.3	UP	0.086	4.28
Coalinga, CA; Aftshck 13 (H)	07/21/83	TH	4.9	67	10.2	N00E	0.30	
				67	10.2	N90W	0.25	
				67	10.2	UP	0.08	
				65	11.8	N00E	0.13	
				65	11.8	N90W	0.14	
				65	11.8	UP	0.04	
				65	11.8	N00E	0.13	
				65	11.8	N90W	0.16	
				65	11.8	UP	0.04	
				61	13.3	N00E	0.09	
				61	13.3	N90W	0.15	
				61	13.3	UP	0.04	
				46T03	13.7	N90E	0.031	1.05
				46T03	13.7	N00E	0.045	1.79
				46T03	13.7	UP	0.032	1.30
Coalinga, CA; Aftshck 14 (H)	07/25/83	TH	5.2	67	10.0	N00E	0.39	
				67	10.0	N90W	0.28	
				67	10.0	UP	0.12	
				65	11.4	N00E	0.10	
				65	11.4	N90W	0.15	
				65	11.4	UP	0.06	
				65	11.4	N00E	0.12	
				65	11.4	N90W	0.18	
				65	11.4	UP	0.06	
				61	12.8	N00E	0.06	
				61	12.8	N90W	0.14	
				61	12.8	UP	0.09	
				46T03	14.7	N90E	0.201	12.4
				46T03	14.7	N00E	0.178	9.82
				46T03	14.7	UP	0.164	5.23
Coalinga, CA; Aftshck 16 (H)	09/09/83	RV	5.3	65	8.2	N00E	0.14	
				65	8.2	N90W	0.09	
				65	8.2	UP	0.09	
				65	8.2	N00E	0.17	
				65	8.2	N90W	0.12	
				65	8.2	UP	0.07	





Table Q3-2 (continued)

ROCK-SITE STRONG-MOTION RECORDS, REVERSE/THRUST FAULTING
 Data used to develop peak ground acceleration attenuation relationships for earthquakes less than magnitude 6.5 M_w

Earthquake Name	Date	Rupt Mech	M	Stn #	Dist (km)	Comp	PGA (g)	PGV (cm/s)
-----	-----	----	---	-----	-----	----	-----	-----
Coalinga, CA; Aftshck 16 (N) (continued)				46T03	18.4	N90E	0.015	0.72
				46T03	18.4	N00E	0.016	0.90
				46T03	18.4	UP	0.014	0.64
Whittier Narrows, CA; Mrschck (C)	10/01/87	TH	6.0	872	18.3	N12W	0.16	
				872	18.3	S78W	0.11	
				872	18.3	UP	0.07	
				24399	21.2	N90E	0.183	4.05
				24399	21.2	N00E	0.130	4.19
				24399	21.2	UP	0.122	2.52
				141	22.9	N00E	0.13	
				141	22.9	S90W	0.15	
				141	22.9	UP	0.06	
				23328	24.1	N27W	0.07	
				23328	24.1	S63W	0.06	
				23328	24.1	UP	0.07	
				23328	24.1	N27W	0.07	
				23328	24.1	S63W	0.07	
				23328	24.1	UP	0.04	
				23328	24.1	N27W	0.07	
				23328	24.1	S63W	0.05	
				23328	24.1	UP	0.04	
				23328	24.1	N27W	0.08	
				23328	24.1	N63E	0.06	
				23328	24.1	UP	0.06	
				23210	24.6	S30E	0.06	
				23210	24.6	N60E	0.08	
				23210	24.6	UP	0.06	
				108	26.8	S50E	0.22	
				108	26.8	N40E	0.16	
				108	26.8	UP	0.07	
				24464	28.0	N90E	0.09	
				24464	28.0	N00E	0.11	
				24464	28.0	UP	0.07	
				698	28.4	N79W	0.09	
				698	28.4	S11W	0.06	
				698	28.4	UP	0.04	
				287	36.3	N90E	0.04	
				287	36.3	N00E	0.04	
				287	36.3	UP	0.05	
				287	36.3	N90E	0.07	
				287	36.3	N00E	0.05	
				287	36.3	UP	0.04	
				710	37.6	S73W	0.04	
				710	37.6	S17E	0.04	
				710	37.6	UP	0.03	
				24088	37.9	N90E	0.16	
				24088	37.9	N00E	0.16	
				24088	37.9	UP	0.06	
				14405	38.2	N90E	0.02	
				14405	38.2	N00E	0.02	
				14405	38.2	UP	0.02	
				14159	41.3	S90W	0.02	
				14159	41.3	S00W	0.02	
				14159	41.3	UP	0.01	





Table Q3-2 (continued)

ROCK-SITE STRONG-MOTION RECORDS, REVERSE/THRUST FAULTING
 Data used to develop peak ground acceleration attenuation relationships for
 earthquakes less than magnitude 6.5 M_w

Earthquake Name	Date	Rupt Mech	M	Stn #	Dist (km)	Comp	PGA (g)	PGV (cm/s)
Whittier Narrows, CA; Mshck(C) (continued)				24207	42.5	S00W	0.02	
				24207	42.5	S90W	0.04	
				24207	42.5	UP	0.02	
				14404	43.8	N90E	0.02	
				14404	43.8	N00E	0.02	
				14404	43.8	UP	0.02	
				24047	52.4	N90E	0.07	
				24047	52.4	N00E	0.05	
				24047	52.4	UP	0.04	
				5235	56.3	S05E	0.05	
				5235	56.3	N85E	0.05	
				5235	56.3	UP	0.04	
				707	59.7	S72W	0.05	
				707	59.7	S18E	0.09	
				707	59.7	UP	0.05	
				13326	60.2	N75E	0.05	
				13326	60.2	N15W	0.07	
				13326	60.2	UP	0.03	
				24469	74.4	N90E	0.03	
				24469	74.4	N00E	0.03	
				24469	74.4	UP	0.03	
				24523	74.3	S67E	0.03	
				24523	74.3	N23E	0.02	
				24523	74.3	UP	0.02	
				24280	75.6	S85W	0.05	
				24280	75.6	S05E	0.04	
				24280	75.6	UP	0.02	
				24082	85.6	N90E	0.05	
				24082	85.6	N00E	0.04	
				24082	85.6	UP	0.02	
				13198	98.6	N90E	0.02	
				13198	98.6	N00E	0.02	
				13198	98.6	UP	0.01	
				24269	98.9	N90E	0.06	
				24269	98.9	N00E	0.04	
				24269	98.9	UP	0.02	
				13199	99.3	N90E	0.03	
				13199	99.3	N00E	0.02	
				13199	99.3	UP	0.03	

NOTE:

(C) Denotes that distance used was closest distance to fault rupture surface

(H) Denotes that distance used was Hypocentral distance





Table Q3-3

ROCK-SITE STRONG-MOTION RECORDS, STRIKE-SLIP AND NORMAL FAULTING
 Peak ground acceleration data used for comparisons with selected
 strike-slip attenuation relationships

Earthquake Name	Date	Rupt Mech	M	Stn #	Dist (km)	Comp	PGA (g)	PGV (cm/s)
Helena, MT; Mainshock (H)	10/31/35	MM	5.6	2229	8.0	N00E	0.141	7.30
				2229	8.0	N90E	0.156	13.30
				2229	8.0	D04N	0.099	9.70
Helena, MT; Aftershock (H)	11/28/35	MM	5.0	2229	8.0	N00E	0.076	3.20
				2229	8.0	N90E	0.088	3.90
				2229	8.0	UP	0.042	1.40
San Francisco, CA (C)	03/22/57	SS	5.3	1117	9.5	N10E	0.105	4.90
				1117	9.5	S80E	0.127	4.60
				1117	9.5	VERT	0.051	1.20
Parkfield, CA (C)	06/27/66	SS	6.1	1438	9.9	N65W	0.282	14.5
				1438	9.9	S25W	0.411	22.5
				1438	9.9	VERT	0.165	4.40
Koyna, India (C)	12/10/67	SS	6.3	9001	3.0	LONG	0.631	32.0
				9001	3.0	TRAN	0.490	19.4
				9001	3.0	VERT	0.341	21.6
Borrego Mountain, CA (C)	04/09/68	SS	6.6	803	113.	S83E	0.019	
				803	113.	S07W	0.013	
				803	113.	VERT	0.006	
				116	150.	S00W	0.009	
				116	150.	N90E	0.011	
				116	150.	VERT	0.007	
				111	156.	S20E	0.007	
				111	156.	N70E	0.007	
				111	156.	VERT	0.003	
				104	197.	N03E	0.003	
				104	197.	N87W	0.004	
				104	197.	VERT	0.001	
				266	207.	TRAN	0.007	
				266	207.	LONG	0.006	
				266	207.	VERT	0.002	
				136	209.	S52E	0.008	2.20
				136	209.	S38W	0.012	3.10
				136	209.	VERT	0.005	1.20
				121	261.	N34W	0.003	
				121	261.	N56E	0.003	
				121	261.	VERT	0.001	
Santa Rosa, CA; Shock A (H)	10/02/69	SS	5.6	1057	80.0	N0RT	0.005	
				1057	80.0	EAST	0.007	
				1057	80.0	VERT	0.002	
Santa Rosa, CA; Shock B (H)	10/02/69	SS	5.7	1057	78.9	N0RT	0.009	
				1057	78.9	EAST	0.008	
				1057	78.9	VERT	0.002	
Hollister, CA (H)	11/28/74	SS	5.2	1202	39.0	N87E	0.030	
				1202	39.0	S03E	0.020	
				1202	39.0	VERT	0.050	



Table Q3-3 (continued)

ROCK-SITE STRONG-MOTION RECORDS, STRIKE-SLIP AND NORMAL FAULTING
 Peak ground acceleration data used for comparisons with selected
 strike-slip attenuation relationships

Earthquake Name	Date	Rupt Mech	M	Stn #	Dist (km)	Comp	PGA (g)	PGV (cm/s)
Oroville, CA; Main shock (C)	08/01/75	NM	5.9	1051	9.5	N53W	0.103	4.80
				1051	9.5	N37E	0.108	4.10
				1051	9.5	UP	0.139	4.90
				1293	35.8	S07E	0.030	
				1293	35.8	N83E	0.040	
				1293	35.8	VERT	0.030	
Oroville, CA; Aftershock A (H)	08/03/75	NM	4.6	1543	8.4	S00E	0.255	2.92
				1543	8.4	N90E	0.140	1.50
				1543	8.4	DOWN	0.106	4.35
Oroville, CA; Aftershock F (H)	08/06/75	NM	4.7	1543	10.9	S00E	0.470	2.90
				1543	10.9	N90E	0.229	4.20
				1543	10.9	DOWN	0.147	1.70
Oroville, CA; Aftershock K (H)	08/08/75	NM	4.9	1543	6.5	S00E	0.274	2.70
				1543	6.5	N90E	0.116	1.90
				1543	6.5	DOWN	0.086	0.90
				1551	8.6	S55E	0.077	1.30
				1551	8.6	N35E	0.109	2.50
				1551	8.6	DOWN	0.066	0.80
Calipatria Swarm, CA (H)	11/04/76	SS	4.9	286	26.4	N45W	0.06	
				286	26.4	S45W	0.03	
				286	26.4	UP	0.02	
Coyote Lake, CA (C)	08/06/79	SS	5.7	1413	3.1	S40E	0.319	25.1
				1413	3.1	N50E	0.422	43.8
				1413	3.1	UP	0.153	16.5
				1445	3.2	N70E	0.250	20.5
				1445	3.2	N20W	0.141	11.5
				1445	3.2	UP	0.105	7.23
				1408	9.3	S40E	0.118	10.3
				1408	9.3	N50E	0.095	3.99
				1408	9.3	UP	0.067	2.56
				1483	59.5	S50E	0.05	
				1483	59.5	N40E	0.08	
				1483	59.5	UP	0.02	
Imperial Valley, CA; Mn shck(C)	10/15/79	SS	6.5	286	26.0	S45E	0.202	9.02
				286	26.0	N45E	0.115	4.86
				286	26.0	UP	0.082	2.10
				6604	26.5	N57E	0.149	14.5
				6604	26.5	N33W	0.167	11.9
				6604	26.5	DOWN	0.198	5.74
				5049	74.8	N45W	0.04	
				5049	74.8	S45W	0.03	
				5049	74.8	UP	0.02	
				5094	119.	S26E	0.02	
				5094	119.	N64E	0.02	
				5094	119.	UP	0.01	
Imperial Valley, CA; Aftshk 31(H)	10/15/79	SS	5.5	286	27.4	S45E	0.031	
				286	27.4	N45E	0.025	
				286	27.4	UP	0.021	

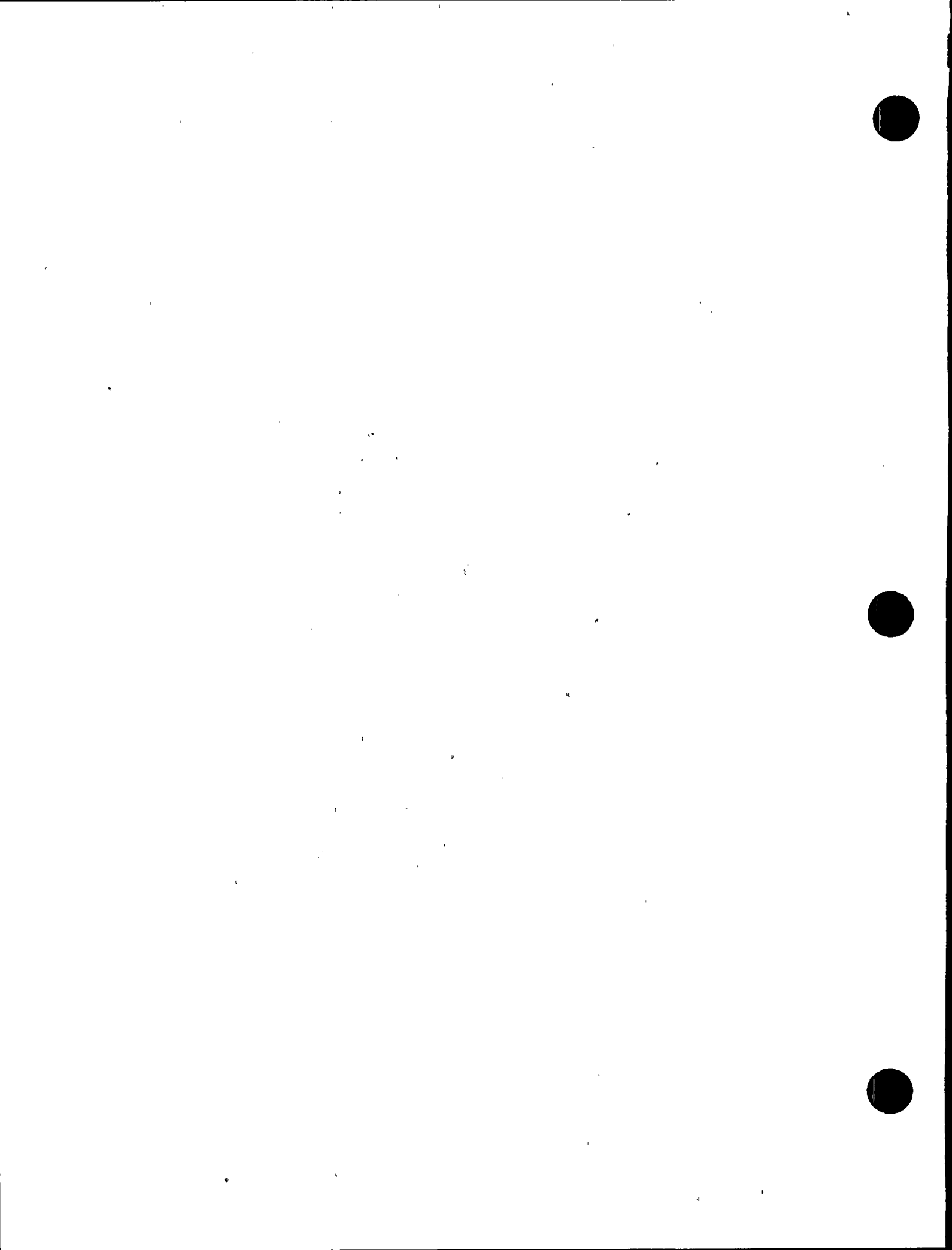


Table Q3-3 (continued)

ROCK-SITE STRONG-MOTION RECORDS, STRIKE-SLIP AND NORMAL FAULTING
 Peak ground acceleration data used for comparisons with selected
 strike-slip attenuation relationships

Earthquake Name	Date	Rupt Mech	M	Stn #	Dist (km)	Comp	PGA (g)	PGV (cm/s)
Livermore, CA; Shock A (H)	01/24/80	SS	5.8	58364	25.2	S00E	0.027	
				58364	25.2	S90E	0.031	
				58364	25.2	UP	0.025	
				58354	31.0	N90E	0.032	
				58354	31.0	N00E	0.043	
				58354	31.0	UP	0.015	
				58219	31.2	S56W	0.077	
				58219	31.2	S34E	0.060	
				58219	31.2	UP	0.023	
				58359	37.1	S00E	0.01	
				58359	37.1	S90W	0.02	
				58359	37.1	UP	0.01	
				58183	48.4	S40E	0.04	
				58183	48.4	N50E	0.03	
				58183	48.4	UP	0.03	
				57180	62.4	S90W	0.02	
				57180	62.4	S00W	0.02	
				57180	62.4	UP	0.01	
				47125	86.4	S48E	0.01	
				47125	86.4	N42E	0.03	
47125	86.4	UP	0.02					
Livermore, CA; Shock B (C)	01/26/80	SS	5.4	57102	8.0	N05W	0.272	
				57102	8.0	S85W	0.189	
				57102	8.0	UP	0.078	
				58354	31.0	N90E	0.032	
				58354	31.0	N00E	0.062	
				58354	31.0	UP	0.021	
				58219	31.2	S56W	0.044	
				58219	31.2	S34E	0.076	
				58219	31.2	UP	0.016	
				58364	33.1	N90E	0.059	
				58364	33.1	S00W	0.054	
				58364	33.1	UP	0.020	
				58359	43.6	S00E	0.01	
				58359	43.6	S90W	0.02	
				58359	43.6	UP	0.01	
				58183	48.4	S38E	0.03	
				58183	48.4	N52E	0.04	
58183	48.4	UP	0.01					
58263	58.9	S37W	0.005					
58263	58.9	S53E	0.005					
58263	58.9	UP	0.005					
Horse Canyon, CA (H)	02/25/80	SS	5.3	5045	5.8	S45E	0.09	
				5045	5.8	N45E	0.12	
				5045	5.8	UP	0.07	
				5044	13.0	S45E	0.13	
				5044	13.0	N45E	0.11	
				5044	13.0	UP	0.06	
				901	36.0	N25W	0.08	
				901	36.0	S65W	0.11	
				901	36.0	UP	0.17	
Hornet Lakes, CA; Shock A (H)	05/25/80	SS	6.2	54214	15.5	N90E	0.079	7.12
				54214	15.5	N00E	0.125	7.12
				54214	15.5	UP	0.112	7.12





Table Q3-3 (continued)

ROCK-SITE STRONG-MOTION RECORDS, STRIKE-SLIP AND NORMAL FAULTING
 Peak ground acceleration data used for comparisons with selected
 strike-slip attenuation relationships

Earthquake Name	Date	Rupt Mech	M	Stn #	Dist (km)	Comp	PGA (g)	PGV (cm/s)
Mammoth Lakes, CA; Shock A (H) (continued)				54214	15.5	N90E	0.068	6.15
				54214	15.5	N00E	0.109	15.8
				54214	15.5	UP	0.081	4.78
				1539	33.1	LONG	0.052	
				1539	33.1	TRAN	0.070	
				1539	33.1	VERT	0.049	
Mammoth Lakes, CA; Shock B (H)	05/25/80	SS	5.7	54214	24.3	N90E	0.01	
				54214	24.3	N00E	0.04	
				54214	24.3	UP	0.02	
Mammoth Lakes, CA; Shock C (H)	05/25/80	SS	6.0	54214	19.7	N90E	0.075	6.25
				54214	19.7	N00E	0.088	6.78
				54214	19.7	UP	0.073	4.05
				54214	19.7	N90E	0.060	5.63
				54214	19.7	N00E	0.112	5.77
				54214	19.7	UP	0.075	4.71
				1539	31.8	LONG	0.073	
				1539	31.8	TRAN	0.064	
				1539	31.8	VERT	0.049	
Mammoth Lakes, CA; Aftshk C01(H)	05/25/80	SS	5.7	54214	14.4	N90E	0.063	3.58
				54214	14.4	N00E	0.099	7.63
				54214	14.4	UP	0.055	2.66
				54214	14.4	N90E	0.043	2.12
				54214	14.4	N00E	0.083	6.86
				54214	14.4	UP	0.069	2.31
Mammoth Lakes, CA; Shock D (H)	05/27/80	SS	6.0	54214	20.0	N90E	0.207	20.8
				54214	20.0	N00E	0.208	12.4
				54214	20.0	UP	0.119	7.35
				54214	20.0	N90E	0.180	17.7
				54214	20.0	N00E	0.219	8.01
				54214	20.0	UP	0.089	5.94
				54424	24.5	S20E	0.119	5.46
				54424	24.5	N70E	0.093	5.85
				54424	24.5	UP	0.087	2.97
				1539	28.7	LONG	0.114	
				1539	28.7	TRAN	0.102	
				1539	28.7	VERT	0.082	
Mexicali Valley, Mexico (C)	06/09/80	SS	6.4	6604	8.5	N45E	0.611	32.5
				6604	8.5	S45E	0.603	23.3
				6604	8.5	DOWN	0.297	12.7
Westmorland, CA (H)	04/26/81	SS	5.6	286	26.5	N45E	0.090	
				286	26.5	S45E	0.110	
				286	26.5	UP	0.060	
Morgan Hill, CA (C)	04/24/84	SS	6.2	57217	0.1	N75W	1.304	79.7
				57217	0.1	S15W	0.707	51.9
				57217	0.1	UP	0.401	15.4
				57383	11.8	N90E	0.293	36.6
				57383	11.8	N00E	0.228	11.3
				57383	11.8	UP	0.426	14.5
				47379	16.2	N40W	0.100	2.66
				47379	16.2	S50W	0.073	2.52
				47379	16.2	UP	0.096	1.61





Table Q3-3 (continued)

ROCK-SITE STRONG-MOTION RECORDS, STRIKE-SLIP AND NORMAL FAULTING
 Peak ground acceleration data used for comparisons with selected
 strike-slip attenuation relationships

Earthquake Name	Date	Rupt Mech	M	Stn #	Dist (km)	Comp	PGA (g)	PGV (cm/s)
Morgan Hill, CA (C) (continued)				57180	25.6	N90E	0.02	
				57180	25.6	N00E	0.02	
				57180	25.6	UP	0.01	
				1032	40.3	N00E	0.026	
				1032	40.3	S90W	0.010	
				1032	40.3	UP	0.026	
				58135	44.1	N50E	0.040	1.85
				58135	44.1	N40W	0.076	3.65
				58135	44.1	UP	0.033	1.18
				1602	46.2	N00E	0.027	
				1602	46.2	S90W	0.016	
				1602	46.2	UP	0.020	
				1601	46.9	N00E	0.031	
				1601	46.9	S90W	0.032	
				1601	46.9	UP	0.022	
				58354	49.8	N35E	0.02	
				58354	49.8	N55W	0.01	
				58354	49.8	UP	0.01	
				58183	52.8	HOR1	0.02	
				58183	52.8	HOR2	***	
				58183	52.8	VERT	0.01	
				58263	53.3	S37W	0.01	
				58263	53.3	N53W	0.01	
				58263	53.3	UP	0.01	
				1160	57.7	S47W	0.03	
				1160	57.7	S43E	0.03	
				1160	57.7	UP	0.02	
				1343	60.5	S40E	0.016	
				1343	60.5	N40E	0.011	
				1343	60.5	UP	0.019	
				58364	73.7	N77E	0.01	
				58364	73.7	S13E	0.01	
				58364	73.7	UP	0.01	
				1483	75.9	N50W	0.021	
				1483	75.9	S40W	0.028	
				1483	75.9	UP	0.010	
				1475	79.1	N50W	0.024	
				1475	79.1	S40W	0.016	
				1475	79.1	UP	0.005	
Bishop, CA (H)	11/23/84	SS	5.8	54424	13.3	S20E	0.24	
				54424	13.3	N70E	0.20	
				54424	13.3	UP	0.20	
				54T04	35.6	S00W	0.04	
				54T04	35.6	N90E	0.02	
				54T04	35.6	UP	0.02	
Hollister, CA (H)	01/26/86	SS	5.5	1032	17.3	N00E	0.04	
				1032	17.3	S90W	0.04	
				1032	17.3	UP	0.04	
				1343	21.0	S50E	0.03	
				1343	21.0	N40E	0.04	
				1343	21.0	UP	0.02	
				1210	28.5	N50W	0.04	
				1210	28.5	S40W	0.04	
				1210	28.5	UP	0.02	





Table Q3-3 (continued)

ROCK-SITE STRONG-MOTION RECORDS, STRIKE-SLIP AND NORMAL FAULTING
 Peak ground acceleration data used for comparisons with selected
 strike-slip attenuation relationships

Earthquake Name	Date	Rupt Mech	M	Stn #	Dist (km)	Comp	PGA (g)	PGV (cm/s)
.....
Hollister, CA (H)				1475	38.1	N50W	0.02	
(continued)				1475	38.1	S40W	0.01	
				1475	38.1	UP	0.01	
North Palm Springs, CA (C)	07/08/86	SS	5.9	12206	25.8	N90E	0.119	3.60
				12206	25.8	N00E	0.145	3.82
				12206	25.8	UP	0.099	2.65
				5044	40.2	S45E	0.067	
				5044	40.2	N45E	0.053	
				5044	40.2	UP	0.058	
				5230	43.8	N00E	0.088	
				5230	43.8	S90W	0.120	
				5230	43.8	UP	0.057	
				5224	45.6	N00E	0.141	
				5224	45.6	S90W	0.100	
				5224	45.6	UP	0.083	
				13200	51.9	N00E	0.079	1.27
				13200	51.9	S90W	0.089	1.27
				13200	51.9	UP	0.043	0.81
				5231	55.4	N00E	0.103	
				5231	55.4	S90W	0.107	
				5231	55.4	UP	0.043	
				13199	57.6	N90E	0.096	1.84
				13199	57.6	N00E	0.072	1.67
				13199	57.6	UP	0.079	1.27
				720	61.4	S02E	0.078	
				720	61.4	N88E	0.083	
				720	61.4	UP	0.037	
				13198	63.3	N90E	0.051	1.30
				13198	63.3	N00E	0.054	1.42
				13198	63.3	UP	0.034	0.84
				13326	73.0	N75E	0.09	
				13326	73.0	N15W	0.07	
				13326	73.0	UP	0.03	
				12330	73.6	N90E	0.03	
				12330	73.6	N00E	0.03	
				12330	73.6	UP	0.03	
				707	73.7	S72W	0.056	
				707	73.7	S18E	0.066	
				707	73.7	UP	0.041	
				287	93.2	N90E	0.010	
				287	93.2	N00E	0.005	
				287	93.2	UP	0.011	
				5033	101.	N60W	0.021	
				5033	101.	S30W	0.026	
				5033	101.	UP	0.010	
				698	106.	N79W	0.017	
				698	106.	S11W	0.022	
				698	106.	UP	0.010	
				710	154.	S15E	0.021	
				710	154.	N75E	0.021	
				710	154.	UP	0.016	
Chalfant Valley, CA (C)	07/21/86	SS	6.0	54424	20.2	S20E	0.170	
				54424	20.2	N70E	0.170	
				54424	20.2	UP	0.140	





Table Q3-3 (continued)

ROCK-SITE STRONG-MOTION RECORDS, STRIKE-SLIP AND NORMAL FAULTING
 Peak ground acceleration data used for comparisons with selected
 strike-slip attenuation relationships

Earthquake Name	Date	Rupt Mech	M	Stn #	Dist (km)	Comp	PGA (g)	PGV (cm/s)
-----	-----	-----	---	-----	-----	-----	-----	-----
Chalfant Valley, CA (C)				54214	29.4	EAST	0.060	
(continued)				54214	29.4	NORT	0.100	
				54214	29.4	UP	0.050	
Whittier Narrows, CA; Aftshk (C)	10/04/87	SS	5.3	872	18.6	N12W	0.08	
				872	18.6	S78W	0.08	
				872	18.6	UP	0.05	
				24399	20.4	N90E	0.16	
				24399	20.4	N00E	0.15	
				24399	20.4	UP	0.09	
				141	22.8	N00E	0.04	
				141	22.8	S90W	0.05	
				141	22.8	UP	0.05	
				23210	25.5	S30E	0.04	
				23210	25.5	N60E	0.04	
				23210	25.5	UP	0.03	
				24464	26.9	N90E	0.04	
				24464	26.9	N00E	0.04	
				24464	26.9	UP	0.02	
				108	32.5	S50E	0.05	
				108	32.5	N40E	0.05	
				108	32.5	UP	0.03	
				108	32.5	S50E	0.07	
				108	32.5	N40E	0.05	
				108	32.5	UP	0.03	
				698	34.2	N79W	0.02	
				698	34.2	S11W	0.03	
				698	34.2	UP	0.01	
				24088	35.8	N90E	0.06	
				24088	35.8	N00E	0.04	
				24088	35.8	UP	0.03	
				24047	50.9	N90E	0.07	
				24047	50.9	N00E	0.07	
				24047	50.9	UP	0.03	
Superstition Hills, CA; Shk A (C)	11/23/87	SS	6.2	286	12.5	S45E	0.13	
				286	12.5	N45E	0.11	
				286	12.5	UP	0.12	
Superstition Hills, CA; Shk B (C)	11/24/87	SS	6.6	286	5.7	S45E	0.91	
				286	5.7	N45E	0.73	
				286	5.7	UP	0.65	
				5045	85.3	S45E	0.02	
				5045	85.3	N45E	0.02	
				5045	85.3	UP	0.01	
				5044	86.2	S45E	0.01	
				5044	86.2	N45E	0.01	
				5044	86.2	UP	0.01	
				13198	135.	N90E	0.01	
				13198	135.	N00E	0.01	
				13198	135.	UP	0.01	

NOTE:

(C) Denotes that distance used was closest distance to fault rupture surface

(H) Denotes that distance used was Hypocentral distance





Table Q3-4

**ROCK-SITE STRONG-MOTION RECORDS, REVERSE/THRUST, STRIKE-SLIP
AND NORMAL FAULTING**

Data used to develop magnitude-dependent spectral shape relationships

Earthquake Name	Date	Rupt Mech	M	Stn #	Dist (km)	Comp	PGA (g)	PGV (cm/s)
San Fernando, CA (C)	02/09/71	TH	6.6	279	2.8	S16E	1.170	113.2
				279	2.8	S74W	1.080	57.7
				279	2.8	DOWN	0.710	58.3
				220	15.3	N00E	0.181	12.4
				220	15.3	S90W	0.154	15.0
				220	15.3	DOWN	0.085	5.00
				141	17.4	S00W	0.188	20.5
				141	17.4	S90W	0.180	14.6
				141	17.4	DOWN	0.138	7.40
				266	19.1	S00W	0.096	6.00
				266	19.1	S90W	0.204	11.6
				266	19.1	DOWN	0.093	5.90
				128	20.3	N21E	0.374	14.7
				128	20.3	N69W	0.288	12.8
				128	20.3	DOWN	0.164	4.10
				127	23.5	N21E	0.147	4.80
				127	23.5	N69W	0.131	4.50
				127	23.5	DOWN	0.089	3.00
				126	24.2	S69E	0.200	5.70
				126	24.2	S21W	0.159	8.60
				126	24.2	DOWN	0.170	7.10
				104	27.0	N03E	0.172	5.30
				104	27.0	N87W	0.223	6.70
				104	27.0	DOWN	0.070	4.50
				121	29.1	N56E	0.068	3.80
				121	29.1	N34W	0.103	8.40
				121	29.1	UP	0.034	3.40
				278	50.4	N55E	0.078	4.60
				278	50.4	N35W	0.059	4.40
				278	50.4	DOWN	0.039	2.20
				287	58.1	N15E	0.058	3.10
				287	58.1	N75W	0.081	3.70
				287	58.1	DOWN	0.032	1.60
				1027	68.0	S00W	0.026	1.08
				1027	68.0	N90E	0.057	2.13
				1027	68.0	DOWN	0.047	2.07
Gazli, USSR (C)	05/17/76	RV	6.8	9201	3.0	NORT	0.655	44.4
				9201	3.0	EAST	0.699	47.2
				9201	3.0	VERT	1.413	53.5
Tabas, Iran (C)	09/16/78	TH	7.4	9101	3.0	N16W	0.700	105.0
				9101	3.0	N74E	0.810	91.5
				9101	3.0	VERT	0.739	41.5
				9102	17.0	N80W	0.379	36.7
				9102	17.0	N10E	0.391	27.5
				9102	17.0	VERT	0.189	12.2
Coalinga, CA; Mainshock (H)	05/02/83	RV	6.5	36177	33.7	N65E	0.179	12.6
				36177	33.7	N25W	0.122	14.6
				36177	33.7	UP	0.069	6.55
				46175	35.0	N45E	0.173	15.7
				46175	35.0	S45E	0.137	15.6
				46175	35.0	UP	0.053	7.22





Table Q3-4 (continued)

**ROCK-SITE STRONG-MOTION RECORDS, REVERSE/THRUST, STRIKE-SLIP
AND NORMAL FAULTING**

Data used to develop magnitude-dependent spectral shape relationships

Earthquake Name	Date	Rupt Mech	M	Stn #	Dist (km)	Comp	PGA (g)	PGV (cm/s)
Coaltinga, CA; Mainshock (H) (continued)				36453	39.6	N90E	0.087	6.63
				36453	39.6	N00E	0.079	10.8
				36453	39.6	UP	0.043	5.02
				36176	41.2	S70E	0.139	13.6
				36176	41.2	N20E	0.101	11.7
				36176	41.2	UP	0.056	6.23
				36444	41.3	N90E	0.133	15.9
				36444	41.3	N00E	0.075	16.2
				36444	41.3	UP	0.046	5.92
				36438	43.2	N90E	0.065	8.05
				36438	43.2	N00E	0.074	7.80
				36438	43.2	UP	0.029	3.60
				36422	49.1	N90E	0.089	7.48
				36422	49.1	N00E	0.062	8.12
				36422	49.1	UP	0.033	3.81
				36420	50.2	N90E	0.123	8.17
				36420	50.2	N00E	0.138	11.6
				36420	50.2	UP	0.067	7.63
				36450	52.7	N90E	0.046	6.83
				36450	52.7	N00E	0.044	5.57
				36450	52.7	UP	0.027	3.21
				36230	54.5	N90E	0.039	5.78
				36230	54.5	N00E	0.027	3.65
				36230	54.5	UP	0.017	2.60
Nahanni, Canada (C)	12/23/85	TH	6.8	E6097	6.0	N10E	1.101	46.2
				E6097	6.0	N80W	1.345	45.1
				E6097	6.0	VERT	2.367	42.9
				E6098	8.0	N30W	0.390	32.6
				E6098	8.0	S60W	0.545	30.3
				E6098	8.0	VERT	***	***
				E6099	16.0	N00E	0.194	3.43
				E6099	16.0	N90W	0.186	6.29
				E6099	16.0	VERT	0.181	6.09
Lytile Creek, CA (H)	09/12/70	RV	5.3	111	20.6	S85E	0.086	5.60
				111	20.6	S05W	0.057	2.00
				111	20.6	DOWN	0.093	2.60
Coaltinga, CA; Aftshck 03 (H)	05/09/83	RV	5.1	65	12.1	N00E	0.177	5.10
				65	12.1	N90W	0.240	7.74
				65	12.1	UP	0.168	3.52
				61	12.4	N00E	0.114	4.99
				61	12.4	N90W	0.152	7.61
				61	12.4	UP	0.128	3.41
				46T06	12.7	N90E	0.353	9.85
				46T06	12.7	N00E	0.302	9.52
				46T06	12.7	UP	0.220	3.64
Coaltinga, CA; Aftshck 10 (H)	07/09/83	TH	5.2	46T03	17.0	N90E	0.074	2.12
				46T03	17.0	N00E	0.056	1.94
				46T03	17.0	UP	0.040	1.20





Table Q3-4 (continued)

**ROCK-SITE STRONG-MOTION RECORDS, REVERSE/THRUST, STRIKE-SLIP
AND NORMAL FAULTING**

Data used to develop magnitude-dependent spectral shape relationships

Earthquake Name	Date	Rupt Mech	M	Stn #	Dist (km)	Comp	PGA (g)	PGV (cm/s)
Coalinga, CA; Aftshck 12 (H)	07/21/83	TH	5.9	67	9.5	N00E	0.961	46.8
				67	9.5	N90W	0.838	46.6
				67	9.5	UP	0.426	10.7
				65	11.3	N00E	0.219	16.8
				65	11.3	N90W	0.218	16.9
				65	11.3	UP	0.157	7.33
				65	11.3	N00E	0.194	15.9
				65	11.3	N90W	0.219	16.8
				65	11.3	UP	0.130	6.57
				61	12.4	N00E	0.231	14.9
				61	12.4	N90W	0.375	16.2
				61	12.4	UP	0.247	9.36
				46T03	15.3	N90E	0.116	5.63
				46T03	15.3	N00E	0.136	5.57
46T03	15.3	UP	0.086	4.28				
Coalinga, CA; Aftshck 13 (H)	07/21/83	TH	4.9	46T03	13.7	N90E	0.031	1.05
				46T03	13.7	N00E	0.045	1.79
				46T03	13.7	UP	0.032	1.30
Coalinga, CA; Aftshck 14 (H)	07/25/83	TH	5.2	46T03	14.7	N90E	0.201	12.4
				46T03	14.7	N00E	0.178	9.82
				46T03	14.7	UP	0.164	5.23
Helena, MT; Mainshock (H)	10/31/35	NM	5.6	2229	8.0	N00E	0.141	7.30
				2229	8.0	N90E	0.156	13.30
				2229	8.0	DOWN	0.099	9.70
Helena, MT; Aftershock (H)	11/28/35	NM	5.0	2229	8.0	N00E	0.076	3.20
				2229	8.0	N90E	0.088	3.90
				2229	8.0	UP	0.042	1.40
San Francisco, CA (C)	03/22/57	SS	5.3	1117	9.5	N10E	0.105	4.90
				1117	9.5	S80E	0.127	4.60
				1117	9.5	VERT	0.051	1.20
Parkfield, CA (C)	06/27/66	SS	6.1	1438	9.9	N65W	0.282	14.5
				1438	9.9	S25W	0.411	22.5
				1438	9.9	VERT	0.165	4.40
Koyna, India (C)	12/10/67	SS	6.3	9001	3.0	LONG	0.631	32.0
				9001	3.0	TRAN	0.490	19.4
				9001	3.0	VERT	0.341	21.6
Oroville, CA; Main shock (C)	08/01/75	NM	5.9	1051	9.5	N53W	0.103	4.80
				1051	9.5	N37E	0.108	4.10
				1051	9.5	UP	0.139	4.90
Oroville, CA; Aftershock A (H)	08/03/75	NM	4.6	1543	8.4	S00E	0.255	2.92
				1543	8.4	N90E	0.140	1.50
				1543	8.4	DOWN	0.106	4.35
Oroville, CA; Aftershock F (H)	08/06/75	NM	4.7	1543	10.9	S00E	0.470	2.90
				1543	10.9	N90E	0.229	4.20
				1543	10.9	DOWN	0.147	1.70





Table Q3-4 (continued)

**ROCK-SITE STRONG-MOTION RECORDS, REVERSE/THRUST, STRIKE-SLIP
AND NORMAL FAULTING**

Data used to develop magnitude-dependent spectral shape relationships

Earthquake Name	Date	Rupt Mech	M	Stn #	Dist (km)	Comp	PGA (g)	PGV (cm/s)
Oroville, CA; Aftershock K (H)	08/08/75	MM	4.9	1543	6.5	S00E	0.274	2.70
				1543	6.5	N90E	0.116	1.90
				1543	6.5	D0LN	0.086	0.90
				1551	8.6	S55E	0.077	1.30
				1551	8.6	N35E	0.109	2.50
				1551	8.6	D0LN	0.066	0.80
Coyote Lake, CA (C)	08/06/79	SS	5.7	1413	3.1	S40E	0.319	25.1
				1413	3.1	N50E	0.422	43.8
				1413	3.1	UP	0.153	16.5
				1445	3.2	N70E	0.250	20.5
				1445	3.2	N20W	0.141	11.5
				1445	3.2	UP	0.105	7.23
				1408	9.3	S40E	0.118	10.3
				1408	9.3	N50E	0.095	3.99
				1408	9.3	UP	0.067	2.56
Imperial Valley, CA; Mn shck (C)	10/15/79	SS	6.5	286	26.0	S45E	0.202	9.02
				286	26.0	N45E	0.115	4.86
				286	26.0	UP	0.082	2.10
				6604	26.5	N57E	0.149	14.5
				6604	26.5	N33W	0.167	11.9
				6604	26.5	D0WN	0.198	5.74
Mammoth Lakes, CA; Shock A (H)	05/25/80	SS	6.2	54214	15.5	N90E	0.079	7.12
				54214	15.5	N00E	0.125	15.1
				54214	15.5	UP	0.112	4.79
				54214	15.5	N90E	0.068	6.15
				54214	15.5	N00E	0.109	15.8
				54214	15.5	UP	0.081	4.78
Mammoth Lakes, CA; Shock C (H)	05/25/80	SS	6.0	54214	19.7	N90E	0.075	6.25
				54214	19.7	N00E	0.088	6.78
				54214	19.7	UP	0.073	4.05
				54214	19.7	N90E	0.060	5.63
				54214	19.7	N00E	0.112	5.77
				54214	19.7	UP	0.075	4.71
Mammoth Lakes, CA; Aftshk C01 (H)	05/25/80	SS	5.7	54214	14.4	N90E	0.063	3.58
				54214	14.4	N00E	0.099	7.63
				54214	14.4	UP	0.055	2.66
				54214	14.4	N90E	0.043	2.12
				54214	14.4	N00E	0.083	6.86
				54214	14.4	UP	0.069	2.31
Mammoth Lakes, CA; Shock D (H)	05/27/80	SS	6.0	54214	20.0	N90E	0.207	20.8
				54214	20.0	N00E	0.208	12.4
				54214	20.0	UP	0.119	7.35
				54214	20.0	N90E	0.180	17.7
				54214	20.0	N00E	0.219	8.01
				54214	20.0	UP	0.089	5.94
				54424	24.5	S20E	0.119	5.46
				54424	24.5	N70E	0.093	5.85
				54424	24.5	UP	0.087	2.97



Table Q3-4 (continued)

**ROCK-SITE STRONG-MOTION RECORDS, REVERSE/THRUST, STRIKE-SLIP
AND NORMAL FAULTING**

Data used to develop magnitude-dependent spectral shape relationships

Earthquake Name	Date	Rupt Mech	M	Stn #	Dist (km)	Comp	PGA (g)	PGV (cm/s)
Mexicali Valley, Mexico (C)	06/09/80	SS	6.4	6604	8.5	N45E	0.611	32.5
				6604	8.5	S45E	0.603	23.3
				6604	8.5	DOWN	0.297	12.7
Westmorland, CA (H)	04/26/81	SS	5.6	286	26.5	N45E	0.090	
				286	26.5	S45E	0.110	
				286	26.5	UP	0.060	
Morgan Hill, CA (C)	04/24/84	SS	6.2	57217	0.1	N75W	1.304	79.7
				57217	0.1	S15W	0.707	51.9
				57217	0.1	UP	0.401	15.4
				57383	11.8	N90E	0.293	36.6
				57383	11.8	N00E	0.228	11.3
				57383	11.8	UP	0.426	14.5
				47379	16.2	N40W	0.100	2.66
				47379	16.2	S50W	0.073	2.52
				47379	16.2	UP	0.096	1.01
				58135	44.1	N50E	0.040	1.85
				58135	44.1	N40W	0.076	3.65
				58135	44.1	UP	0.033	1.18
North Palm Springs, CA (C)	07/08/86	SS	5.9	12206	25.8	N90E	0.119	3.60
				12206	25.8	N00E	0.145	3.82
				12206	25.8	UP	0.099	2.65
				13200	51.9	N00E	0.079	1.27
				13200	51.9	S90W	0.089	1.27
				13200	51.9	UP	0.043	0.81
				13199	57.6	N90E	0.096	1.84
				13199	57.6	N00E	0.072	1.67
				13199	57.6	UP	0.079	1.27
				13198	63.3	N90E	0.051	1.30
				13198	63.3	N00E	0.054	1.42
				13198	63.3	UP	0.034	0.84

NOTE:

(C) Denotes that distance used was closest distance to fault rupture surface

(H) Denotes that distance used was Hypocentral distance





QUESTION 4

The median and 84% spectra resulting from the numerical modeling studies have a dip in amplitude between 5 and 10 Hertz. PG&E stated that this is an artifact of the random number set used in the calculations. Substantiate this by providing spectra generated with a different set of random numbers where this dip does not occur.

The median and 84th-percentile horizontal response spectra presented in the Final Report for the 116 simulated accelerograms are shown in Figure Q4-1. In exploring the cause of the dip in response spectral amplitude at just below 6 Hz, we found that it was less pronounced when a different random number set was used in the simulations, as shown in Figure Q4-2. Random numbers are used to incorporate a stochastic component in an otherwise uniform rupture velocity and slip velocity. Because the dip in amplitude was still present, the effect of other parameters on the response spectral shape was examined. Particular attention was paid to the assumed rise time of 0.2 seconds of the empirical source functions, as the corresponding frequency of 5 Hz is close to the dip in the response spectrum at 6 Hz. We found that varying the rise time does not affect either the amplitude of the dip, or the frequency at which it occurs.

Investigation of the effects of the rise time and other source parameters indicates that the dip in the response spectrum is not due to the parameters of the simulation procedure. Accordingly, we examined the response spectra of the contributions of individual empirical source functions. It was found that both the Imperial Valley and Coalinga empirical source sets contain individual empirical source functions whose response spectral peaks occur more commonly at 4 and 8 Hz than at 6 Hz. This was especially the case for the SH component of the Imperial Valley source functions and the SV component of the Coalinga source functions, whose normalized average spectra over all stations after correction for propagation effects are shown in Figure Q4-3. Both normalized spectra show a dip between 5 and 6 Hz.

The effect that the suite of source functions has on the response spectral shape of an individual simulation depends strongly on the shape of the source functions that are used at asperities, especially those source functions that have large amplitudes. The response spectra of individual simulations are quite variable, as summarized in the response to Question 18, January 1989, and do not always show a dip in the response spectrum. However, averaging the response spectra of many simulations sometimes caused the dip to become prominent, as shown in Figure Q4-1. It appears to be coincidental that the average of both the Imperial Valley and the Coalinga empirical source function sets have a similar bimodal spectral composition, and the dip in the response spectrum is not considered significant.

If the simulation procedure itself were introducing the dip in the response spectrum, it would be present even if the empirical source functions were replaced by source functions having a smooth analytical shape that contained no spectral bumps. We have tested this by using a single source function whose time and frequency domain shapes are both Gaussian. The resulting averaged response spectrum for a suite of 11 bilateral strike-slip simulations is shown in Figure Q4-4. The absence of a dip in this response spectrum, in contrast to the dip shown at the top of Figure Q4-2, indicates that the simulation procedure itself does not introduce a dip in the response spectrum.



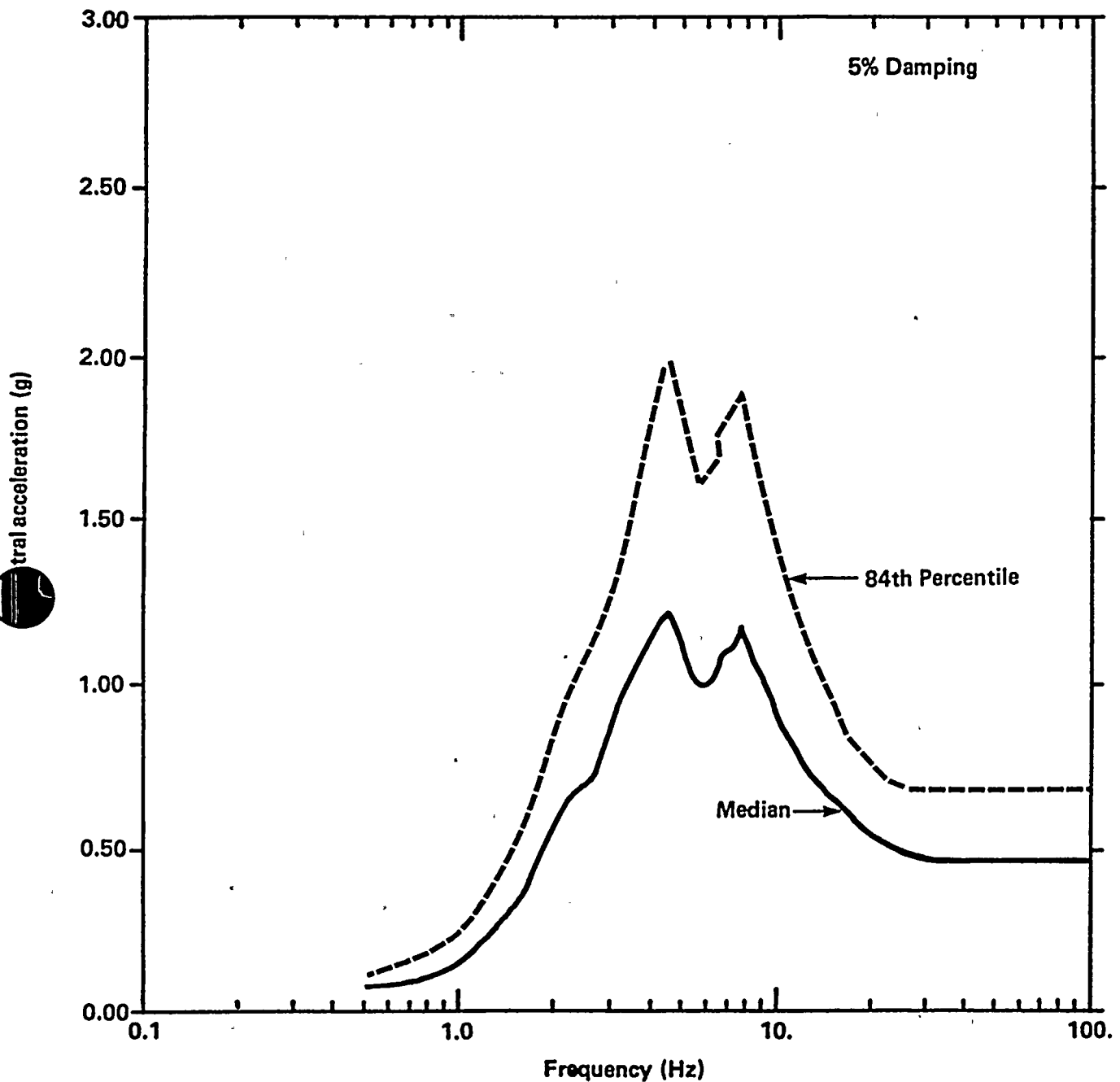


Figure Q4-1

Median and 84th-percentile horizontal acceleration response spectra from a magnitude 7.2 earthquake at 4.5 kilometers, based on numerical modeling studies, and weighted for style of faulting: 0.65, strike-slip; 0.30, oblique; 0.05, thrust.



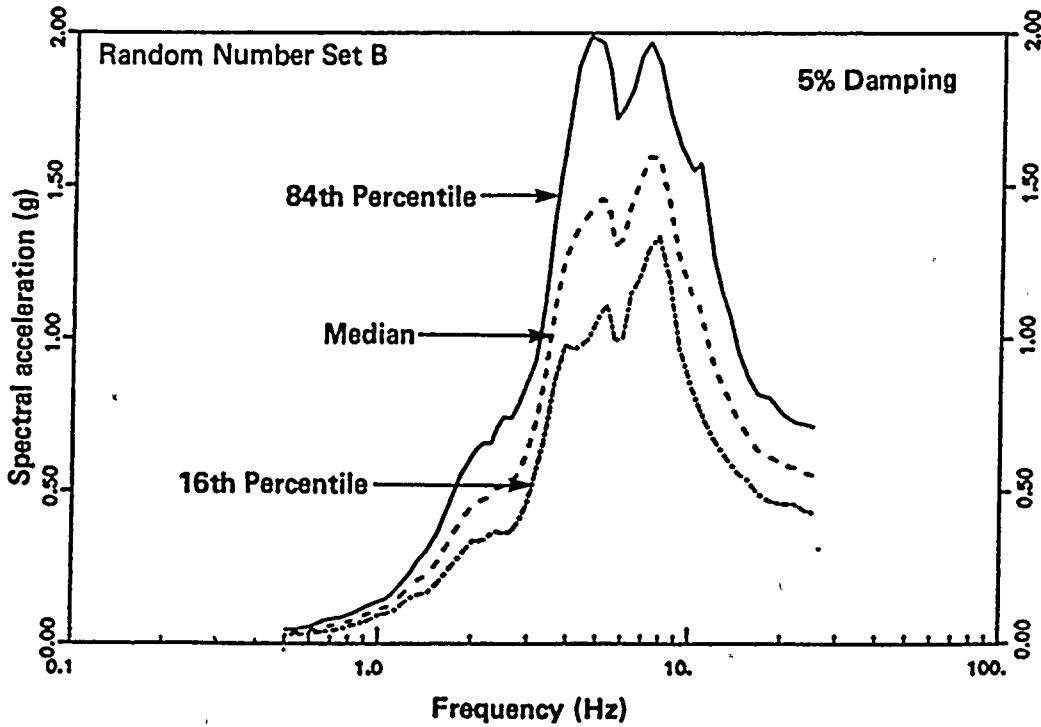
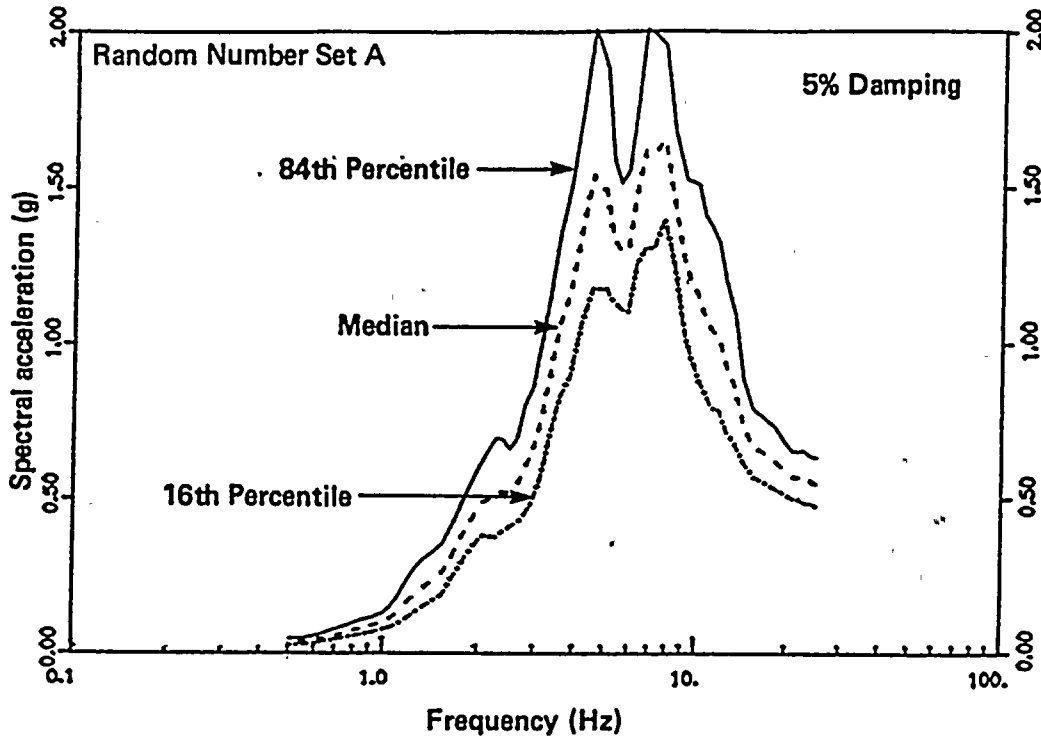


Figure Q4-2

Comparison of averaged response spectra of 11 bilateral strike-slip simulation using different sets of random numbers.



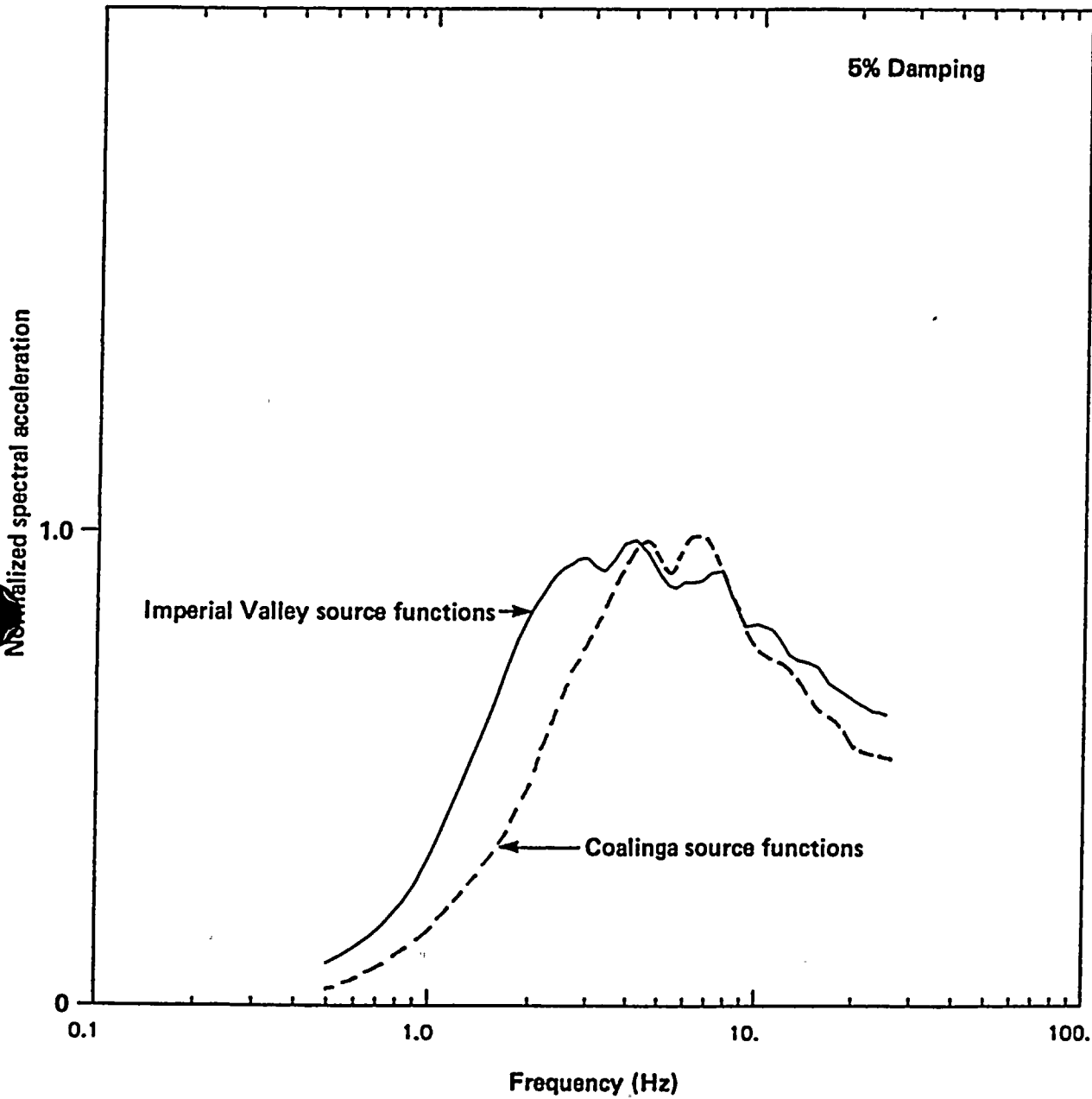


Figure Q4-3

Comparison of average response spectra of the suite of Imperial Valley Source functions (SH component) and the suite of Coalinga source functions (SV component); note that each average spectrum was normalized with respect to its own peak.



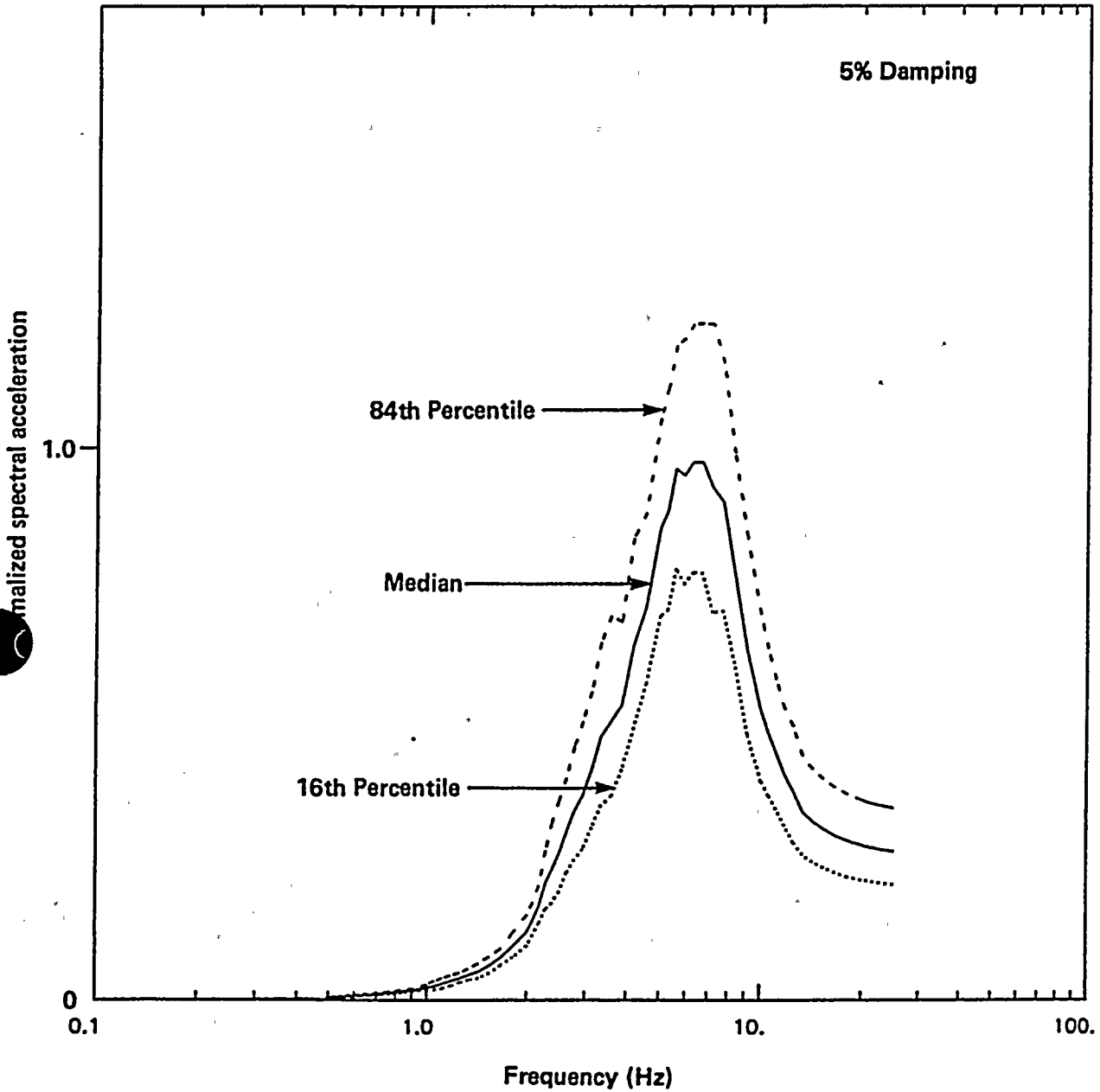


Figure Q4-4

Average response spectra of 11 strike-slip simulations using an analytical source function having a Gaussian Fourier amplitude spectrum. Note that the spectra were normalized with respect to the peak value of the median spectrum.



**QUESTION 5**

How much would the empirical ground motion estimates change if the type of faulting was assumed to be all oblique slip rather than 65% strike slip, 30% oblique slip, and 5% reverse slip?

The assessment of the sense of slip on the Hosgri fault zone, particularly along the reach of the fault proximate to the site, was the focus of extensive study during the Long Term Seismic Program. The conclusion of that study, which is based on a large body of geology, seismology, geophysics, and tectonics data, is that the sense of slip on Hosgri fault zone is strike slip. For the purpose of the characterization of site-specific ground motions, a weighted combination of ground motions for various slip types was used to conservatively allow for variations in interpretation. The weights were strike slip, 0.65; oblique slip, 0.30; and thrust, 0.05.

In response to Question 5, results have been generated for an assumed case in which the weights are strike slip, 0; oblique slip, 1.00; and thrust, 0. The response spectrum for this assumed case is shown on Figure Q5-1. The difference between the response spectrum for this assumed case and the site-specific response spectrum is about 5 percent.





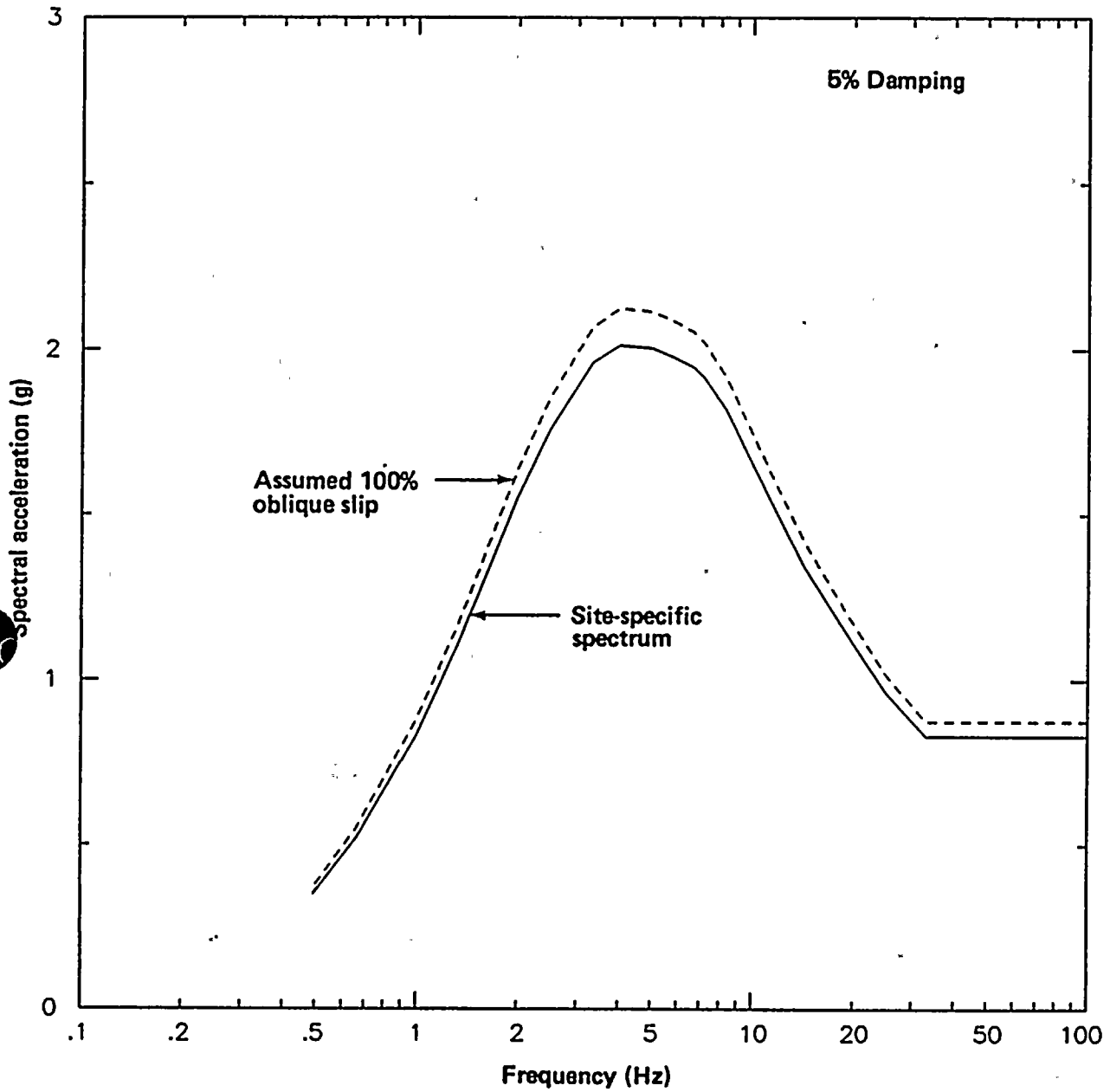


Figure Q5-1

Comparison of site-specific spectrum with assumed 100 percent oblique spectrum, 84th percentile level of ground motions



QUESTION 7

Provide a step-by-step discussion of the uncertainty in the numerical modeling study.

Introduction

In recent years, numerical modeling methods have been developed to simulate recorded strong ground motions and to predict future ground motions. Simulations of recorded ground motions have been used to estimate source parameters and to demonstrate the validity of the numerical methods. Once validated, numerical modeling can be used to predict ground motions due to future earthquakes.

Estimation of source parameters and validation of the numerical model both involve estimation of how well the simulated ground motions match the recorded ground motions. Generally, the goodness of fit has been subjective: the simulated time histories are said to show excellent, good, fair, or poor agreement with the recorded time histories. We have developed a quantitative measure of the goodness of fit for strong motion simulations and have used it to estimate the uncertainty of simulated ground motions.

To use predicted strong ground motions computed by numerical modeling in engineering analyses, an estimate of their uncertainty, analogous to the uncertainty given for empirical attenuation models, is needed. The total uncertainty of the predicted strong ground motion should include all sources of uncertainty: modeling uncertainty (adequacy of the form of the model); random uncertainty (event-to-event and station-to-station variability that is not accounted for in the source or wave propagation models); and parametric uncertainty (uncertainty in the values of source parameters for future earthquakes).

In the following, we quantify the goodness of fit between simulated and recorded ground motions. We also present a general method for estimating the total uncertainty of predicted ground motions for future earthquakes in terms of modeling uncertainty, random uncertainty, and parametric uncertainty. Finally, the application of the method to the Diablo Canyon site is given.

Goodness of Fit of Simulations of Recorded Earthquakes

For simulated time histories that are intended to be used for engineering purposes, a reasonable approach for quantifying the goodness of fit of simulations of recorded earthquakes is to consider the differences in the response spectra of the observed and simulated ground motions. Response spectral values are usually assumed to be log-normally distributed (Joyner and Boore, 1988); therefore, the natural logarithm of spectral acceleration is used to compare the observed and simulated spectra. Specifically, we take the natural logarithm of the spectral acceleration at 5 percent damping on each horizontal component, and then average the log spectral values for the two horizontal components. This average horizontal spectral acceleration, $\ln SA$, for the j^{th} station of the i^{th} earthquake is given by

$$\ln SA_{ij}^o(f) = \ln SA_{ij}^c(f) + \mu(f) + \epsilon_{ij}(f) \quad (1)$$

where f is frequency, superscripts o and c refer to observed and calculated, respectively, $\mu(f)$ is the model bias, and $\epsilon_{ij}(f)$ is the error term. The model bias term, $\mu(f)$, is included in Eq. 1 because a specific numerical simulation model may produce systematically high or low ground motions. The estimated model bias can be used to put limits on the frequency band for which the model is valid. The model bias can also be used to correct the predicted motions. The $\epsilon_{ij}(f)$ are assumed to be normal variates with mean zero and variance $\sigma_\epsilon^2(f)$. The variance of the error term is estimated by

$$\sigma_\epsilon^2(f) = \frac{1}{N-1} \sum_i \sum_j \epsilon_{ij}^2(f) \quad (2)$$





(If the model bias is assumed to be zero, then N-1 should be replaced by N in Eq. 2.)

The bias and variance are frequency dependent. They can be reduced to single values by averaging over a frequency band. For a specific frequency band, $[f_1, f_2]$, the mean spectral acceleration is

$$SA_{ij}(f_1, f_2) = \frac{\sum_k w_k SA_{ij}(f_k)}{\sum_k w_k} \quad (3)$$

where w_k is a weight function to account for possible uneven sampling of the frequency band. (Response spectra are often computed at uneven frequency intervals.) If this type of frequency-averaged spectrum is used, then there is an additional source of variation to consider: peak-to-trough variations about the mean level. The peak-to-trough variance is given by

$$\sigma_{pt}^2(f_1, f_2) = \frac{\sum_i \sum_j \sum_k w_k (SA_{ij}(f_k) - SA_{ij}(f_1, f_2))^2}{\left\{ \sum_i \sum_j \sum_k w_k \right\} - 1} \quad (4)$$

Uncertainty of Numerical Predictions

The total uncertainty in the response spectrum derived from numerical modeling has three parts: modeling, random, and parametric. The modeling uncertainty represents differences between the actual physical process that generates the strong ground motion and the simulation of those processes in the numerical procedure. Random uncertainty represents detailed aspects of the earthquake source and wave propagation that cannot be modeled deterministically using our current level of knowledge. The parametric uncertainty represents uncertainty in the values of source parameters for future earthquakes.

For a given prediction application, the parametric uncertainty is estimated from the suite of ground motions produced by probabilistically varying the free source-parameter values; the free source parameters are those that were determined externally for each event used in the validation procedure. These include asperity location, for example. The separation of the source parameters into those contributing to modeling uncertainty and those contributing to parametric uncertainty is not absolute; it depends on the modeling procedure used in the validation process and the subsequent prediction process. Free source parameters belong under parametric uncertainty, whereas fixed source parameters belong under modeling uncertainty. For example, if the rupture velocity is estimated independently for each event in the validation process (for example, by inversion of strong-motion records), then the rupture velocity uncertainty is part of the parametric uncertainty. On the other hand, if a single value or rule is used to estimate the rupture velocity V_r (for example, $V_r = 0.8\beta$ where β is the shear wave velocity) for all the events, then rupture velocity uncertainty is already included as part of the modeling uncertainty. Selection of the magnitude, site-to-source distance, and focal mechanism of future earthquakes is considered part of the seismic source characterization. This is consistent with the current use of empirical attenuation relations. Therefore, the uncertainties in these three source-parameter values are not included in this analysis; they can be considered by conventional seismic hazard analysis using event and/or logic trees.

In nature, earthquake source parameters cannot be controlled, and we cannot obtain repetitions of the same earthquake. As a result, the modeling and random uncertainties cannot be estimated separately; we can only estimate the combined effect of modeling and random uncertainty. The combined modeling plus random variance, σ_{mr}^2 , is estimated from the simulations of recorded earthquakes:

$$\sigma_{mr}^2(f) = \sigma_e^2(f) \quad (5)$$



For prediction, the parametric uncertainty is estimated from the suite of ground motions produced by varying selected model parameter values. That is

$$\sigma_p^2(f) = \frac{\sum_{n=1}^M \sum_{a=1}^{N_n} (\ln SA_{na}(f) - \overline{\ln SA}(f))^2}{\left\{ \sum_{n=1}^M N_n \right\} - 1} \quad (6)$$

where M is the number of free source parameters to be varied, N_m is the number of different values of the m^{th} parameter, and $\overline{\ln SA}(f)$ is the mean predicted log spectral acceleration.

The overall estimate of the uncertainty of the predicted response spectrum derived from numerical modeling is obtained by combining the modeling plus random uncertainty, σ_{mr}^2 , with the parametric uncertainty, σ_p^2 . The total variance, σ_T^2 , is approximated by

$$\sigma_T^2(f) = \sigma_{mr}^2(f) + \sigma_p^2(f), \quad (7)$$

where the modeling and random variations are assumed to be uncorrelated with the parametric variations.

Application of the Method at the Diablo Canyon Site

In this application of the method, we consider the numerical modeling procedure used by Wald and others (1988a), described in the response to Question 12, January 1989. Their model is a semi-empirical method that uses theoretical Greens functions and empirical source functions. The source parameters that are required for this model have been separated into those contributing to modeling uncertainty and those contributing to parametric uncertainty in Table Q7-1. A brief description of the method used to estimate each source parameter to justify its placement in either the modeling or parametric uncertainty column is given in Table Q7-2.

Table Q7-1

CLASSIFICATION OF SOURCE PARAMETERS INTO MODELING AND PARAMETRIC UNCERTAINTY TERMS FOR THE WALD AND OTHERS (1988) NUMERICAL MODELING METHOD

Modeling Uncertainty Terms

- Average Rupture Velocity
- Variation in Rupture Velocity and Slip Velocity
- Source Functions
- Rise Time
- Fault Element Size
- Slip Distribution (detailed features)

Parametric Uncertainty Terms

- Rupture Location
- Rupture Mode
- Slip Distribution (gross features)

The slip distribution could not be exclusively associated with either modeling uncertainty or parametric uncertainty; therefore, the slip distribution is included in both columns in Table Q7-1.



Table Q7-2

**METHODS USED TO ESTIMATE THE SOURCE PARAMETERS
FOR THE VALIDATION PROCEDURE**

Modeling Uncertainty Parameters

Average rupture velocity:	A single rule for average rupture (0.8β) is used for all events.
Variation in rupture velocity and slip velocity:	The same degree of randomness is used in both rupture velocity and slip velocity for all events. The degree of randomness is such that the probability of slip initiating outside the time window of smooth rupture propagation across a fault element, or outside the time window of smooth slip on a subevent is 0.05.
Source functions:	A single set of source functions computed from the magnitude 5.0 aftershock of the 1979 Imperial Valley earthquake is used for all events.
Rise time:	The Geller (1976) relation is used for all events. (See response to Question 12, January 1989.)
Fault element size:	A constant element size of 4 km x 3 km is used for all events.
Slip distribution (detailed features):	Detailed aspects of the slip distribution beyond the 4 x 3 km fault discretization are not modeled in any of the events.

Parametric Uncertainty Parameters

Rupture location:	The location of the rupture surface is identified from the modeling of strong motion velocity recordings by other investigators and from the aftershock distribution.
Rupture mode:	Unilateral or bilateral rupture is determined for each event by the location of the hypocenter with respect to the rupture surface.
Slip distribution (gross features):	The gross features of the slip distribution for each event are based on inversion of strong-motion or teleseismic velocity data, or on the inverse correlation between slip and aftershock locations (Mendoza and Hartzell, 1988).



For recorded events that have been simulated, the gross features of the slip distribution are considered to be known based on waveform inversion or aftershock locations. For future earthquakes, the gross slip distribution is unknown and will be varied, so the gross slip distribution belongs under parametric uncertainty. On the other hand, detailed features of the slip distribution beyond the 4 km x 3 km discretization cannot be modeled for either recorded earthquakes or future earthquakes. Differences between the slip distribution used in the validation process and the actual slip distribution will manifest themselves as modeling uncertainty. Thus, the detailed slip distribution belongs under modeling plus random uncertainty.

There were no free source parameters involved in the validation of the Wald and others (1988a) modeling procedure. That is, the model parameter values were not varied to find the best fit using the goodness-of-fit criterion; instead, a single model and single set of preselected parameter values or rules were used. The comparison between the observed and calculated ground motions was only used to estimate the modeling plus random uncertainty, not to select between competing models. For the simulations of recorded earthquakes, reasonable assumptions were made about the values of the parameters on the left side of Table Q7-1, whereas the values of the parameters on the right side of Table Q7-1 were constrained by data. For the predictions, the former remain fixed as part of the model, whereas the latter, being unknown for future earthquakes, are varied probabilistically.

At Diablo Canyon, the selected seismic source is a moment magnitude 7.2 earthquake at a distance of 4.5 km. Three focal mechanisms were considered: strike-slip, oblique, and thrust. In the Final Report, these three mechanisms were assigned probabilities of 0.65, 0.30, and 0.05, respectively.

Both the uncertainty in the spectral acceleration at individual frequencies and the uncertainty in the average response over a frequency band are considered. For Diablo Canyon, the frequency band of main interest is 3.0 to 8.5 Hz. For convenience, the spectrum averaged over this frequency band is called the "frequency-averaged spectrum" in the following discussion.

Estimation of Modeling Plus Random Uncertainty. Multiple recordings of three events were used to estimate the modeling plus random uncertainty, σ_{mr}^2 . These include the 1979 Imperial Valley event (six stations) (Wald and others, 1988a), the 1985 Nahanni event (three stations) in response to Question 13f, January 1989, and the 1987 Whittier Narrows event (nine stations) (Wald and others, 1988b). The 18 stations used in the validation are listed in Table Q7-3. The individual residuals from all 18 stations are shown in Figure Q7-1. The model bias and the 90-percent confidence interval of the bias are shown in Figure Q7-2, which indicates that the bias for this particular numerical model is not significantly different from zero at frequencies higher than 3 Hz. The modeling plus random standard error, $\sigma_{mr}(f)$, is shown in Figure Q7-3. The standard error is shown corrected and not corrected for model bias; the difference is small. (For the "not corrected for model bias" case, we assume that $\mu(f) = 0$ in Eq. 1.)

The observed and simulated peak acceleration and frequency-averaged spectral values for the 18 records are listed in Table Q7-4. The model bias is 0.003 and -0.128, and the standard error is 0.31 and 0.34 (0.35 if not corrected for model bias) for the peak acceleration and frequency-averaged spectral values, respectively. The bias and standard error is given separately for each event in Table Q7-5. Of these three events, the Nahanni event has by far the largest uncertainty, although its bias is similar to that of the other two events. The standard error of the peak-to-trough variation, $\sigma_{PT}(3,8.5)$, is 0.14.

The variation in the bias estimates for the individual earthquakes indicates the event-to-event (inter-event) variability, whereas the variation in the individual residuals indicates the station-to-station (intra-event) variability. The inter-event standard error is 0.04, which is much smaller than the intra-event standard error of 0.34. Although only a small sample of earthquakes was used in the validation to estimate the bias, the large difference between the inter-event and intra-event standard errors suggests that the inter-event variation is not significant.

As shown in Table Q7-5, all three events yield a negative model bias for the frequency-averaged spectrum. The negative model bias indicates that the simulation procedure is overpredicting the



Table Q7-3

STRONG MOTION DATA USED IN THE VALIDATION STUDY

<u>Event</u>	<u>Station</u>
1979 Imperial Valley	EC Sta 4 EC Sta 5 EC Sta 6 EC Sta 7 EC Sta 8 EC Sta 10
1985 Nahanni	Site 1 Site 2 Site 3
1987 Whittier Narrows	Cal State LA Whittier Alhambra Downey Garvey Obregon Park Whittier Dam San Marino Bulk Mail



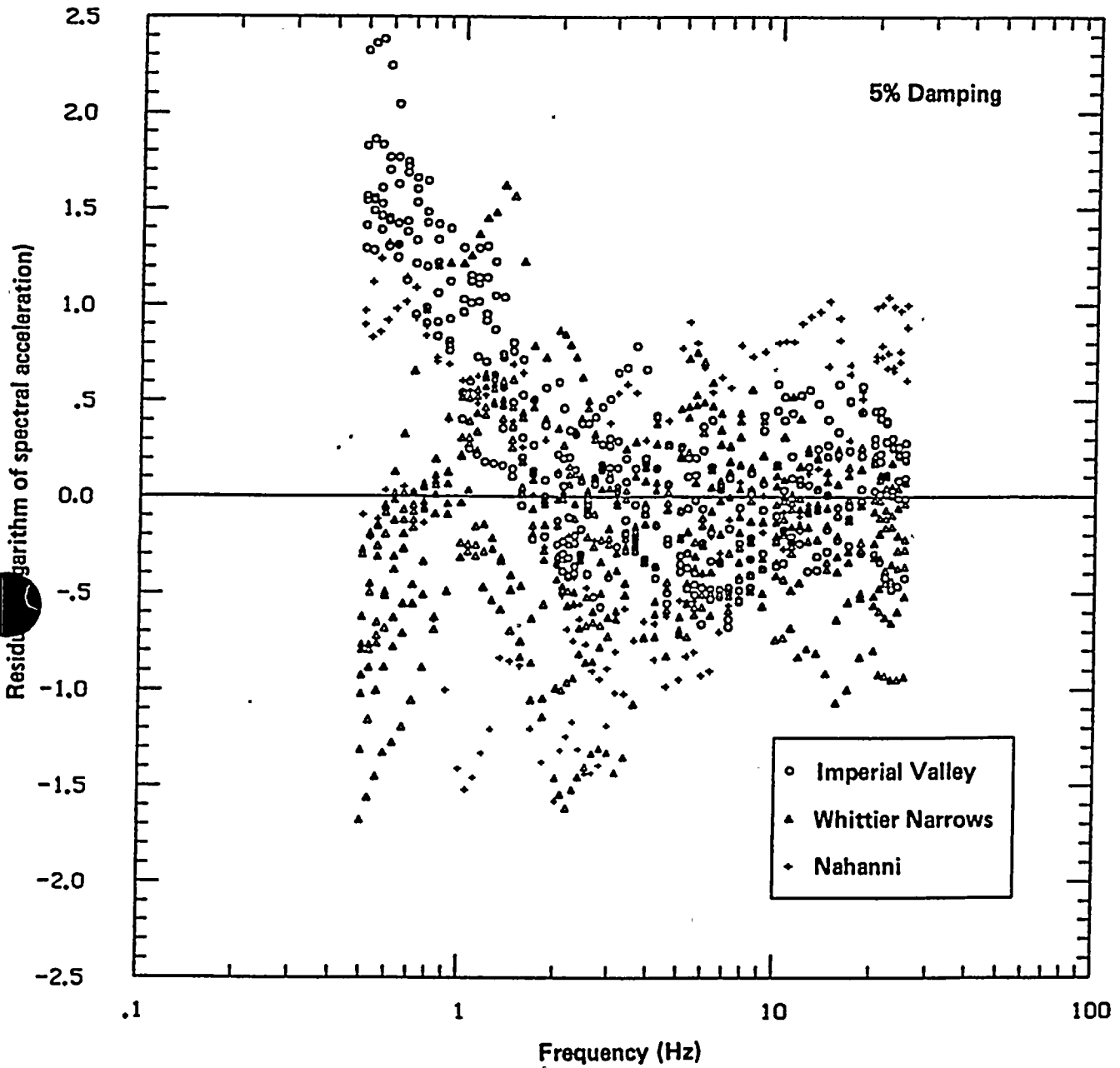


Figure Q7-1

Residuals of the natural logarithm of spectral acceleration at 5 percent damping for the three events used in the validation study.



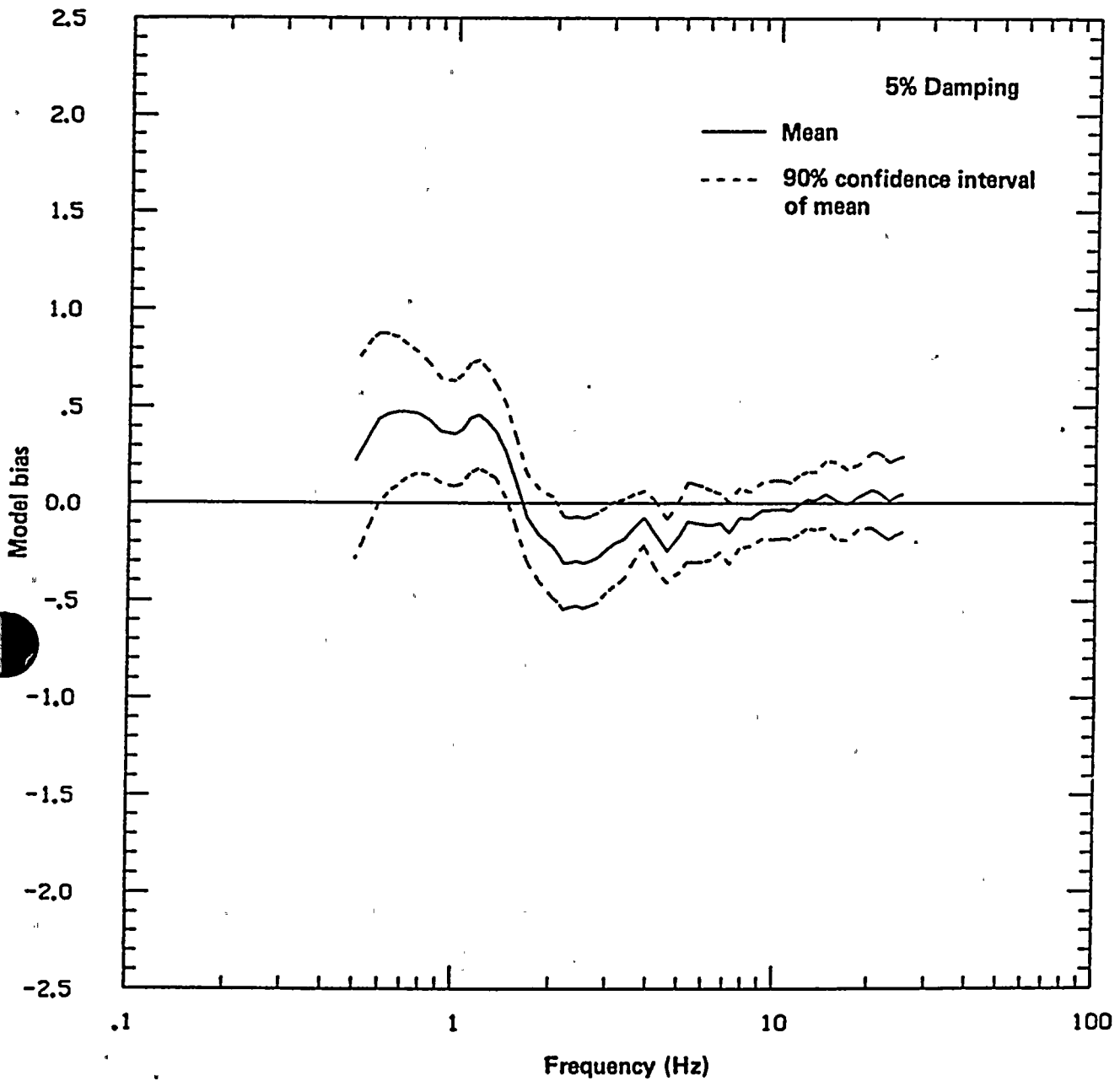


Figure Q7-2

Model bias of the natural logarithm of spectral acceleration. A positive bias indicates the model underpredicts the spectrum, whereas a negative bias indicates the model over predicts the spectrum.



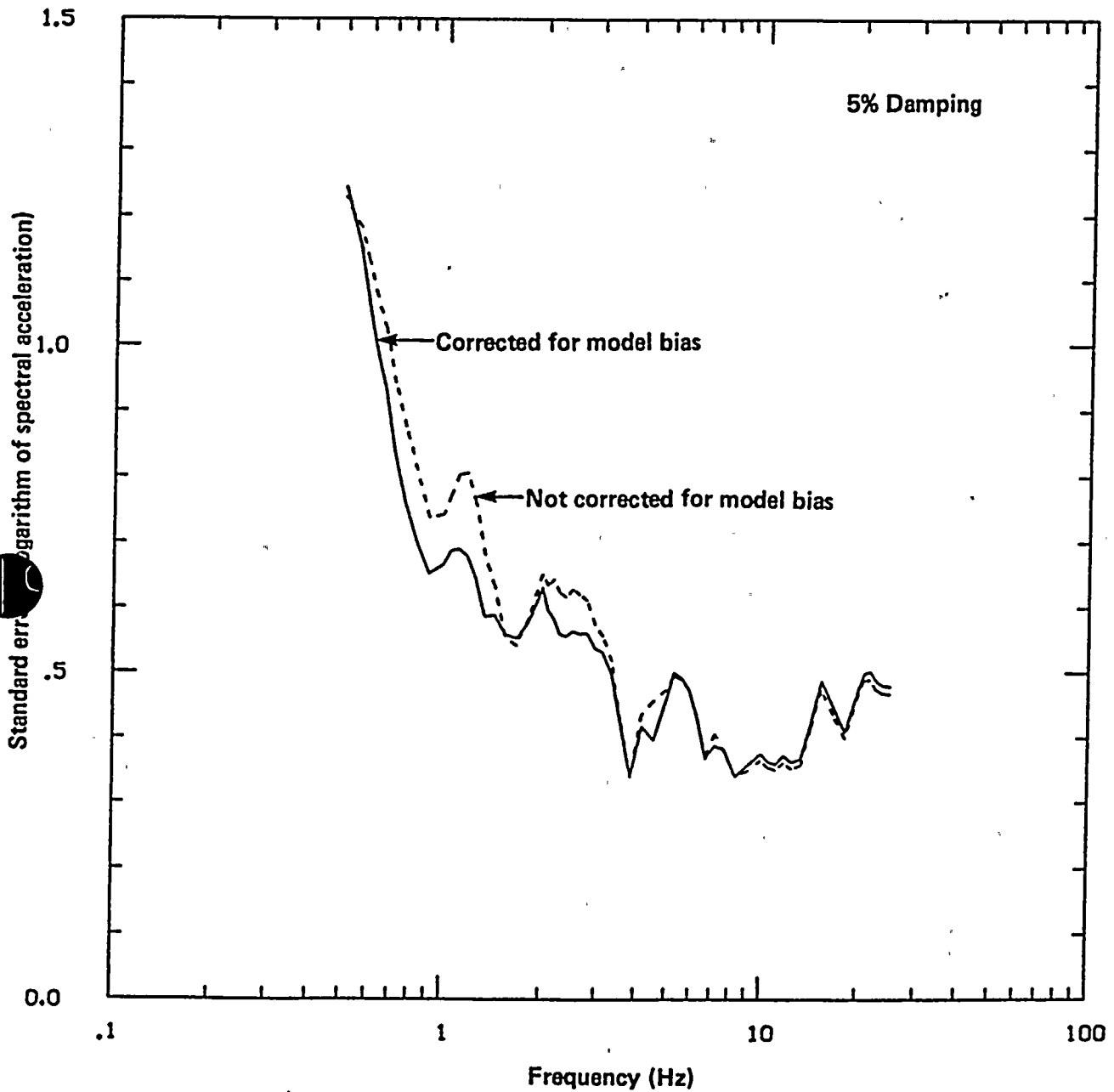


Figure Q7-3

Standard error of the simulated spectrum due to modeling plus random uncertainty.



Table Q7-4

**FREQUENCY-AVERAGED SPECTRA (3.0 TO 8.5 HZ) AND PEAK ACCELERATION
USED IN ESTIMATING MODELING PLUS RANDOM UNCERTAINTY**

Units are natural logarithm of acceleration, in g

<u>Earthquake</u>	<u>Station</u>	<u>Observed</u>		<u>Calculated</u>		<u>Residual</u>	
		<u>ln SA</u>	<u>ln PGA</u>	<u>ln SA</u>	<u>ln PGA</u>	<u>ln SA</u>	<u>ln PGA</u>
Imperial Valley	EC Sta 4	-0.333	-0.870	-0.357	-1.266	0.024	0.396
	EC Sta 5	-0.053	-0.812	-0.069	-0.805	0.016	-0.007
	EC Sta 6	-0.377	-0.947	-0.075	-1.034	-0.302	0.087
	EC Sta 7	-0.551	-0.936	-0.120	-1.161	-0.431	0.225
	EC Sta 8	-0.026	-0.629	-0.100	-0.911	0.074	0.282
	EC Sta 10	-0.792	-1.627	-0.424	-1.317	-0.368	-0.310
Nahanni	Site 1	0.693	-0.340	0.088	-0.664	0.605	0.324
	Site 2	-0.764	-0.774	-0.176	-0.923	-0.588	0.149
	Site 3	-1.473	-1.661	-0.994	-1.928	-0.478	0.267
Whittier	Alhambra	-0.235	-1.060	-0.260	-1.206	0.025	0.146
	Bulk Mail	-0.015	-0.779	-0.111	-0.779	0.096	0.000
	Cal State LA	-0.271	-1.073	0.047	-0.773	-0.317	-0.300
	Downey	-1.087	-1.721	-0.814	-1.434	-0.272	-0.287
	Garvey	0.118	-0.810	0.017	-0.604	0.101	-0.206
	Obregon Park	-0.012	-0.862	-0.341	-1.087	0.330	0.225
	San Marino	-1.016	-1.753	-0.391	-0.981	-0.624	-0.772
	Whittier Dam	-0.421	-1.354	-0.031	-0.971	-0.390	-0.383
	Whittier	-0.109	-0.689	-0.312	-0.908	0.203	0.219

Table Q7-5

**BIAS AND STANDARD ERROR OF THE FREQUENCY-AVERAGED
SPECTRUM (3.0 TO 8.5 HZ) AND THE PEAK ACCELERATION**

Units are natural logarithm of acceleration, in g

<u>Earthquake</u>	<u>Bias</u>		<u>Standard Error</u>		<u>No. of Stations</u>
	<u>ln SA</u>	<u>ln PGA</u>	<u>ln SA</u>	<u>ln PGA</u>	
Imperial Valley	-0.164	0.122	0.226	0.251	6
Nahanni	-0.154	0.247	0.660	0.089	3
Whittier Narrows	-0.094	-0.151	0.318	0.330	9
Combined	-0.128	0.003	0.34	0.31	18



frequency-averaged spectrum. For all events, the overprediction is about 14 percent. We have chosen not to correct for model bias, thus the predicted frequency-averaged spectrum is conservative.

A possible source of underestimation of σ_{mr}^2 results from the use of the Imperial Valley mainshock as part of the modeling plus random uncertainty estimation. In the prediction stage, the Imperial Valley aftershock source functions are used to compute the ground motions at Diablo Canyon. Intuitively, transporting these source functions to a region other than Imperial Valley should increase the uncertainty of the simulations; however, this effect does not appear to be large. Over the frequency band 3 to 8.5 Hz, the bias of the model is larger for the Imperial Valley mainshock than for either Whittier or Nahanni (Table Q7-5). The frequency-dependent bias estimated from just the Whittier and Nahanni earthquakes is shown in Figure Q7-4. Comparing this with Figure Q7-2 shows that at frequencies above 3 Hz the bias is about the same with or without the Imperial Valley mainshock, although the uncertainty is slightly larger without Imperial Valley. If the Imperial Valley mainshock is excluded from the frequency-averaged spectrum, then σ_{mr} increases from 0.35 to 0.39.

This small difference indicates that transporting the Imperial Valley source functions to other regions does not greatly increase the uncertainty of the simulations. Therefore, including the Imperial Valley mainshock in the estimation of σ_{mr}^2 is not expected to significantly underestimate its value. Furthermore, any underestimation is likely to be offset by the overestimation due to the double counting of uncertainty in the gross features of the slip distribution. This double counting occurs because we treat the gross features of the slip distribution as parametric uncertainty, and assume that the gross features of the slip distribution are known exactly for the three events used in estimating the modeling plus random uncertainty. Any error in the gross features of the assumed slip models of these three earthquakes will contribute to the measured modeling plus random uncertainty, causing overestimation of the modeling plus random uncertainty.

Estimation of Parametric Uncertainty. The source-parameter values that were varied probabilistically in the predictions include rupture mode (unilateral or bilateral) and location of the rupture surface (and the asperities on it) with respect to the site. The rupture location and asperity locations were varied simultaneously. The motion was simulated at several sites along the rupture plane, which contained multiple asperities at various depths. This is equivalent to shifting the rupture plane and computing the motion at a single site. A rigorous approach should vary the rupture location and asperity locations separately; however, the most important distance is the distance from the site to the closest asperity. The approach used in this study generates a wide range of asperity-to-site distances for the given closest distance to the fault plane. The variation of ground motion from this sample of asperity-to-site distances should yield a good approximation to a more rigorous estimation of the parametric uncertainty.

The estimate of modeling uncertainty already includes a component due to differences between the selected source function and the actual process as contained in the data. Therefore, the variability in source functions should not be included in the estimation of parametric uncertainty; only one set of source functions should be used. In this study, the Imperial Valley source functions are used because the event that produced them has been extensively studied (Liu and Helmberger, 1985), and many Imperial Valley mainshock recordings are available to test their effectiveness in simulations. The number of simulations for each mechanism is listed in Table Q7-6.

Table Q7-6

PARAMETRIC VARIATIONS FOR PREDICTIONS

<u>Mechanism</u>	<u>Rupture Mode</u>	<u>Rupture Location</u>	<u>Total</u>
Strike-slip	6	11	22
Oblique	2	10	20
Thrust	2	8	16
Total			58



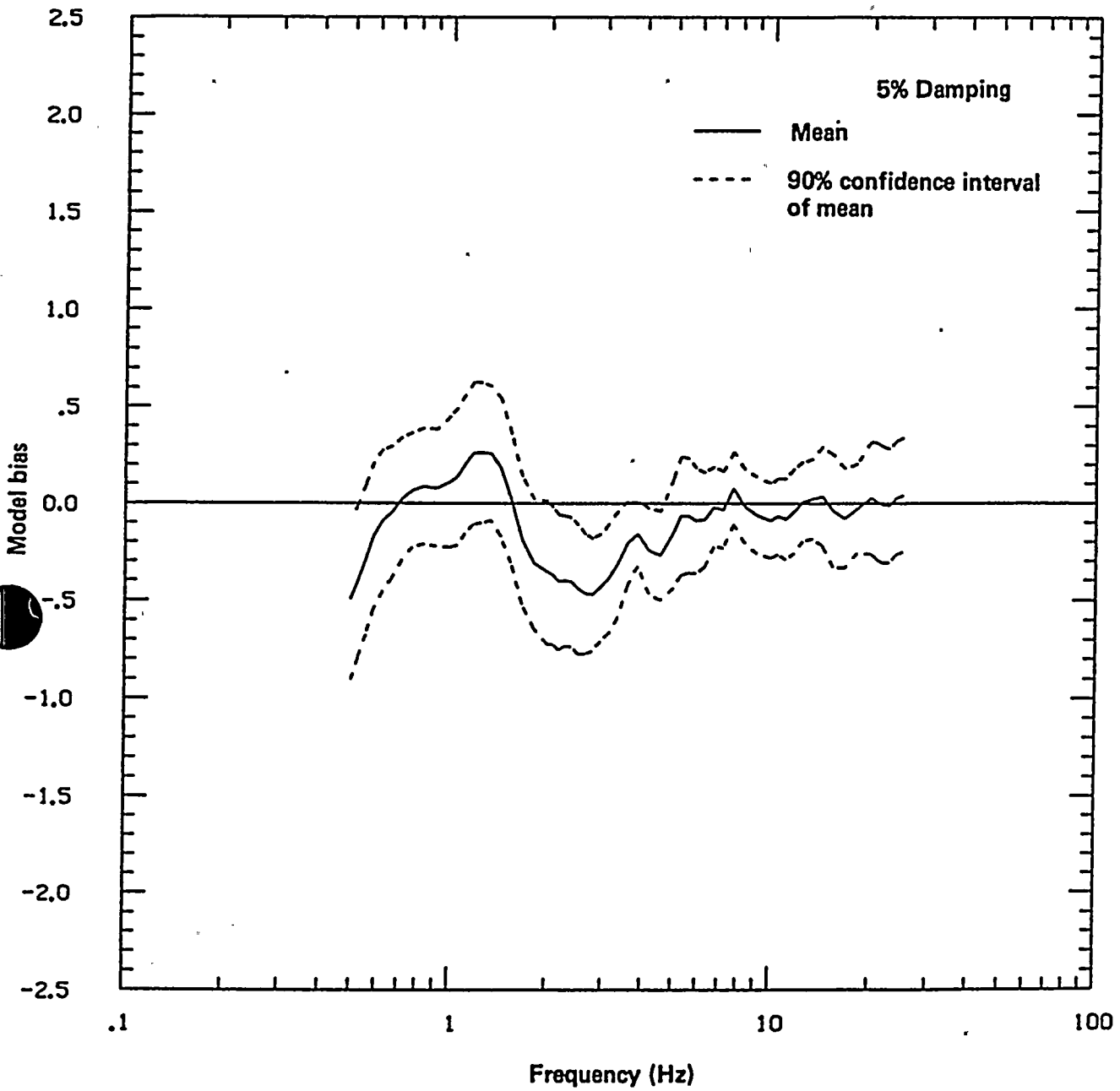


Figure Q7-4

Model bias for the Imperial Valley source functions excluding the Imperial Valley mainshock.



The parametric standard errors, $\sigma_p(f)$, for each focal mechanism are shown in Figure Q7-5. The mean parametric standard error is computed from the weighted sum of the variances where the weights are given by the probabilities assigned to each mechanism. The frequency-averaged spectra for the 58 simulations are listed in Table Q7-7. The parametric standard errors of the frequency-averaged spectrum are 0.37, 0.39, and 0.29 for strike-slip, oblique, and reverse mechanisms, respectively. Again using the probabilities as weights, the mean parametric standard error is 0.37. The parametric standard error (0.37) is about the same size as the modeling plus random standard error (0.35).

The sensitivity of the parametric uncertainty to the particular set of random numbers used in the simulation procedure is illustrated in Figure Q7-6, which shows the parametric uncertainty for a second realization of the simulations using a different set of random numbers than those used in Figure Q7-5. The random numbers introduce a stochastic component into an otherwise uniform rupture velocity and slip velocity. The parametric uncertainty from this second realization is similar to that of the first realization (Figure Q7-5) with expected variations in the individual peaks and troughs. Overall, the comparison indicates that the parametric uncertainty estimate from 58 simulations is stable.

The parametric uncertainty includes the effects of uncertainty in both the rupture mode and the rupture (and asperity) location. The relative importance of these two sources of parametric uncertainty can be estimated. The parametric uncertainty is separated into the standard errors due to rupture mode and rupture location uncertainty in Figure Q7-7. It is clear that the uncertainty in rupture location leads to much larger variation in ground motion than the uncertainty in rupture mode. The standard errors of the frequency-averaged spectral acceleration due to uncertainty in rupture location and rupture mode are 0.38 and 0.11, respectively. This indicates that the effect of rupture mode is relatively insignificant. (The loss of degrees of freedom in the estimation of the parametric standard errors due to individual source parameters results in a larger standard error due to rupture location, 0.38, than the total parametric standard error of 0.37. Therefore, a simple square-root-of-the-sum-of-squares combination of the standard errors due to rupture mode and rupture location will overestimate the total parametric uncertainty.)

The assumption of lognormality of the simulated response spectra was checked by comparing the 50th- and 84th-percentile spectra with the mean and mean plus sigma spectra. These four spectra computed for the 116 simulations presented in the Final Report are shown in Figure Q7-8. The 50th- and 84th-percentile spectra slightly exceed the mean and mean plus sigma spectra in the frequency band of 4 to 10 Hz, but overall the agreement is good. Therefore, the assumption of lognormality is justified.

Overall Estimate of Uncertainty. The overall estimate of uncertainty of the predicted response spectra derived from numerical modeling is obtained by combining the modeling plus random uncertainty with the parametric uncertainty using Eq. 7. The total standard error, $\sigma_T(f)$, is shown in Figure Q7-9. For the frequency-averaged spectrum, the total standard error (without correction for model bias) is 0.51. This value of total uncertainty does not include the peak-to-trough variability; however, its effect is quite small. Including the peak-to-trough variability will increase the total standard error by less than 0.02.

A comparison of the modeling plus random, parametric, and total uncertainties is shown in Figure Q7-10. At frequencies above 3 Hz, the modeling plus random uncertainty and the parametric uncertainty contribute about equally to the total uncertainty. The uncertainties for the frequency-averaged spectrum are listed in Table Q7-8. The modeling plus random uncertainty and the parametric uncertainty contribute about equally to the total uncertainty of the frequency-averaged spectrum.

To estimate the 84th-percentile spectrum, the total uncertainty shown in Figure Q7-9 is added to the median of the 116 simulations from the Final Report. This 84th-percentile spectrum is shown in Figure Q7-11. It is based on modeling plus random uncertainty and parametric uncertainty estimated using the Imperial Valley source functions. The 84th-percentile of the frequency-averaged spectrum is 1.85 g, compared to 1.94 g for the site-specific spectrum. This is lower than the 84th-percentile spectrum shown in Figure Q7-11 because the frequency-averaged spectrum is more stable (has smaller uncertainty) than the spectral values at individual frequencies. (This is analogous to the uncertainty



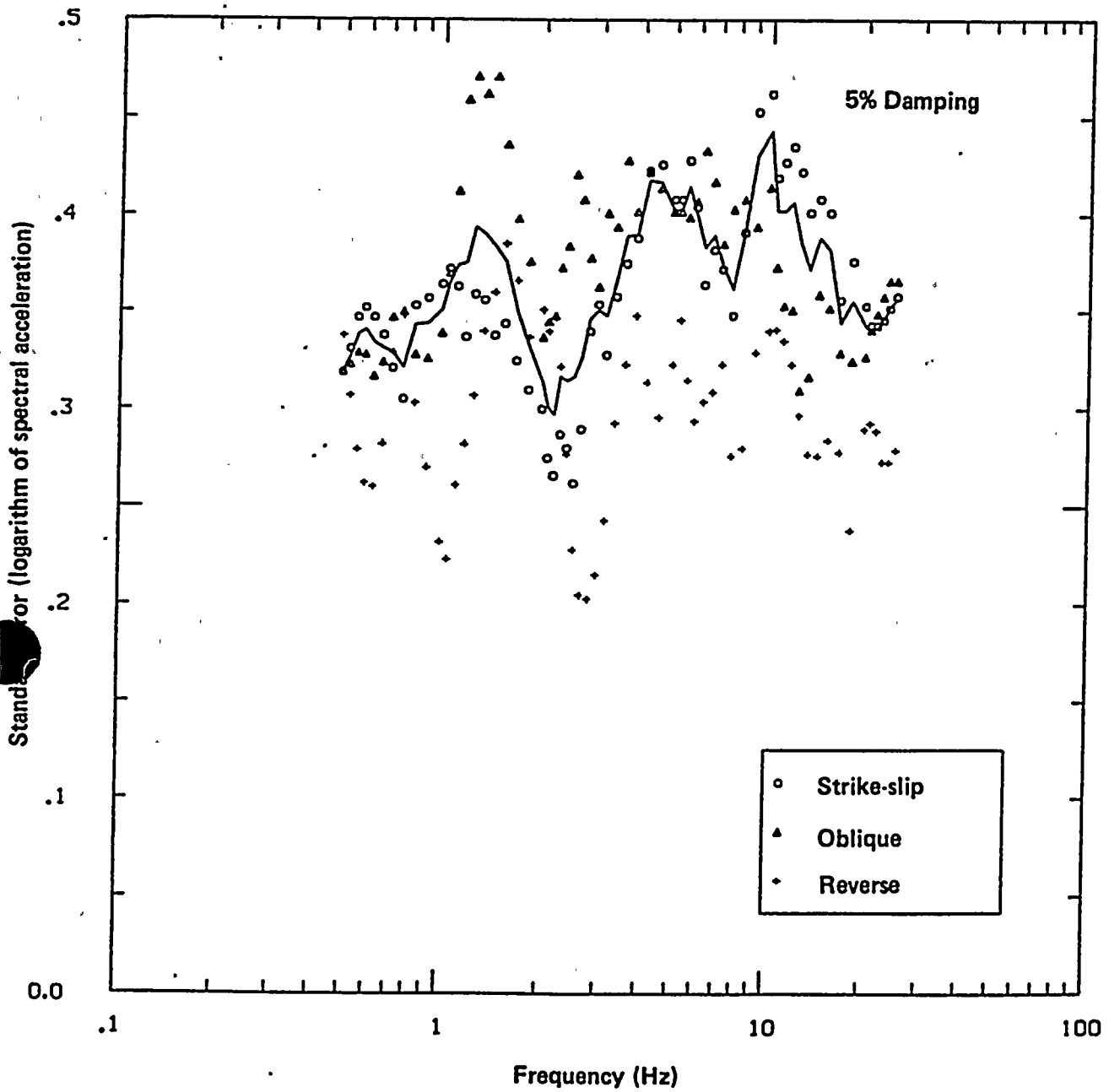


Figure Q7-5

Standard error of the predicted spectrum due to parametric uncertainty.



Table Q7-7

SUITE OF FREQUENCY-AVERAGED SPECTRA FROM THE PARAMETRIC
 VARIATIONS LISTED IN TABLE Q7-6.
 Units are natural logarithm of acceleration, in g

<u>Mechanism</u>	<u>Rupture Location</u>	<u>Rupture Mode</u>	
		<u>Unilateral</u>	<u>Bilateral</u>
Strike-slip	1	-0.5492	-0.9247
	2	-0.1474	-0.1068
	3	0.1695	0.2913
	4	-0.4720	-0.2775
	5	-0.1220	-0.7921
	6	0.2851	0.0226
	7	-0.2851	-0.1506
	8	-0.7704	-0.6595
	9	0.0580	-0.0919
	10	0.3201	0.2899
	11	-0.2289	-0.1568
Oblique	1	-0.7797	-0.8766
	2	-0.1377	-0.2068
	3	0.3677	0.4400
	4	-0.0212	0.1913
	5	-0.4531	-0.2689
	6	-0.2286	-0.2035
	7	0.2427	0.3307
	8	0.3532	0.3366
	9	-0.3772	-0.3178
	10	-0.4967	-0.3412
Reverse	1	-0.5529	-0.6857
	2	-0.1400	-0.2404
	3	-0.0684	-0.0182
	4	-0.1626	-0.3442
	5	-0.0537	-0.1713
	6	0.4384	0.3330
	7	-0.0150	0.2155
	8	-0.1985	-0.0154





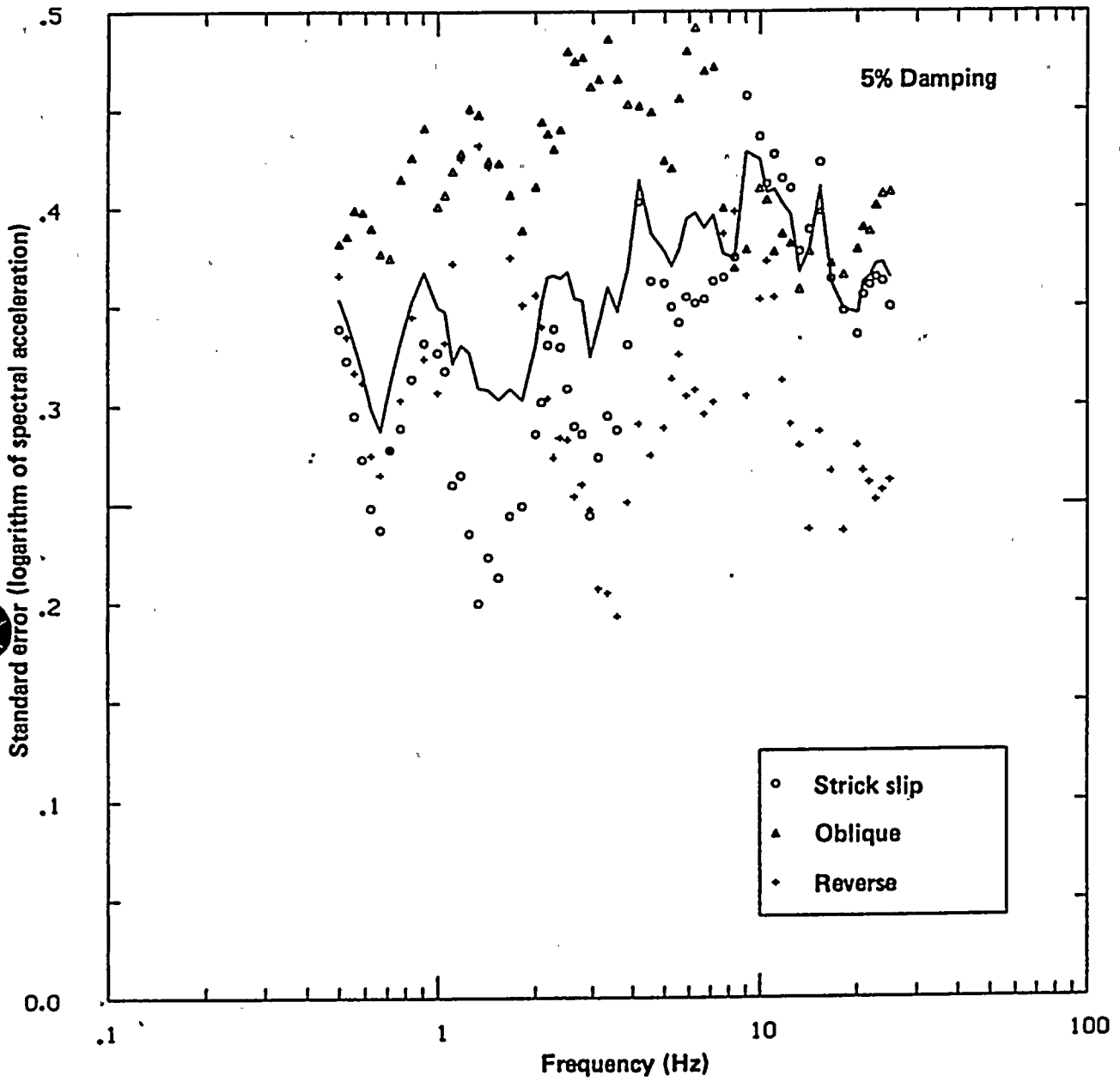


Figure Q7-6

Standard error of the predicted spectrum due to parametric uncertainty for the second set of random numbers.



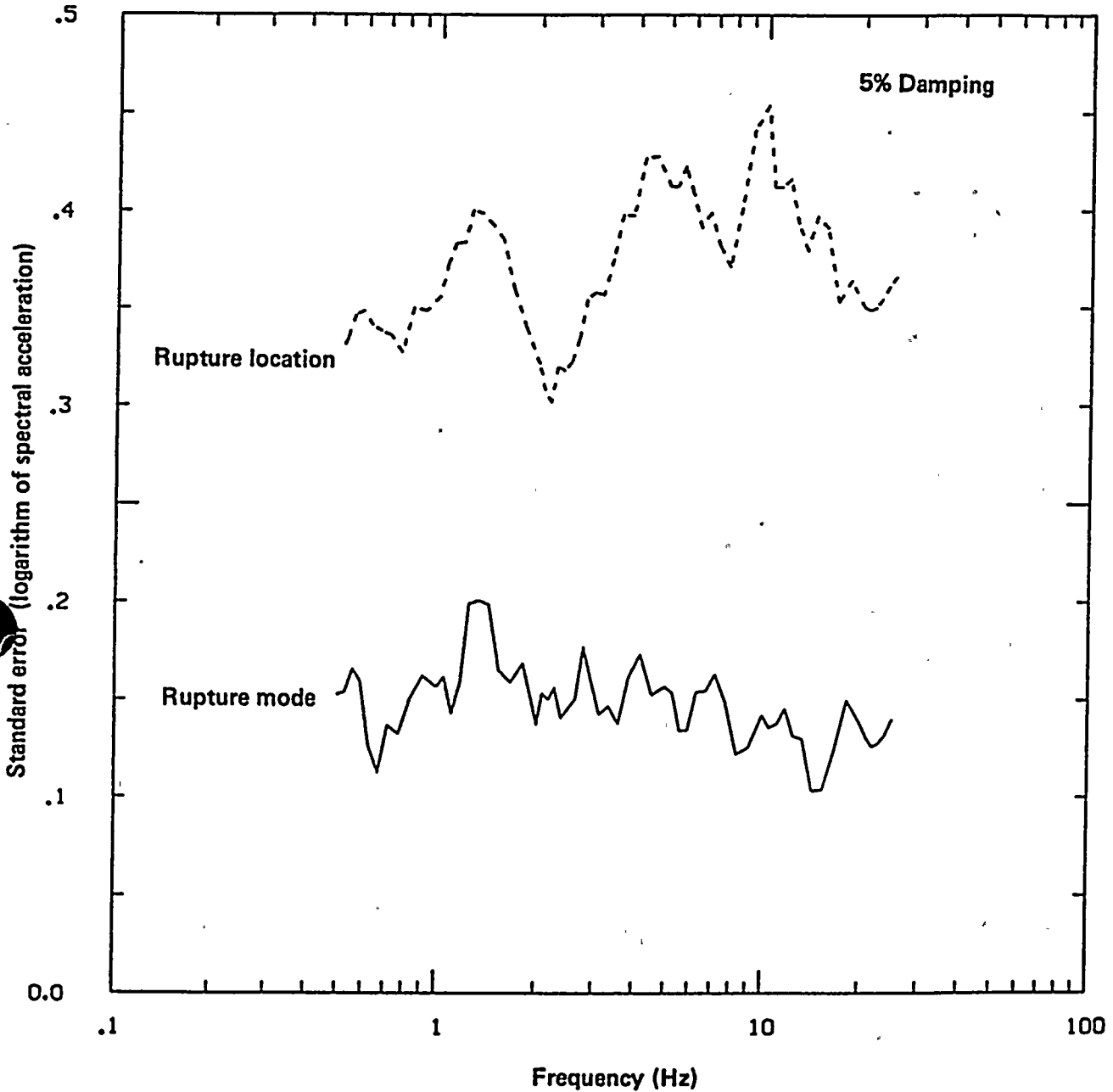


Figure Q7-7

The parametric uncertainty broken down into rupture mode uncertainty and rupture location uncertainty.



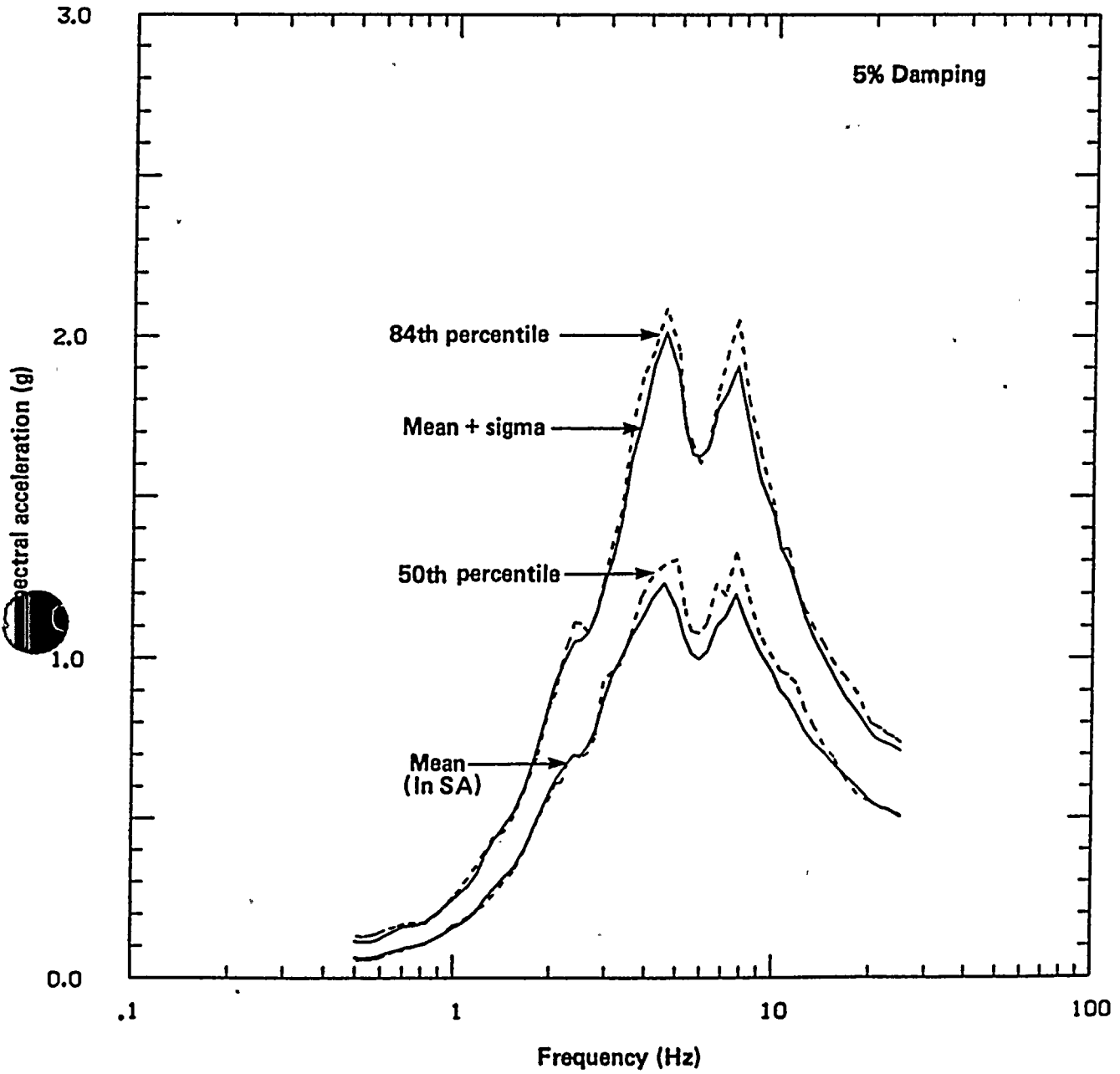


Figure Q7-8

Comparison of the mean, mean plus sigma, 50th-percentile, and 84th-percentile spectra based on the natural logarithmic values for the 116 simulations presented in the Final Report.



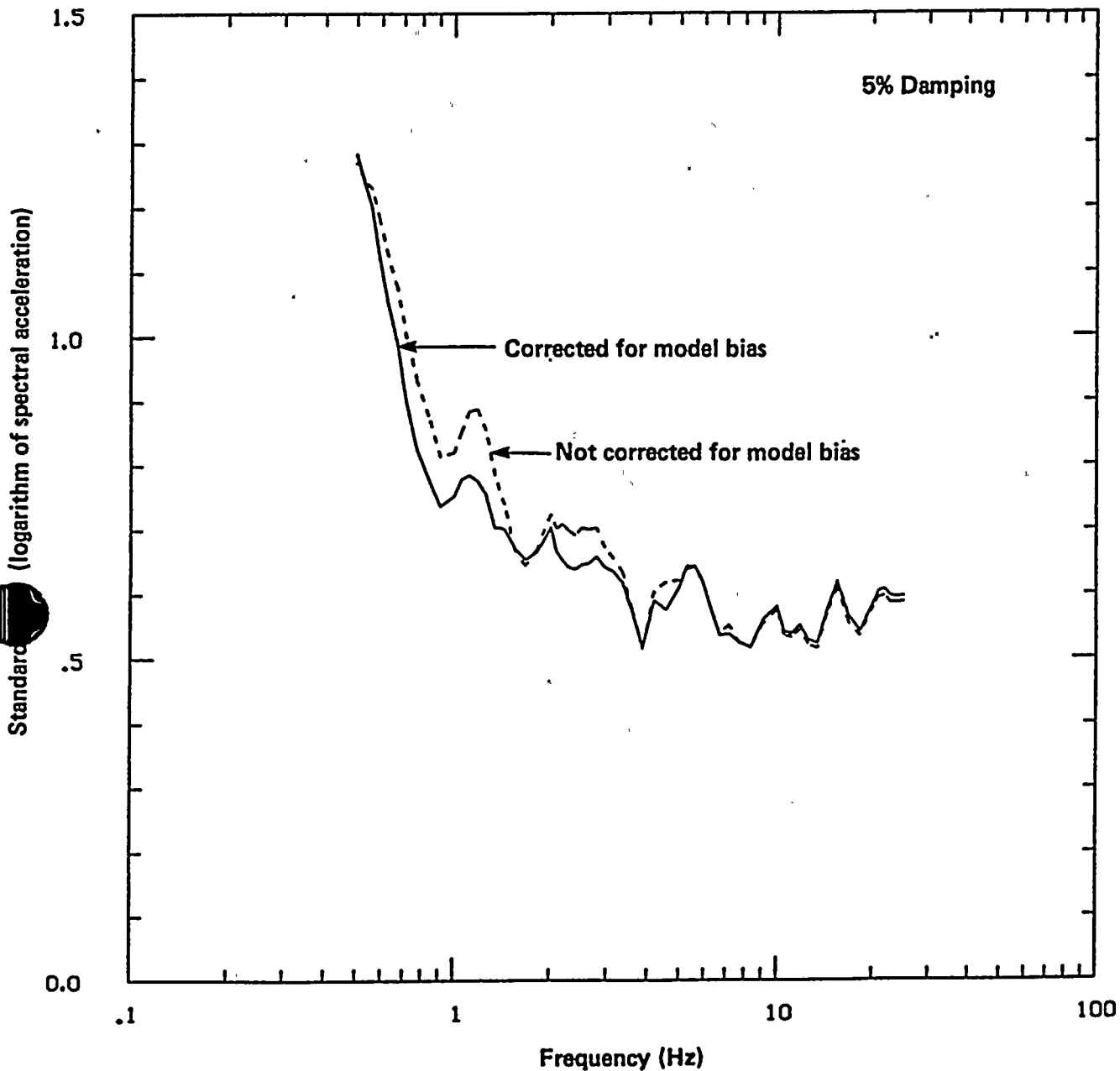


Figure Q7-9

The total uncertainty of the predicted spectrum.



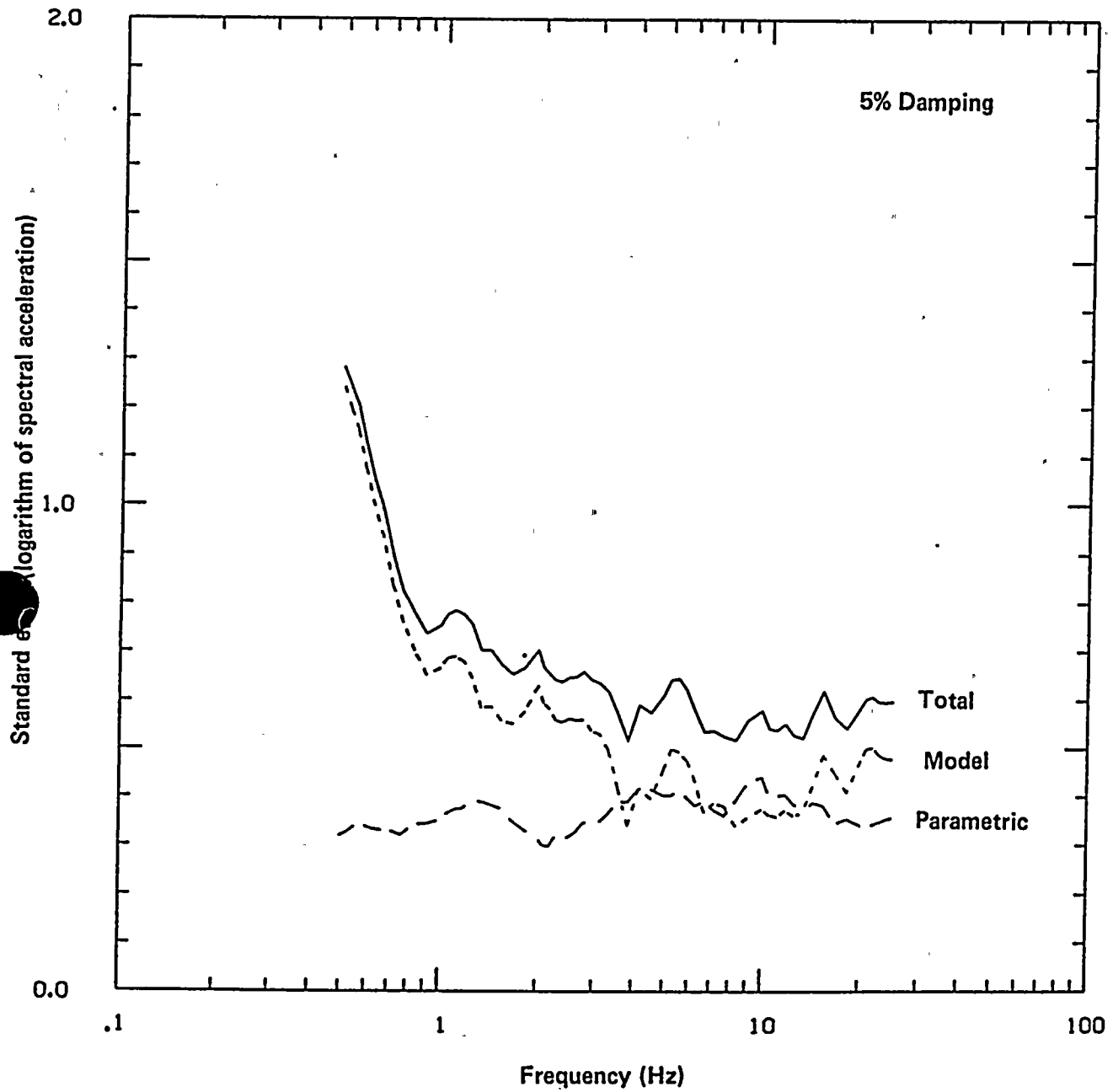


Figure Q7-10

Comparison of the modeling plus random, parametric, and total uncertainty, not corrected for model bias.



Table Q7-8

UNCERTAINTY OF THE FREQUENCY-AVERAGED SPECTRUM
Units are in natural logarithm of acceleration, in g

<u>Component of Uncertainty</u>	<u>Standard Error</u>	
	<u>Corrected for Model Bias</u>	<u>Not Corrected for Model Bias</u>
Modeling plus Random	0.34	0.35
Parametric	0.37	0.37
Total	0.50	0.51





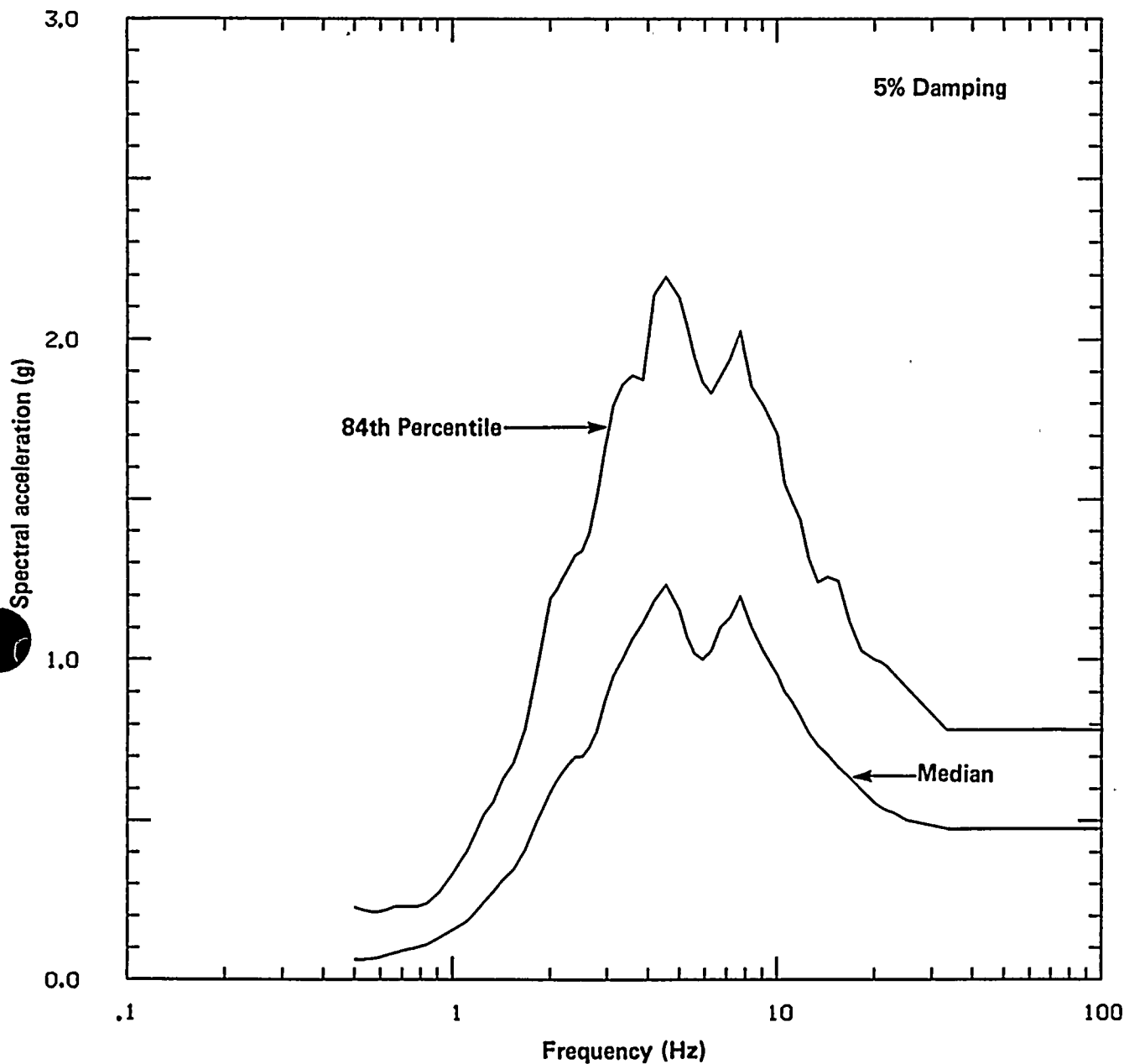


Figure Q7-11

Median and 84th-percentile response spectra derived by numerical modeling. The median response spectrum is from the Final Report, and the 84th-percentile response spectrum is from the overall uncertainty estimate described in this response.



of a mean value being less than the uncertainty of a single observation.) The 84th-percentile estimated here differs from that shown in the Final Report; the two spectra are shown in Figure Q7-12. The 84th-percentile response spectrum shown in the Final Report lacked rigor in the following two respects: the parametric uncertainty was overestimated by double counting it due to the use of two sets of empirical source functions, and an estimate of modeling plus random uncertainty was not included. The present estimate of the 84th-percentile response spectrum treated both of these aspects much more rigorously.

An assessment of the stability of the 84th-percentile spectrum is made by comparing the 84th-percentile spectra based on the two sets of random numbers discussed earlier. The two 84th-percentile spectra shown in Figure Q7-12 are quite similar, indicating that a sufficient number (58) of simulations was made to ensure a stable estimate of the 84th-percentile spectrum. As shown in Figure Q7-12, the newly derived numerical modeling spectra exceed the site-specific response spectrum in the frequency ranges of 4 to 5 Hz and 7 to 8 Hz by less than about 8 percent.

References

Geller, R. J., 1976, Scaling relations for earthquake source parameters and magnitudes, *Bulletin of the Seismological Society of America*, v. 66, p. 1501-1523.

Liu, H.-L., and Helmberger, D. V., 1985, The 23:19 aftershock of the October 1979 Imperial Valley earthquake: more evidence for an asperity, *Bulletin of the Seismological Society of America*, v. 75, p. 689-708.

Joyner, W. B., and Boore, D. M., 1988, Measurement, characterization, and prediction of strong ground motion, *Proceedings of Earthquake Engineering Soil Dynamics II - Recent Advances in Ground-Motion Evaluation*, Park City, Utah, p. 43-102.

Mendoza, C., and Hartzell, S. H., 1988, Inversion for slip-distribution using teleseismic waveforms: North Palm Springs, Borah Peak, and Michoacan earthquakes, *Bulletin of the Seismological Society of America*, v. 78, p. 1092-1111.

Wald, D. J., Burdick, L. J., and Somerville, P. G., 1988a, Simulation of acceleration time histories close to large earthquakes: *Proceedings of Earthquake Engineering Soil Dynamics II - Recent Advances in Ground-Motion Evaluation*, Park City, Utah, p. 430-444.

Wald, D., Somerville, P. G., and Burdick, L. J., 1988b, The Whittier Narrows, California earthquake of October 1, 1987 - Simulation of recorded accelerations: *Earthquake Spectra*, v. 4, p. 139-156.



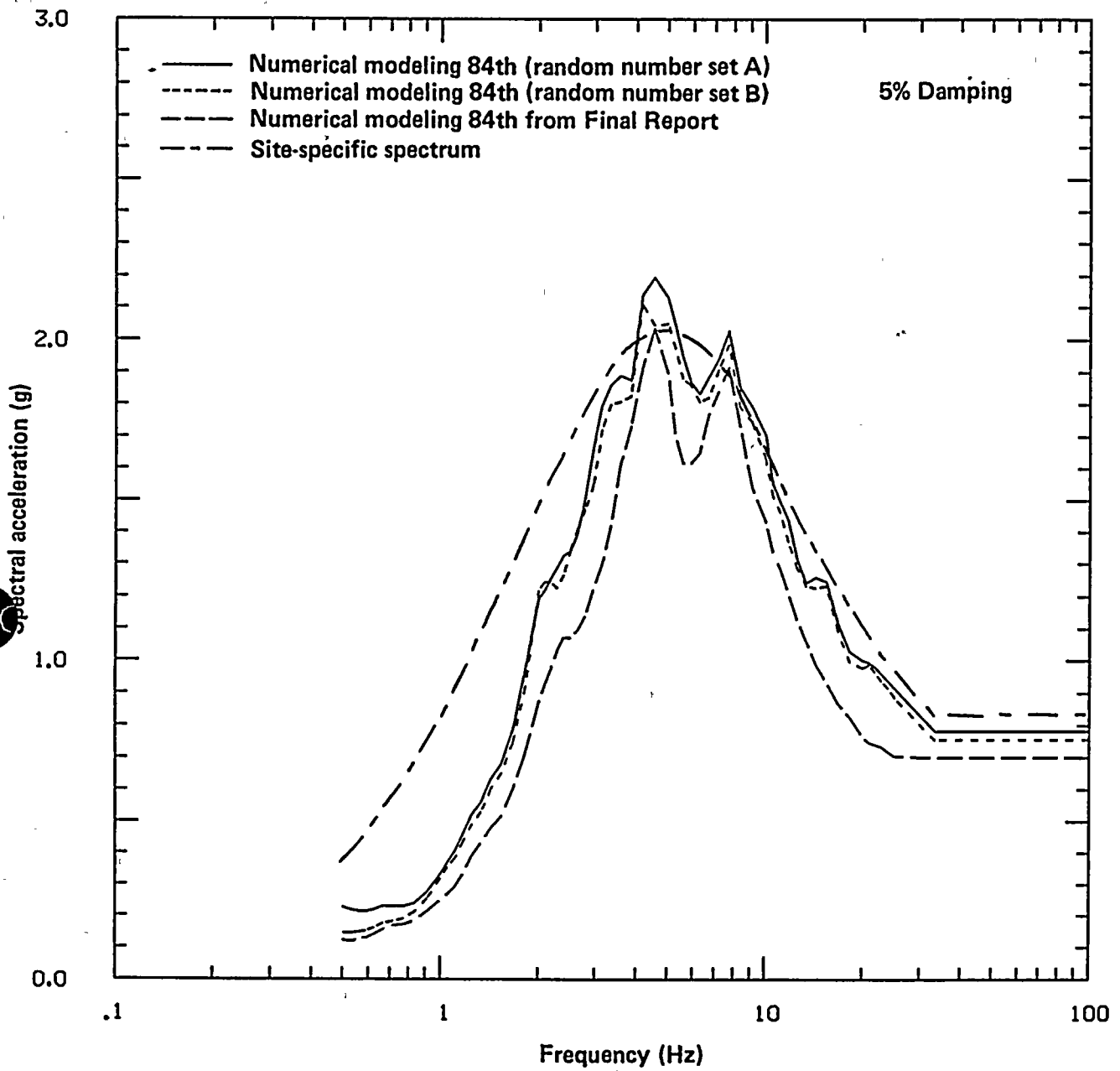


Figure Q7-12

Comparison of the 84th-percentile response spectra derived from numerical modeling with the site-specific 84th-percentile response spectrum.




QUESTION 10

Provide the eleven three-component time series for bilateal rupture for both the Imperial Valley and Coalinga aftershock sources from the numerical modeling study.

The locations of the 11 stations used in the strike-slip simulations are shown on Figure Q10-1; the slip distribution model is shown in Table Q10-1 (Table 13b-2, Question 13b, January 1989). The simulated acceleration time histories for bilateral, strike-slip faulting using the Imperial Valley source functions are given in Figures Q10-2 through Q10-12, and for the Coalinga source functions on Figures Q10-13 through Q10-23. The time histories have been highpass filtered at a frequency of 0.2 Hz.





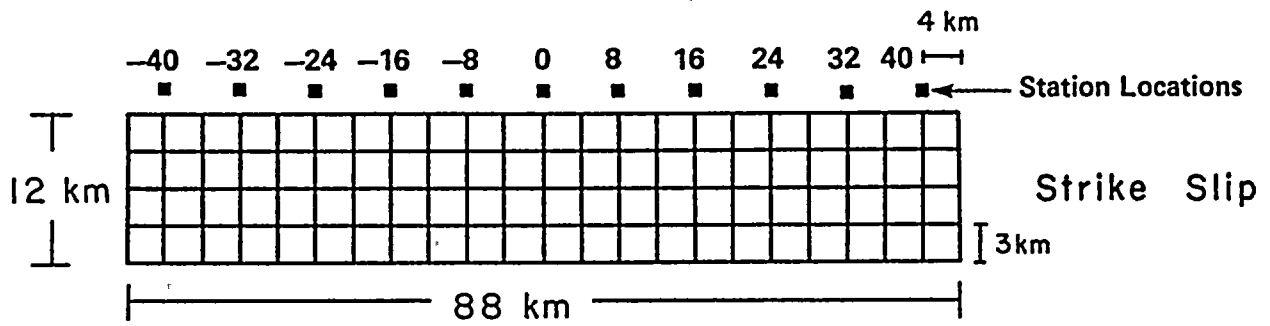


Figure Q10-1

Fault element geometry and station locations of Hosgri strike-slip fault model to simulate time histories for site-specific spectra.



Table Q10-1

SLIP (m) ON THE FAULT ELEMENTS OF THE STRIKE-SLIP MODEL

1.0	1.0	1.0	1.6	2.0	1.6	1.0	1.0	1.0	1.6	2.0	1.6	1.0	1.0	1.0	1.0	1.0	3.1	5.1	3.1	1.0	1.0
1.0	1.0	1.0	3.0	5.0	3.0	1.0	1.0	1.0	1.0	3.0	5.0	3.0	1.0	1.0	1.0	2.0	5.0	10.1	5.0	2.0	1.0
1.0	1.0	2.0	5.0	10.1	5.0	2.0	1.0	1.0	2.0	5.0	10.1	5.0	2.0	1.0	1.0	2.0	5.0	10.1	5.0	2.0	1.0
1.0	1.0	1.0	3.0	5.0	3.0	1.0	1.0	1.0	1.0	3.0	5.0	3.0	1.0	1.0	1.0	1.0	3.0	5.0	3.0	1.0	1.0



DCP SS BIL M=7.2 IV SRCS 5/18/88 4X3 4.1 km W=0-12 RT=3.5 (K)
SS-40
1 g

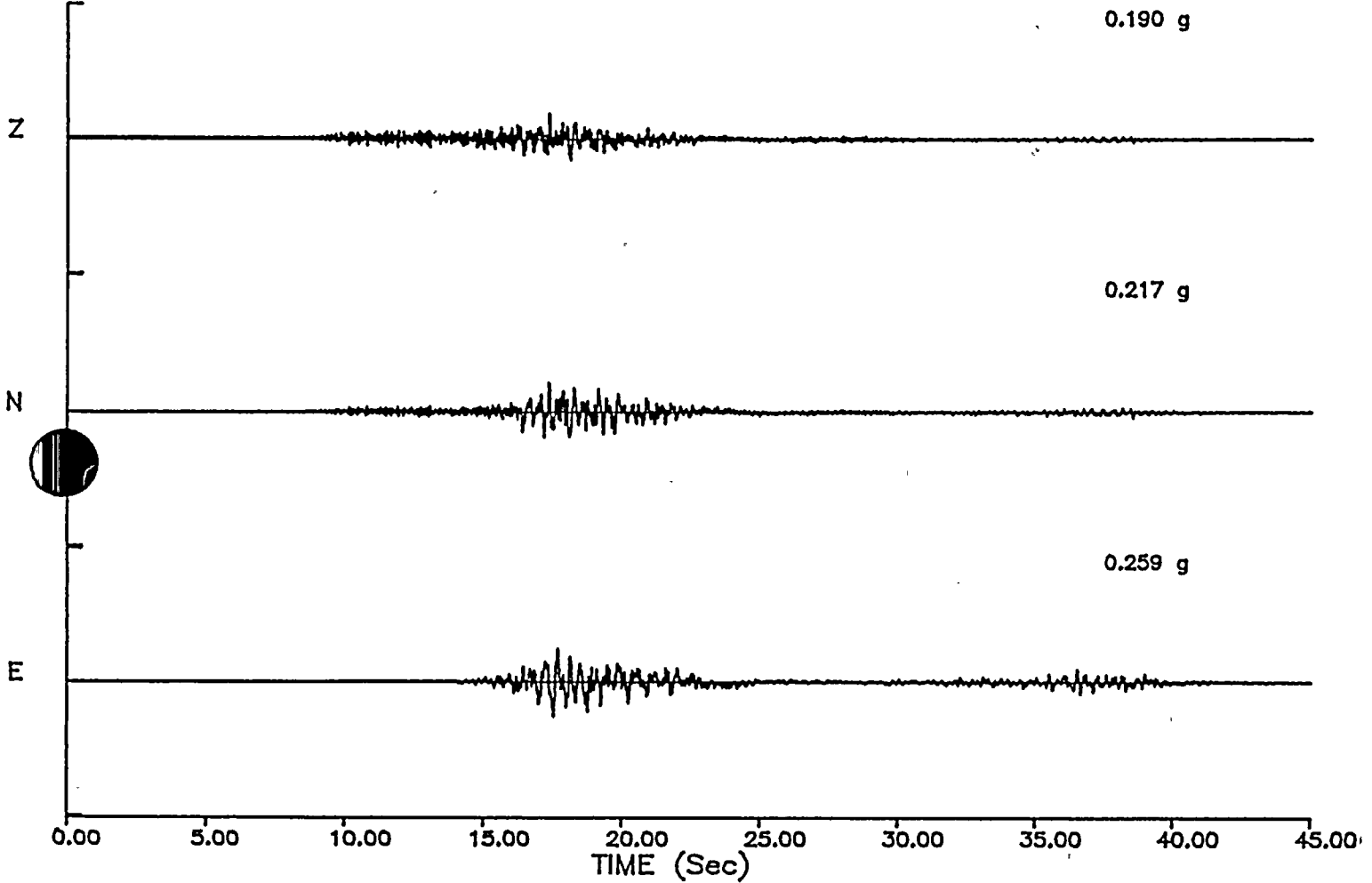


Figure Q10-2

Simulated accelerogram for magnitude 7.2 strike-slip, bilateral rupture at station -40 using Imperial Valley aftershock source functions.



DCP SS BIL M=7.2 IV SRCS 5/18/88 4X3 4.1 km W=0-12 RT=3.5 (K)
SS-32

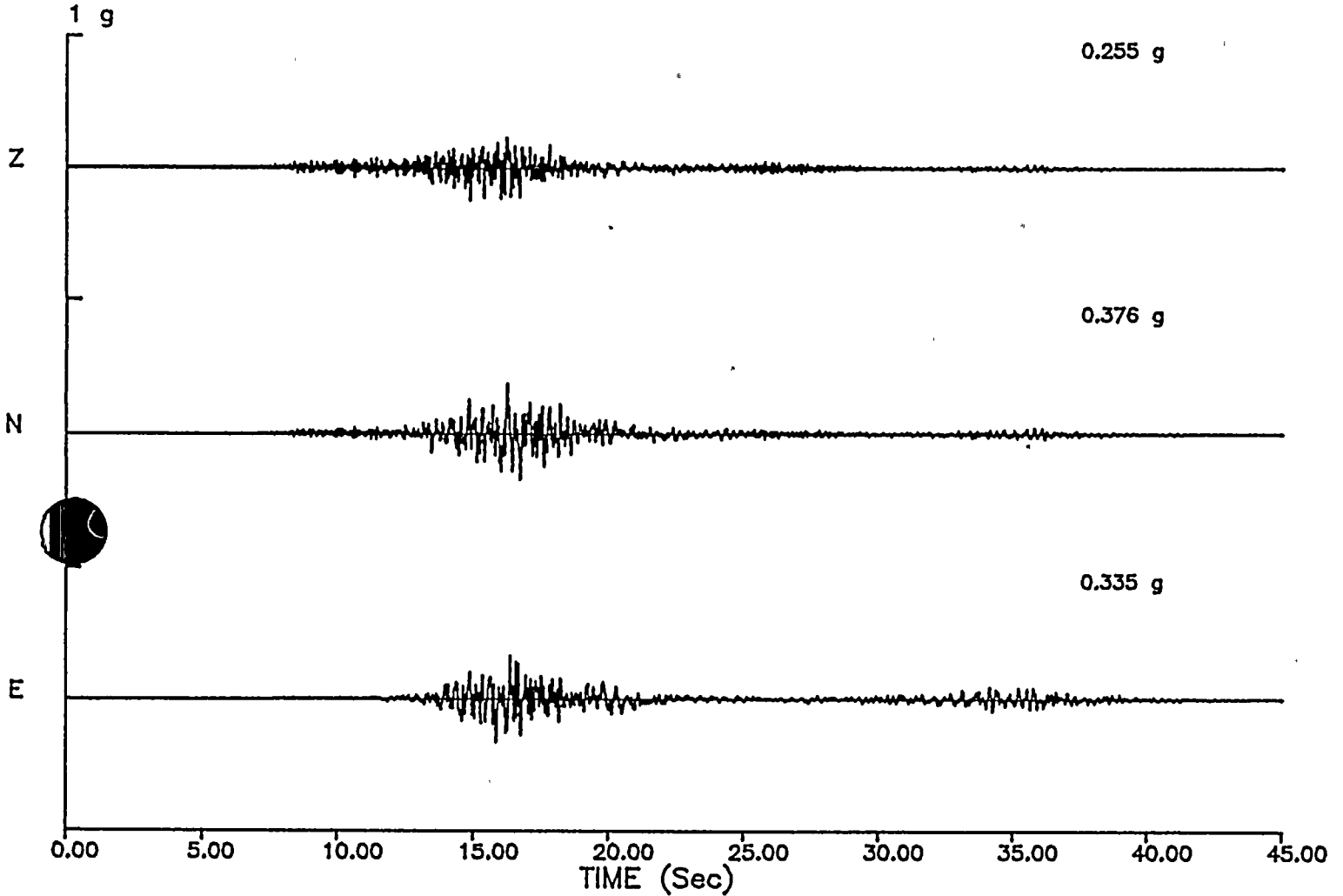


Figure Q10-3

Simulated accelerogram for magnitude 7.2, strike-slip, bilateral rupture at station -32 using Imperial Valley aftershock source functions.



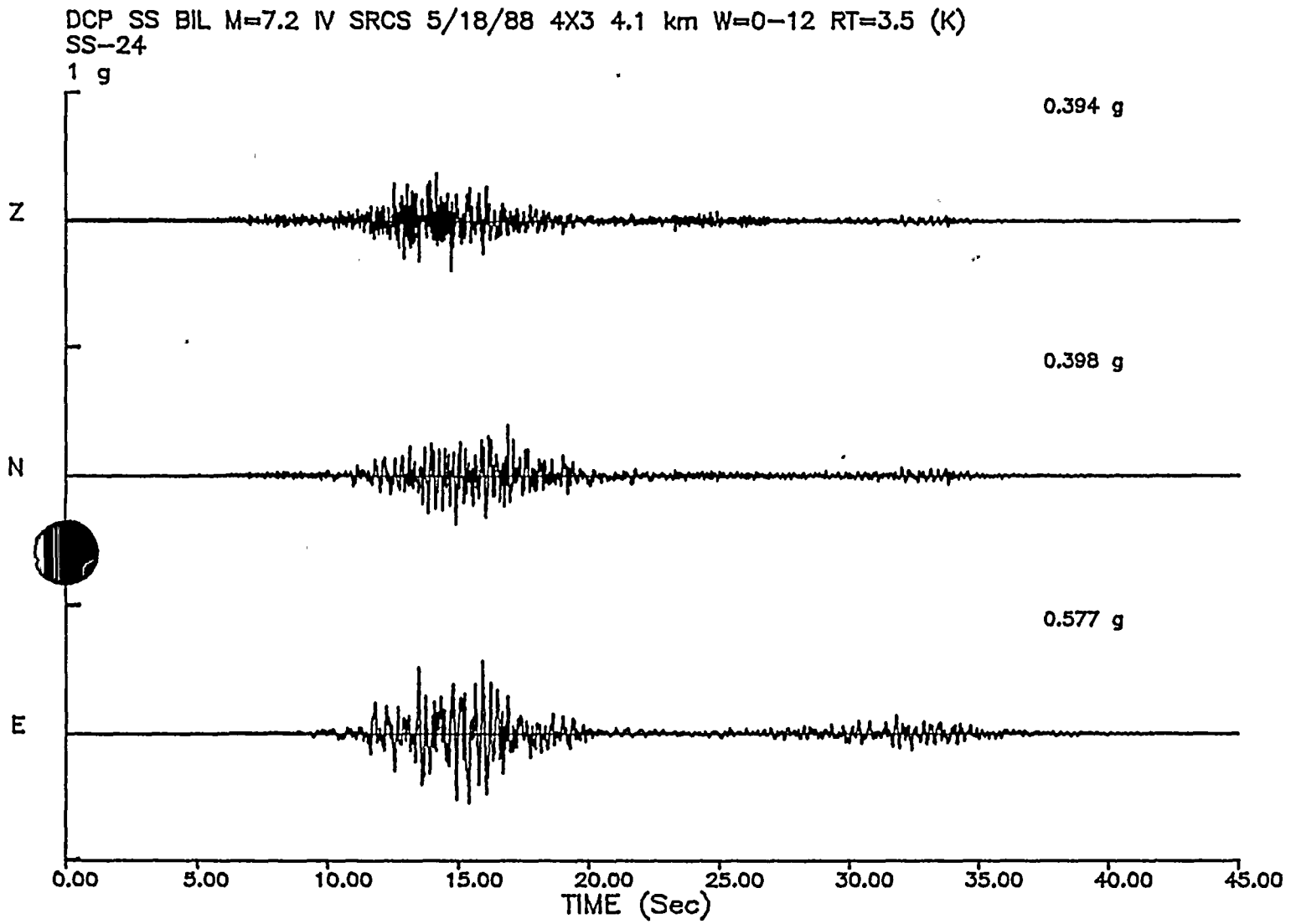


Figure Q10-4

Simulated accelerogram for magnitude 7.2, strike-slip, bilateral rupture at station -24 using Imperial Valley aftershock source functions.



DGP SS BIL M=7.2 IV SRCS 5/18/88 4X3 4.1 km W=0-12 RT=3.5 (K)
SS-16

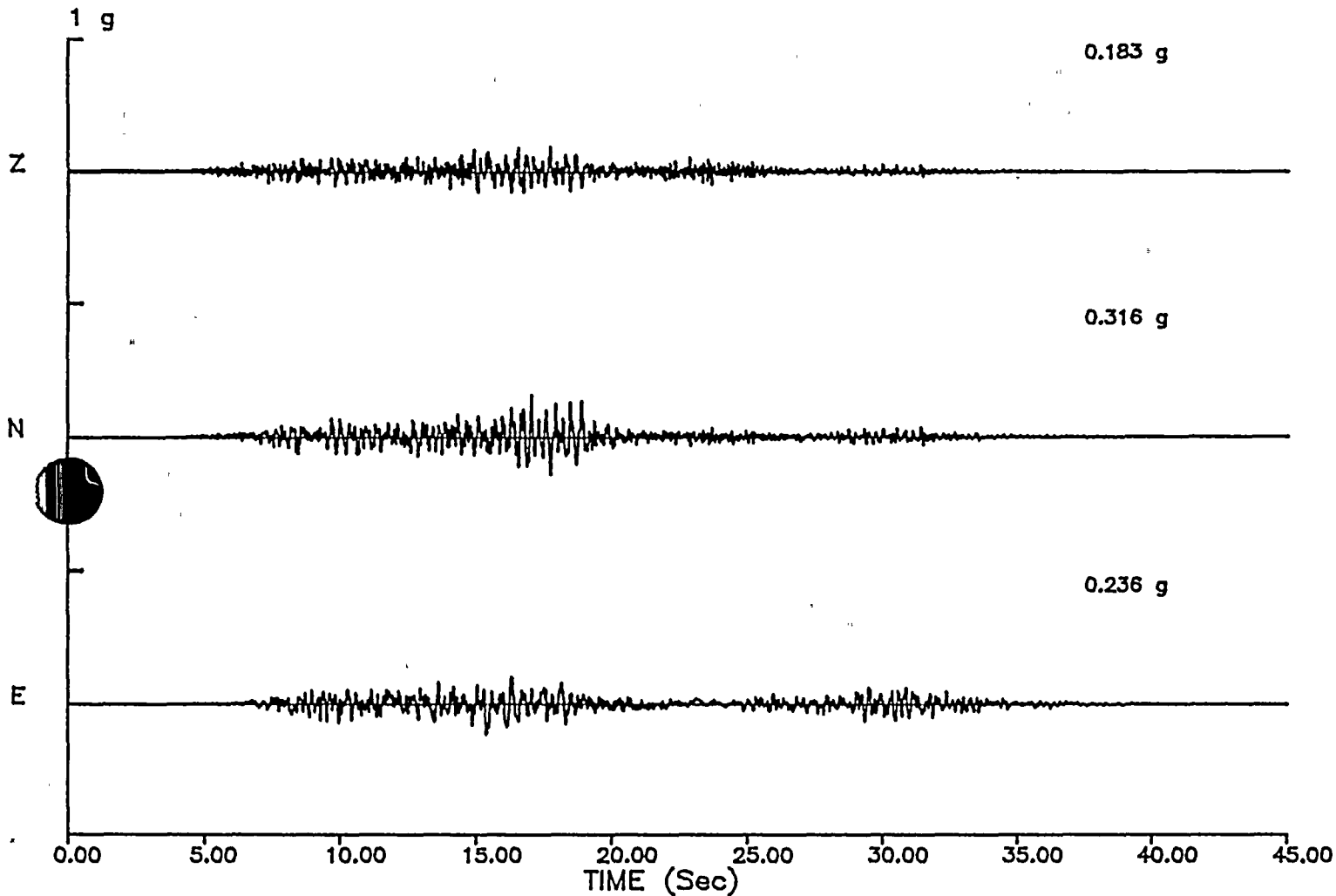


Figure Q10-5

Simulated accelerogram for magnitude 7.2, strike-slip, bilateral rupture at station -16 using Imperial Valley aftershock source functions.



DCP SS BIL M=7.2 IV SRCS 5/18/88 4X3 4.1 km W=0-12 RT=3.5 (K)
SS-8
1 g

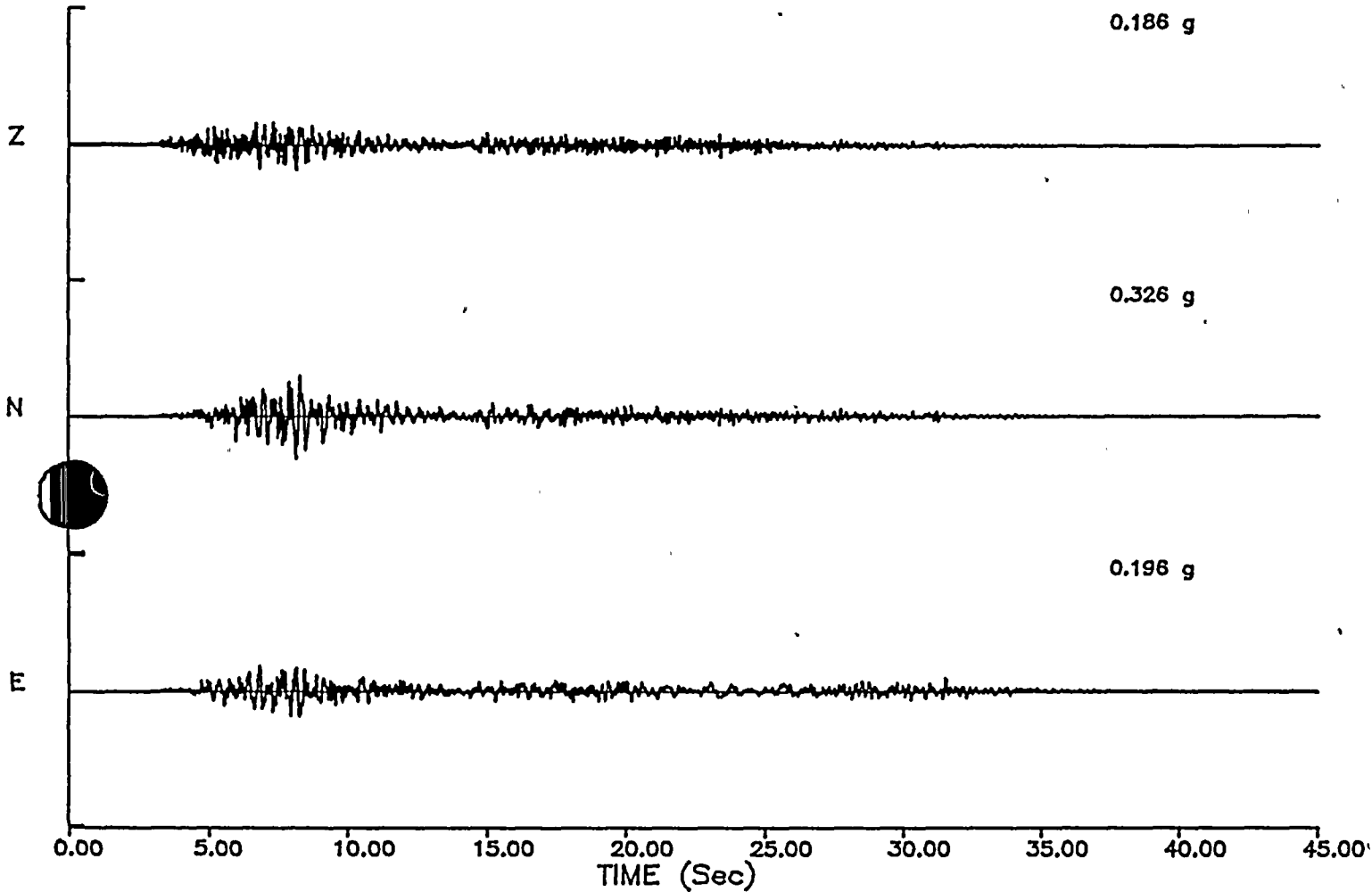


Figure Q10-6

Simulated accelerogram for magnitude 7.2, strike-slip, bilateral rupture at station -8 using Imperial Valley aftershock source functions.



DCP SS BIL M=7.2 IV SRCS 5/18/88 4X3 4.1 km W=0-12 RT=3.5 (K)
SS-0

1 g

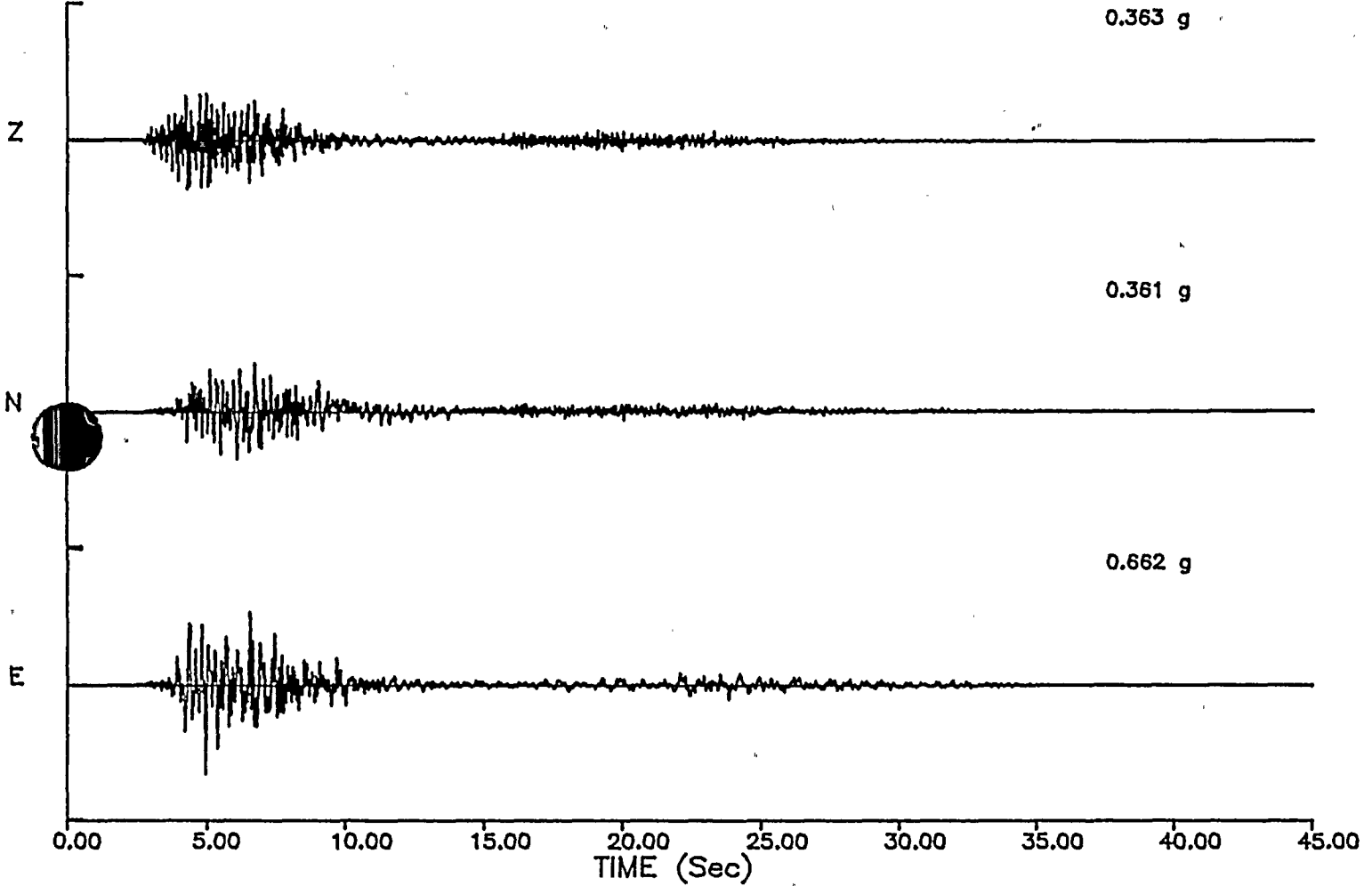


Figure Q10-7

Simulated accelerogram for magnitude 7.2, strike-slip, bilateral rupture at station 0 using Imperial Valley aftershock source functions.



DCP SS BIL M=7.2 IV SRCS 5/18/88 4X3 4.1 km W=0-12 RT=3.5 (K)
SS+8
1 g

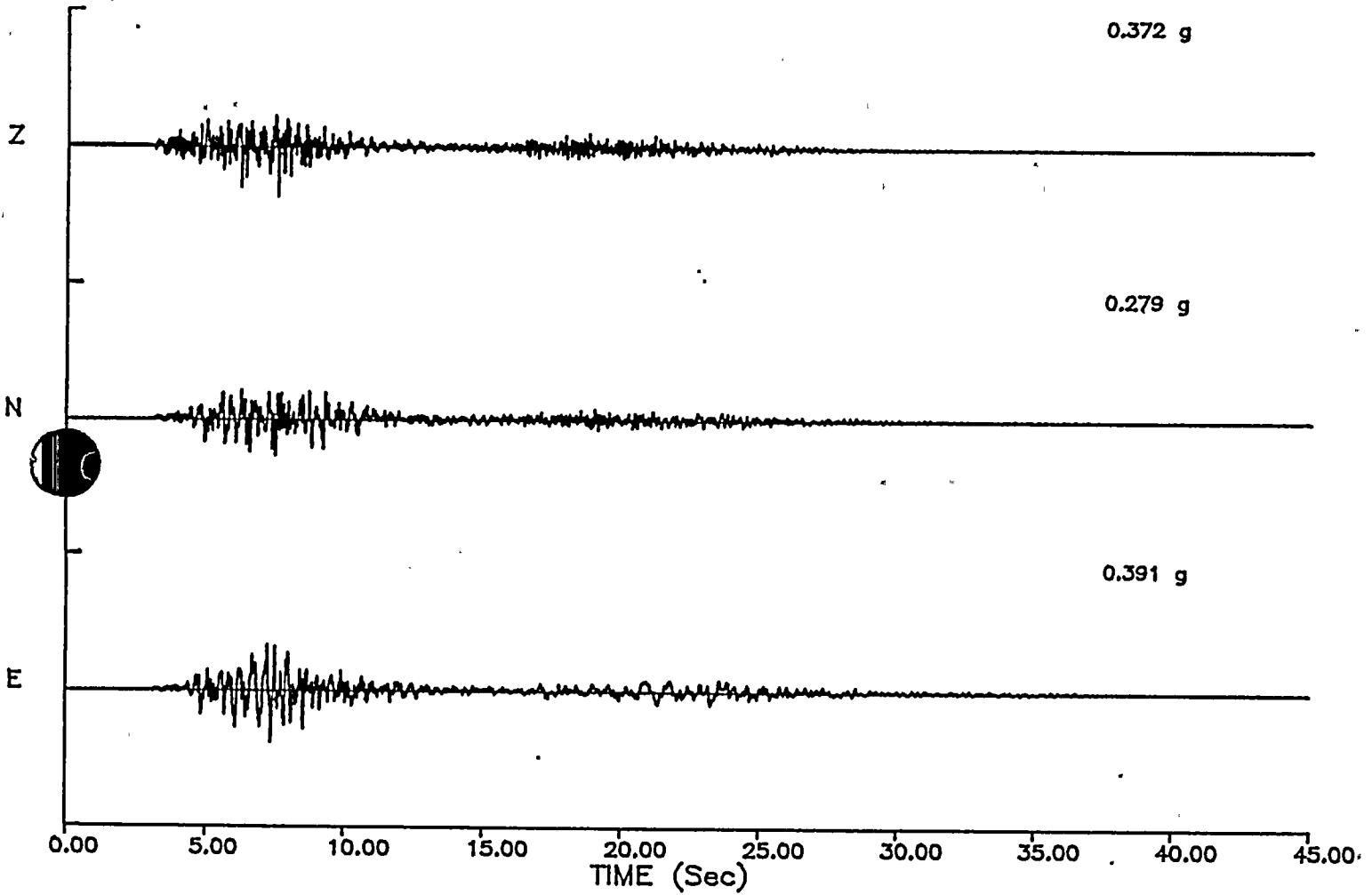


Figure Q10-8

Simulated accelerogram for magnitude 7.2, strike-slip, bilateral rupture at station 8 using Imperial Valley aftershock source functions.



DCP SS BIL M=7.2 IV SRCS 5/18/88 4X3 4.1 km W=0-12 RT=3.5 (K)
SS+16

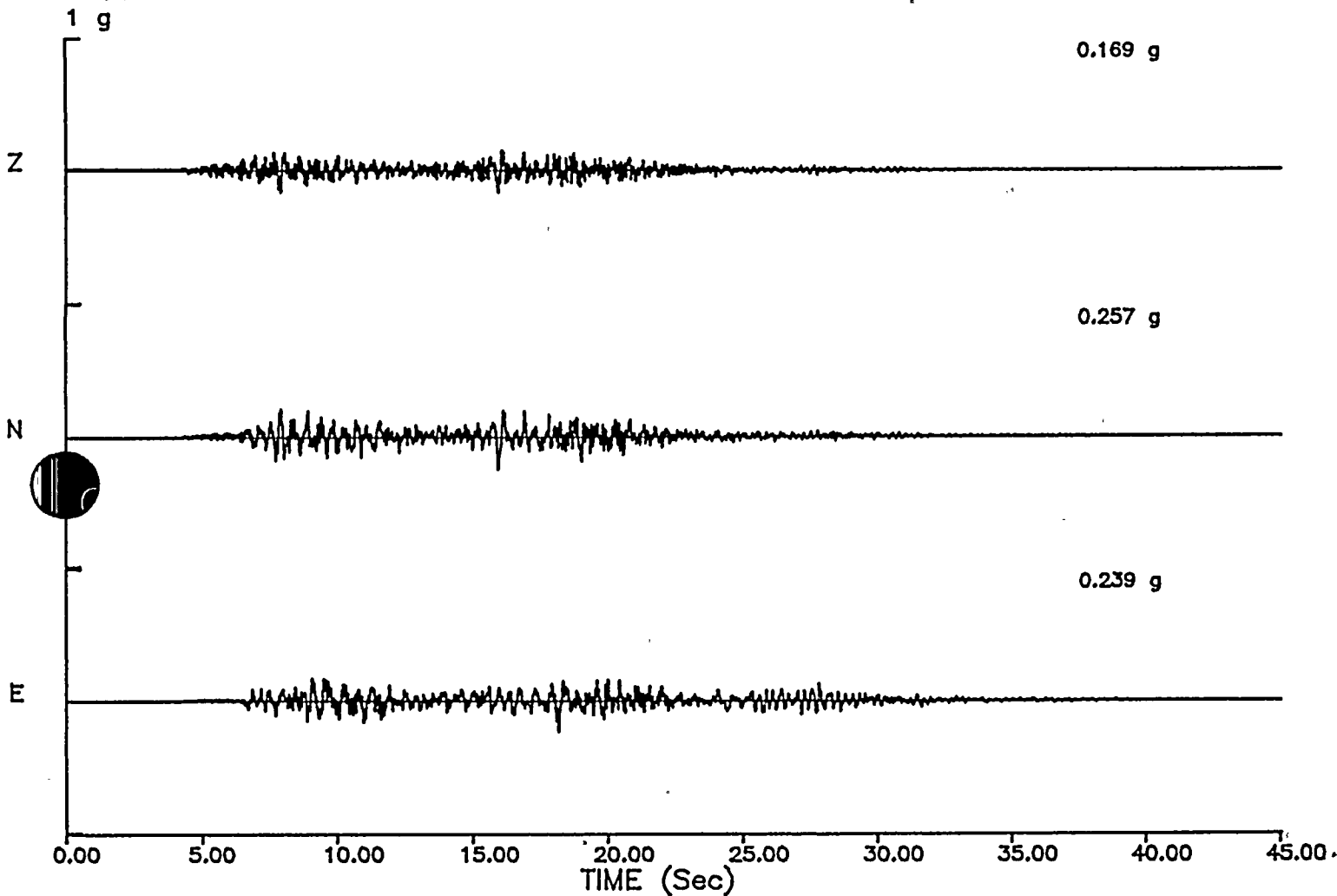


Figure Q10-9

Simulated accelerogram for magnitude 7.2, strike-slip, bilateral rupture at station 16 using Imperial Valley aftershock source functions.



DCP SS BIL M=7.2 IV SRCS 5/18/88 4X3 4.1 km W=0-12 RT=3.5 (K)
SS+24
1 g

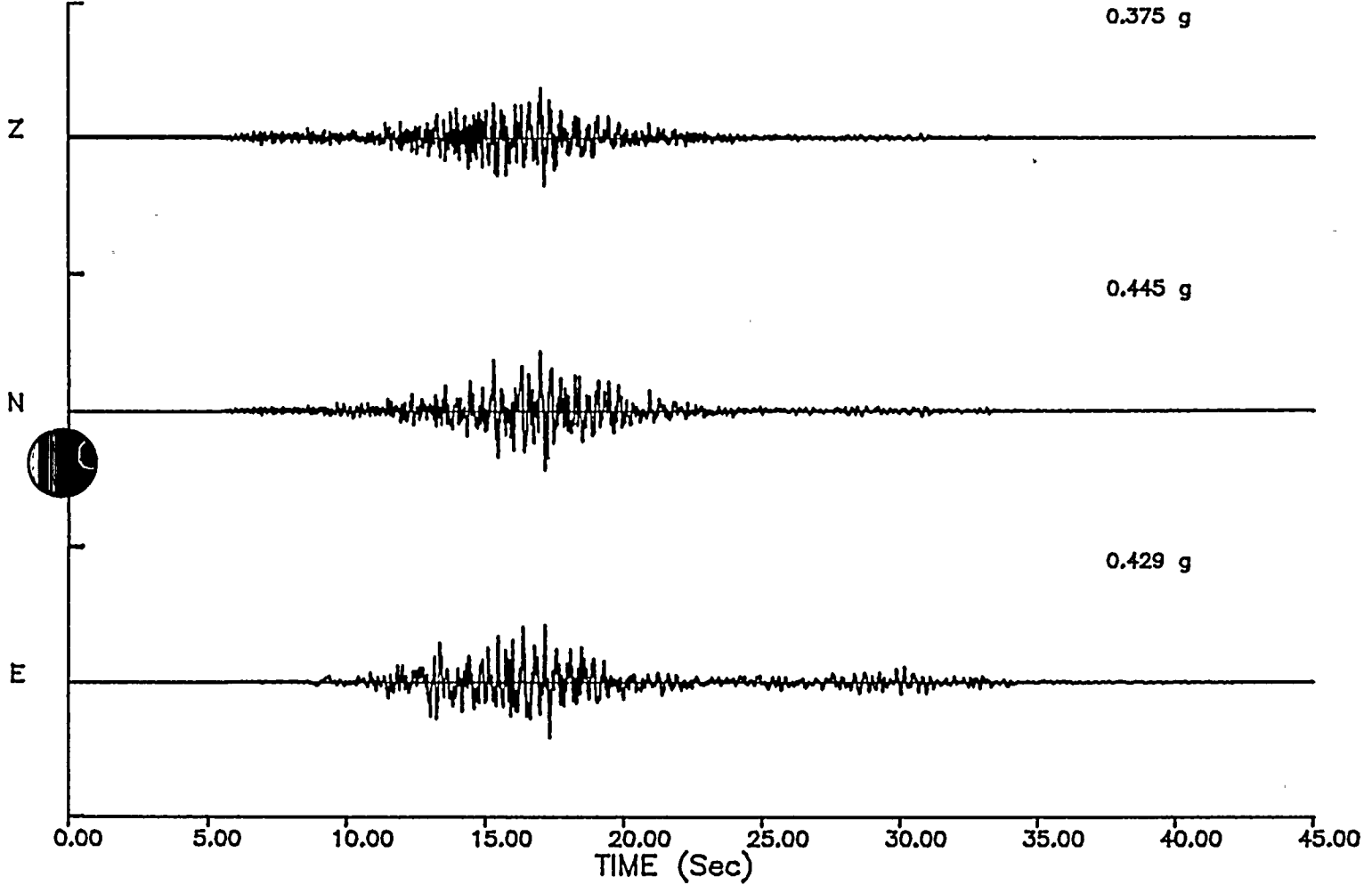


Figure Q10-10

Simulated accelerogram for magnitude 7.2, strike-slip, bilateral rupture at station 24 using Imperial Valley aftershock source functions.



DCP SS BIL M=7.2 IV SRCS 5/18/88 4X3 4.1 km W=0-12 RT=3.5 (K)
SS+32

1 g

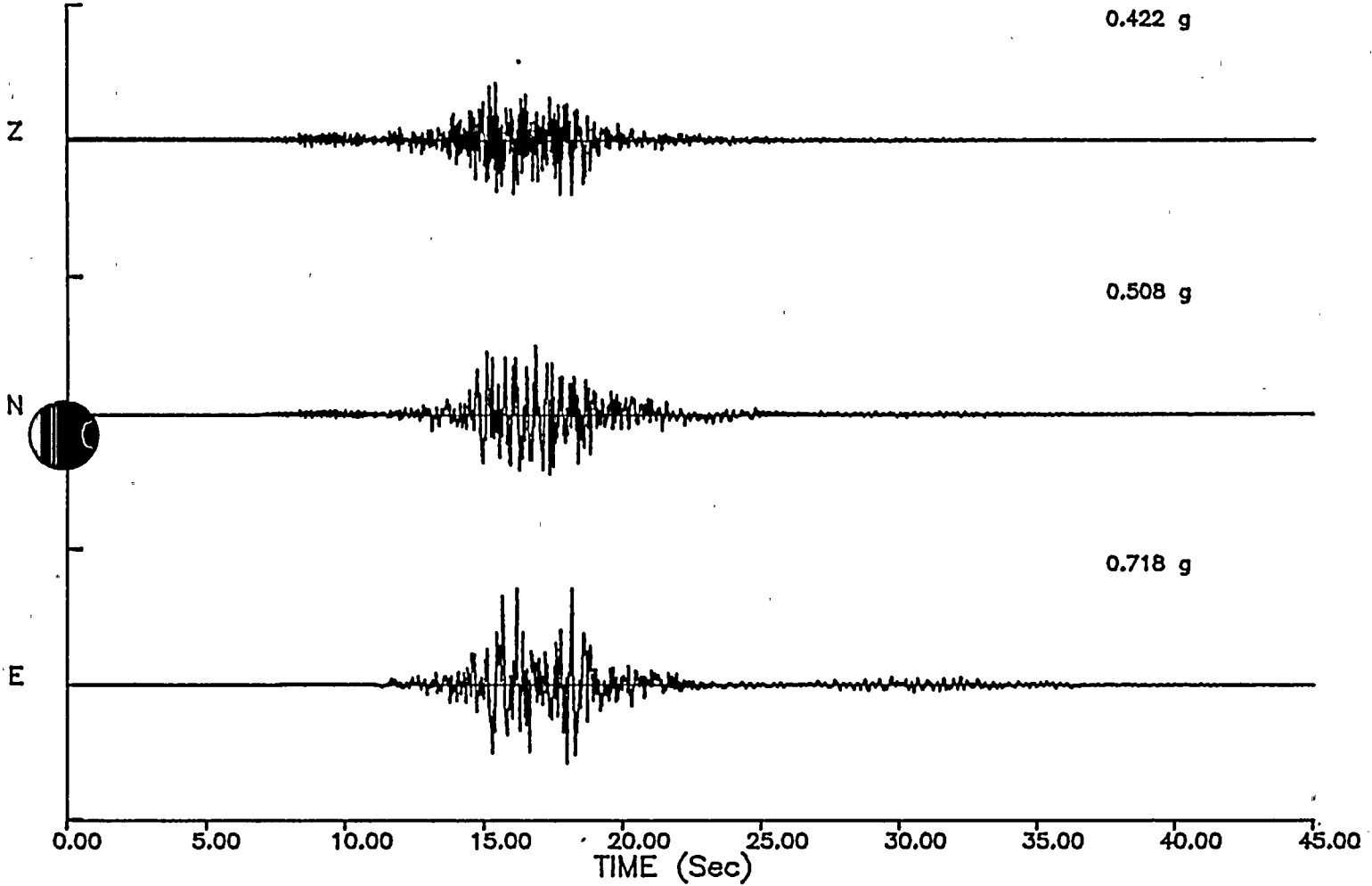


Figure Q10-11

Simulated accelerogram for magnitude 7.2, strike-slip, bilateral rupture at station 32 using Imperial Valley aftershock source functions.



DCP SS BIL M=7.2 IV SRCS 5/18/88 4X3 4.1 km W=0-12 RT=3.5 (K)
SS+40

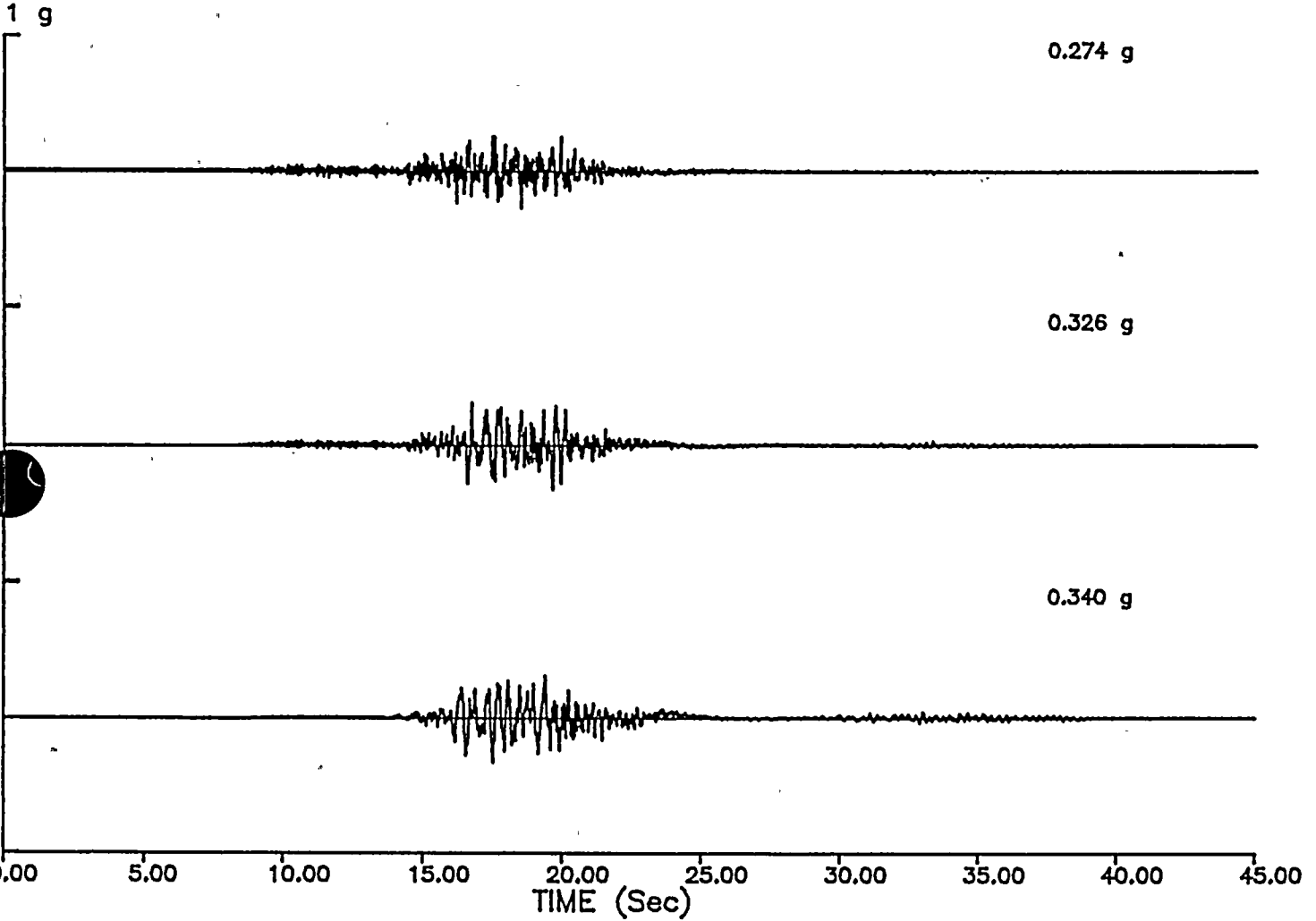


Figure Q10-12

Simulated accelerogram for magnitude 7.2, strike-slip, bilateral rupture at station 40 using Imperial Valley aftershock source functions.



DCP SS BIL M=7.2 COAL SRCS 5/17/88 4X3 4.1 km W=0-12 RT=3.5
SS-40

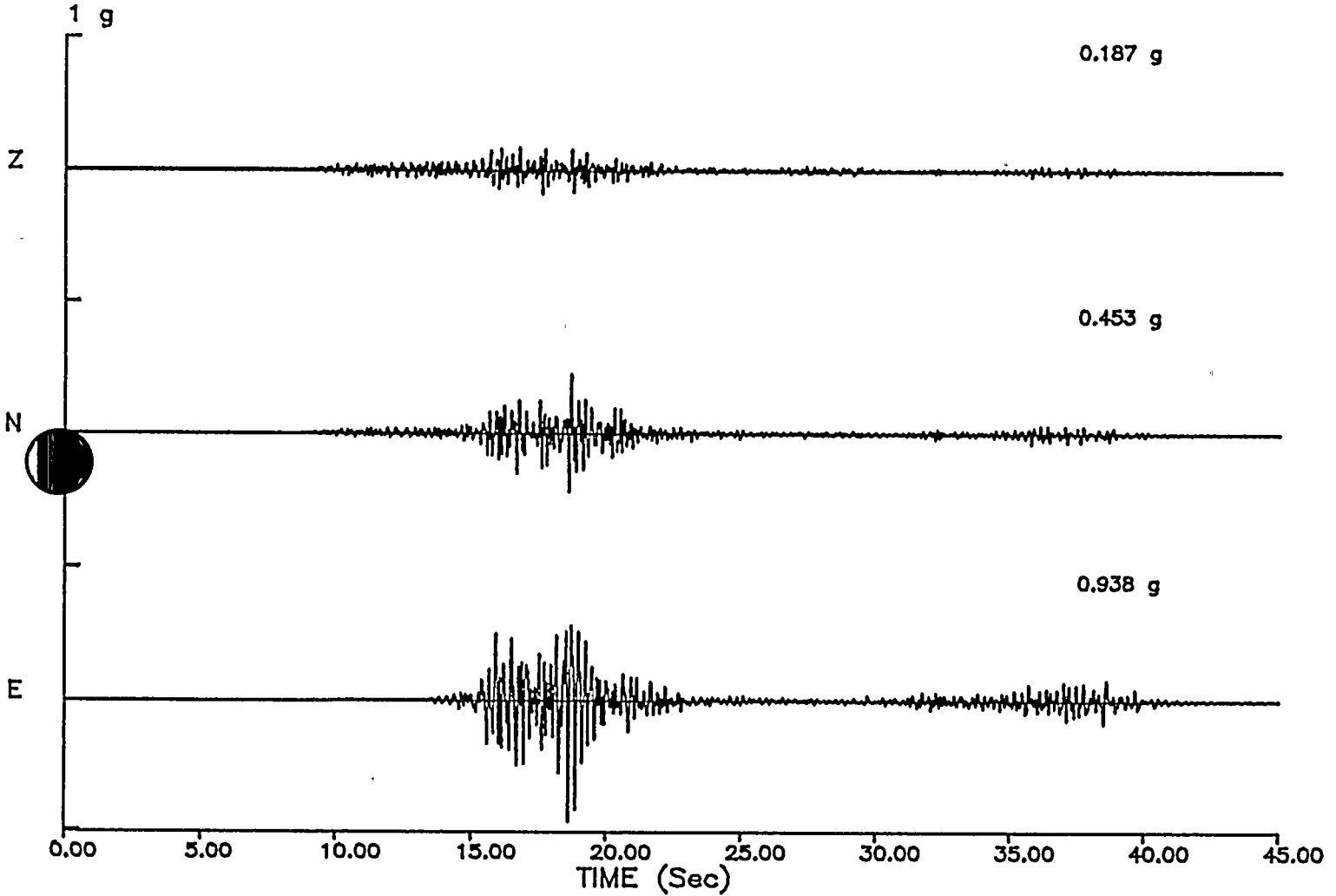


Figure Q10-13

Simulated accelerogram for magnitude 7.2, strike-slip, bilateral rupture at station -40 using Coalinga aftershock source functions.



DCP SS BIL M=7.2 COAL SRCS 5/17/88 4X3 4.1 km W=0-12 RT=3.5
SS-32

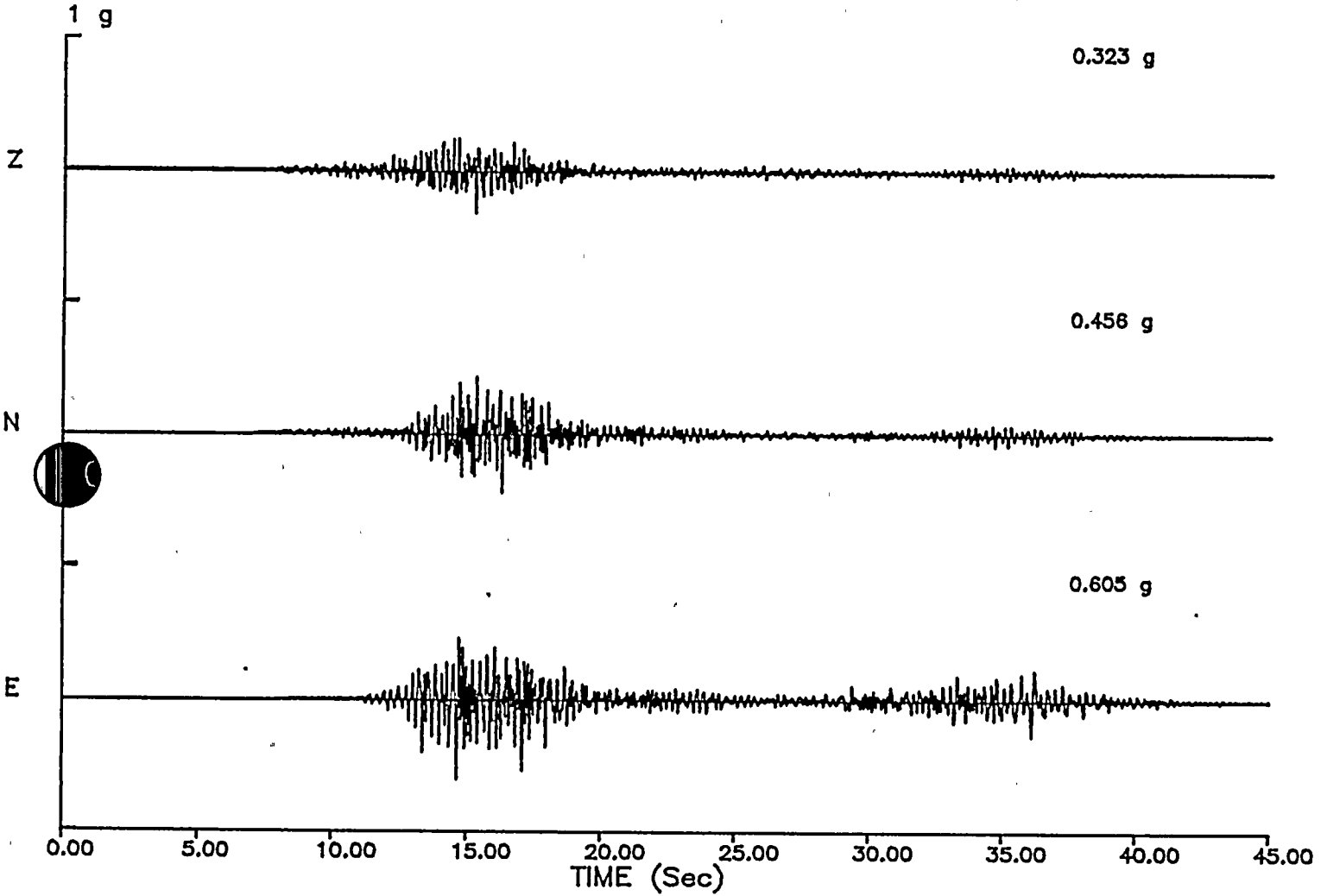
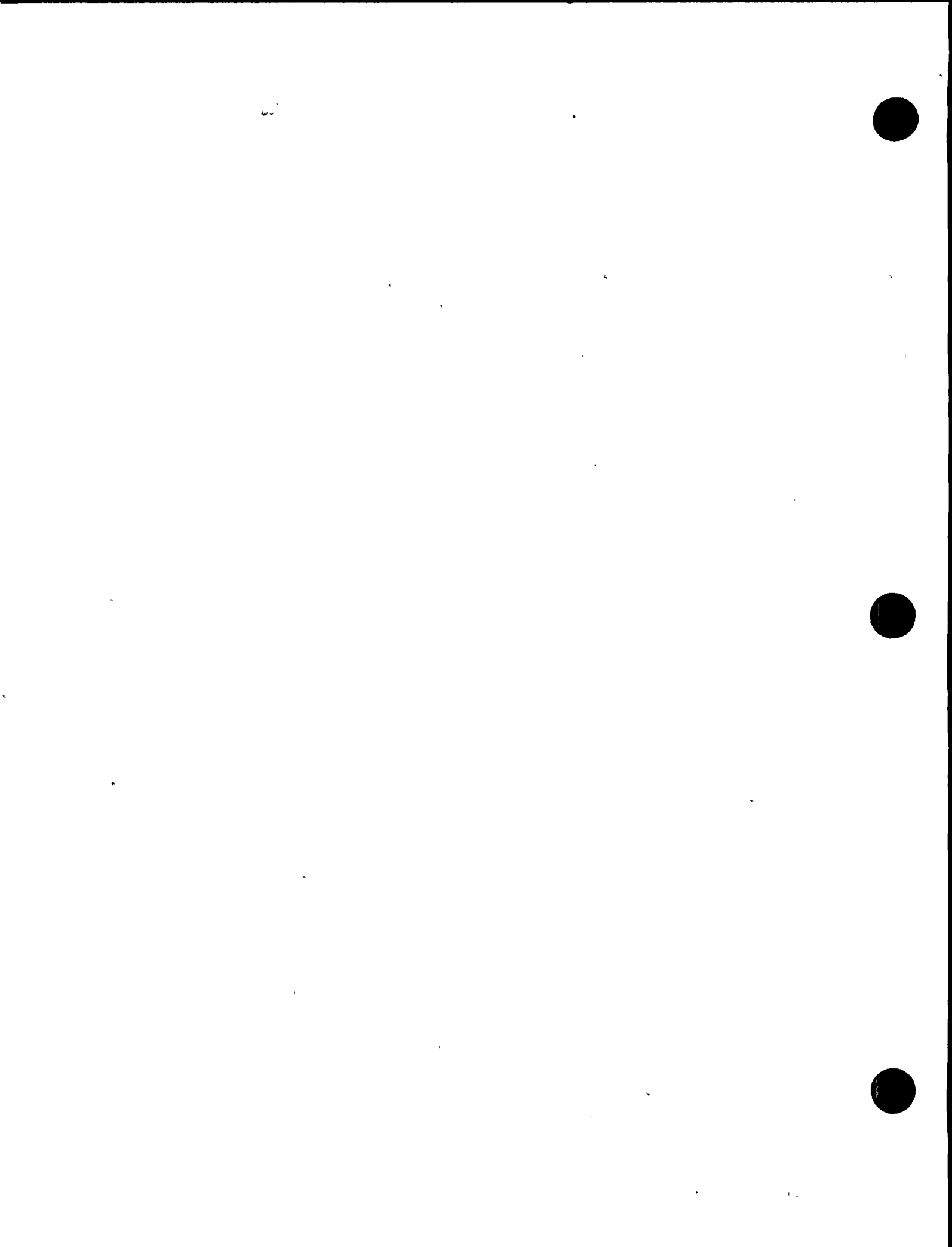


Figure Q10-14

Simulated accelerogram for magnitude 7.2, strike-slip, bilateral rupture at station -32 using Coalinga aftershock source functions.



DCP SS BIL M=7.2 COAL SRCS 5/17/88 4X3 4.1 km W=0-12 RT=3.5
SS-24

1 g

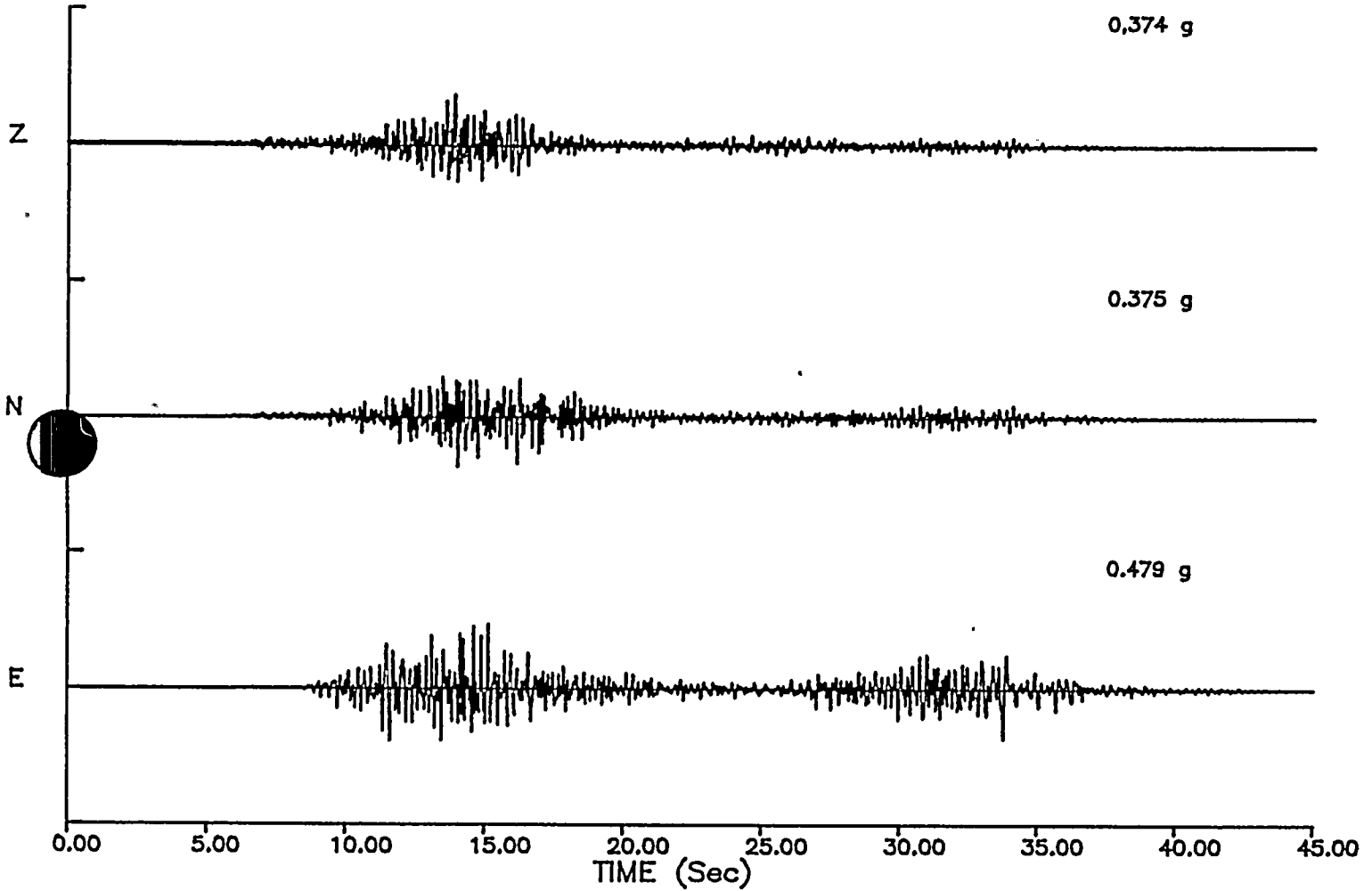


Figure Q10-15

Simulated accelerogram for magnitude 7.2, strike-slip, bilateral rupture at station -24 using Coalinga aftershock source functions.



DCP SS BIL M=7.2 COAL SRCS 5/17/88 4X3 4.1 km W=0-12 RT=3.5
SS-16
1 g

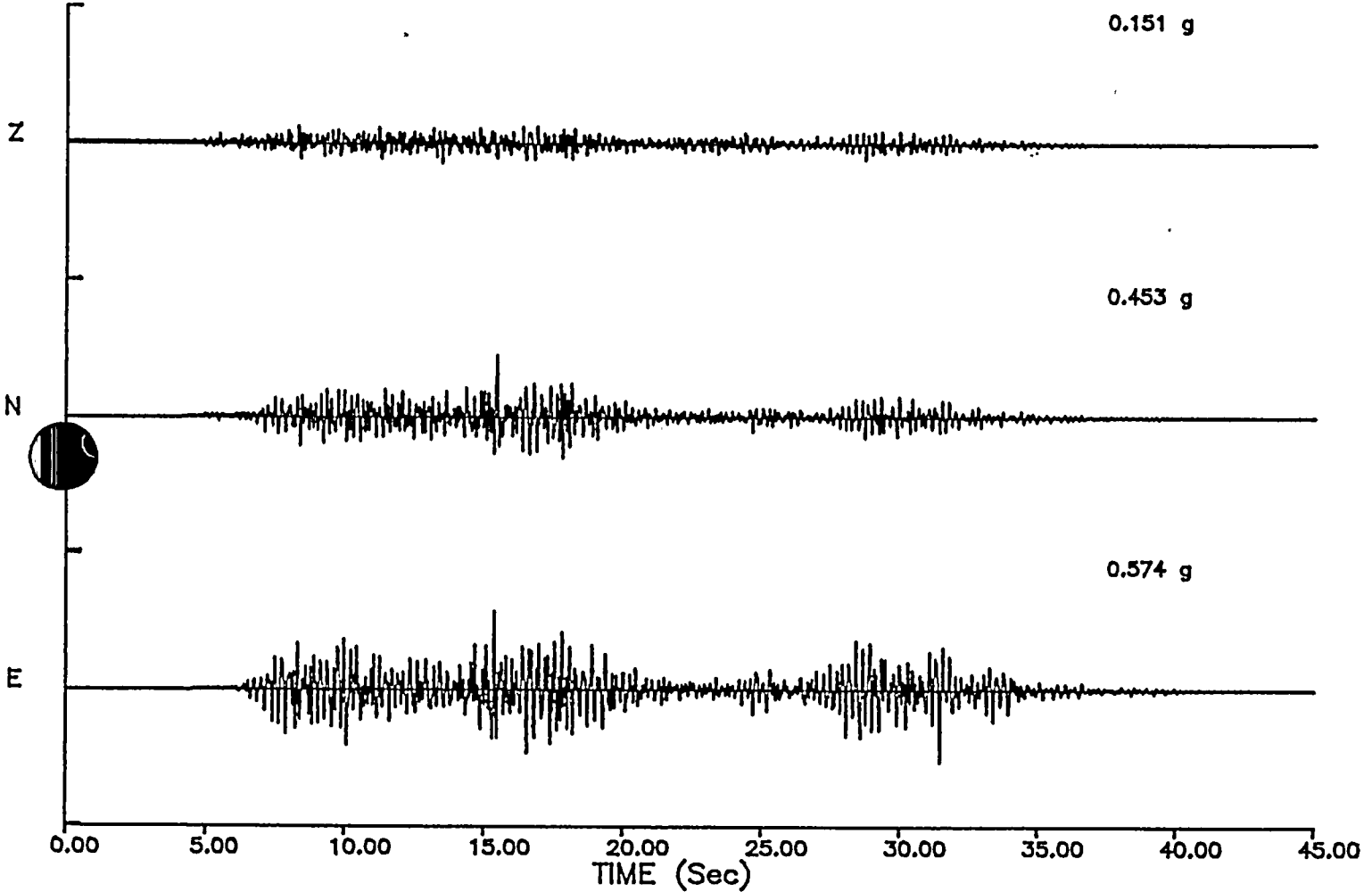


Figure Q10-16

Simulated accelerogram for magnitude 7.2, strike-slip, bilateral rupture at station -16 using Coalinga aftershock source functions.



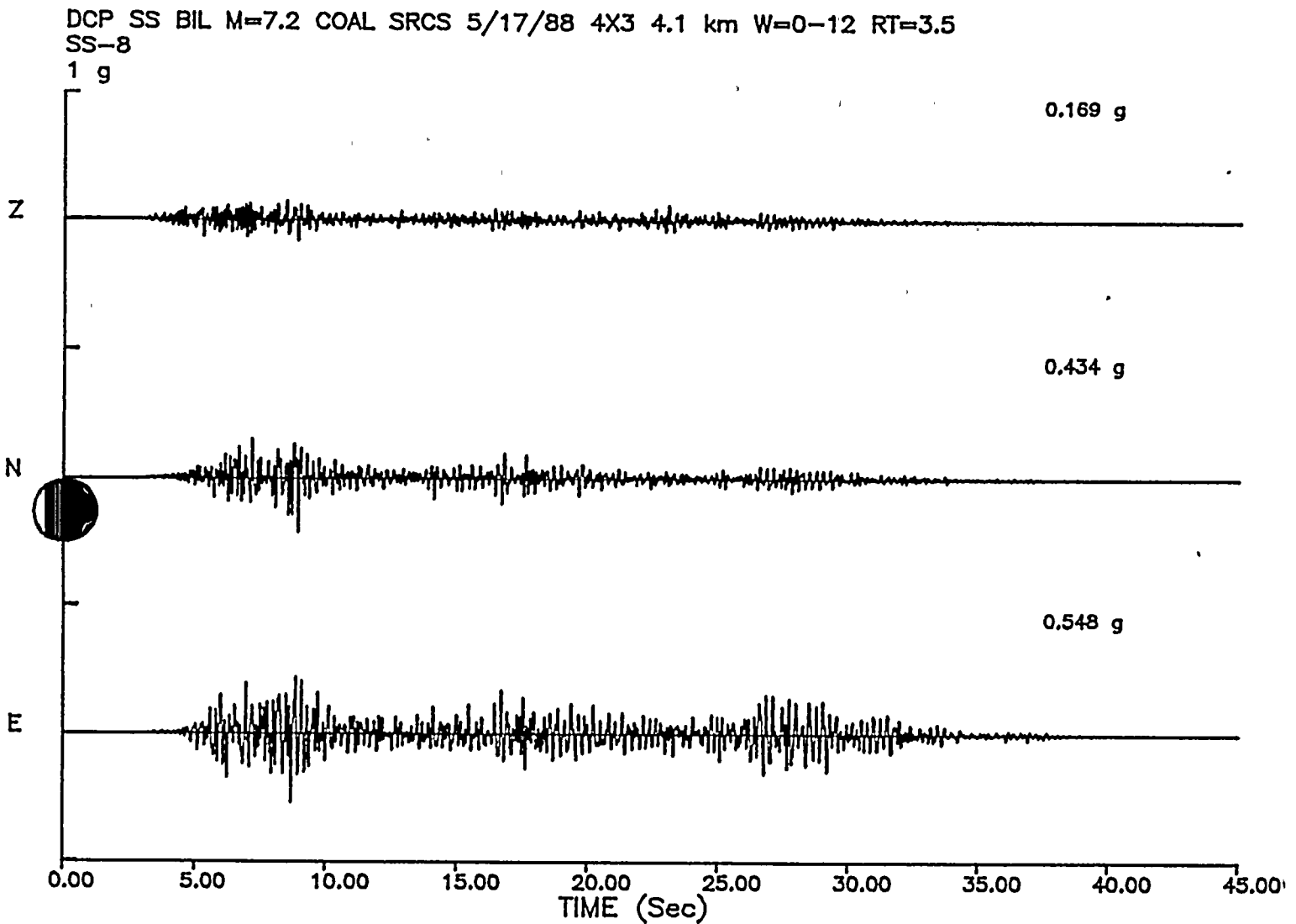


Figure Q10-17

Simulated accelerogram for magnitude 7.2, strike-slip, bilateral rupture at station -8 using Coalinga aftershock source functions.



DCP SS BIL M=7.2 COAL SRCS 5/17/88 4X3 4.1 km W=0-12 RT=3.5
SS-0

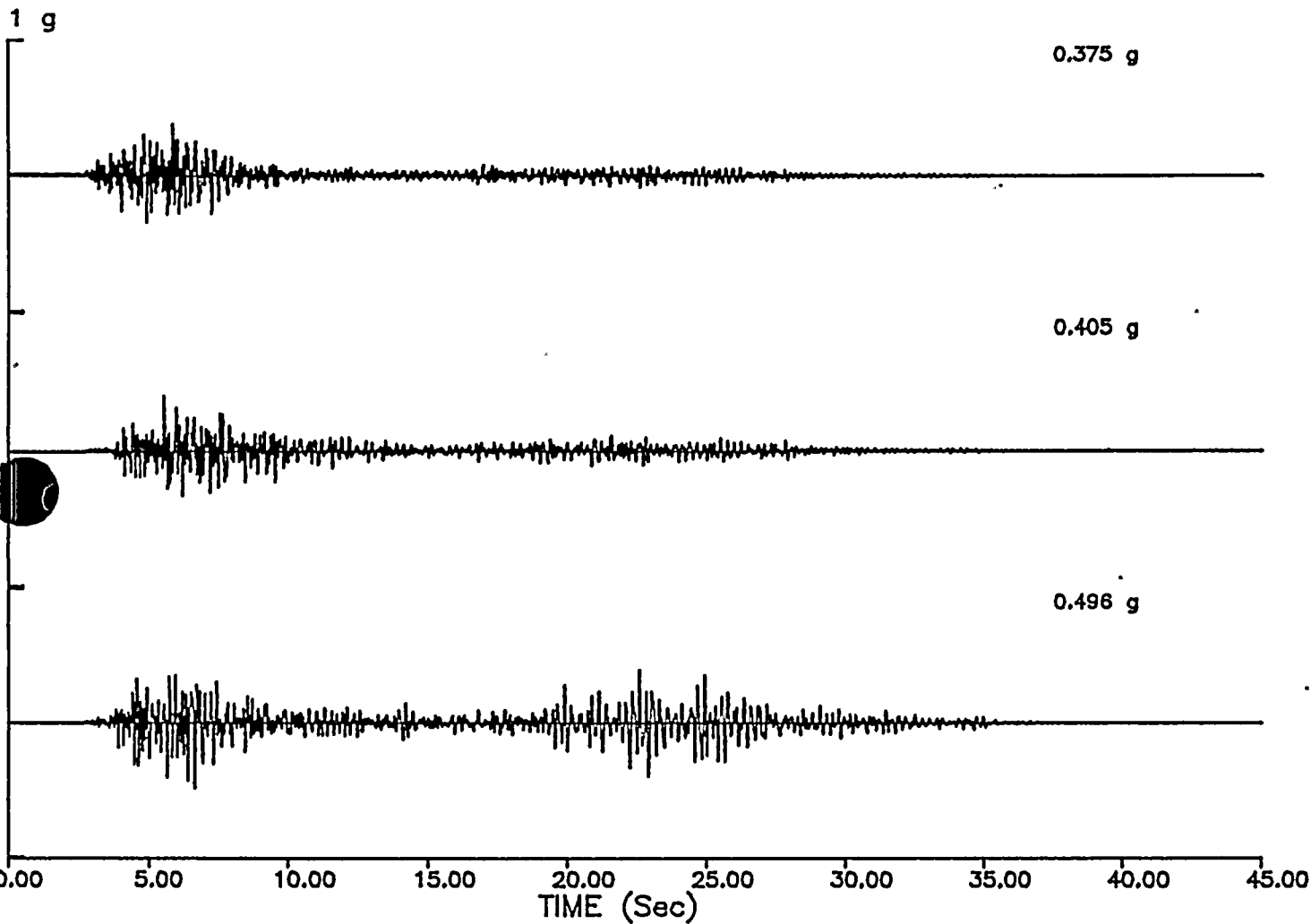


Figure Q10-18

Simulated accelerogram for magnitude 7.2, strike-slip, bilateral rupture at station 0 using Coalinga aftershock source functions.



DCP SS BIL M=7.2 COAL SRCS 5/17/88 4X3 4.1 km W=0-12 RT=3.5
SS+8
1 g

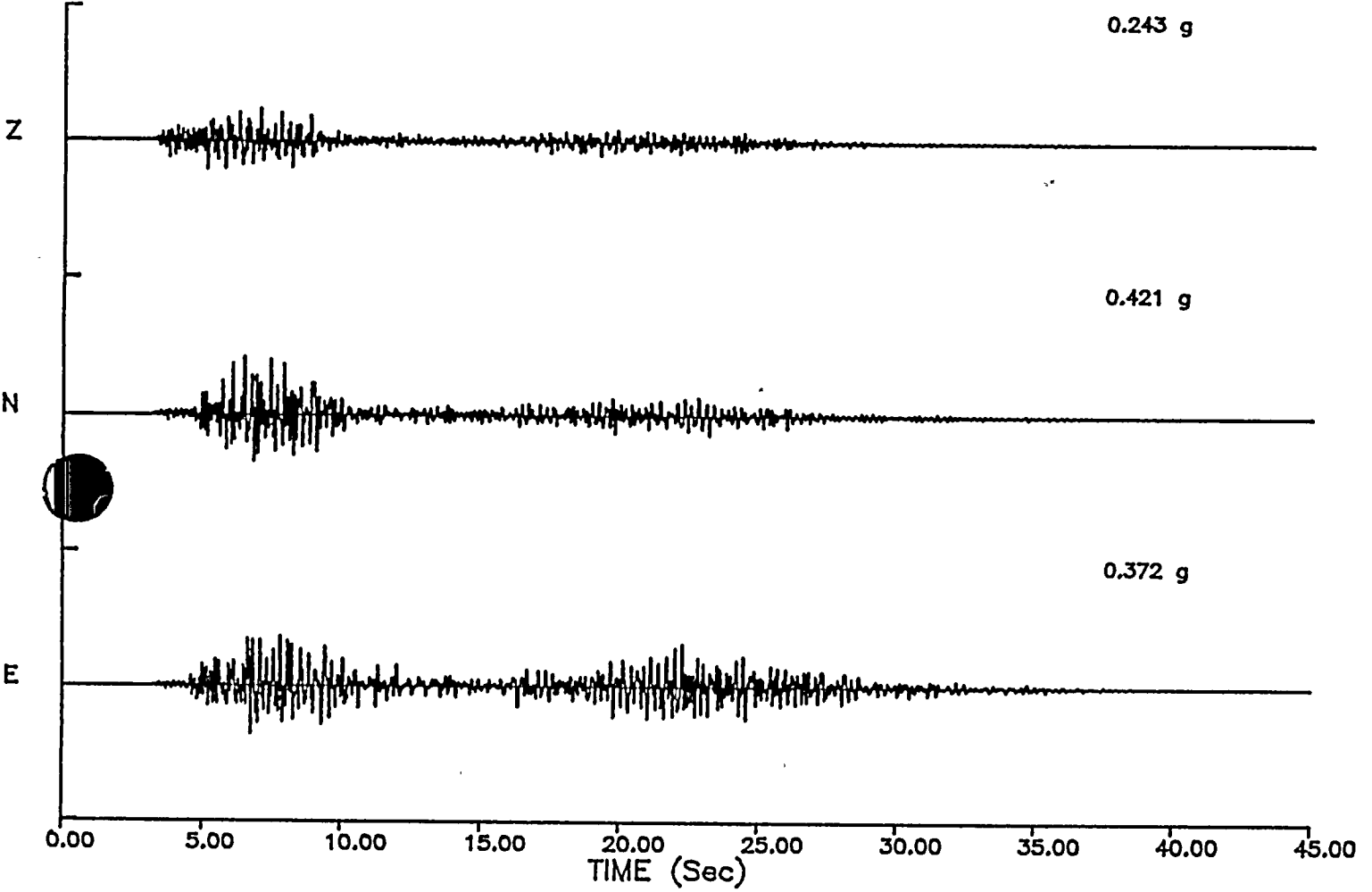


Figure Q10-19

Simulated accelerogram for magnitude 7.2, strike-slip, bilateral rupture at station 8 using Coalinga aftershock source functions.



DCP SS BIL M=7.2 COAL SRCS 5/17/88 4X3 4.1 km W=0-12 RT=3.5
SS+16
1 g

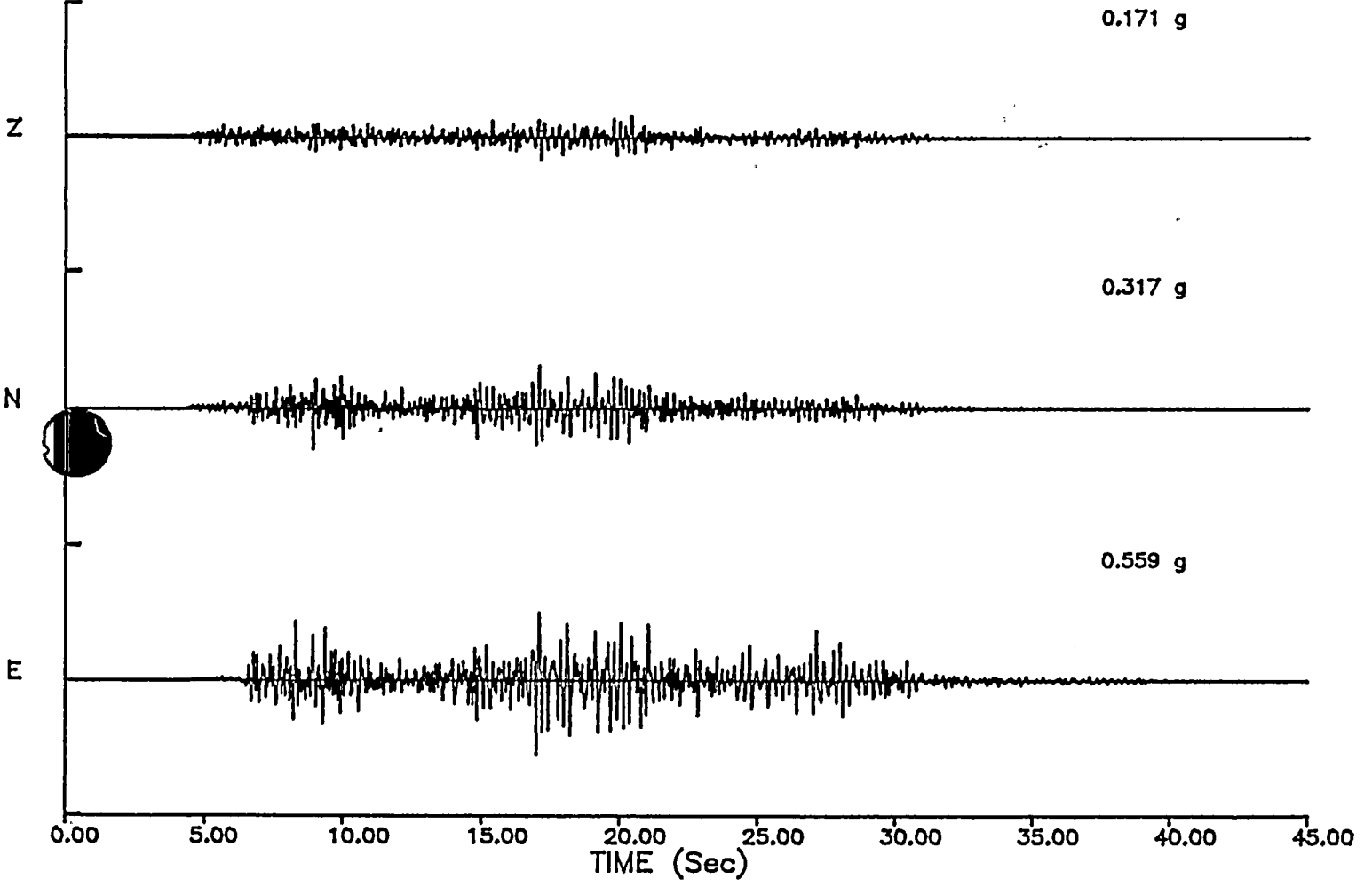


Figure Q10-20

Simulated accelerogram for magnitude 7.2, strike-slip, bilateral rupture at station 16 using Coalinga aftershock source functions.



DCP SS BIL M=7.2 COAL SRCS 5/17/88 4X3 4.1 km W=0-12 RT=3.5
SS+24

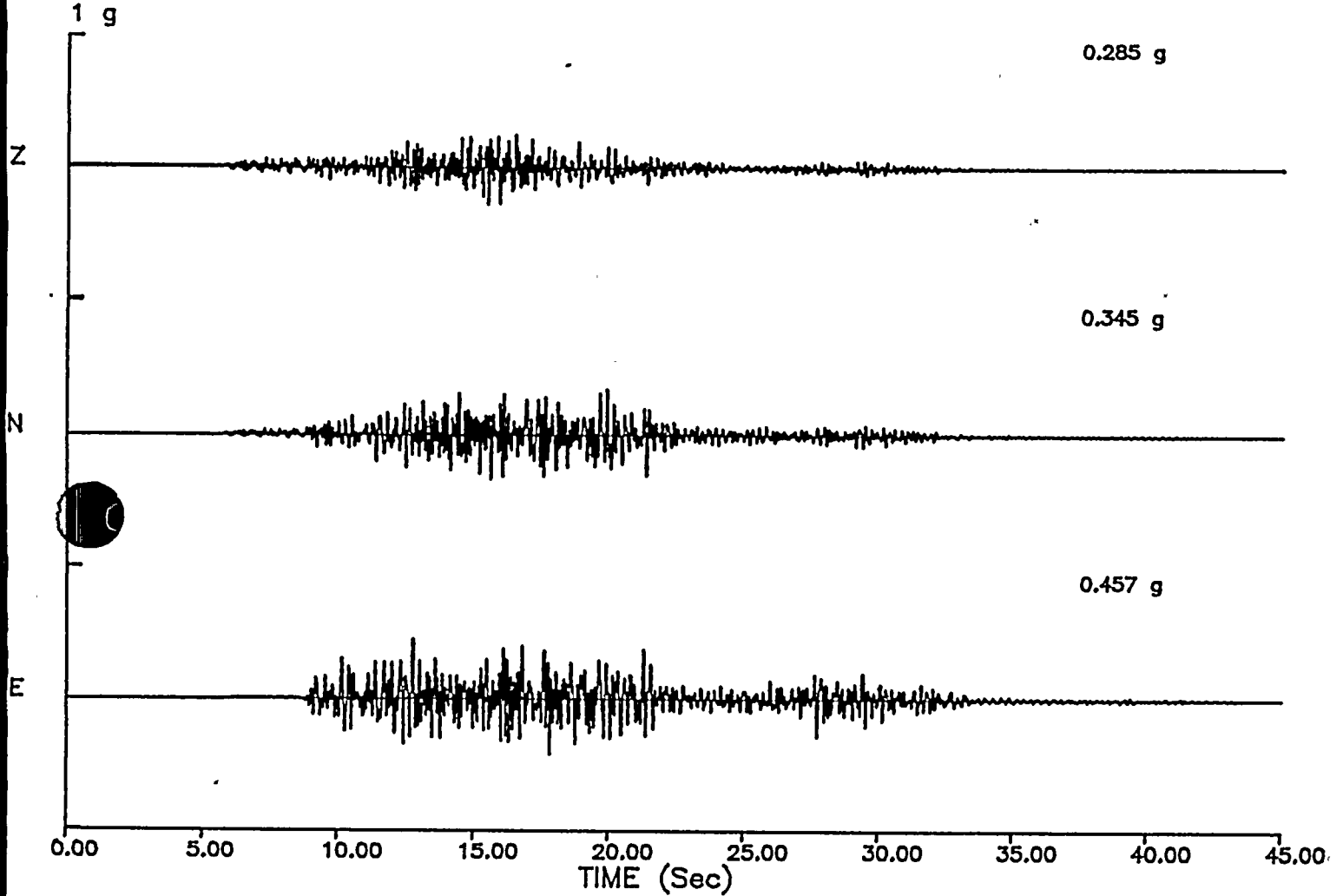


Figure Q10-21

Simulated accelerogram for magnitude 7.2, strike-slip, bilateral rupture at station 24 using Coalinga aftershock source functions.



DCP SS BIL M=7.2 COAL SRCS 5/17/88 4X3 4.1 km W=0-12 RT=3.5
SS+32

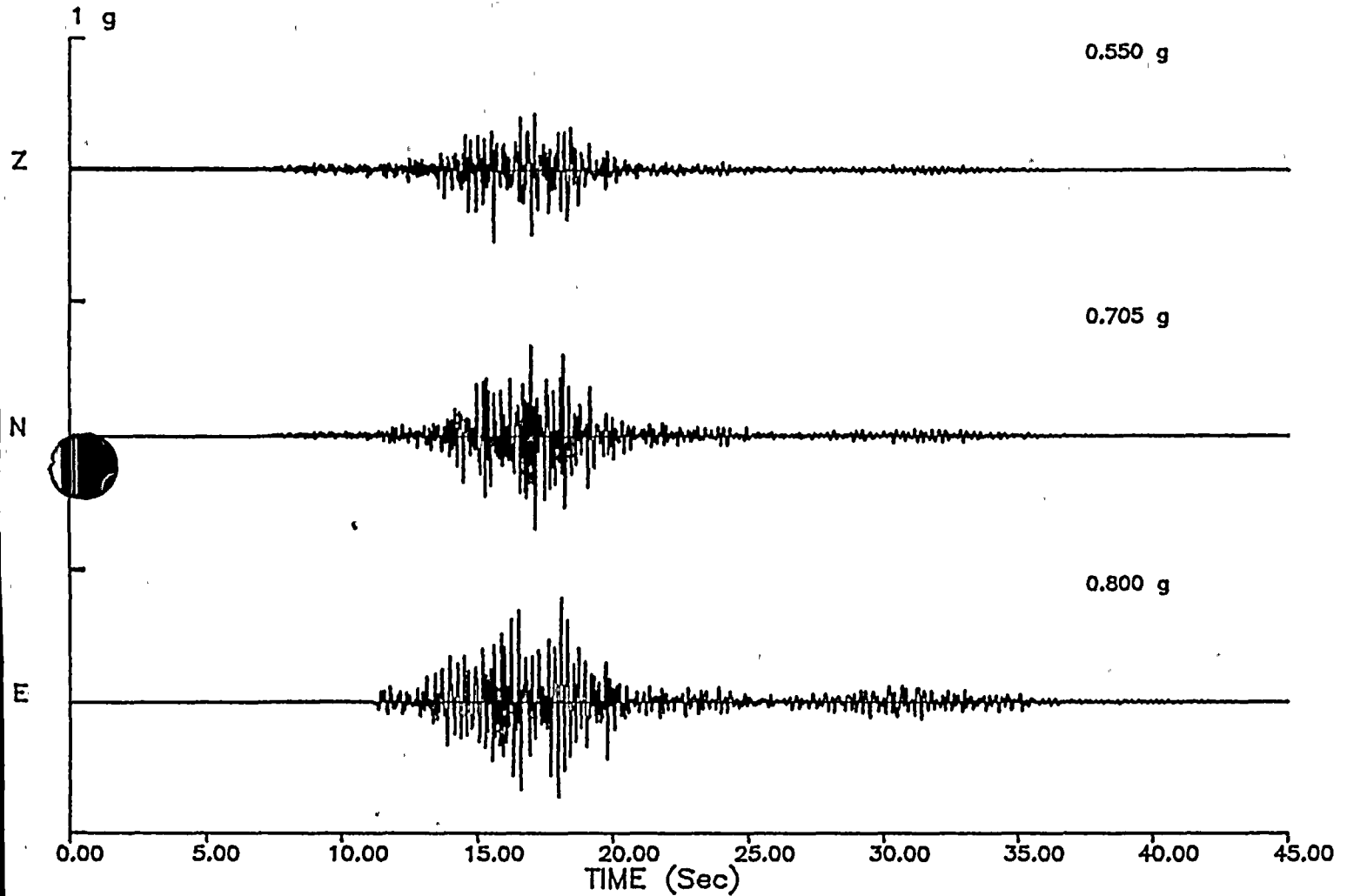


Figure Q10-22

Simulated accelerogram for magnitude 7.2, strike-slip, bilateral rupture at station 32 using Coalinga aftershock source functions.



DCP SS BIL M=7.2 COAL SRCS 5/17/88 4X3 4.1 km W=0-12 RT=3.5
SS+40
1 g

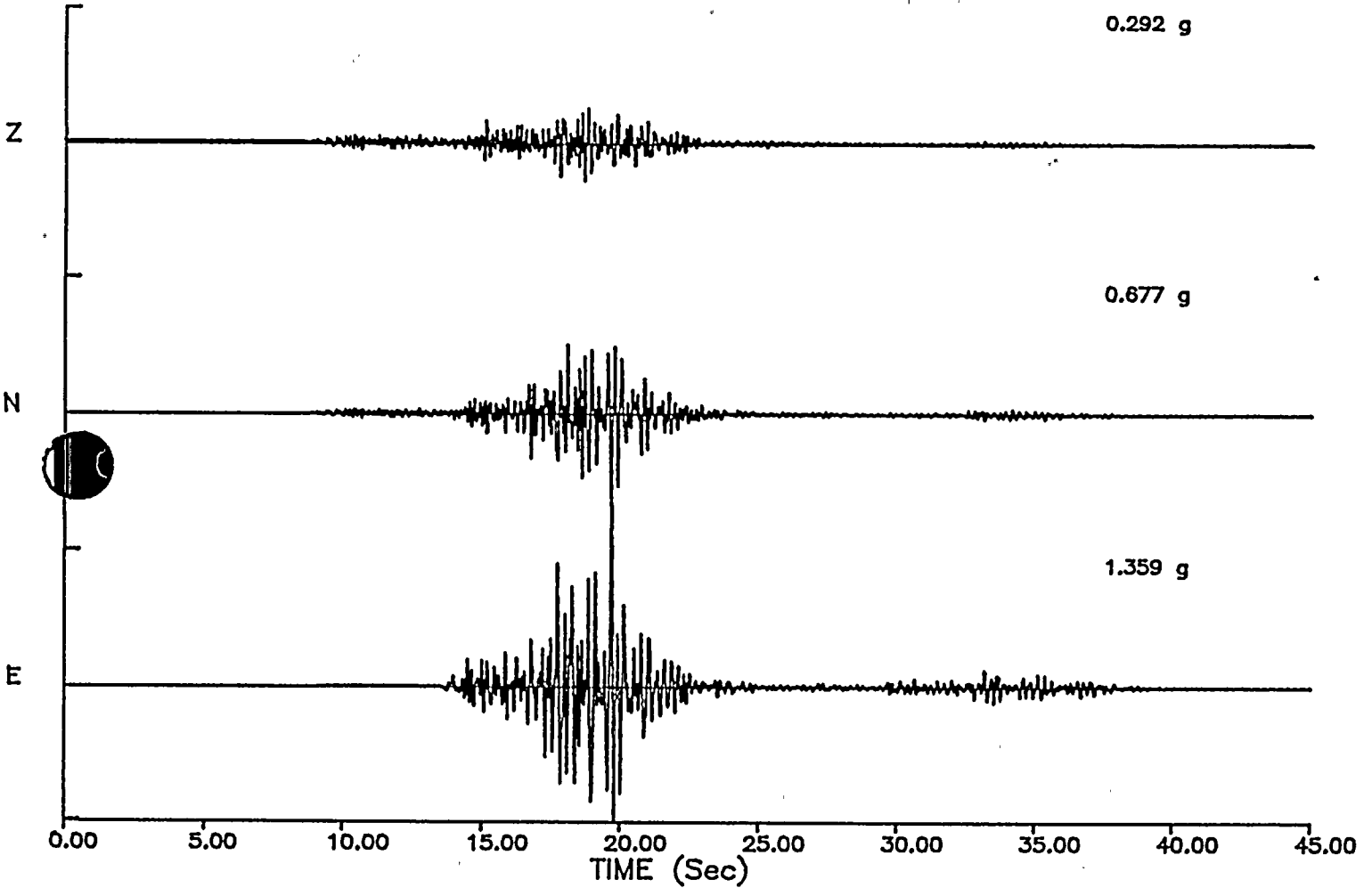


Figure Q10-23

Simulated accelerogram for magnitude 7.2, strike-slip, bilateral rupture at station 40 using Coalinga aftershock source functions.



QUESTION 11

The amplitudes of low frequency portion of the spectra generated in the numerical modeling study appear to be deficient. At what frequencies are these spectra dependable?

The response spectra of the time histories generated by numerical modeling are dependable for frequencies of 2 Hz and above. This is demonstrated in the deviation between recorded and simulated response spectral acceleration from a total of 18 recordings of three earthquakes (see response to Question 16, February 1989). The deviation is small; it either slightly overpredicts or is not significantly different from zero for all frequencies above 2 Hz, as shown in Figure Q11-1 (Figure Q16-2, February 1989). Note that the negative sign of the deviation between 2 and 10 Hz indicates that the simulation procedure overpredicts the data by 5 to 30 percent.

Below 2 Hz, the deviation changes abruptly, becoming positive and significantly different from zero; the simulation procedure underpredicts the low frequency response by a factor of up to 1.6. The reason for this underprediction is related to the method that was used to calculate the simplified theoretical Green's functions in the simulation procedure. Because the frequencies of interest at the plant are above 2 Hz, the generalized ray method was chosen for its computational efficiency and accuracy at high frequencies. This method does not include surface wave contributions. Surface waves are not significant above 2 Hz, however, and we conclude that the response spectra of the time histories generated by numerical modeling are dependable for frequencies of 2 Hz and above.





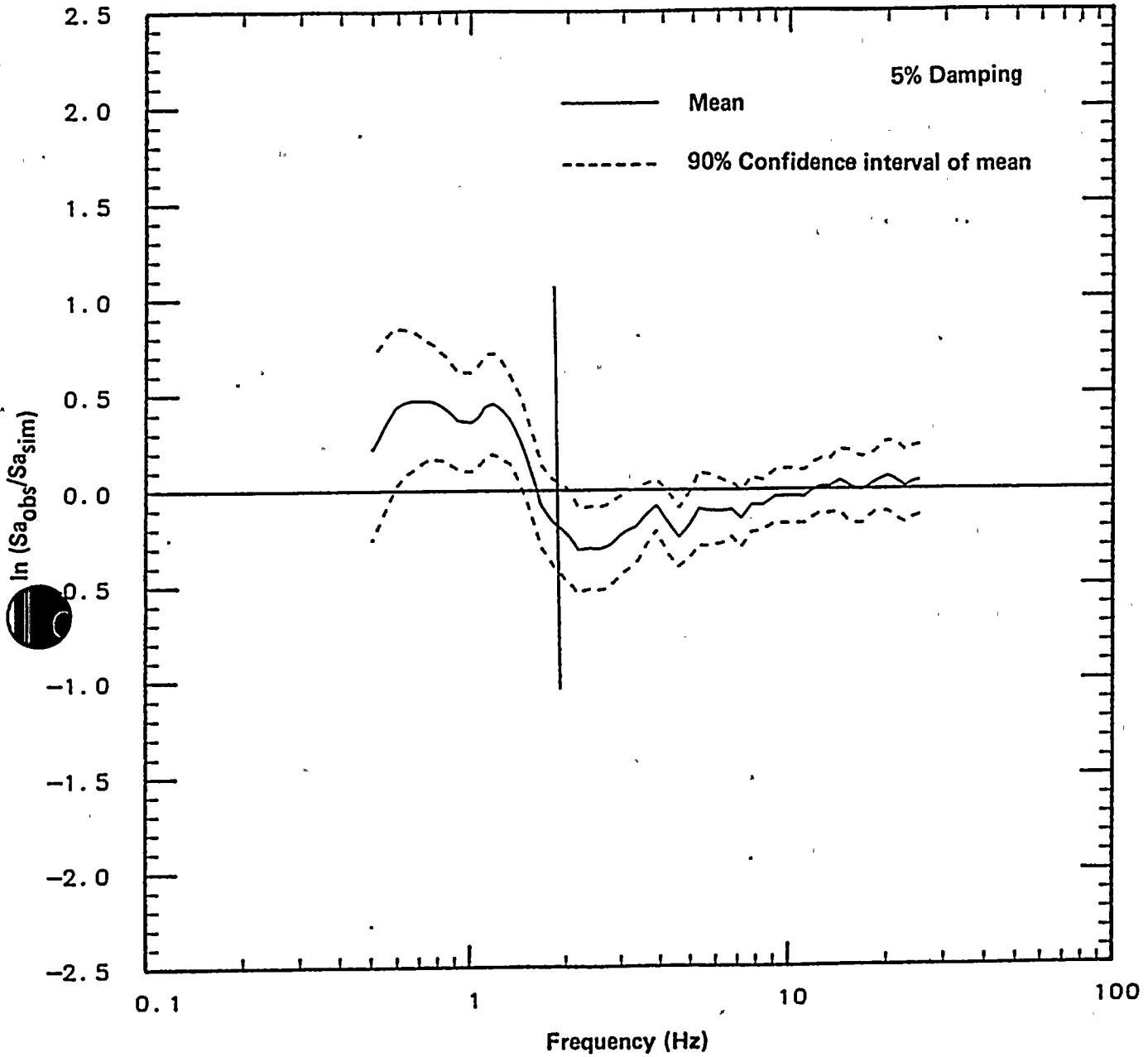


Figure Q11-1

Deviation between recorded and simulated horizontal response spectral acceleration averaged over all earthquake-station pairs.



QUESTION 12

To aid in assessing the proposed lack of topographic effect at the Diablo Canyon site, provide a numerical study using vertically polarized shear waves with ground motion amplitude referenced to sea level.

The lack of significant topographic effects on ground motions at the Diablo Canyon site was demonstrated using finite difference modeling for SH waves. The results were presented in the Final Report, July 1988, and in our response to Question 17a, January 1989.

In response to the present question, we have made two additional studies. Both studies were based on SV waves incident on a cross section selected to have the maximum topographic relief in the site area. Furthermore, rock properties identical to those used in the soil/structure interaction analyses presented in the Final Report, July 1988, were incorporated into this cross section.

The first study described below extended our earlier finite difference modeling to using SV pulses having Gaussian Fourier acceleration spectra. This study was made to assess the sensitivity of potential topographic effects to incident wave type and wave frequency, as well as incidence angle. The second study was based on finite element modeling using one of the site-specific acceleration time histories used in the soil/structure interaction analyses as the input control motion. This study was made to show potential topographic effects on the site-specific ground motions for the Diablo Canyon site.

The results of both studies, as presented below, further confirm the lack of significant topographic effects on ground motions at the location of the power block structures at the Diablo Canyon site.

Finite Difference Modeling

In this study, the effects of topography on ground motions at the site were investigated using finite difference calculations that assumed linear elasticity of the foundation rock. A site plan showing the location of the cross section analyzed is shown on Figure Q12-1. A topographic profile of this section is shown at the bottom of Figure Q12-2. The material properties of the rock are summarized in Table Q12-1. The input ground motion was a Gaussian pulse whose Fourier acceleration spectrum was centered at a frequency of 2.5 Hz, which is comparable to the Fourier spectra of the suite of empirical strong motion records used to develop the input spectrum for the soil/structure interaction analyses. An example of the accelerograms calculated for a vertically incident SV wave is shown at the top of Figure Q12-2. The delay between stations 15 and 1 represents the propagation time of the wave between sea level and the elevation of the top of the ridge. Peak amplitudes are shown to the right of the accelerograms for station locations along the topographic profile shown at the bottom of Figure Q12-2.

Figure Q12-3 shows the response of the site region for a series of different input ground motions. The response is represented by the ratio of peak acceleration for the model having topography to the peak acceleration for the model having no topography, which defines the free-field control motion. The response of the site region to a vertically propagating SV wave shows a slight deamplification at the base of the sea cliff and a peak amplification of about 17 percent at its crest. The motion at the location of the power block structures is generally deamplified; at its greatest, the deamplification is about 15 percent.

The sensitivity of this response to incidence angle is illustrated using an SV wave incident from the left (ocean side) at 20 degrees from vertical. The response is quite similar to that for vertical incidence, but the regions of amplification at the crest of the sea cliff and the crest of the ridge, and the region of deamplification at the base of the ridge are extended toward the east due to the excitation of Rayleigh waves. The location of the power block structures is again within a region of mostly deamplification, which in this case now extends farther right to the lower part of the ridge.



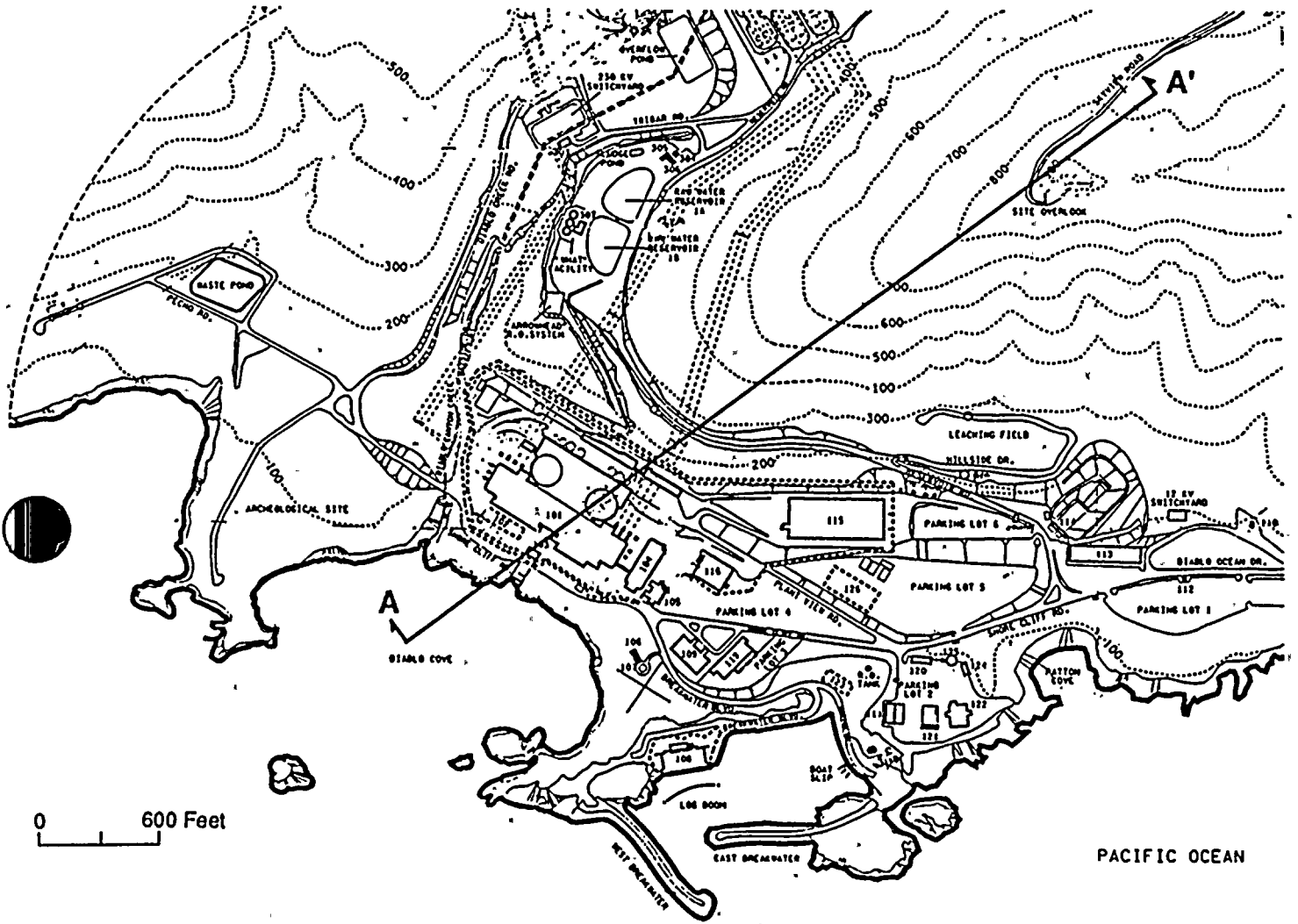
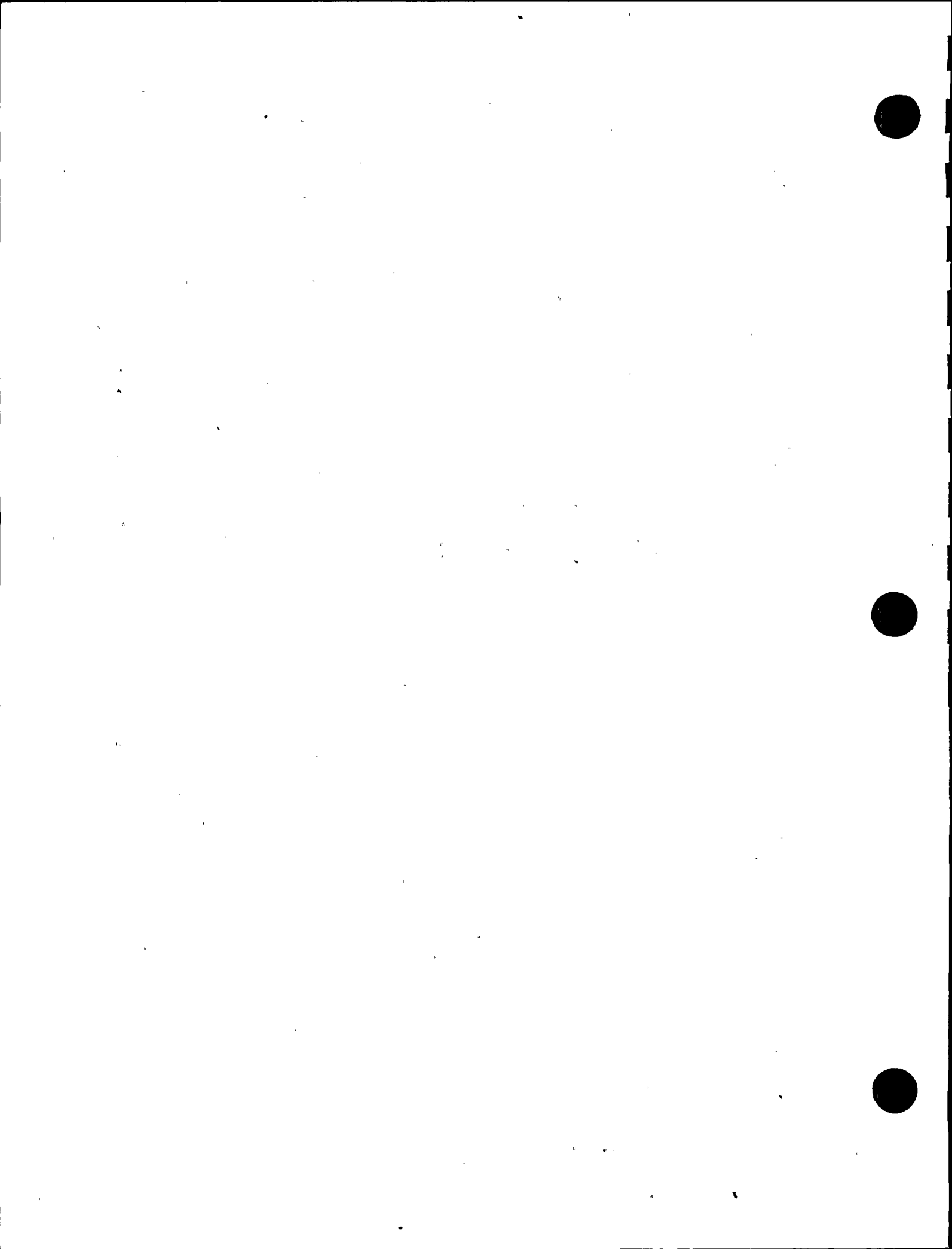


Figure Q12-1

Site plan showing location of cross section A-A' analyzed for topographic effects on ground motions in the Plant area.



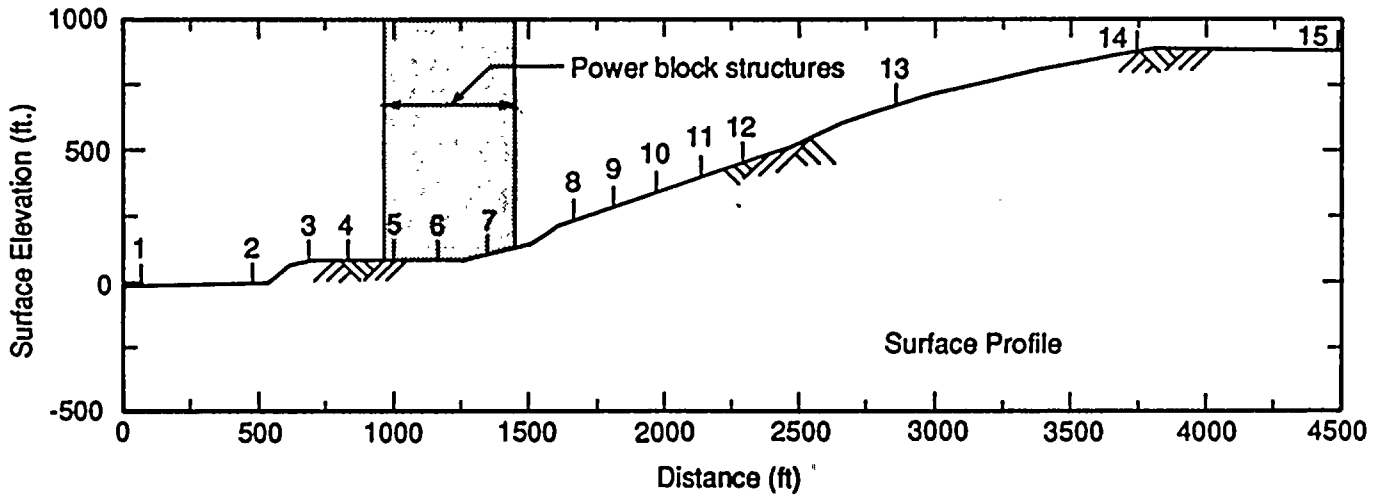
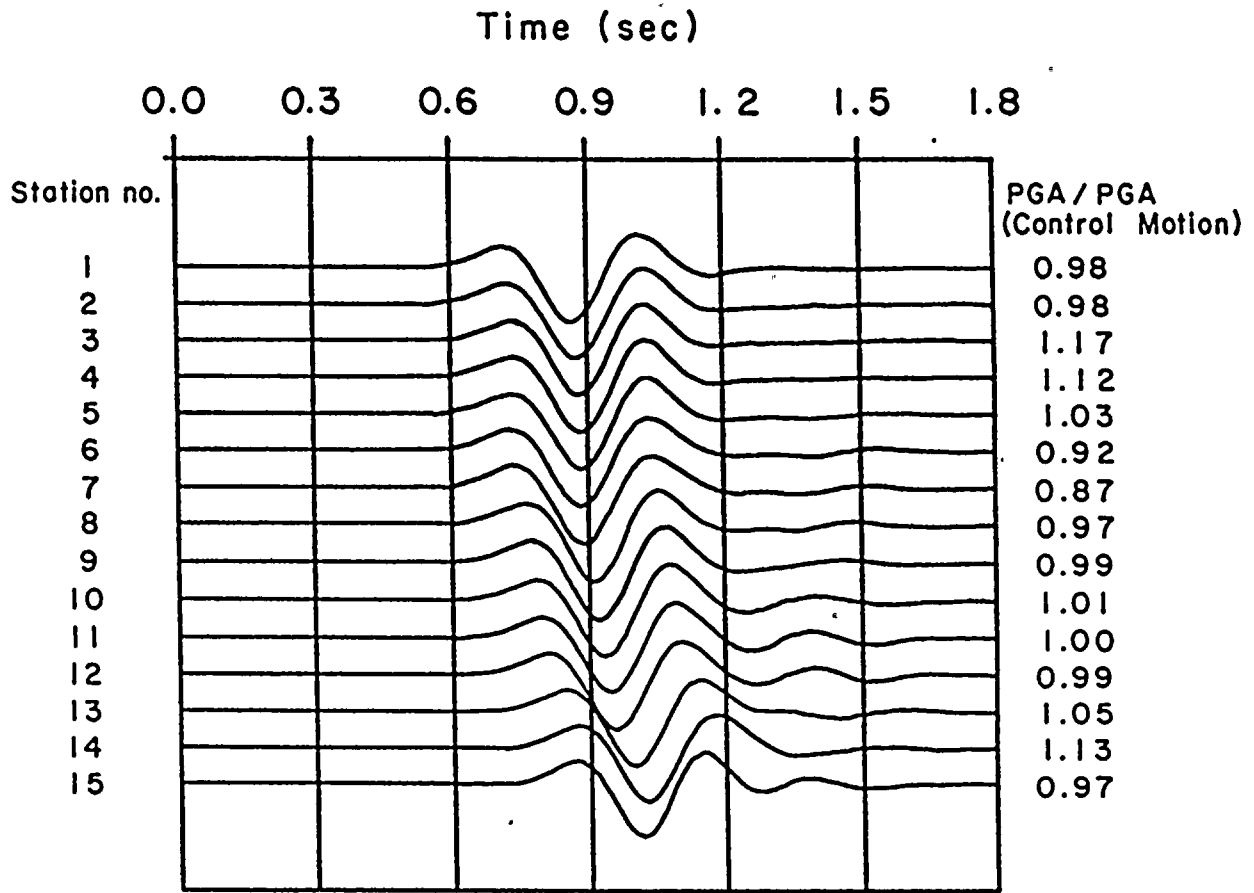


Figure Q12-2

Accelerogram calculated for a vertically incident SV wave, and topographic profile, cross section A-A'.



Table Q12-1
ROCK PROPERTIES USED IN ANALYSIS

Depth (ft)	Layer Thickness (ft)	Density (pcf)	Shear Wave Velocity (fps)	Poisson's Ratio
	15	140	2600	0.45
15 -				
	20	140	3300	0.40
35 -				
	125	145	4000	0.37
160 -				
	100	150	4800	0.35
260 -				
	∞	150	5900	0.22





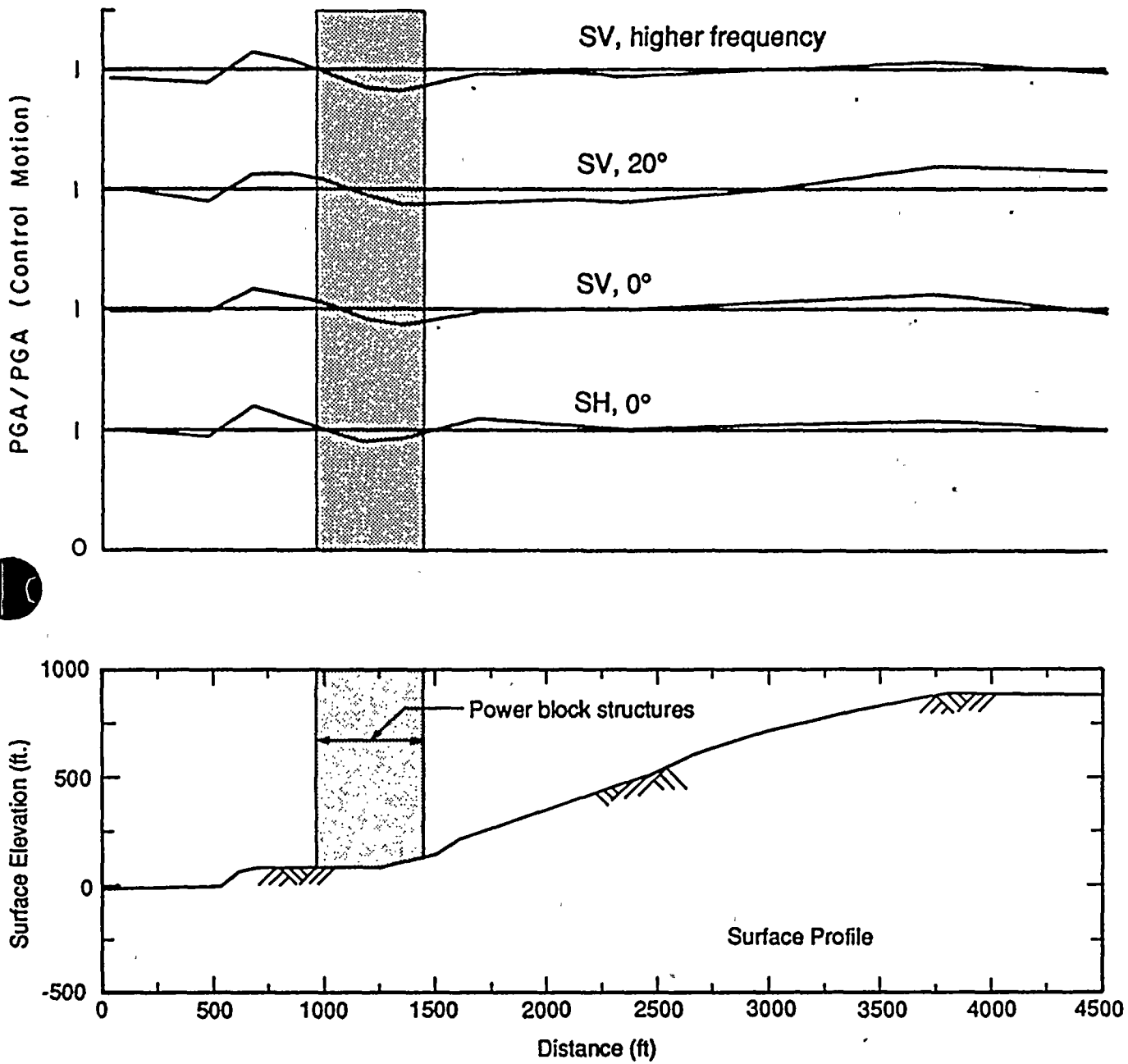


Figure Q12-3

Response of the plant site region for different input ground motions.



The sensitivity of the vertically propagating SV wave response to higher frequencies was examined by increasing the center frequency of the Fourier spectrum of the input pulse to 3 Hz. The response of the 3-Hz pulse is very similar to that for the 2.5-Hz pulse. The main effect of shifting the frequency content to higher frequencies, as shown at the top of Figure Q12-3, is to deepen and broaden the troughs at the base of the sea cliff and at the location of the power block structures, and to move the latter trough to the left.

The response to a vertically propagating SH wave is very similar to that for a vertically propagating SV wave (Figure Q12-3). For both SV and SH waves, the topography causes amplification near the crests of the sea cliff and the ridge, and deamplification near the bases of the sea cliff and the ridge.

For the entire range of input motions tested in this sensitivity study, the effect of the topography is to generally deamplify the ground motions at the location of the power block structures with respect to free-field conditions.

Finite Element Analysis

To further aid in assessing possible effects of topography at the plant site, we conducted a two-dimensional finite element analysis using vertically propagating SV waves. The cross section (Figure Q12-1) was selected to traverse the area of maximum topographic relief. The finite element discretization of the cross section was constructed to transmit ground motions having frequencies as high as 25 Hz. A viscous boundary was provided at the base of the finite element model to simulate an elastic half-space below. Transmitting boundaries were provided on the right side (uphill side) and left side (ocean side) of the model. The analysis was made using the computer program SuperFLUSH (Earthquake Engineering Technology, 1983).

The low-strain shear wave velocities and Poisson's ratios of the site rock used in the analysis are the same as those used in the soil/structure interaction analyses, summarized in the Final Report, July 1988. These properties were used throughout the two-dimensional model at the depths below the existing ground surface indicated in Table Q12-1. Below a depth of 260 feet, the shear wave velocity is 5900 ft/sec. This velocity was also used for the half-space below. The strain-dependent variations of shear modulus and damping ratio for the site rock used in the analysis are also the same as those used in the soil/structure interaction analyses. Values of strain-compatible shear modulus and damping ratio used for the two-dimensional model were estimated on the basis of a one-dimensional ground response analysis of the site. The results of the one-dimensional analysis showed very minor strain-dependent effects, with reduction in shear wave velocities less than 6 percent below the low-strain values.

The input control motion used in the analysis was the same horizontal motion used in the soil/structure interaction analyses. This motion is a modification of the longitudinal component of the Pacoima Dam record (1971 San Fernando earthquake), which matches the median site-specific acceleration response spectrum for the Diablo Canyon site. As was done for the soil/structure interaction analyses, this motion is specified as a free-field control motion at the ground surface (Elevation 85 feet). Using this motion, the outcrop motion of the underlying rock half-space was calculated and used as the rock outcrop motion of the half-space of the finite element model. The input motion was applied in the direction of the plane of the model, thus representing vertically propagating SV waves.

Results of the analysis in terms of peak ground acceleration and average spectral acceleration (5 percent damped) in the 3 to 8.5 Hz range versus location along the cross section are shown in Figure Q12-4. Values of the peak acceleration and average spectral acceleration of the free-field control motion are also shown in these plots for comparison purposes. In Figure Q12-5, these results are normalized to the control motion, that is, divided by the corresponding amplitudes of the control motion at the ground surface in the free field. Figure Q12-5 shows that ground motions at the location of the power block structures on the average are about 10 percent less than the control motion. Ground motions near the crest of the sea cliff are amplified by about 25 percent. These results show trends almost identical to those obtained from the finite difference calculations shown



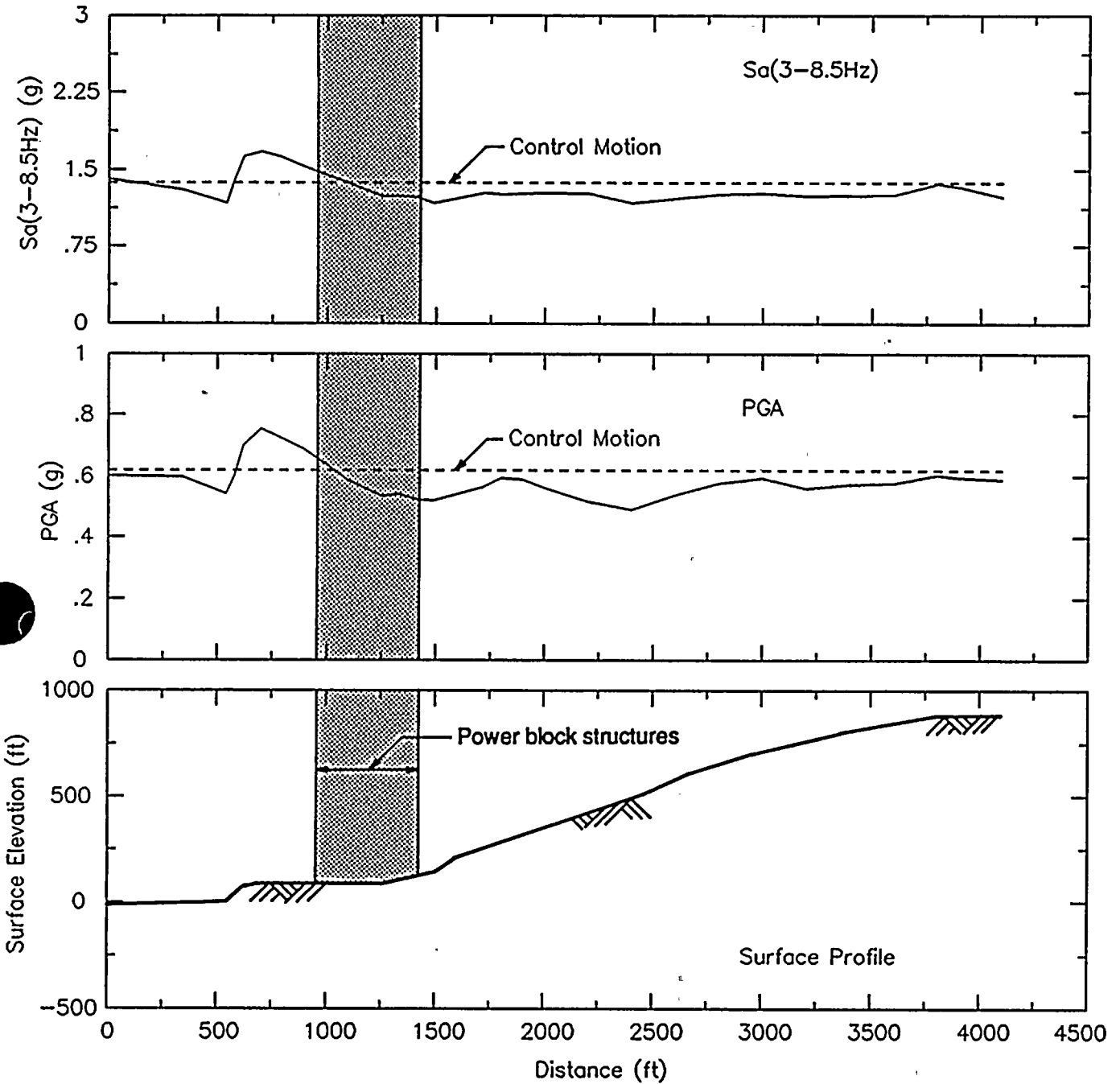


Figure Q12-4

Effects of topography on peak ground acceleration and spectral acceleration values for horizontal motions along the ground surface.



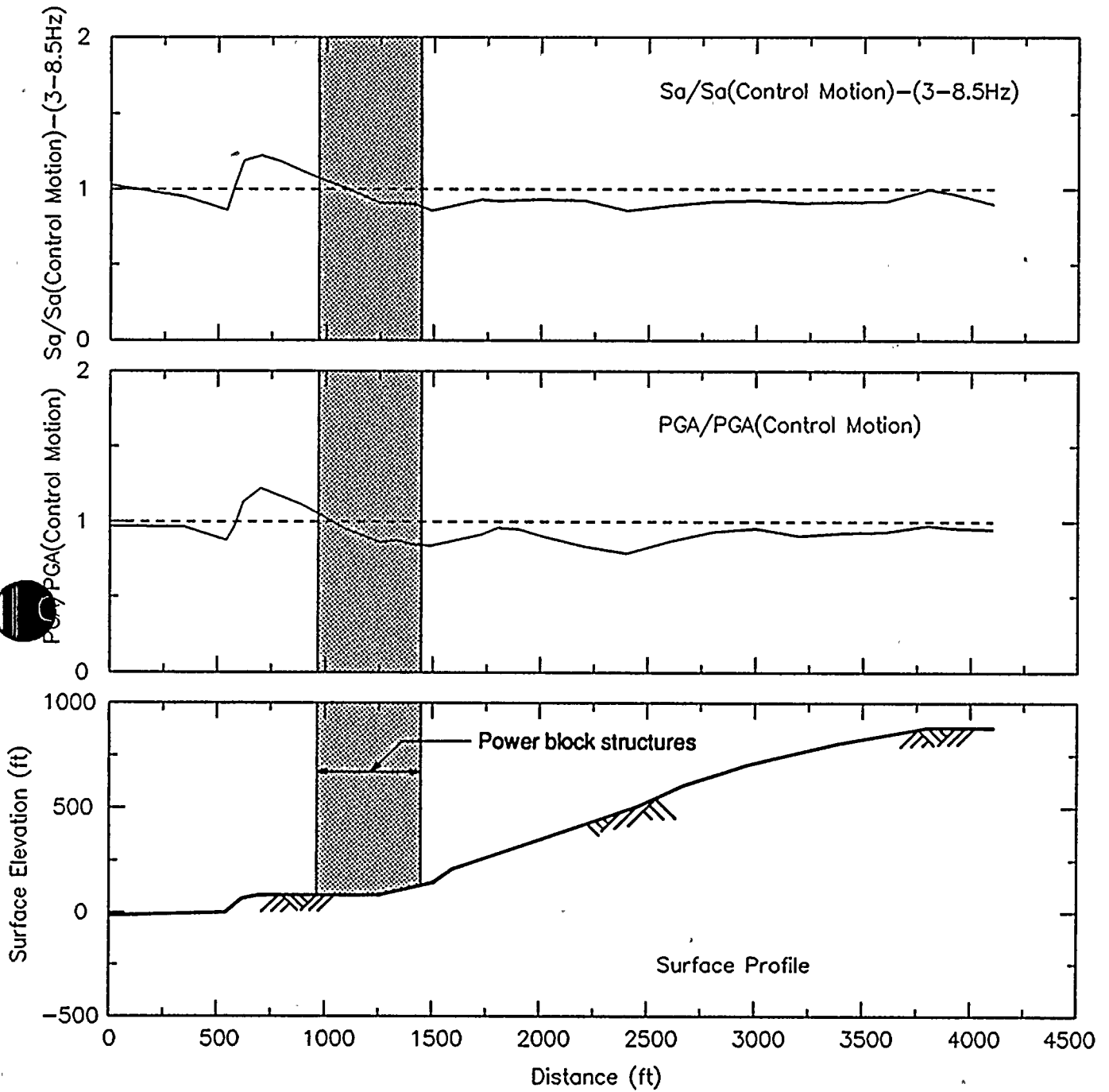


Figure Q12-5

Effects of topography on normalized peak ground acceleration and normalized spectral acceleration values for horizontal motions along the ground surface.





on Figure Q12-3.

Figures Q12-6 through Q12-8 show response spectra (5 percent damped) of ground motions near the crest of the sea cliff, at the location of the power block structures, and at both the left and right boundaries of the finite element model. The response spectrum of the free-field control motion is also plotted in Figures Q12-6 through Q12-8 for comparison purposes. The comparison in Figure Q12-7 also illustrates that ground motions at the power block structures are very little different from the free-field control motion. The ground motions near the crest of the sea cliff are amplified at frequencies higher than about 2 Hz (Figure Q12-6). However, the ground motions at the left boundary (ocean side) and the right boundary (ridge side) are equal to or slightly lower than the input free-field control motion (Figure Q12-8). Thus, the analysis indicates that topographic effects on ground motions at the location of the power block structures at the Diablo Canyon site are insignificant.

REFERENCES

Earthquake Engineering Technology, Inc, 1983, SuperFLUSH: Volume 1 - Basic Users' Guide; Volume 2 - Theoretic Manual; and Volume 3 - Verification and Example Problems: San Ramon, California.



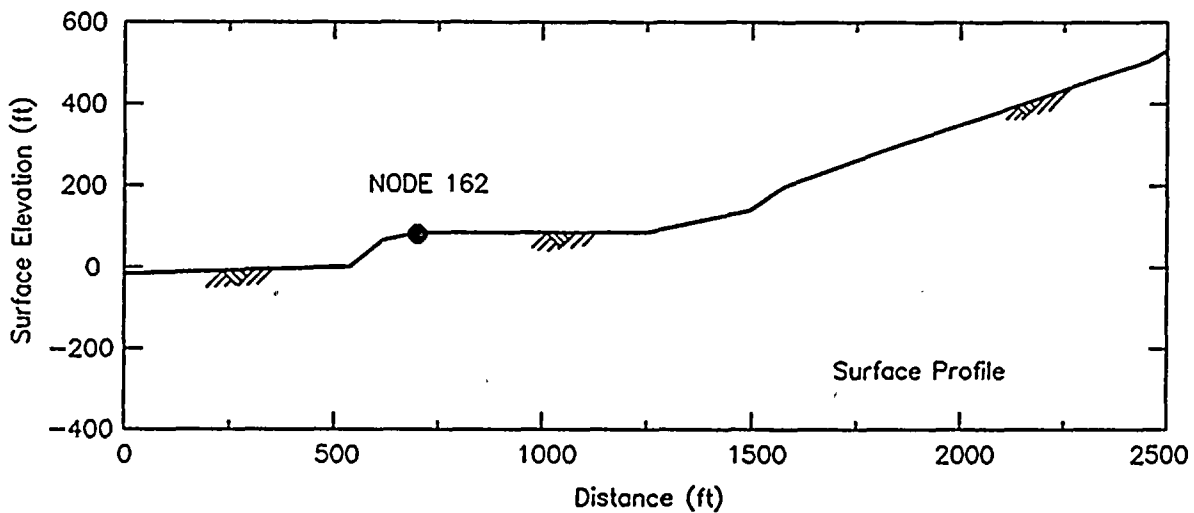
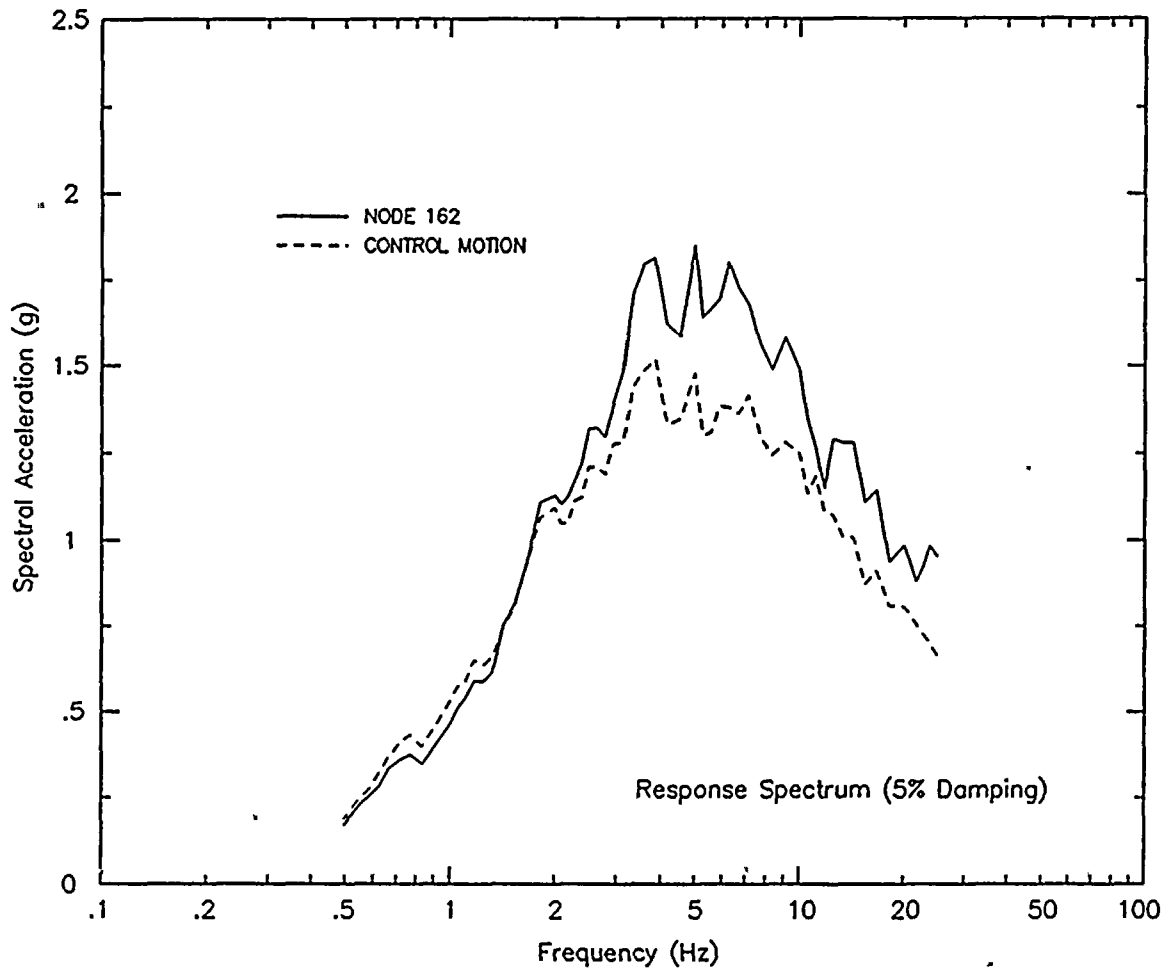


Figure Q12-6

Comparison of response spectra of the control motion and computed horizontal motion at node 162.



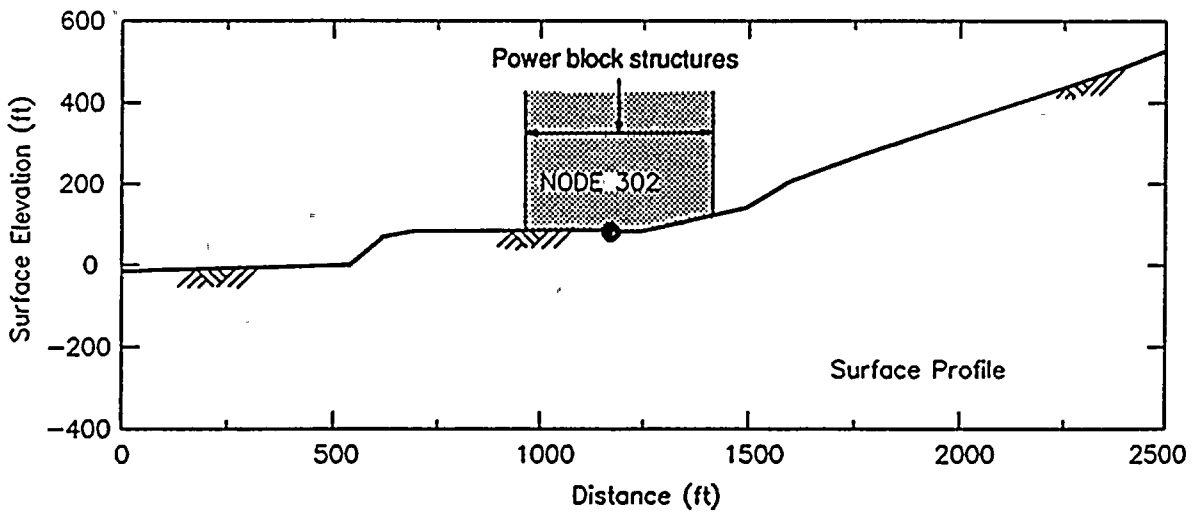
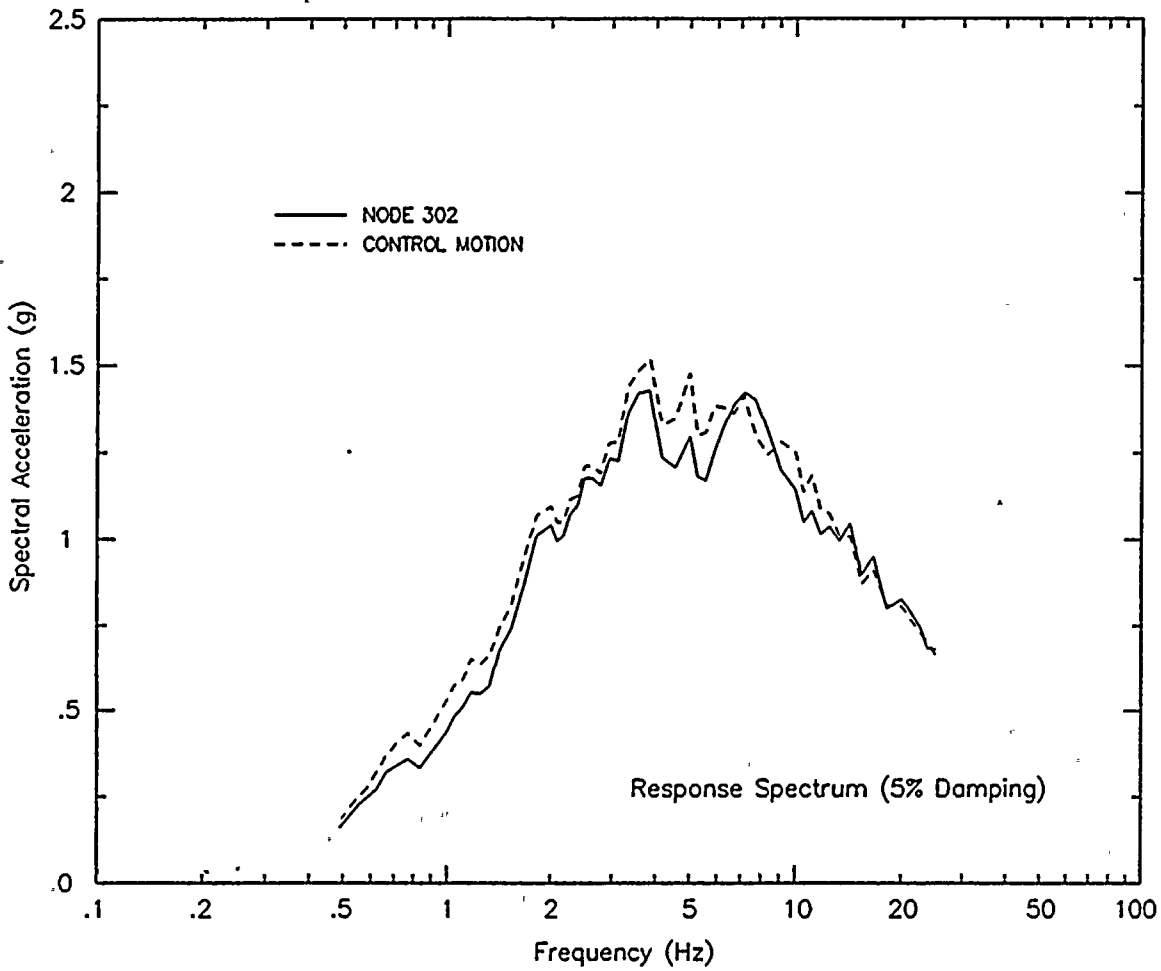


Figure Q12-7

Comparison of response spectra of the control motion and computed horizontal motion at node 302.



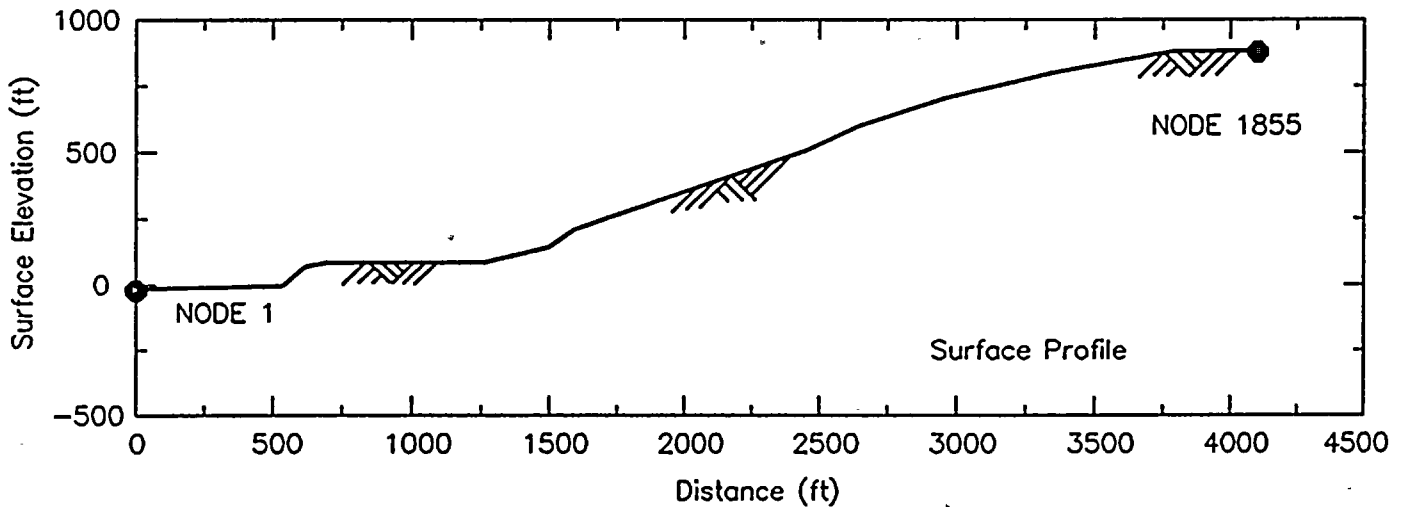
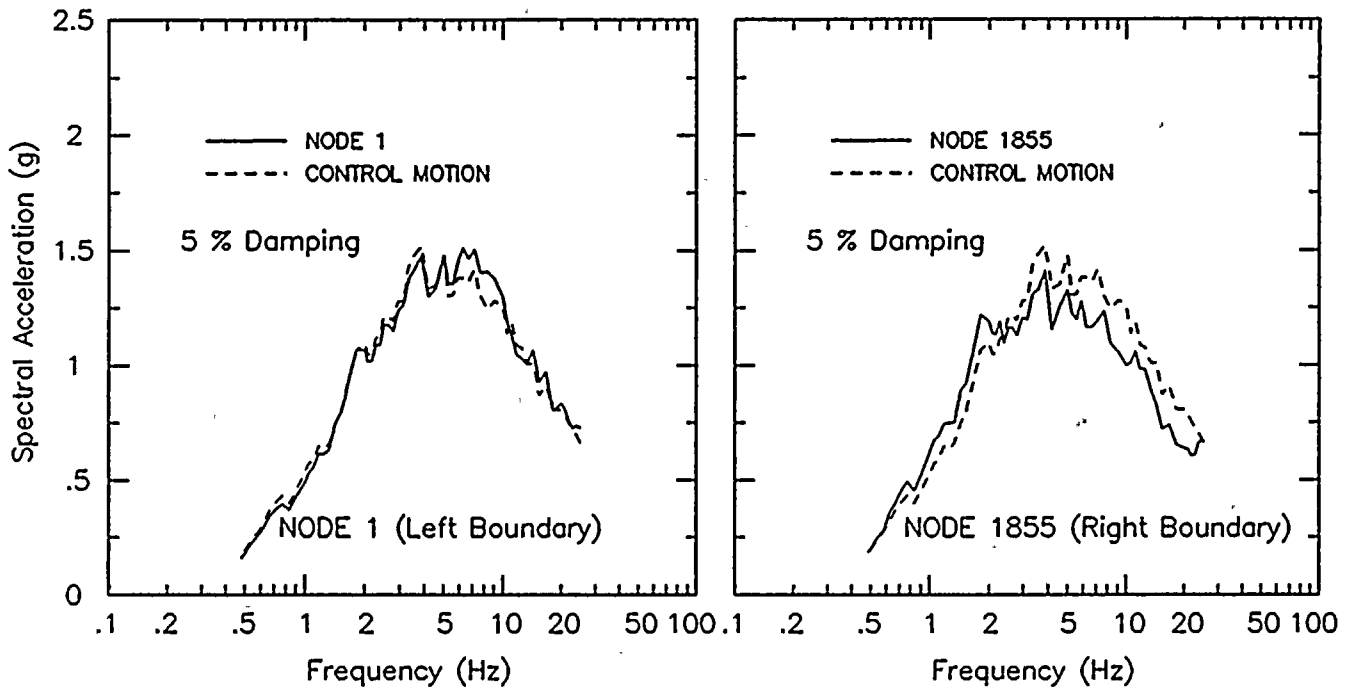


Figure Q12-8

Comparisons of response spectra of the control motion and computed horizontal motions at the left and right boundaries of the model.



QUESTION 13

Limits on parameters used to establish the empirical data base appear to be constrained to the point where some earthquakes which may be important are not included. To determine the significance of the choice of magnitude and distance ranges to the LTSP site specific spectra, expand the data base to include earthquakes down to magnitude 6, particularly the Parkfield and Morgan Hill events, and distances to about 30 kilometers and provide the resulting spectra.

In our response to Question 2 of this submittal, we conducted sensitivity studies to show the effects of the selection criteria on the estimates of near-source ground motions. In one of the sensitivity studies (Case 5 of Table Q2-1), the magnitude and distance ranges were expanded to include earthquakes having magnitudes of 6.0 M_w or greater and recording sites at distances within 30 kilometers. This resulted in a set of 35 ground-motion records from rock sites, and includes those recorded during the Parkfield and Morgan Hill earthquakes. The set consisted of 20 recordings from earthquakes having reverse/thrust fault mechanisms, and 15 recordings from strike-slip earthquakes (Table Q13-1). The records shown in Table Q13-1 were scaled to a moment magnitude of 7.2 and a distance of 4.5 km, and weighted for style of faulting assumed applicable at the plant site. The results of the statistical analysis for this set of records, which gives the most conservative estimates of the four cases studied, are compared with those of the Final Report in Figures Q13-1 and Q13-2 for the median and the 84th-percentile levels of ground motions. Also shown on these figures are the site-specific spectra based on the regression analysis. The scaling and weighting factors for both sets are the same as those described earlier in our response to Question 9, January 1989. The results are presented in terms of spectral acceleration values (5 percent damped) for the entire frequency range.

As can be seen from Figures Q13-1 and Q13-2, the spectra presented in the Final Report derived from near-source statistics provide equal or more conservative estimates in the high frequency range (about 5 to 25 Hz). At lower frequencies (less than 5 Hz), the response spectra obtained using the expanded selection criteria provide more conservative estimates of ground motions. A more relevant comparison is with the site-specific spectra based on the regression analysis. This comparison shows that the site-specific response spectra essentially equal or envelop the other spectra over the entire frequency range at the median level, and over a frequency range of about 1.5 to 25 Hz at the 84th-percentile level.



Table Q13-1

**ROCK-SITE RECORDS FOR EARTHQUAKES OF MOMENT MAGNITUDE 6.0 OR
GREATER AT SOURCE-TO-SITE DISTANCES WITHIN 30 KM**

EARTHQUAKE NAME	DATE	MECH	Mw	Stn #	Cl Dist (km)	PGA (g)	PGV (cm/sec)	PGD (cm)
Parkfield, CA	6/27/66	SS	6.1	1438	9.9	0.340	18.06	5.08
Koyna, India	12/10/67	SS	6.3	9001	3.0	0.556	24.93	5.62
San Fernando, CA	2/9/71	TH	6.6	279	2.8	1.124	80.82	20.18
San Fernando, CA	2/9/71	TH	6.6	266	19.1	0.140	8.34	2.92
San Fernando, CA	2/9/71	TH	6.6	126	24.2	0.178	7.00	1.43
San Fernando, CA	2/9/71	TH	6.6	127	23.5	0.139	4.65	2.19
San Fernando, CA	2/9/71	TH	6.6	128	20.3	0.328	13.72	4.00
San Fernando, CA	2/9/71	TH	6.6	220	15.3	0.167	13.64	5.14
San Fernando, CA	2/9/71	TH	6.6	141	17.4	0.184	17.30	6.34
San Fernando, CA	2/9/71	TH	6.6	121	29.1	0.084	5.65	1.43
San Fernando, CA	2/9/71	TH	6.6	104	27.0	0.196	5.96	4.35
Gazli, USSR	5/17/76	RV	6.8	9201	3.0	0.677	45.81	8.74
Tabas, Iran	9/16/78	TH	7.4	9101	3.0	0.753	98.02	57.30
Tabas, Iran	9/16/78	TH	7.4	9102	17.0	0.385	31.77	26.86
Imperial Valley (H)	10/15/79	SS	6.5	286	26.0	0.152	6.62	1.79
Imperial Valley (H)	10/15/79	SS	6.5	6604	26.5	0.158	13.14	10.51
Hammoth Lakes - A	5/25/80	SS	6.2	54214	15.5	0.099	10.37	4.37
Hammoth Lakes - A	5/25/80	SS	6.2	54214	15.5	0.086	9.86	3.97
Hammoth Lakes - C	5/25/80	SS	6.0	54214	19.7	0.081	6.51	1.34
Hammoth Lakes - C	5/25/80	SS	6.0	54214	19.7	0.082	5.70	1.28
Hammoth Lakes - D	5/27/80	SS	6.0	54214	20.0	0.207	16.06	2.13
Hammoth Lakes - D	5/27/80	SS	6.0	54214	20.0	0.199	11.91	1.66
Hammoth Lakes - D	5/27/80	SS	6.0	54424	24.5	0.105	5.65	1.52
Hexicali Valley, MX	6/9/80	SS	6.4	6604	8.5	0.607	27.51	35.32
Coalinga, CA Main	05/02/83	RV	6.5	46175	27.6	0.154	15.65	3.58
Coalinga, CA Main	05/02/83	RV	6.5	36177	24.6	0.148	13.56	5.07
Coalinga, CA Main	05/02/83	RV	6.5	36438	29.6	0.069	7.92	2.42
Coalinga, CA Main	05/02/83	RV	6.5	36453	28.4	0.083	8.46	2.44
Horgan Hill, CA	04/24/84	SS	6.2	57217	0.1	0.960	64.32	10.40
Horgan Hill, CA	04/24/84	SS	6.2	57383	11.8	0.258	20.34	3.08
Horgan Hill, CA	04/24/84	SS	6.2	47379	16.2	0.085	2.59	0.38
Nahanni, Canada	12/23/85	TH	6.8	6097	6.0	1.217	45.61	12.60
Nahanni, Canada	12/23/85	TH	6.8	6098	8.0	0.461	31.43	37.11
Nahanni, Canada	12/23/85	TH	6.8	6099	16.0	0.190	4.64	1.38
Whittier Nar.(H),CA	10/01/87	TH	6.0	24399	21.2	0.154	4.12	0.00



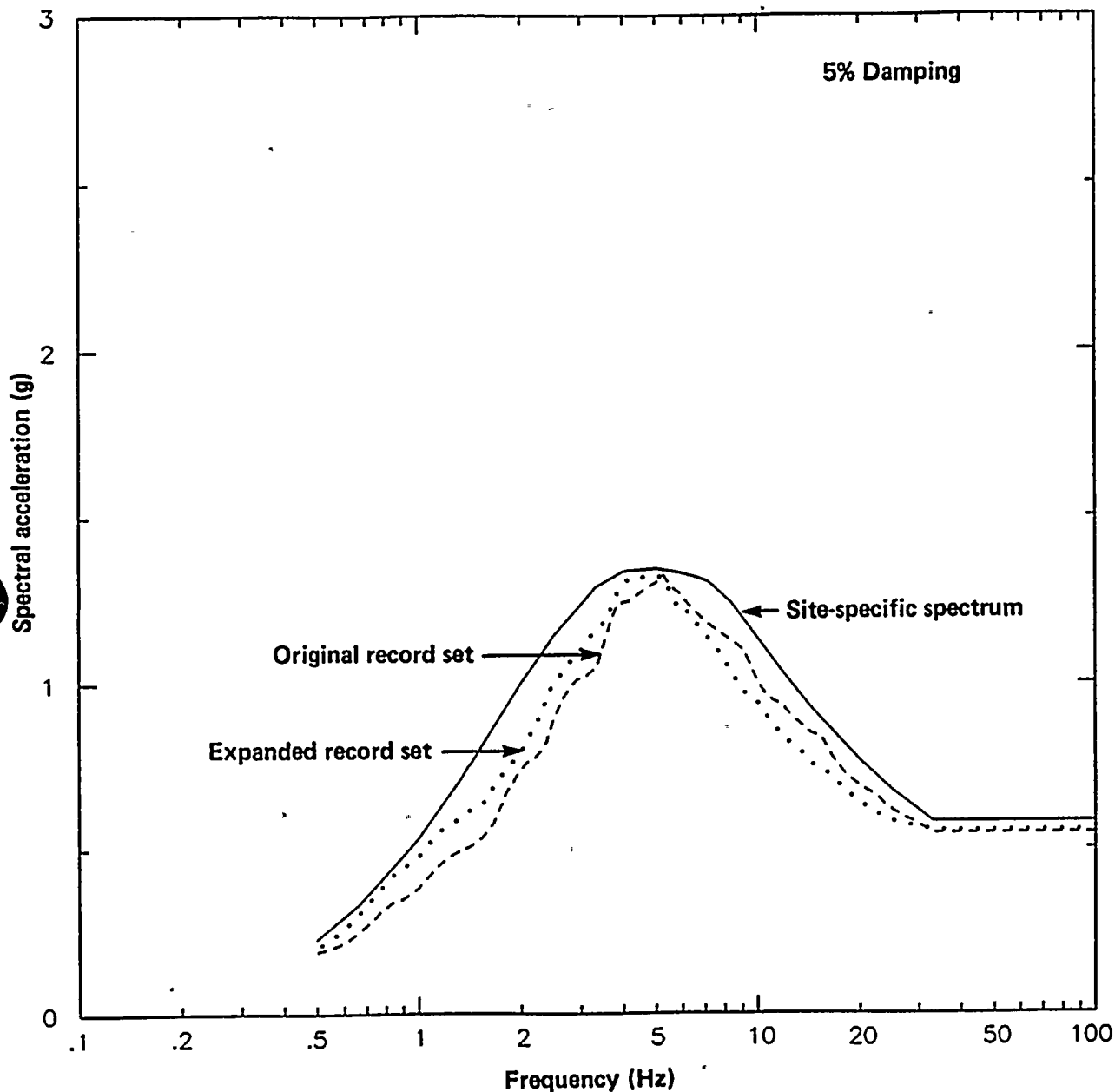


Figure Q13-1

Median horizontal response spectra showing effects of magnitude and distance selection criteria on statistics of near-source ground motions.



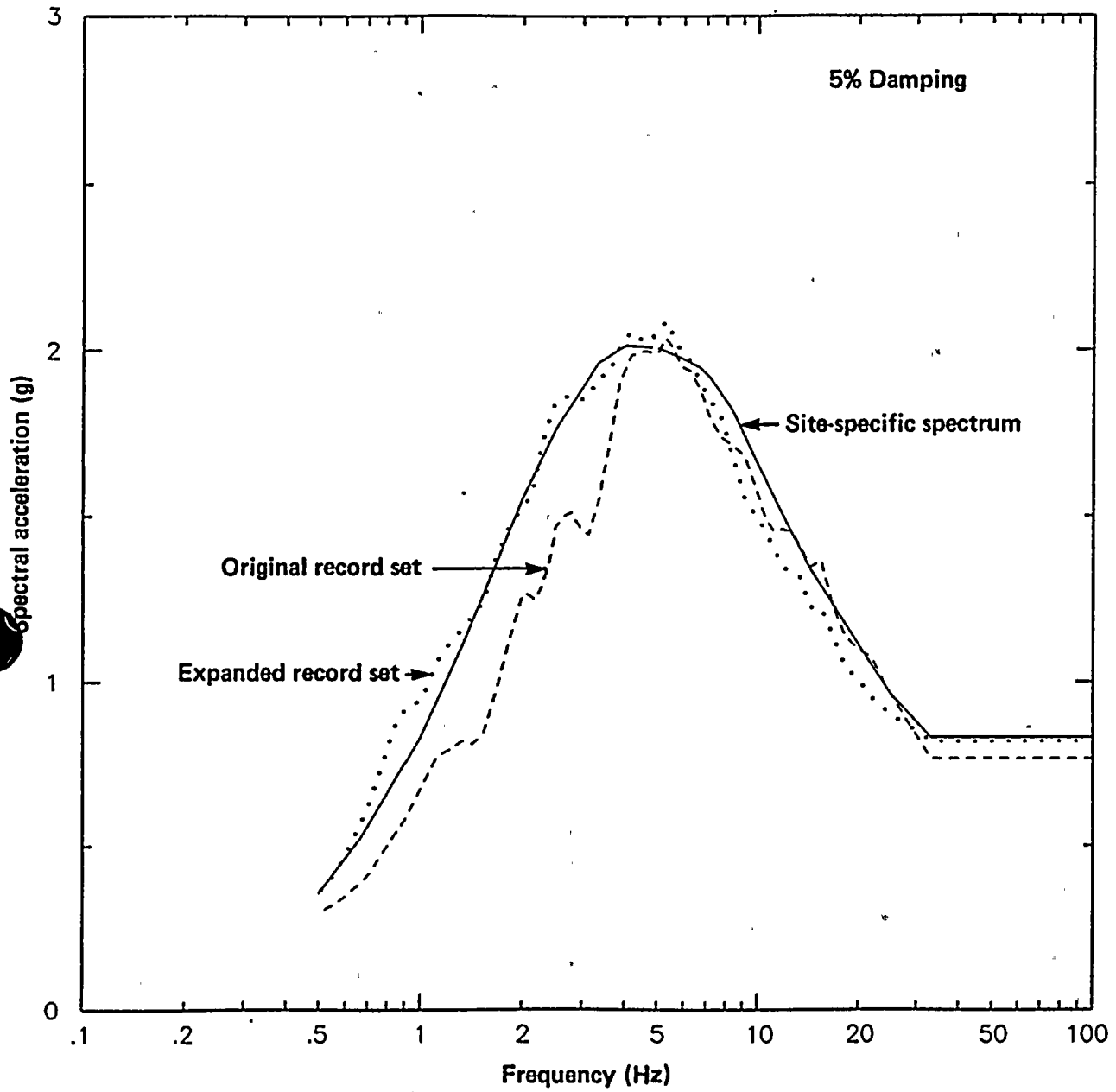


Figure Q13-2

84-percentile horizontal response spectra showing effects of magnitude and distance selection criteria on statistics of near-source ground motions.



QUESTION 14

Since the Imperial Valley earthquake data were recorded on deep soil sites, their use in developing the site specific response spectra for Diablo Canyon has been questioned. Provide site specific response spectra obtained without the use of the Imperial Valley earthquakes.

Five Imperial Valley records from soil sites were used in our statistical analysis of near-source records for two reasons. The first was to enlarge the sample of 13 near-source rock records and to improve its statistical significance. The second was to supplement the sample of 13 rock records with records from strike-slip events, because the original sample contained 11 reverse/thrust records and only 2 strike-slip records. The Imperial Valley records were modified to rock-site conditions before being used in the statistical analyses. Details of the modification procedure were presented in our response to Question 9, January 1989.

In response to the current question, a sensitivity study was performed of the set of near-source records, excluding the five Imperial Valley records. The results are compared with those for the original 18-record set, in terms of 5 percent damped spectral acceleration, on Figure Q14-1 for the median and the 84th-percentile levels. As can be seen from Figure Q14-1, the agreement between the two spectra at the median level is very close, differing by less than 4 percent for the peak ground acceleration values, about 2 percent for the spectral acceleration values averaged over the 3 to 8.5 Hz frequency band, and about 4 percent for the spectral acceleration values averaged over the 5 to 14 Hz frequency band. At the 84th-percentile level, Figure Q14-1 shows the differences are about 7 percent for the peak ground acceleration values, about 9 percent for the spectral acceleration (3 to 8.5 Hz) values, and slightly less than 10 percent for the spectral acceleration (5 to 14 Hz) values. The somewhat larger differences observed at the 84th-percentile level may be due to the modest number of records; it is expected that there will be greater variability at the 84th-percentile level than at the median level.

It is also of interest to note that in our responses to Questions 2 and 13 of this submittal, we examined several expanded sets of near-source strong-motion records, and presented the response spectra based on statistical analyses of these records, which contained ground motions from rock sites only. The most conservative case of the sensitivity studies in Question 2 contained 35 records of earthquakes having moment magnitudes of 6 or greater and within 30 km of the recording stations. The 84th-percentile response spectrum obtained from this set of records is compared with the near-source statistics (with and without the soil-site records) in Figure Q14-2, together with the corresponding site-specific spectrum obtained from the regression analysis. The estimated spectral accelerations from this larger set of rock-site recordings are very similar to those estimated for the site-specific spectrum over the entire frequency range.



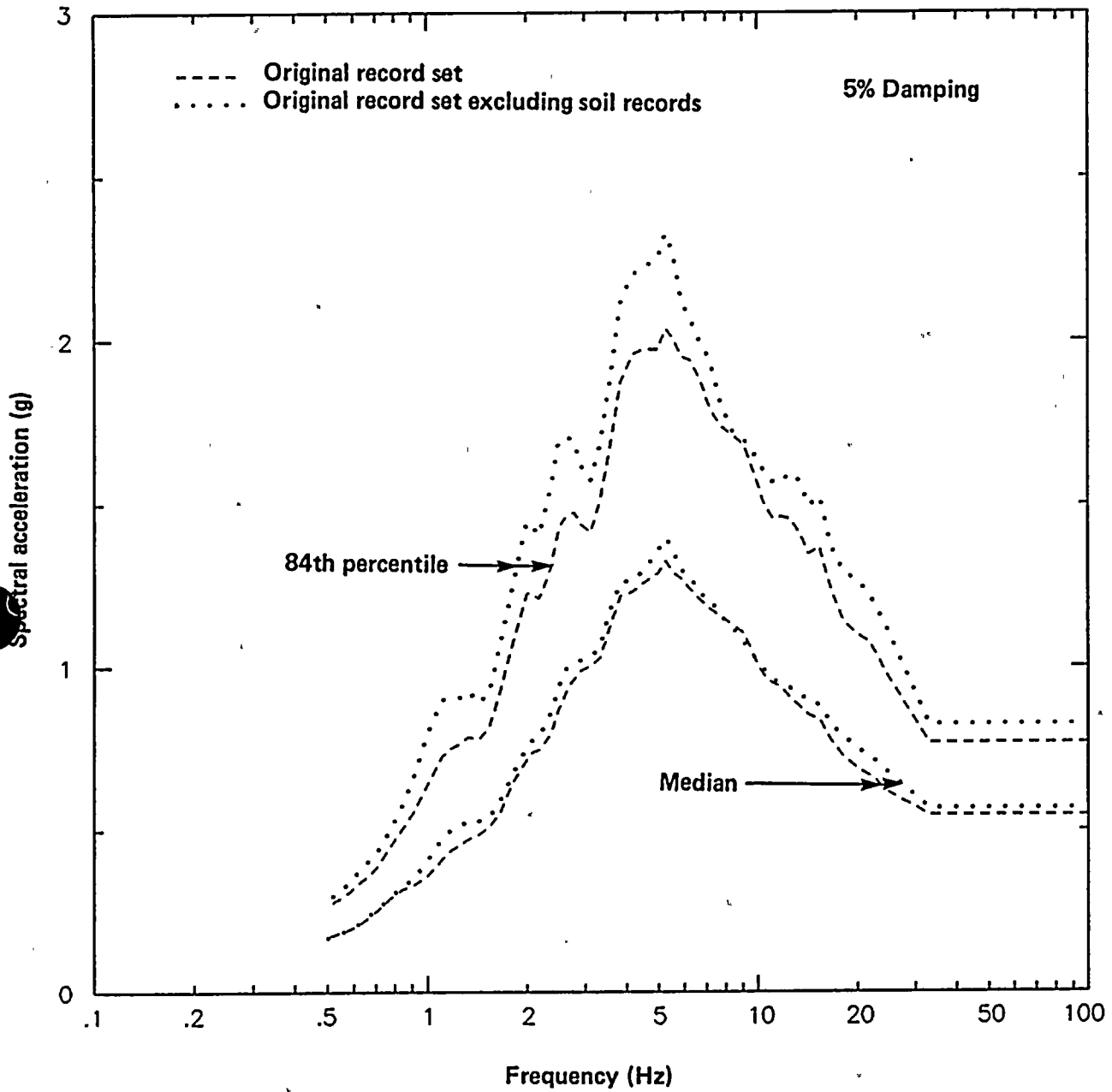


Figure Q14-1

Median and 84th-percentile horizontal response spectra showing effects of including and excluding records from soil sites.



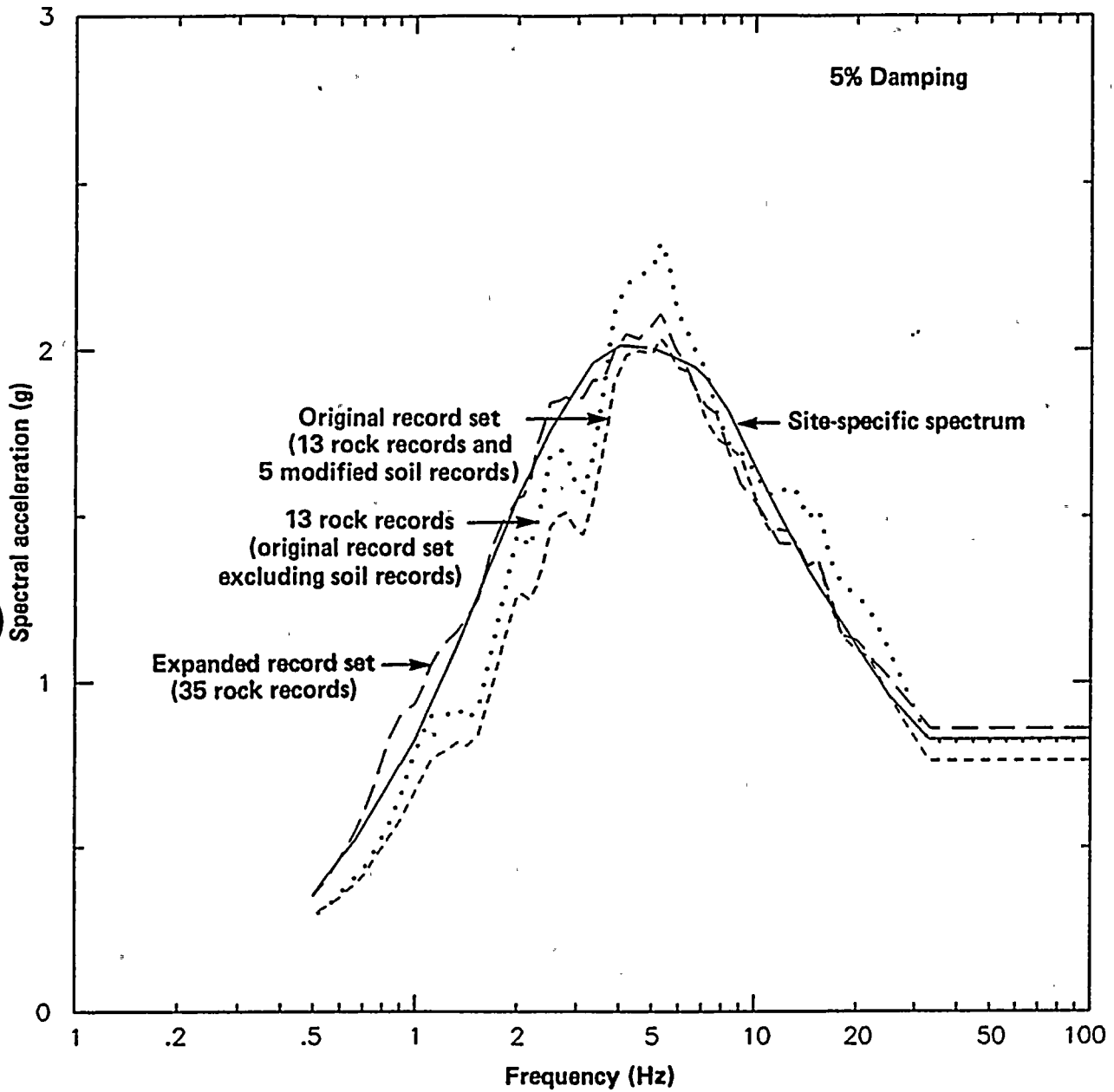


Figure Q14-2

Comparison of the 84th-percentile Long Term Seismic Program site-specific and near-source statistics spectra with the spectra obtained from near-source statistics using the expanded data base from Question 13, and excluding the soil-site records from the original record set.



QUESTION 16

Recent work on the Nahanni earthquake Site 2 data (Weichert, 1989) and in the San Fernando earthquake Pacoima Dam recording (Anooshehpoor, 1988) indicate that the high ground motions recorded may not be due to site effects. In view of this, modification of these records to account for topographic amplification is questionable. What would the ground motion estimates be without these modifications?

There is strong evidence for topographic amplification of ground motions at ridge sites, as indicated by numerous empirical observations and supported by numerical modeling studies, and reviewed recently by Geli and others (1988) and Aki (1988). Both the Nahanni earthquake recording Sites 1 and 2 and the San Fernando earthquake Pacoima Dam accelerograph site were located on ridges. Possible topographic amplification of the ground motions recorded at these sites has been the subject of several studies.

In response to this question we have reviewed the published studies. In the case of the Nahanni earthquake, we also have conducted a numerical modeling study of topographic effects at both Site 1 and Site 2 using a finite difference method. Results from both the literature review and our numerical modeling study confirm that the ground motions recorded at these sites were significantly affected by topographic amplification.

Topographic Amplification at the Pacoima Dam Accelerograph Site

Possible topographic amplification of the ground motions in the Pacoima Dam accelerogram recorded during the 1971 San Fernando earthquake has been the subject of several studies, because the peak ground accelerations were among the highest ever recorded and because the accelerograph site was located on a steep ridge forming the left abutment of the 111-meter-high concrete arch dam. These investigations can be broadly grouped into three types, namely, comparative studies of aftershock accelerograms, numerical modeling studies, and foam-rubber model studies.

Comparative Studies of Aftershock Accelerograms. Studies by Mickey and others (1973) and by Reimer (1973) compared the ground motions in the accelerograms recorded at the Pacoima Dam accelerograph site with those recorded at a free-field site in the downstream valley floor.

Mickey and others (1973) compared the ground motions from eight aftershocks having magnitudes from 2.7 to 3.7 M_L recorded at the Pacoima Dam accelerograph site with those recorded at a free field site downstream in the valley floor. These aftershocks were located at epicentral distances from 4.5 to 30 km over a wide azimuthal range from the dam, as shown in Figure Q16-1. The results showed that the average overall amplification in response spectral acceleration was about 1.4 in the north-south direction, and about 1.65 in the east-west direction for the Pacoima Dam accelerograph site, as compared to the free-field site. Figure Q16-2 shows the average ratio of north-south response spectra for the eight aftershocks. Amplification occurred at all frequencies above 0.5 Hz.

Reimer (1973) used a set of accelerograms from three different aftershocks having magnitudes from 2.0 to 3.3 M_L to compare the ground motions at the Pacoima Dam accelerograph site (Station 1) and at a valley floor site (Station 2) about 600 meters downstream. Figure Q16-3 shows the epicenters of these aftershocks. Figure Q16-4 shows the locations of the recording stations. Station 1 was on the ridge and Station 2 was in the free-field. Figure Q16-5 shows the acceleration response spectra of the two horizontal components at the two recording sites for one of the events (Event 3). Figure Q16-6 shows the ratio of acceleration spectral ordinates for 5 percent damping recorded at Station 1, divided by those recorded at Station 2. It is clear from these figures that there was amplification of peak ground acceleration, as well as response spectral acceleration for all frequencies above 1 Hz.

Further evidence for topographic amplification of ground motions at the Pacoima Dam accelerograph site was provided by the accelerograms recently obtained at that site and at the dam base from the 1987 Whittier Narrows earthquake (Shakal and others, 1987). As shown in Figure Q16-7, the peak accelerations are 0.01 g for both horizontal components at the dam base, and 0.04 and 0.05 g for the



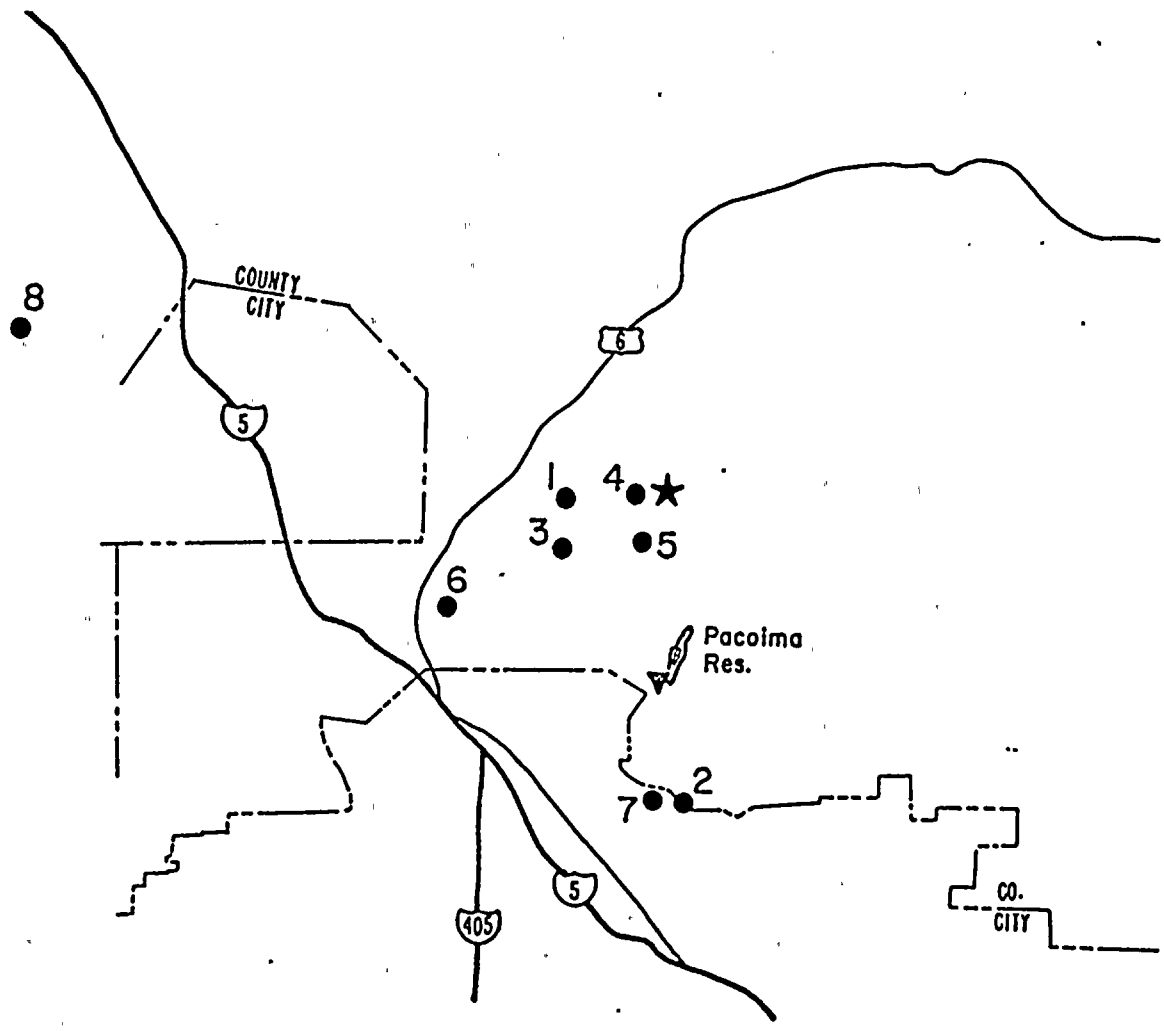


Figure Q16-1

February 9, 1971 earthquake (star); Pacoima Dam (triangle); and eight aftershocks numbered in order of occurrence (circle) (from Mickey and others, 1973).



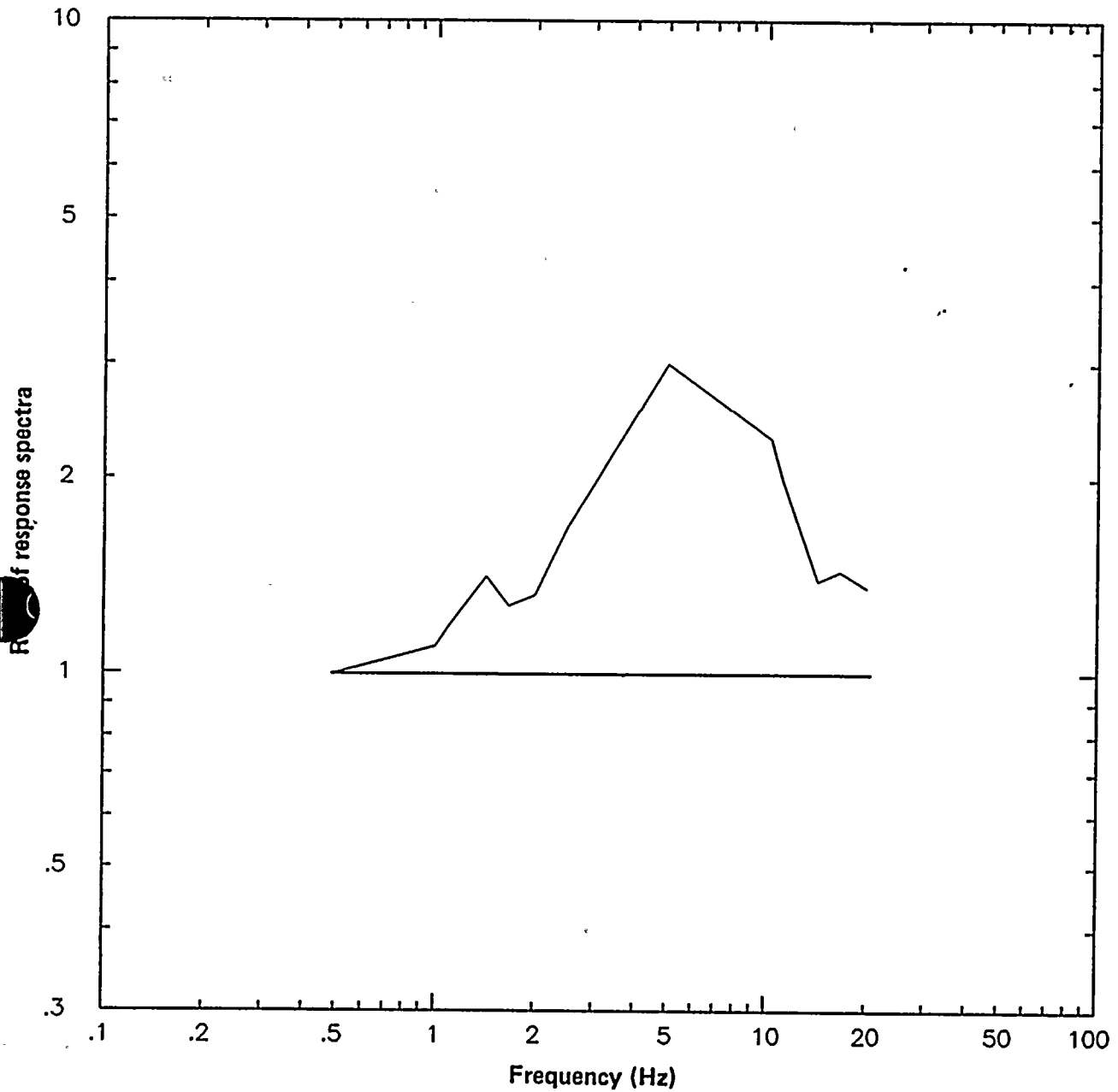


Figure Q16-2

Overall average ratio of the response spectra at the Pacoima Dam accelerograph site to a free-field site for the eight aftershocks, north component (based on Mickey and others, 1973).



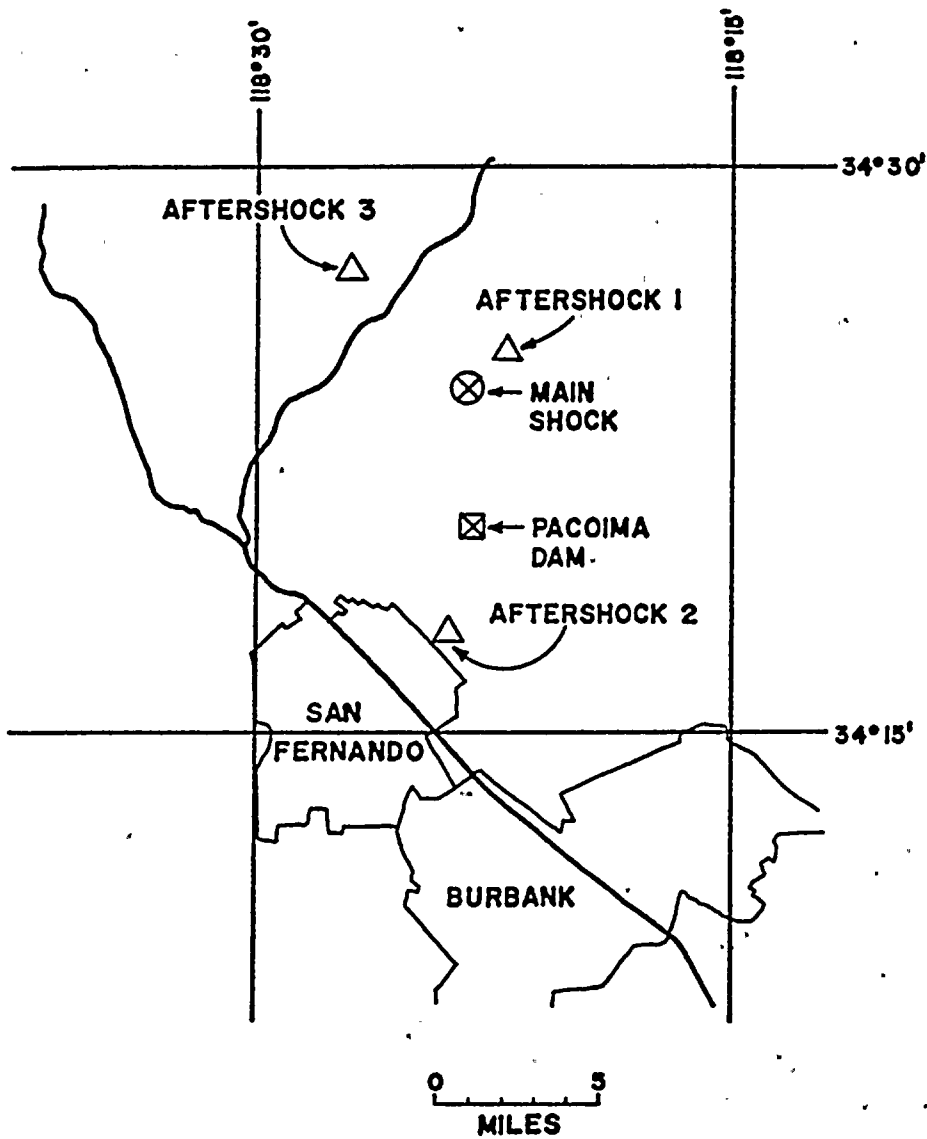


Figure Q16-3

Epicentral locations of aftershocks of the 1971 San Fernando earthquake recorded at Pacoima Dam (from Reimer, 1973).



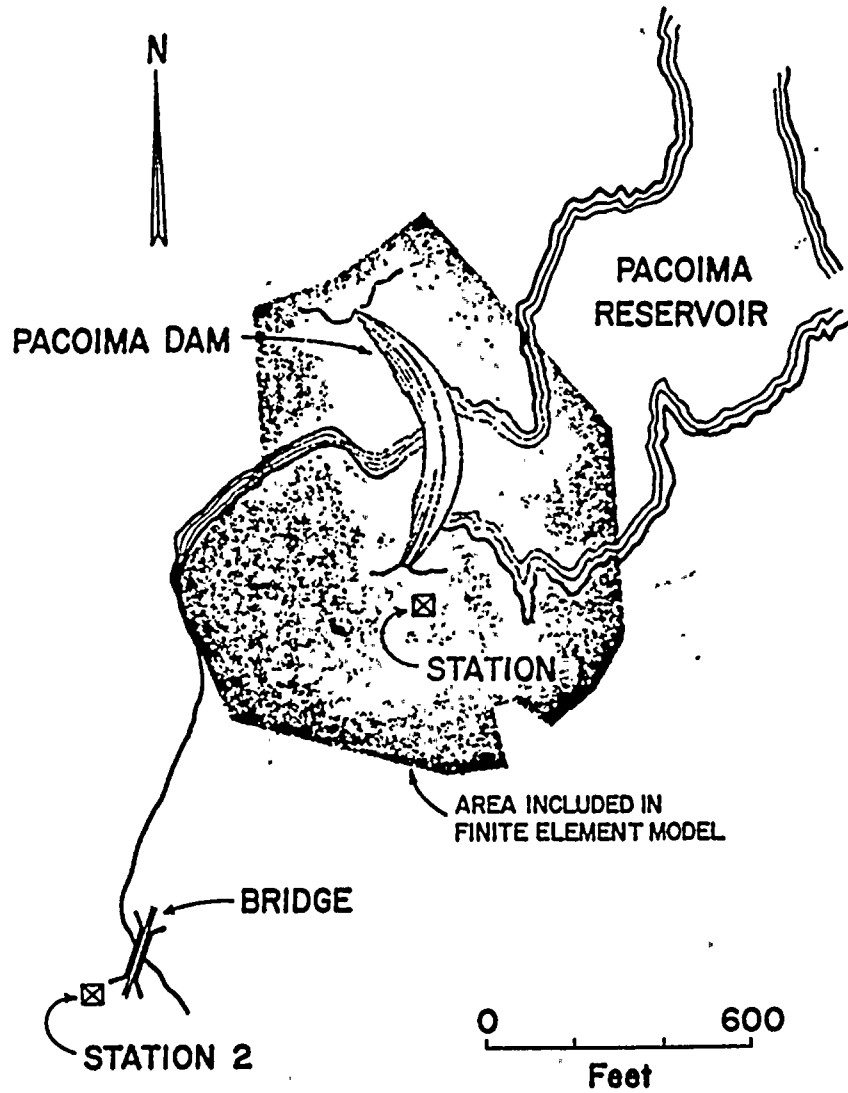


Figure Q16-4

Locations of accelerograph stations used in the study of 1971 San Fernando earthquake aftershocks by Reimer (1973).



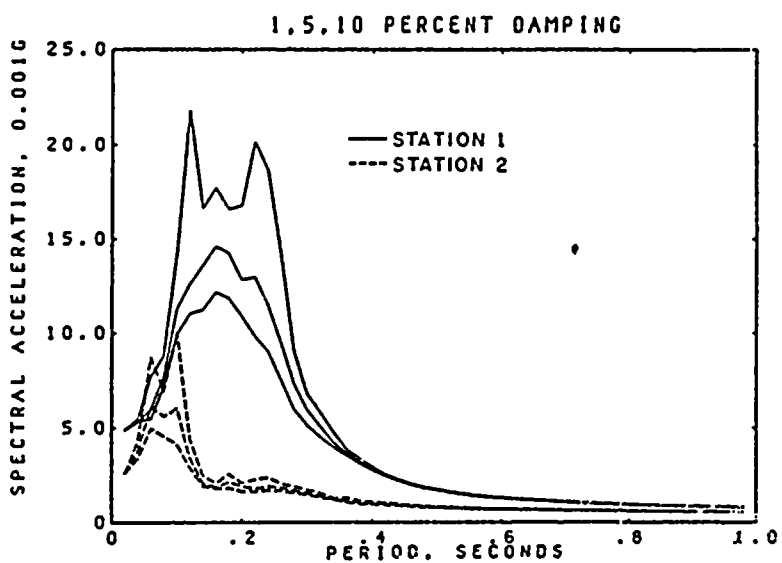
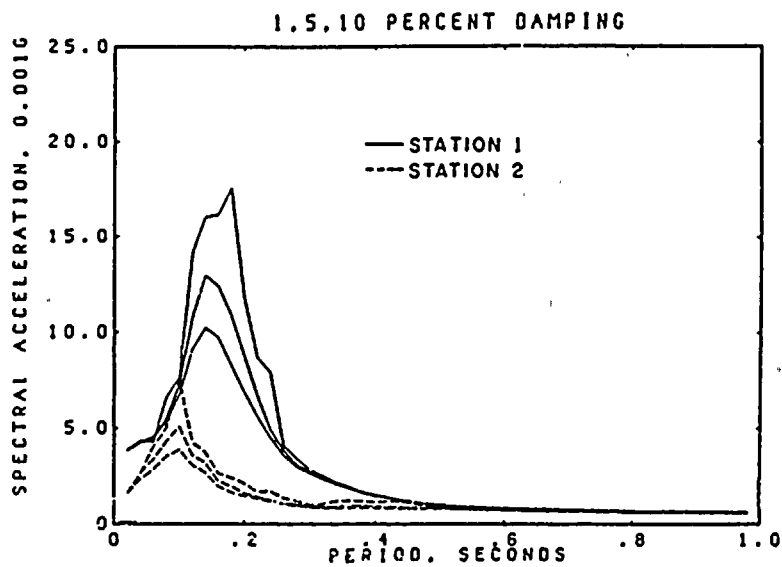


Figure Q16-5

Acceleration response spectra of the two horizontal components for the third aftershock of the 1971 San Fernando earthquake recorded at Pacoima Dam: top, S14°W component; bottom, N76°W component (from Reimer, 1973).



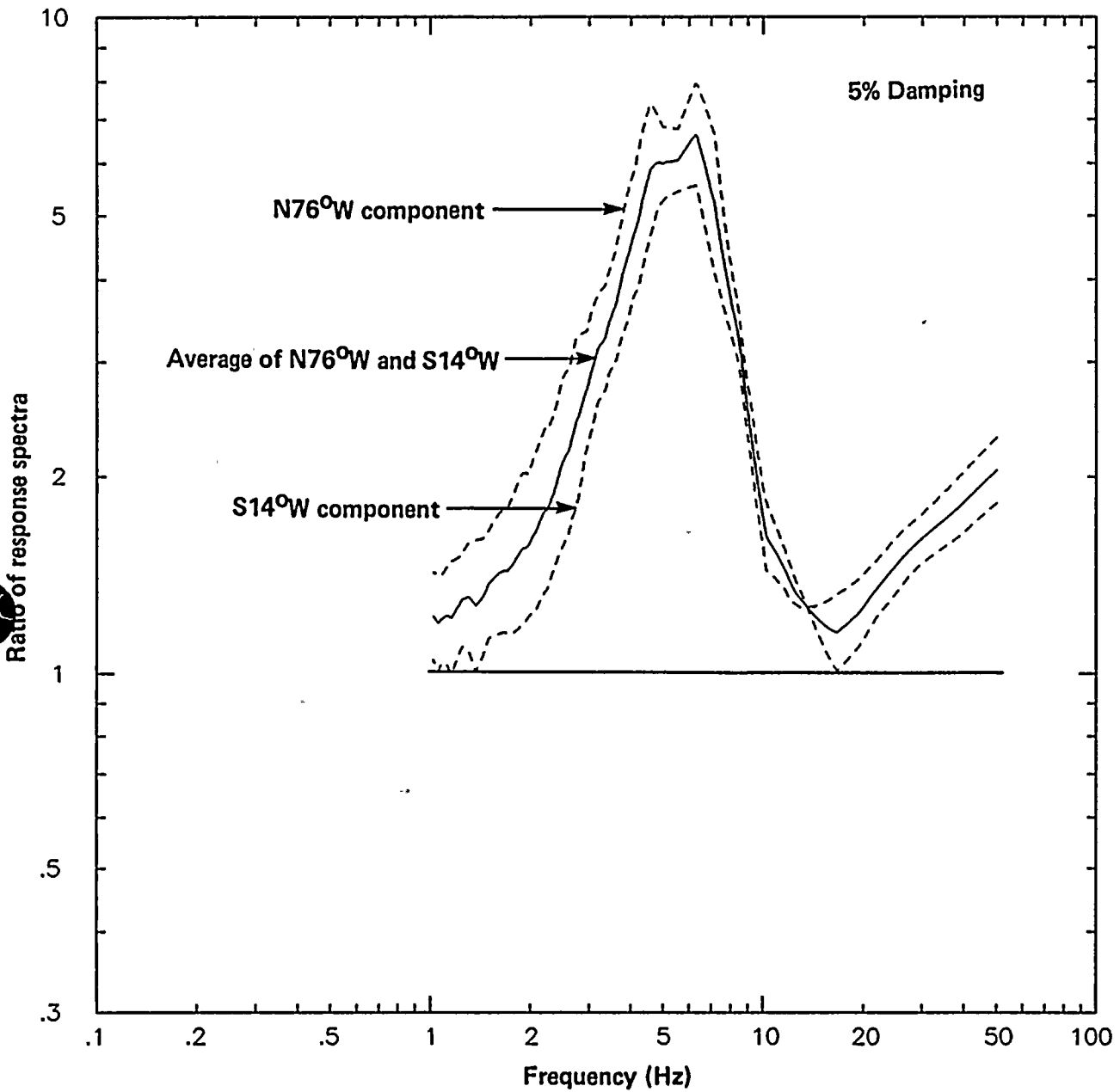


Figure Q16-6

Ratio of the horizontal response spectra at the Pacoima Dam accelerograph site to a free-field site for Event 3 (based on Reimer, 1973).



Pacoima Dam

(CSMIP Station No. 24207)

Record 24207-S2485-87278.01

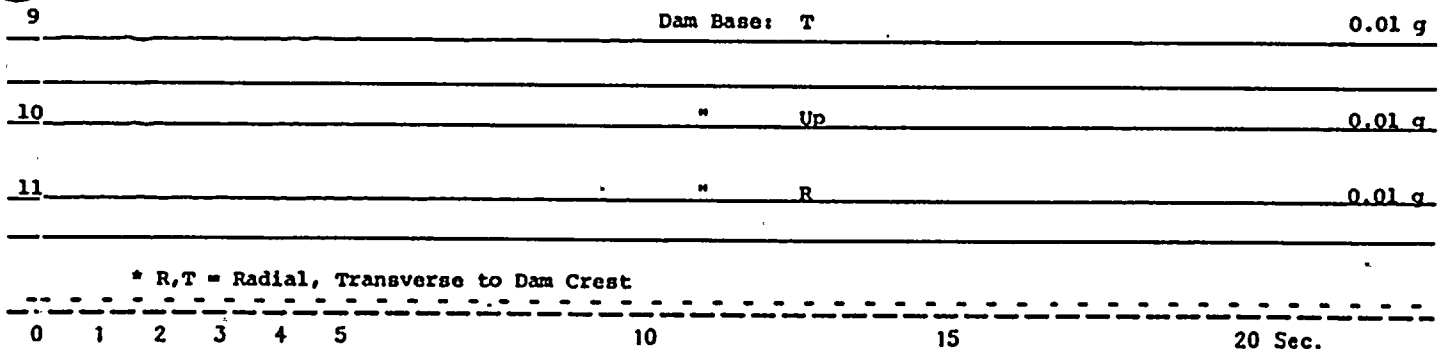
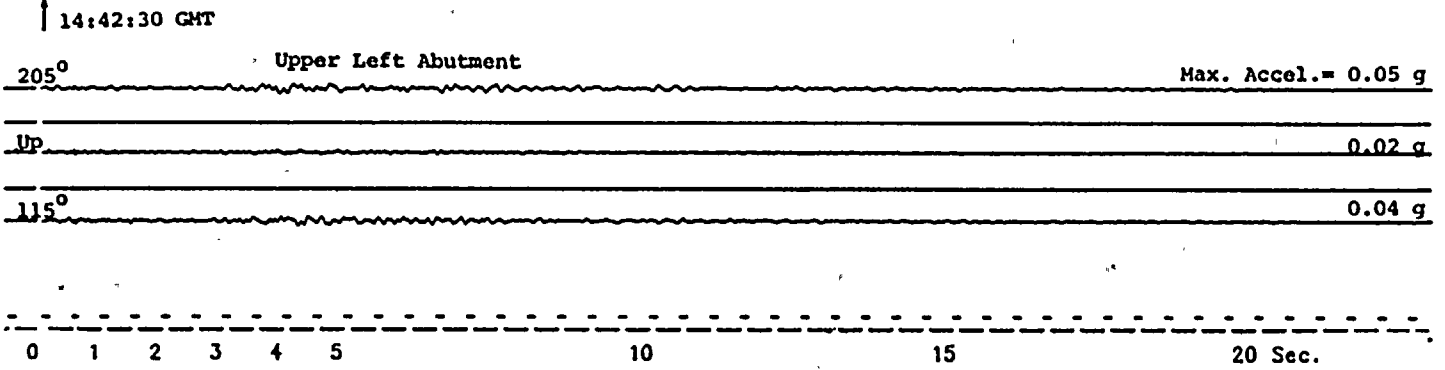


Figure Q16-7

Accelerograms from the 1987 Whittier Narrows earthquake recorded Pacoima Dam. Top: upper left abutment (Pacoima Dam accelerograph site). Bottom: base of dam (from Shakal and others, 1987).





two horizontal components at the Pacoima Dam accelerograph site. Again, there was significant amplification of ground motions at the accelerograph site at the upper left abutment.

Numerical Modeling Studies. Three numerical modeling studies on possible amplification of ground motions at the Pacoima Dam accelerograph site have been published. Studies by Bouchon (1973) and Boore (1973) were made using two-dimensional topographic models. The third study, by Reimer and others (1973), was made using a three-dimensional finite element model for the dam and the topography of the region. A summary of the results of these studies follows.

Bouchon (1973) studied possible topographic effects on ground motions due to incident SH, P, and SV waves using the method developed by Aki and Larner (1970). Figure Q16-8 shows the two-dimensional topographic profiles at the Pacoima Dam accelerograph site that were used in the study. Also shown in the figure is the direction of incident waves normal to the fault plane. Table Q16-1 summarizes the computed amplification factors for incident SH, P, and SV waves at a frequency of 10 Hz. The calculated amplification varied with the component considered, and was at least 40 percent higher than the flat surface case. Computations were also made for waves coming from directions other than normal to the fault plane. The results were similar in all cases considered.

Boore (1973) studied possible topographic effects on the Pacoima Dam accelerogram using a finite difference simulation method with an incident plane SH wave. Figure Q16-9 shows the two-dimensional topographic profiles used in his calculations. The Pacoima Dam accelerograph site was located at point 1 on the ridge model and at point 4 in the canyon model. Figure Q16-10 shows the topographic effect on the S14°W component. The original trace recorded in this direction was low-pass filtered with a cutoff of 15 Hz, which decreased the peak acceleration slightly from 1.17 g to 1.12 g. The filtered trace is shown in the upper part of the figure. (This low-pass filtering was necessary because the theoretical amplitude ratios were not computed for higher frequencies.) The deconvolved trace after the effect of the ridge was removed is shown in the lower part of the figure. It may be seen that the peak acceleration was reduced from 1.12 g to 0.73 g after the topographic amplification was removed.

Reimer and others (1973) studied possible topographic amplification of ground motions in the Pacoima Dam accelerogram using a three-dimensional finite element model for the dam and the surrounding rock. The model was based on the topography and physical properties obtained from field surveys, and further refined by comparison of computed mode shapes and frequencies with the results of forced vibration tests of the dam. Figure Q16-11 shows an aerial view of the dam and the finite element model of the area. The model excitation that would produce the Pacoima Dam accelerogram at the instrument location on the model was computed. The time histories and acceleration response spectra of the three components of this excitation are compared with those of the original accelerogram in Figure Q16-12. Results in this figure show amplification due to topography for frequencies above 1 Hz. For example, the peak horizontal acceleration of the computed input motion was about 0.4 g, corresponding to an amplification factor of over 2.5.

It may be further noted that in our response to Question 12 regarding possible topographic effect on ground motions at the plant site, we have made two independent numerical modeling studies. The results from both studies showed that the ground motions at the crest of a 85-foot-high sea cliff could be amplified by a factor of about 1.2. The topographic relief in the immediate vicinity of the Pacoima Dam accelerograph site is about four times greater. Thus, the corresponding topographic amplification could be larger than the case analyzed in Question 12.

Foam-rubber Model Studies. Brune and others (1985) and Anooshehpour (1988) reported results of a study on possible topographic effects on ground motions at the Pacoima Dam accelerograph site using a three-dimensional foam-rubber model for the surrounding topography subject to incident SH waves. For vertically incident SH waves, the spectral ratio of the ground acceleration on the ridge to the free-field (flat surface) indicates an amplification of about 60 percent at a frequency of 6.5 Hz on the N76°W component, and very little effect on the S14°W component. At a frequency of 10 Hz, the motion on the ridge was about 30 percent lower than the free-field motion for both horizontal components. For nonvertically incident SH waves, their results showed that the topographic effect



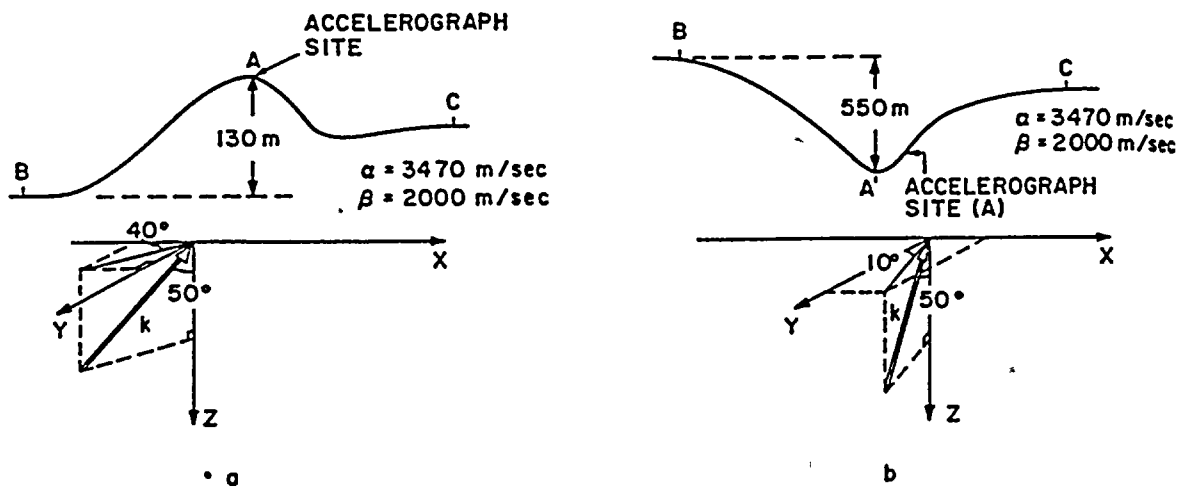


Figure Q16-8

Problem configuration for waves arriving at the Pacoima Dam accelerograph site from the fault plane: (a) ridge (local topography), (b) canyon (regional topography) (from Bouchon, 1973).



Table Q16-1

VALUES OF THE AMPLIFICATION OF THE HORIZONTAL COMPONENTS AT
THE PACOIMA DAM ACCELEROGRAPH SITE FOR A FREQUENCY OF 10 HZ
(based on Bouchon, 1973)

	N76°W	S14°W
P	+80%	+50%
SV	Several times larger	Several times larger
SH	+40%	+40%





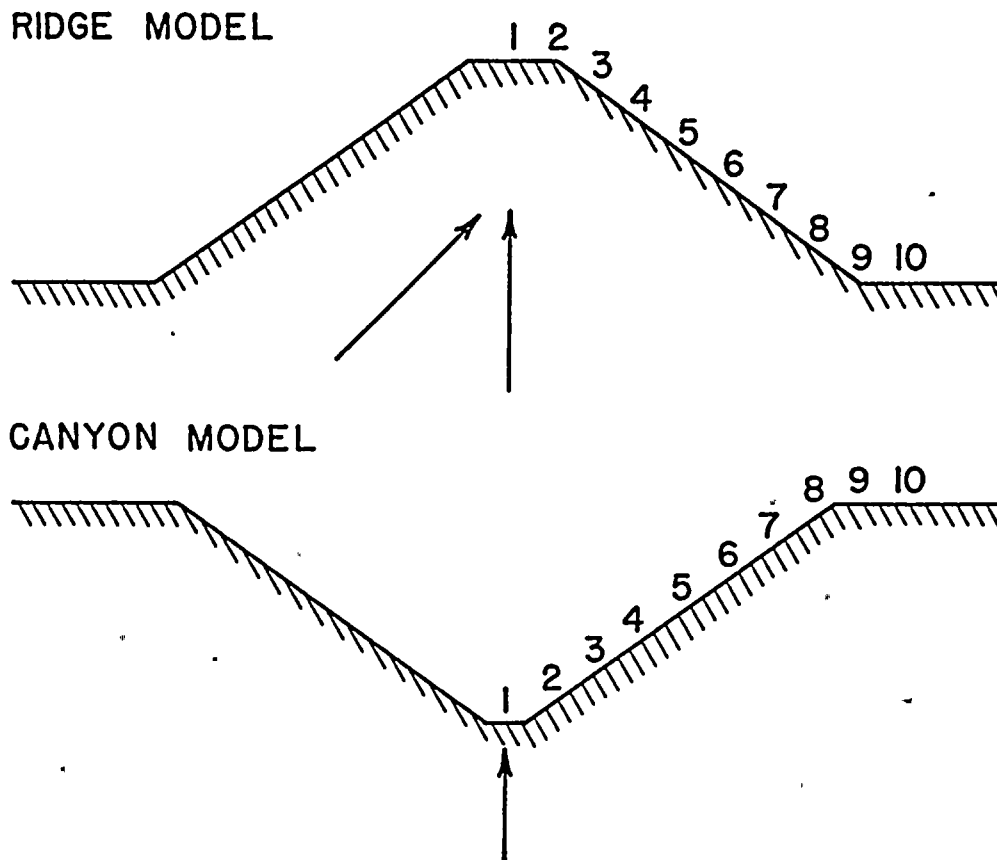


Figure Q16-9

Idealized models of the topography at Pacoima Dam. Two-dimensional geometry is assumed. The arrows indicate the angle of incidence of the *SH* waves used in the analysis. The numbers indicate points at which seismograms are computed. The accelerograph site is approximately at point 1 on the ridge model and point 4 in the canyon model. Because of normalization, the relative sizes of the two models are not shown in this figure (from Boore, 1973).



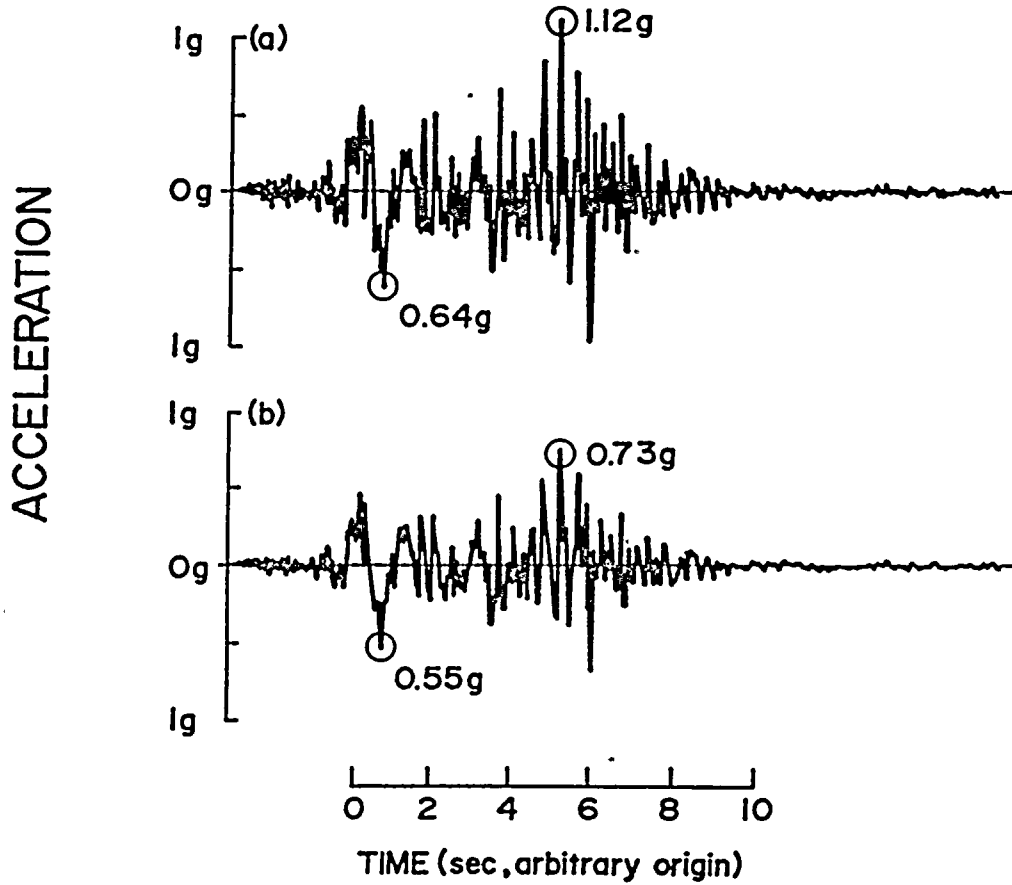


Figure Q16-10

(a) The recorded motion at Pacoima Dam in the S14°W direction during the 1971 San Fernando earthquake, after removing all energy above 15 Hz. (b) The same record after removing the amplification predicted in the ridge model with vertical incidence. The effect is very predictable from the frequency domain result, but would have been less so if the amplification ratio had been more complicated in character (from Boore, 1973).



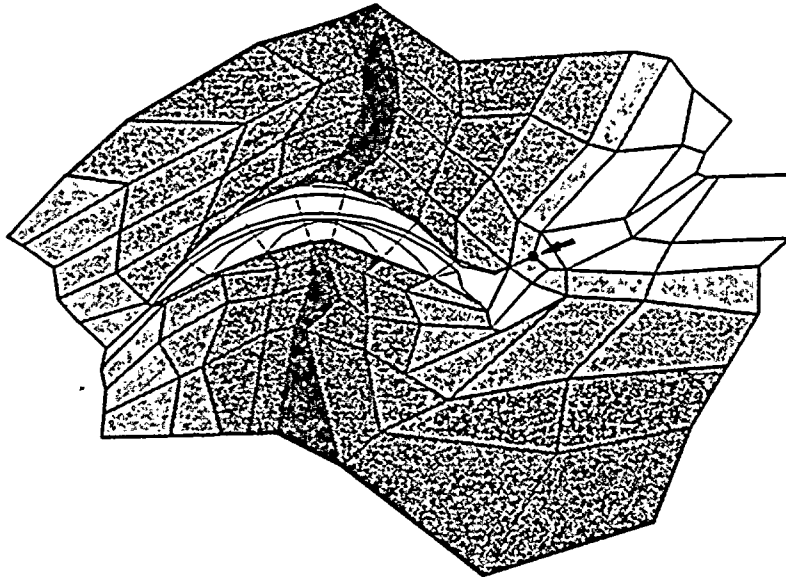


Figure Q16-11

Aerial photograph of the Pacoima Dam and finite element model of the dam and surrounding area (from Reimer and others, 1973).



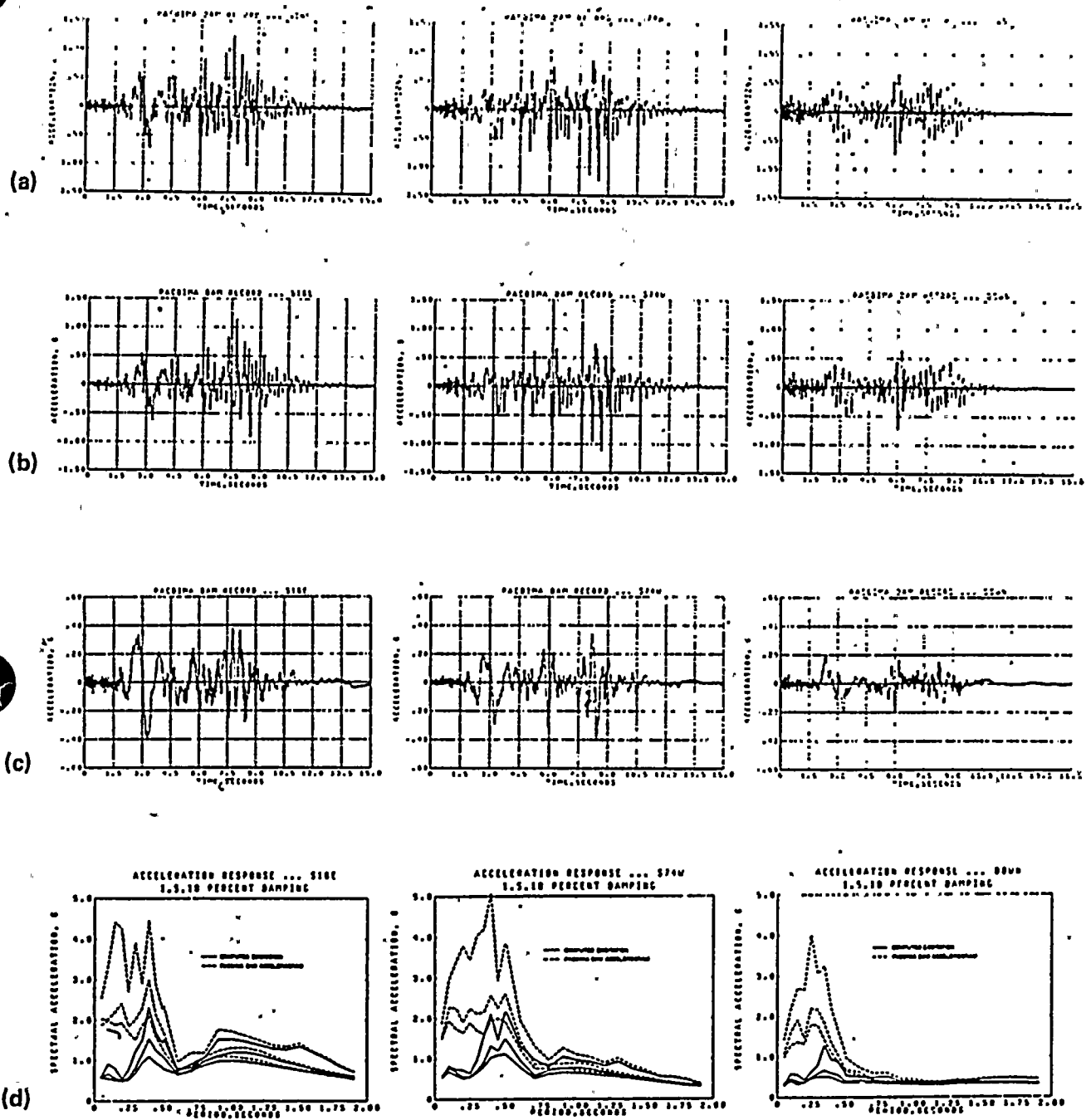


Figure Q16-12

Results of a three-dimensional finite element modeling of the Pacoima Dam accelerogram: (a) the observed accelerogram; (b) the filtered accelerogram; (c) the computed boundary excitation; (d) comparison of acceleration response spectra between the observed accelerogram and the computed excitation (from Reimer and others, 1973).



was dependent on the angle of incidence. The effect could be either deamplification or amplification, depending on whether or not the canyon was on the ray path.

Summary. There is strong evidence for topographic amplification of ground motions at the Pacoima Dam accelerograph site. We found that all the comparative studies of accelerograms from aftershocks and numerical modeling studies consistently indicated significant amplification of ground motions, particularly at high frequencies. The foam-rubber model studies showed mixed results; however, it is not clear how the results from these studies can be extrapolated to the field situation. Furthermore, the studies made thus far were based only on incident SH waves. There is indication, such as in the results from numerical modeling studies shown in Table Q16-1, that topographic effects on ground motions due to incident SV waves could be significantly larger. In view of these limitations, the results from the foam-rubber model studies may not be as directly relevant as those from the other two types of studies for evaluating the topographic effects on ground motions at the Pacoima Dam accelerograph site.

On the basis of the results of both the comparative studies of aftershock accelerograms as well as the numerical modeling studies, we conclude that the topographic amplification of high-frequency ground motions in the Pacoima Dam accelerogram was significant. Accordingly, the ordinates of the horizontal acceleration response spectra of the 1971 Pacoima Dam recording were adjusted by a frequency-dependent factor that varied linearly with frequency on a logarithmic scale from 1 at a frequency of 10 Hz to 1.5 at a frequency of 33 Hz (peak ground acceleration). The adjustment factor is shown in Figure Q16-13 and compared with the results of the various studies discussed above. It is clear that the adjustment factors used in the Long Term Seismic Program are comparable to or smaller than those observed or calculated.

Topographic Amplification at Nahanni Site 1 and Site 2

Weichert and Horner (1987) studied the records obtained at Nahanni Site 1 and Site 2, and described the conditions at these sites as follows. "(Site 1) was on top of the gently undulating plateau, west and on top of the escarpment shown in Figure Q16-14 (top), at a distance of about 30 to 50 m from the 100 to 150 m dropoff, that here marks the Iverson Thrust. Apart from possible topographic amplification due to the nearby 50 to 75 percent slope, Site 1 looked sound, with no nearby loose rock or debris. Site 2 appears much less solid: it is located within a few meters of a steep dropoff near the nose of the helicopter, whose tail is visible in Figure Q16-14 (bottom); behind the photographer, the slope continues down at a more moderate 75% for about 200 m elevation drop. The rather fractured look of the rock rampart in Figure Q16-14 (bottom) qualitatively suggests the possibility of some high-frequency amplification. This may be the explanation of the 20 Hz content seen in the record at Site 2." The topographic elevation in the vicinity of the two sites is shown in contour form in Figure Q16-15 and in cross section in the lower parts of Figures Q16-16 and Q16-17.

The objective of the study by Weichert and Horner (1987) was to determine whether the large phase arriving late in the strong-motion recording of the Nahanni earthquake at Station 1 was attributable to site effects (which might include topographic effects). Their approach was to compare the peak accelerations recorded at Station 1 with those recorded at Station 2 for a series of aftershocks. Plotting the ratio of peak accelerations against the distance ratio, they concluded that, on average, the amplitudes at Station 2 were 30 percent higher than those at Station 1. Thus, it is only in the mainshock that Station 1 has a much larger peak amplitude than Station 2. Weichert and Horner's conclusion was that, since the instrument at Station 1 did not record anomalous (in comparison with Station 2) peak accelerations during the aftershock sequence, there was no evidence that the large later phase recorded during the main shock was due to unusual site amplification.

Weichert and Horner's analysis did not address absolute levels of site amplification; only the relative amplitudes between the two stations. Thus, their conclusion relating to aftershocks is not inconsistent with the hypothesis that both sites experienced topographic amplification that affects the entire duration of the strong motion, but by differing amounts at the two stations. Indeed, in the passage quoted above, it is clear that they expected topographic effects to be present at both sites.



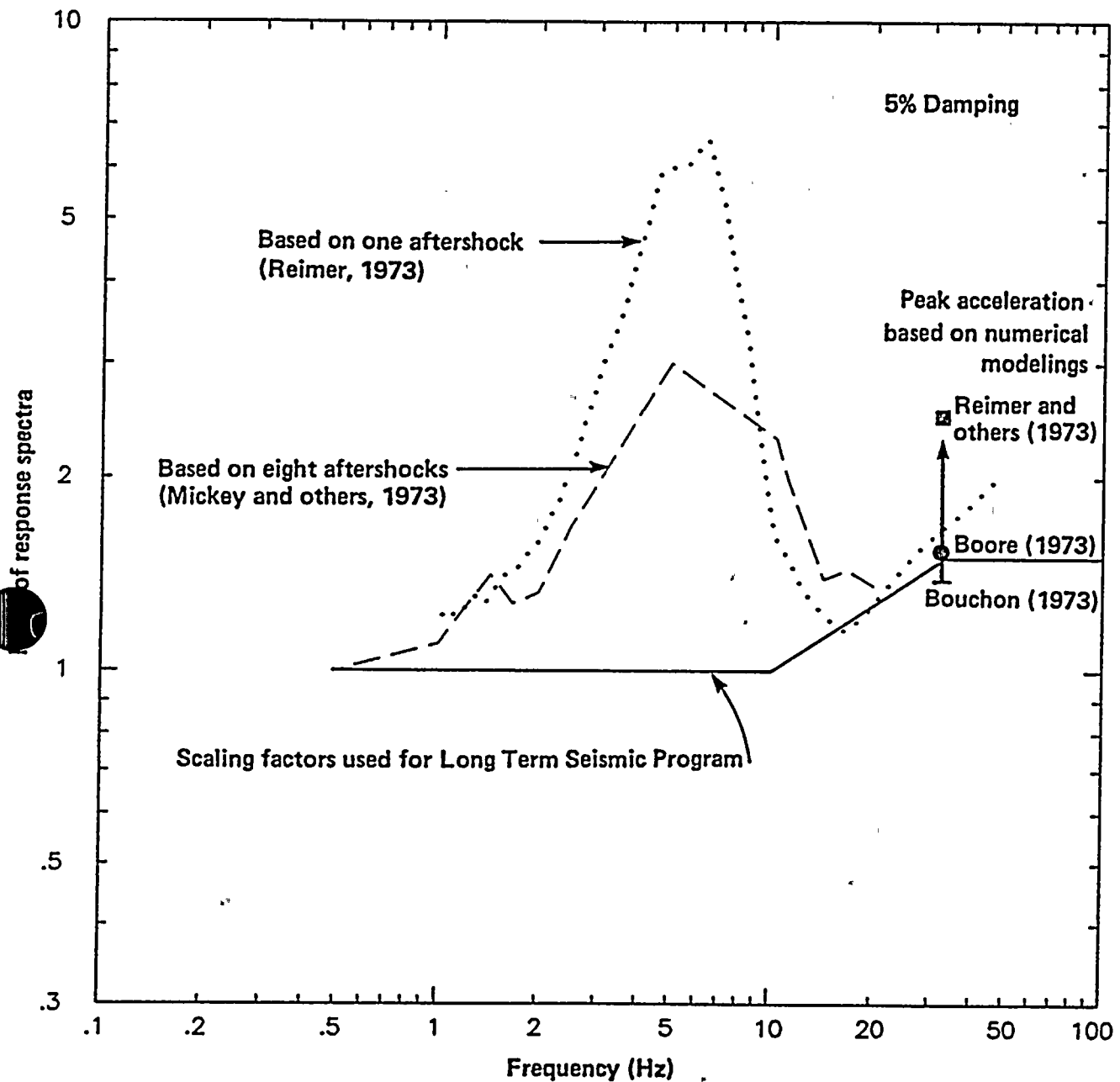


Figure Q16-13

Comparison of the ratio of the response spectra and peak accelerations at the Pacoima Dam seismograph site to the free-field site, from aftershock recordings and numerical modelings, with scaling factors used for the Long Term Seismic Program.



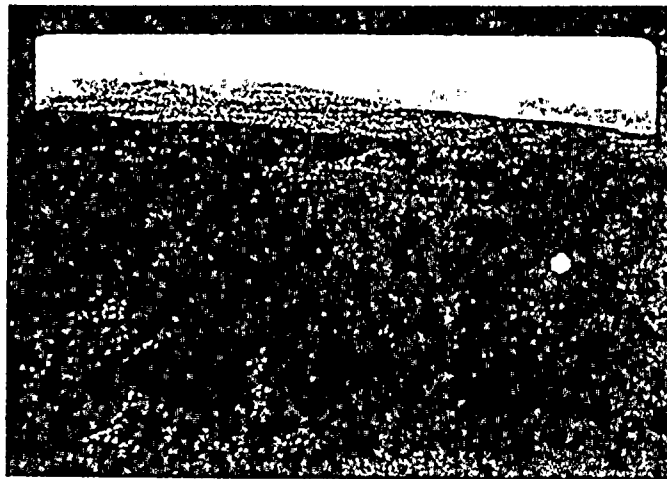


Figure Q16-14

Site conditions at Nahanni Site 1 and Site 2. Top: Site 1, general view, looking southwest. Foreground is Iverson Thrust, MacKenzie Mountains in background. Dot marks approximate site location. Bottom: Site 2, the accelerograph is in front of the helicopter (from Weichert and Horner, 1987).



1:50,000

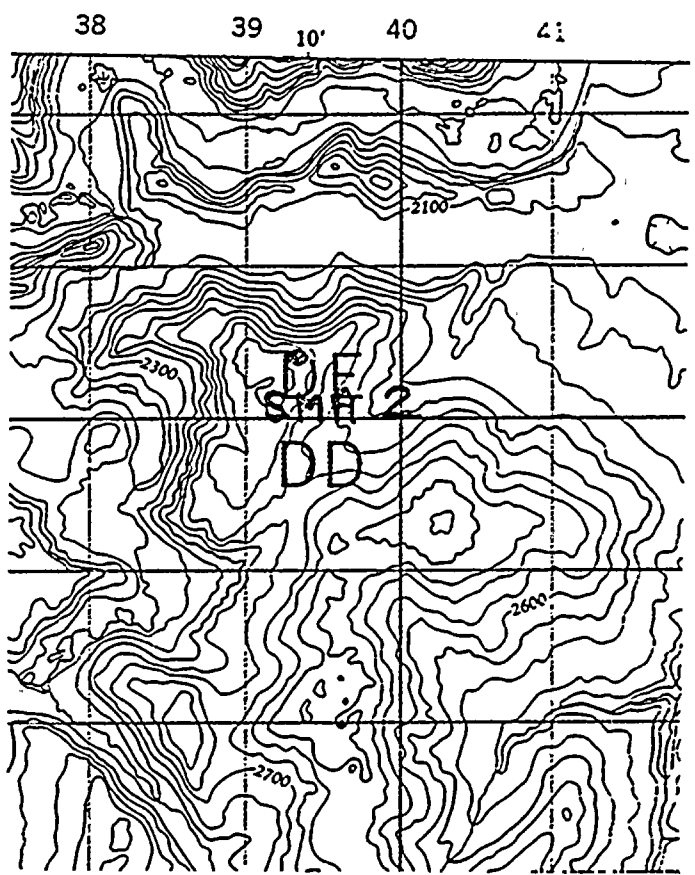
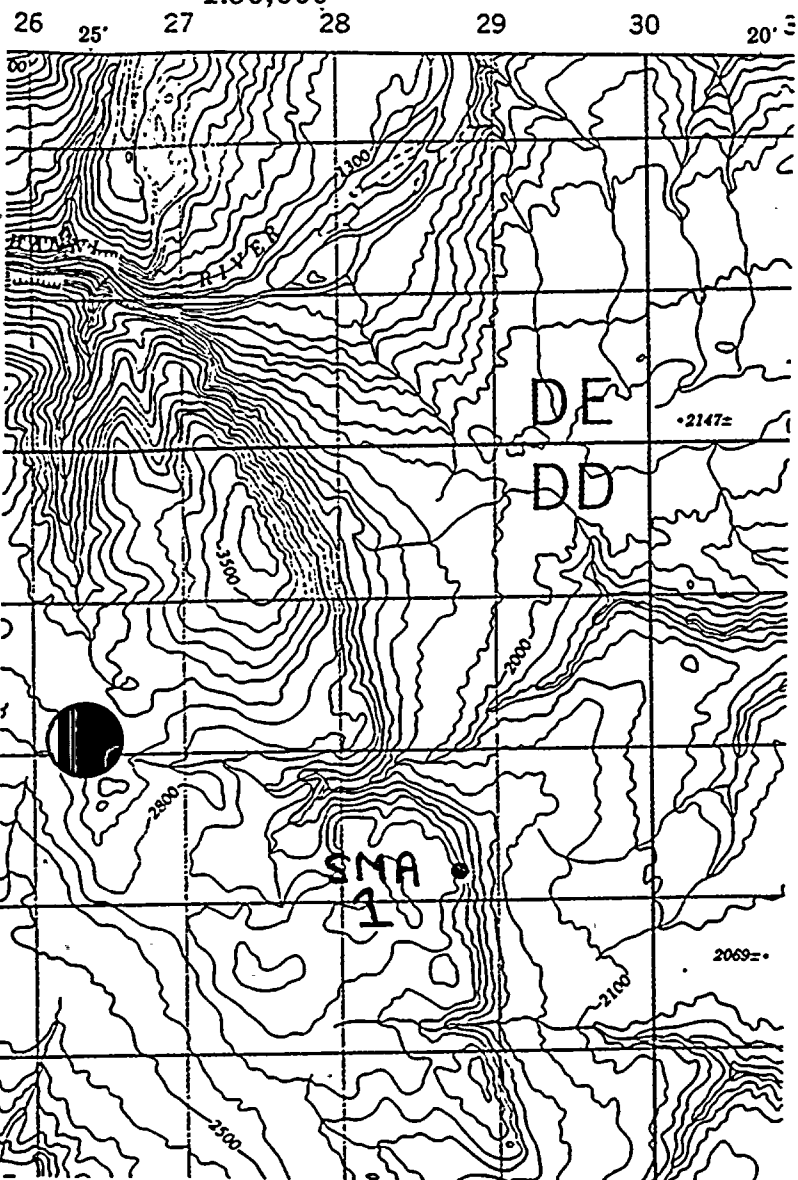


Figure Q16-15

Topographic elevation in the vicinity of Nahanni Sites 1 and 2. Elevation contour intervals are 100 feet.



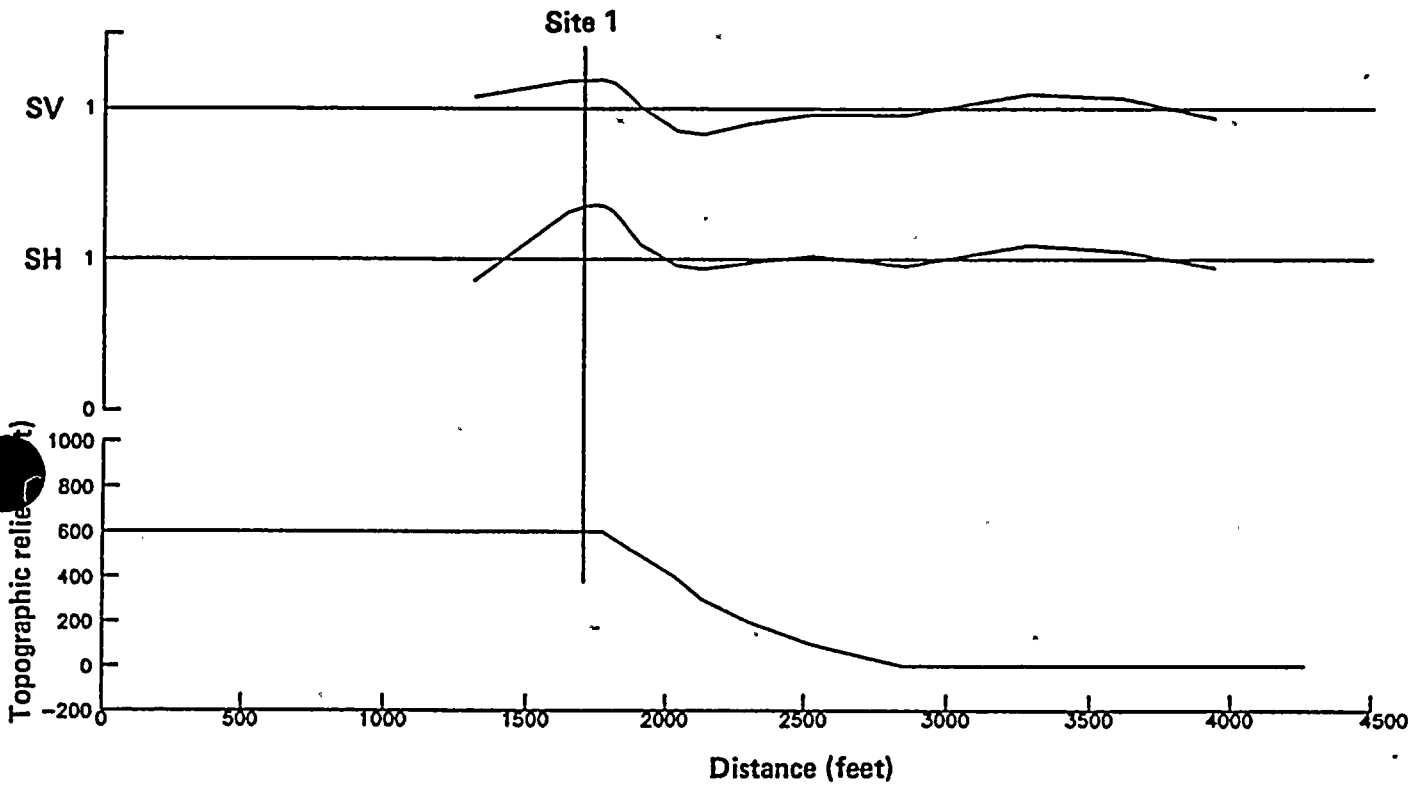


Figure Q16-16

Topographic response to vertically incident SV and SH waves at Nahanni Site 1.



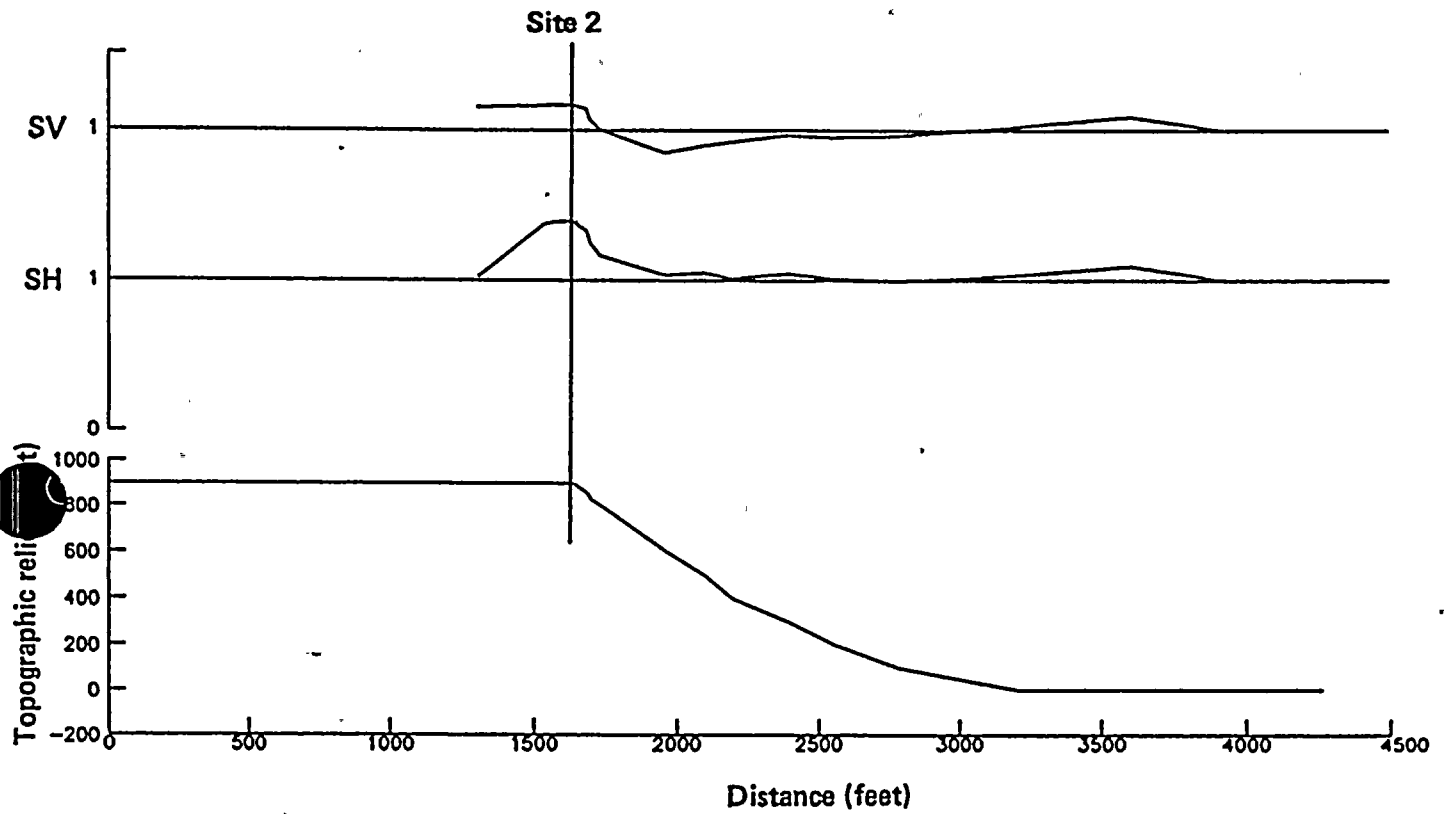


Figure Q16-17

Topographic response to vertically incident SV and SH waves at Nahanni Site 2.



To test this hypothesis, a numerical study of topographic effects at the two Nahanni sites was conducted using finite difference calculations; the results are shown in Figures Q16-16 and Q16-17. The procedure used is the same as that described in the response to Question 12 of this submittal. The topographic profiles were derived from the 1:50,000-scale elevation contour map shown in Figure Q16-15. The upper slopes of the two profiles are very similar, but Station 2 is at about 300 feet higher elevation. At each site, the accelerograph was located close to the edge of a steep slope. The ratio of peak acceleration on the ground surface to that for flat (free-field) conditions shows similar effects, with amplification of both SV and SH waves over the edges of the slopes, and some deamplification over the slopes. At the strong motion sites, there is amplification of SH by 35 and 45 percent for Stations 1 and 2 respectively, and amplification of SV by 10 and 15 percent respectively. For both SH and SV, the amplification at Station 2 is slightly larger than at Station 1. This is consistent with the observation by Weichert and Horner (1987) that the peak accelerations of the aftershocks at Station 2 are larger on the average than at Station 1. We conclude that the strong motion recordings of the Nahanni earthquake at Stations 1 and 2 were both amplified by topographic effects.

Summary

The results of the studies discussed above confirm that the recordings at the Pacoima Dam accelerograph site and at the Nahanni Sites 1 and 2 were affected by topography. They also indicate that the adjustment factors we applied to these recordings are justified and appropriate. (The spectrum derived using these adjustment factors is compared with the spectrum derived using no adjustments in the response to Question 2 of this submittal.)

References

Aki, K., 1988, Local site effects on ground motions: in Van Thun, J. L. (ed.), Proceedings of the Earthquake Engineering and Soil Dynamics II Conference, American Society of Civil Engineers, p. 103-155.

Aki, K., and Larner, K. L., 1970, Surface motion of a layered medium having an irregular interface due to incident plan SH waves: *Journal of Geophysical Research*, v. 75, p. 933-954.

Anooshehpour, A., 1988, Foam rubber model studies of problems in seismology and earthquake engineering: Ph.D. Thesis, University of California at San Diego.

Boore, D. M., 1973, The effect of simple topography on seismic waves; implications for accelerations recorded at Pacoima Dam, San Fernando Valley, California: *Bulletin of the Seismological Society of America*, v. 63, p. 1606-1609.

Bouchon, M., 1973, Effect of topography on surface motion: *Bulletin of the Seismological Society of America*, v. 63, p. 615-632.

Brune, J. N., Anooshehpour, R., Lovberg, R., and Wang, L., 1985, Topographic seismic amplification and dam-foundation interaction on a foam-rubber model of the topography near Pacoima Dam: in Scholl, R. E. and King, J. L. (ed.), *Strong Ground Motion Simulations and Earthquake Engineering Applications*, Earthquake Engineering Research Institute Publication 85-02.

Geli, L., Bard, P. Y., and Jullien, B., 1988, The effect of topography on earthquake ground motion; a review and new results: *Bulletin of the Seismological Society of America*, v. 78, p. 42-63.

Mickey, W. V., Perez, V., and Cloud, W. K., 1973, Amplification studies of the Pacoima Dam from aftershocks of the San Fernando earthquake: *Proceedings of the Fifth World Conference on Earthquake Engineering*, p. 755-762.

Reimer, R. B., 1973, Deconvolution of seismic response for linear systems: Report No. EERC 73-10, Earthquake Engineering Research Center, University of California, Berkeley, 162 p.





Reimer, R. B., Clough, R. W., and Raphaël, J. M., 1973, Evaluation of the Pacoima Dam Accelerogram: Proceedings of the Fifth World Conference on Earthquake Engineering, Paper No. 293, 12 p.

Shakal, A. F., Huang, M. J., Ventura, C. E., Parke, D. L., Cao, T. Q., Sherburne, R. W., and Blazquez, R., 1987, CSMIP strong motion records from the Whittier, California earthquake of 1 October 1987: Report No. OSMS 87-05, California Division of Mines and Geology, 198 p.

Weichert, D. H., and Horner, R. B., 1987, The Nahanni earthquakes: in Proceedings of the Symposium on Seismic Hazards, Ground Motions, Soil Liquefaction and Engineering Practice in Eastern North America, Technical Report NCEER-87-0025, p. 318-328.



